Identification of Nonlinear Model Parameters - Spoiler Aerodynamics of the F-111C Aircraft

by

R.A. Stuckey

B.E. (Aero) University of Sydney, 1991

Submitted to the Department of Aeronautical Engineering
in partial fulfillment of the requirements for the degree of

Doctor of Philosophy

at the

UNIVERSITY OF SYDNEY

August 1995

Signature of Author . . . .
Department of Aeronautical Engineering
31 August 1995

Certified by . . . .
Mr C.A. Martin
Senior Principal Research Scientist, Aeronautical & Maritime Research Laboratory
Thesis Supervisor

Certified by . . . .
Prof G.P. Steven
Head of Department, Department of Aeronautical Engineering
Thesis Supervisor

Certified by . . . .
Dr K.C. Wong
Lecturer, Department of Aeronautical Engineering
Thesis Supervisor

Identification of Nonlinear Model Parameters -

Spoiler Aerodynamics of the F-111C Aircraft

by

R.A. Stuckey

Submitted to the Department of Aeronautical Engineering
on 31 August 1995, in partial fulfillment of the
requirements for the degree of
Doctor of Philosophy

Abstract

An approach for the identification of nonlinear parameters that characterise high-order dynamic systems was developed and then applied to the unsteady aerodynamic behaviour associated with wing-spoilers on the F-111C aircraft.

Prior to analysis, the flight data were first compensated for pressure errors and compressibility effects and then corrected for instrument signal conditioning and recording lags. Careful filtering was also required to set bounds for the removal of outliers and other anomalies from the data.

A Piecewise Regression technique was utilised to estimate the lateral spoiler models from each flight case examined. This approach facilitated the use of tensor-product polynomial splines - which are ideally suited to modelling aerodynamic characteristics - for representation of the nonlinear coefficients. It was found that the estimates obtained were consistently lower than those from scaled-model wind-tunnel tests, particularly at high angles-of-attack where separated flow effects were prominent. Although the characteristic loss/reversal of effectiveness was detected, it occurred at a much higher attitude than expected, due to the difference in Reynold's numbers. Several other phenomena observed in wind-tunnel models were also identified and the final sets of parameters generally compared well.

Methods for partitioning the data were investigated, including two which utilised the statistical significance of each region and an unconstrained optimisation technique. This latter approach employed standard minimisation schemes, such as Simplex Search and nonlinear Least Squares for placement of the bounds.

Following extensive analysis of a range of flight cases, the fundamental model structure was assessed in terms of its efficiency using a stepwise variable-selection scheme. The significance of each parameter was examined, applying various hypothesis tests and a number of selection criteria. Lastly, in order to verify the identification results, a full six degree-of-freedom nonlinear dynamic model was constructed and each response simulated. The resulting time-histories followed the real flight data adequately, even in the presence of excessive measurement noise.

Contents

List of Tables

List of Figures

Acknowledgements

It has been a great privilege to perform this research under the supervision of Mr Colin A. Martin, of the Aeronautical and Maritime Research Laboratory. The encouragement and guidance given to me has been most rewarding and our interaction has contributed much to my understanding of system identification. I would like to thank him for motivating this project and opening the path to many people and resources. Many other staff at AMRL also gave graciously of their time in correspondence and supplied me with the flight-data, as well as all associated material.

Professor Vladislav Klein of the NASA Langley Research Center was an invaluable source of technical reference and experience. I am grateful for our discussions and the publications provided, without which this research would not have been possible.

I wish to thank Dr Daniel M. Newman for his insight and knowledge in flight dynamics. Professor Grant P. Steven & Dr Kee Choon Wong have also afforded considerable time and effort in the evolution of this thesis.

I express my deepest gratitude to my wife Silvia, for her patience and more importantly, for her love and support which has made this task endurable. To my daughter Olivia, who has been the sparkle in my life, I extend my adoration. Lastly, this work is a tribute to the support, encouragement and sacrifice of my parents who first started me along this path.

Chapter 1

Introduction

1.1 Prelude

The aim of this research was to develop an approach for the identification of nonlinear model parameters from flight data and then apply it to the estimation of spoiler characteristics for the F-111C aircraft.

Nonlinear model identification generally represents a complex problem, since the structure of the model is invariably chosen by the analyst and therefore, decisions are made regarding the model's adequacy. It must be determined not only what form the model should take, but also how complex it should be to provide a sufficient representation of the true system.

The aerodynamic characteristics of spoilers have been described as the most difficult to predict among all conventional aircraft control surfaces, due to the present general inability to accurately model separated flows. To add to the problem, the analyst can never be assured of the integrity of scaled-model wind-tunnel tests, since the Reynold's numbers used are often an order of magnitude less than that experienced in real flight. Unlike most control surfaces, the induced wake is turbulent and therefore sensitive to Reynold's number differences.

1.2 Identification Techniques

Equation error methods found their way into the field of aircraft parameter identification several decades ago and constitute one of the main forms of identification used today. Perhaps the most endearing feature of these techniques is their simplicity and ease of application.

This has allowed them to be readily manipulated to suit many engineering problems, including nonlinear model analysis. It has also been shown that if the error is white with zero mean, the parameters will have minimum variance for the class of linear unbiased estimators.

A fundamental drawback of the equation error method is that any measurement noise in the input or output variables will bias the estimates. In addition, any process noise due to say, turbulence or modelling errors, will not only bias the estimates, but will affect their variance as well. Despite this degradation in the accuracy of the estimates, however, the equation error method has been frequently used in parameter identification. More importantly, it has demonstrated the ability to produce results that are comparable to more sophisticated techniques, such as the output error method, which is expected to yield consistent, unbiased estimates.

A collection of equation error techniques were employed in this research - each of them based on the multiple linear regression model - and, although the estimation problem would normally be solved using a standard Least Squares (LS) algorithm, other biased approaches were necessary in the majority of cases examined. Generally speaking, the reason behind this was to avoid the various identification problems that often arise in the analysis of flight-data. For example, the less important terms in the model were biased toward their *a-priori* values using a Mixed Estimation technique, so that unrealistic estimates would not result. The $\dot{\beta}$ terms were also biased, because of their near-linear relationship with the other variables, which would otherwise have produced poorly conditioned matrices. This Bayes-like procedure essentially augments the regression with a second set of equations, describing the relative variance of each parameter, thus 'weighting' each of the estimates accordingly. It is a reasonably simple technique and, as with most biased approaches, is able to reduce the variance of the estimates and possibly even the mean-square error below their LS values.

In those cases that exhibited a high level of collinearity amongst the variables, a Principal Components regression was used. This technique first transforms the regressors into orthogonal components and then removes the components associated with certain 'small' eigenvalues. It is possible to identify those eigenvalues, as well as the regressors likely to cause ill-conditioning, via a variance-proportion decomposition. Following reduction of the regression into principal components, a Least Squares solution is found and the estimates are transformed back onto their original space. Principal Components regression is particularly effective in the analysis of collinear data and can improve the accuracy of the estimates significantly.

1.3 Model Structure Determination

To facilitate use of the equation error method, the aircraft model is formulated through a Taylor series expansion about some trim state. Each of the aerodynamic coefficients in the model can be evaluated from the accelerations and expressed as functions of the state and control variables. The derivatives that parametrize this function comprise terms which are themselves general functions of the aircraft state. For many of these terms, a linear approximation is sufficient, however, for those coefficients in which linearisation cannot be substantiated, nonlinear functions are used.

The nonlinear coefficients are represented by tensor-splines in one and two dimensions, since splines are well-suited to modelling aerodynamic effects. Each spline function is built from a set of parameters, so the model size increases dramatically with the addition of non-linear terms. If too many terms are introduced into the regression, however, identifiability problems may be encountered. On the other hand, too few terms in the model may yield an inadequate representation. This raises the question of required model fidelity.

In order to determine which parameters in the model are significant, a method of selection based on one or more criteria must first be formulated. The Exhaustive search is an extensive procedure that checks the entire space of possible models, or some subspace thereof. A quantity such as the C_p statistic is ideal for the determination of an adequate model from the set examined, as it provides a measure of the model accuracy as well as it's size. A more efficient procedure is that of Stepwise Regression, based on a recursive algorithm in which the model is re-examined at each step. The independent variables are sequentially removed from the regression if their contribution is deemed nonsignificant, while candidate variables are added if their partial correlation is high. The process is allowed to continue until a fully significant model incorporating a (local) maximum number of parameters is attained.

A collection of software routines using these procedures was written for the MATLAB interactive numerical computing environment. The code should prove useful for system analysts, since many in the field of control design and identification will be familiar with the language, or similar high-level ones. It has shown the ability to handle a real-world aircraft identification problem, yet is relatively easy to understand and employ. A user's manual containing several demonstration cases has been included as an introduction to it's use.

1.4 F-111C Results

Before the aircraft's test flight-data were analysed, compensatory measures, including the removal of outliers and application of phase shifts, were required to account for various instrumentation and recording errors. In addition to this pre-processing, a frequency analysis was conducted on the data in order to gain a broader perspective of the aircraft dynamics plus any external disturbances. A considerable amount of noise was found in the yawing acceleration signal, which degraded the resulting accuracy of the estimates significantly.

An examination of the correlation among the variables was also undertaken, since the presence of high collinearity can affect the identification process adversely, as explained beforehand. The greatest degree of collinearity was exhibited between the differential-stabilator and spoiler deflections, with a lesser degree between the sideslip and rudder deflection. Although significant, the limitations on numerical accuracy in MATLAB was such that only a few cases were affected, requiring a biased-estimation technique.

For representation of the spoilers' rolling and yawing contribution functions, first-order polynomial splines in δ_s and α were utilised. Several of the other derivatives also exhibited a significant variation with the angle-of-attack and were consequently represented by splines in α only. A number of data-partitioning approaches were examined, from which it was decided to use a conservative scheme. This scheme makes use of prior information to position the knots within the model and can thus avoid creating sparsely populated regions. A partition-optimisation procedure was also investigated, using both simulated and real flight-data. From this, a nonlinear Least-Squares algorithm proved the most effective - consistently locating the minimum in a fraction of the number of steps taken using the Simplex Search algorithm.

Flight-identified results were obtained for a range of wing-sweep angles and Mach numbers. Only the lateral coefficients were examined in each case, with focus on the nonlinear spoiler terms. The spoilers' sideforce derivative was on average very small and was in fact, the least significant of all of the sideforce coefficients. The rolling-contribution exhibited a general decrease with increasing angle-of-attack, as seen in the wind-tunnel model. However, the change was less marked, indicating a sustained effectiveness at higher attitudes. The characteristic sudden loss in rolling-contribution and subsequent degradation into full control reversal at high angles-of-attack was also detected. Moreover, it was found to constitute a significant effect, although it occurred at a higher angle than observed in the wind-tunnel model. Along with the decrease in the rolling contribution, a corresponding decrease in the yawing contribution was identified. Unlike the former term, however, no rapid change was detected with increasing angle-of-attack. It was concluded that the main cause of disagreement between the wind-tunnel and flight-identified results was the Reynold's number differences present in each case.

1.5 Thesis Outline

The manuscript has been organised in the following manner:

Chapter 2 presents an overview of spoiler aerodynamics. Typical characteristics of the flow are discussed, as well as the resulting effect in terms of control forces on the wing. The spoilers on the F-111C aircraft are also examined in this context.

Chapter 3 introduces the mathematical model of an aircraft and in particular, the F-111C model utilised in the analysis. Model adequacy is discussed and the problems associated with identification. The nonlinear coefficients are formulated using polynomial splines - the properties of which are outlined, as well as simplifications to the resulting model. In addition, the various sources of error are considered, including modelling, systematic and random errors.

Chapter 4 describes the equation error identification technique, including an analysis of the estimated variance and correlation between the variables. The construction of confidence intervals is discussed along with the application of hypothesis tests for the determination of significant parameters. The chapter also compiles a number of accuracy criteria that can be utilised in the selection of an adequate model. Dummy variables are examined, with reference to their use in the analysis of categorical data.

Biased estimation is covered, together with scaling and collinearity. Several approaches for the detection of collinear data are discussed, including an eigensystem analysis. Principal Components regression and Mixed Estimation techniques are detailed, as well as Restricted estimation for the implementation of hard constraints.

The subject of model structure determination is reviewed in the latter sections, covering various procedures that can be used for the identification of a parsimonious model. These include Exhaustive Search, Backward Elimination, Forward Selection and Stepwise Regression. Finally, model analysis and validation methods are examined.

Chapter 5 first summarises the flight-testing and preliminary analysis conducted prior to this work. The aircraft instrumentation and flight-test program are outlined, as well as all data processing and parameter estimation that was performed in the analysis.

The next section details further data pre-processing that was conducted as an integral part of this research. The results of a frequency analysis are studied, in addition to those from an evaluation of the collinearity in the data.

In the last section, data partitioning is investigated and three schemes are examined: conservative placement, based on prior information; various stepping schemes which select significant partitions from the postulated set; and nonlinear optimisation techniques, which utilise minimisation algorithms to partition the data.

Chapter 6 gives the results of system identification on both simulated and real flight-data pertaining to the F-111C aircraft. Following examination of the simulated data results, the details of the real flight-data analysis are discussed. Each wing-sweep configuration is treated separately.

Relevant aspects of the results are interpreted with reference to the aerodynamic behaviour exhibited by spoiler devices.

The significance of certain characteristics of the estimated model are assessed using a Stepwise Regression procedure.

Chapter 7 concludes by summarising the main findings of this work.

As well as the references particular to research in spoiler aerodynamics, an extensive bibliography on aircraft system identification has been included, since a general survey of the field was undertaken during the research. The last bibliography to be compiled in aircraft parameter estimation was almost a decade ago [91] and includes many references not listed. Unlike the previous document, however, the focus of this effort was restricted to system identification and other topics such as instrumentation were not considered.

Chapter 2

Spoiler Aerodynamics

2.1 Introduction

The definition of a spoiler has been given as follows [276]:

> *"A spoiler device is essentially a panel affixed to the surface of a wing - usually the upper surface - which, when deflected, causes separation and thus 'spoils' the streamline flow. This transition generally results in a loss of lift and increase in drag of the wing"*

Spoiler devices were initially employed as roll-controls, though later found a number of alternative uses, such as lift-dumping, airbraking, direct lift control and load-alleviation. They have several features that make them desirable for lateral control in aircraft. In short, spoilers:

- provide an alternative to ailerons for full roll-control - in fact, they can be more effective at high subsonic speeds and are less prone to losing their effectiveness under aeroelastic deformation;
- produce a beneficial, *proverse* yawing moment;
- permit the concurrent use of full-span flaps; and
- can be designed for effective control at high incidence angles.

Unfortunately, the full potential of spoilers as lateral control devices has not been realised due to some of the aerodynamic features they display, including:

- inherent nonlinear characteristics, becoming even more pronounced in the presence of deflected flaps;

- drag increases are introduced;

- they may cause an undesirable lag in the aircraft response; and

- the unsteady wake can cause buffeting loads to be high.

The most common type of spoiler is the "flap-type", illustrated in Figure 2-1. These are used on many transport aircraft and some military aircraft, including the General Dynamics F-111C. This chapter will therefore focus on flap-type spoilers. The following section on the background of spoiler research pertains to spoilers in general, however, the corresponding results and subsequent discussion on spoiler aerodynamics are relevant specifically to flap-type spoilers.

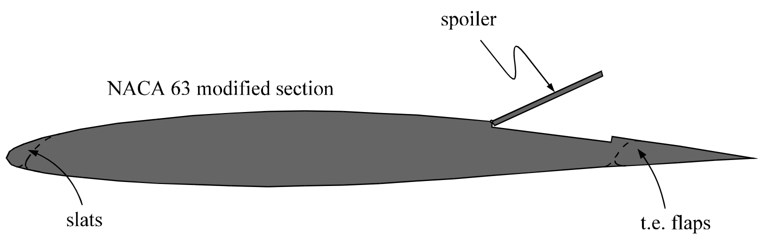

Figure 2-1: Airfoil with a typical flap-type spoiler

Spoiler effectiveness depends on several parameters, including the angle-of-attack, Mach No., Reynold's No., airfoil section, spoiler profile and location as well as other aircraft configuration geometries. Furthermore, the surrounding flow field varies according to the spoiler's deflection and rate of deflection.

Following the first section, the aerodynamic characteristics associated with statically deflected spoilers, including transonic effects will be examined, based on research to-date. The moving spoiler and transient effects will then be discussed in the next section, although there has been little work conducted in this area, so the results are somewhat generalised.

Lastly, differential spoilers used for lateral control will be examined, with particular attention to the spoilers on the F-111C aircraft.

No attempt has been made to give a full account of spoiler aerodynamics - this chapter has been included simply to introduce those aspects directly relevant to this research.

2.2 Background

Experimental research into spoiler aerodynamics dates back to the early 1930's. Weick, *et al* [282] initially investigated the use of spoilers in an effort to obtain satisfactory lateral control through the full angle-of-attack range maintained in flight. A moderate amount of rolling moment with favourable yawing moments was obtained with a large spoiler, tested without the use of ailerons. The principal results were then compared to other control devices in a resumé of the investigation [283]. Spoilers, or "retractable ailerons" presented an attractive possibility for lateral control at that stage, as they required only small control forces in order to produce a significant roll-authority. Rear-mounted spoilers also minimised the response lag inherent with those types of control devices.

Interest in spoiler devices was renewed several years later [281, 272], particularly at high incidence angles, where they lost effectiveness. For one model tested, an increase in the spoiler projection produced a corresponding increase in the rolling moment at low angles-of-attack. However, at angles above 8°, the spoilers' effectiveness decreased rapidly, becoming ineffective at 16°. It was even found that plain outboard ailerons could be much more effective at these high angles-of-attack. Most reports of that time were mainly concerned with the gross aerodynamic forces and moments related to spoiler control [259], rather than the local pressure variation. Very little effort was made to obtain boundary layer and flow field data, mainly due to the lack of adequate instrumentation to measure the separated boundary layer and associated wake. Woods [284] first designed specific experiments to obtain surface pressure distributions on normal spoilers to aid in the theoretical formulation. However, surface pressure distributions were able only to guide this formulation in a limited way. The most important details remained to be measured: complete flow-field information, including the boundary layer development and associated wake characteristics.

During 1974, a series of experimental research programs on spoiler aerodynamics were undertaken at Wichita State University [278]. From these, a complete set of experimental data on airfoil separation was obtained to aid theoretical research on the problem. The data included detailed boundary layer characteristics, static and total pressure fields, velocity vector fields and hot film anemometer surveys. Prominent features of the wake identified through this work included the abrupt termination of the reversed-flow region downstream and the intermittent, unsteady nature of the flow, resulting from the fluctuating separation point on the airfoil. The experiments of Francis, *et al* [258] were also important in addressing the problem of unsteady separated flows and the wake created by a deflected spoiler. Their research mainly concentrated on the unsteady flow characteristics resulting from an oscillating spoiler and the flow properties close to the surface, where the flow-reversal was predominant. Siddalingappa, *et al* [279, 280] continued analysis of both the local flow field around a deflected spoiler and the overall pressure distribution on the airfoil+spoiler combination, acquiring a more detailed understanding. These papers encompassed a discussion of the steady pressures, the transient pressures following a ramp change in spoiler angle and the transient pressures induced by an oscillating spoiler motion. Three-dimensional wing/spoiler effects were also examined over a range of incidence and Mach number. The pertinent results from this and other work will be summarised in the following sections.

Around the same time, Boeing's Stability and Control research group was conducting experiments on typical transport aircraft configurations comprising single- and multi-element airfoils with spoilers. Following an initial investigation restricted to the regions of attached flow, a more comprehensive study [273] took place to obtain detailed flow data. This was motivated by a need to further refine the separated flow model developed by the Aerodynamics group [262]. A number of phenomena associated with deflected spoilers were discussed, including aerodynamic nonlinearities, deadbands, and scale-effect problems, based on two-dimensional experimental and computational data. One of the more important findings, obtained through a spectral analysis of the wake pressure, was the presence of dominant frequencies - a subject attracting much attention in the years to follow [250, 274]. Another interesting aspect of the study was the work done in full-scale flight tests. Flight data were derived from measurements of the speed-brake lift effectiveness and a moment-arm determined empirically from wind-tunnel results. It was found that the low Reynold's number data from the wind-tunnel usually overpredicted the spoiler effectiveness and in conclusion, recommended that predictive techniques be improved to analyse the problem of spoiler-induced separation in full-scale conditions.

In another investigation of the transient pressures and loads associated with sudden changes in spoiler angle [253], large, unsteady nonlinear effects were found to be present.

A full reversal of the control effectiveness was also indicated. Since then, several authors, such as McLachlan and Karamcheti, *et al* [275, 276] and more recently, Lee, *et al* [268, 270] have continued in-depth examination of the two-dimensional flow field. In particular, vortex shedding has been studied and found to characterise the nature of the wake itself.

Over the course of these experimental investigations, a parallel research effort was also being conducted in the theoretical evaluation of spoiler control. Using a simplified lifting-surface theory, it was possible to predict the subsonic rolling effectiveness for plain spoiler ailerons [260]. Subsequent comparison with experimentally obtained results for a number of different models revealed a good agreement. Later, another report [271] presented a method for approximating the loads caused by spoilers in supersonic conditions. These, together with previous theoretical research on antisymmetric wing-span loading [256], were compiled in 1978 to form several sections of the USAF Stability and Control DatCom, [263]. The DatCom provides empirical methods for estimating the rolling and yawing moments due to spoiler deflection at any speed and also summarises important aerodynamic features of spoilers on three-dimensional wings. The latest compilation of information concerning spoiler controls comes from ESDU [257] and essentially covers two topics. Firstly, it provides a brief summary of spoiler types, together with a description of spoiler characteristics and their variation with deflection. Secondly, and more importantly, it provides a method for predicting the lift coefficient decrement and rolling moment coefficient due to spoiler deflection on wings at subsonic speeds with undeflected flaps. The method, which is empirically based, involves determination of the lift characteristics in two dimensions and then correction of those results to allow for three-dimensional effects. Comparisons of test data with predictions have indicated likely errors in the lift coefficient decrement of about ± 0.05 and rolling moment coefficient to within about ± 0.007.

In addition to the experimental and theoretical research on spoiler-induced separated flow, there has been a significant amount of work done in computational modelling. An early attempt [284] to mathematically describe the flow over airfoils with spoilers used a linear perturbation free streamline potential theory to predict the incremental pressure and thence, the incremental lift, drag and pitching moment. However, this approach was limited to small spoilers in low incidence subsonic flow. Barnes [251] modified this theory through a set of empirical relationships to account for the "effective spoiler height" and the base pressure.

More recent development of a powerful panel methods code by Henderson [262] resulted in an effective separated flow model for single- and multi-element airfoil characteristics beyond stall. Using inviscid boundary conditions, the separation streamline shape was initially guessed and then iterated to obtain a stable wake shape. The program was extensively used by Boeing's Research group for the analysis of small spoiler deflections. In cases of larger deflections however, the results were not very encouraging, because the program did not account for turbulent separation and reattachment over the spoiler hinge. Subsequent modifications were made [273] with some success, by prescribing trial pressure distributions around the hinge-line, although it was clear that a greater research effort was required in developing the theoretical models of separating and reattaching flows. Further to the investigation, Lee, *et al* [269] developed a two-dimensional vortex tracing method to simulate the unsteady flow field of an airfoil with deflected spoiler. This method utilised vortex panels to represent the airfoil/spoiler geometry and discrete point vortices with viscous cores to model the wake. Comparison with previously conducted experiments showed that the method described the unsteady flow field reasonably well. The Theoretical Aerodynamics branch at ONERA in France also conducted an investigation aimed at computing the flow around an airfoil equipped with a spoiler [254, 267]. Of late, a three-dimensional inviscid flow model code has been extended to predict the flow about a wing/spoiler configuration. The results presented were compared with experimental data and showed a good agreement.

Estimation of the nonlinear aerodynamics of spoilers from flight data was introduced [222] after successful application of a modified Stepwise Regression procedure to high angle-of-attack manoeuvres [125]. The spoiler characteristics that were obtained compared well with wind-tunnel results, as did the resulting simulated responses to the actual flight recordings. This research has continued and the corresponding findings are presented in this dissertation. Since the identification technique has been outlined in those reports mentioned above, the current discussion will place more emphasis on the aerodynamic significance of the results gathered.

2.3 The Statically Deflected Spoiler

There are a number of characteristics associated with statically deflected spoilers. Much of the work conducted in spoiler aerodynamics has been based on time-averaged measurements of the flowfield and pressures with the spoiler fully deflected at the desired position. In this section, the general behaviour of spoilers - once set in position - will be examined.

2.3.1 Two-Dimensional Aerodynamics

Spoilers operate by inducing a controlled separation of the flow over the wing. The resulting turbulent wake is characterised by vortices shed from the spoiler's (trailing) edge and changes according to the spoiler's angle. As the deflection is increased, the outer streamlines become displaced which, in turn, modifies the potential pressure distribution.

The section pressure distribution for a two-dimensional airfoil (flaps-up case) is shown in Figure 2-2 for the upper and lower surfaces. Ahead of the spoiler, the pressure is increased, resulting in a download; aft of the spoiler, the *base pressure* is decreased, producing an upward force. Pressures around the hinge-line tend toward stagnation ($C_p = +1.0$), however, they never reach that stage because of boundary layer separation in the region. On the lower surface, the pressure is decreased, again producing a download. The loss of lift on the airfoil can therefore be attributed as much to the lower surface as the upper and tends to be associated more with the loading distribution ahead of the spoiler as the circulation diminishes. At angles-of-attack above stall, spoiler deflection has little effect on the pressure distribution, since flow separation occurs so far forward on the airfoil that the spoiler becomes immersed in the "dead-air" region of the resulting wake.

An important feature of bluff-body flows is that the base pressure is less than the free-stream pressure. This negative pressure on the rear side of the body and the positive pressure on the forward side results in a net pressure drag, that is distinct from and many times larger than the skin friction drag. The base pressure is indicative of the pressure drag's behaviour and approximately equal to the total drag of the airfoil/spoiler configuration.

For small deflections, when the discontinuity at the trailing edge of the spoiler is of the same order as the boundary layer thickness, the flow may separate at the spoiler's tip and *reattach* downstream on the surface of the airfoil. For even smaller deflections, the boundary layer may just thicken without separation. As the deflection increases, this reattachment point moves further aft until it reaches the airfoil's trailing edge, upon which complete separation takes place. The spoiler has now reached its design state: attached flow over the airfoil, separating at the spoiler's trailing edge without subsequent reattachment. Increasing the deflection further, the flow over the hinge-line is forced to turn through a progressively larger angle. An increasingly adverse (positive) pressure gradient at the hinge-line confirms that the flow is, in fact, slowing down in this region. Moreover, if the deflection is large enough, separation *ahead* of the spoiler may occur. This phenomena is known as

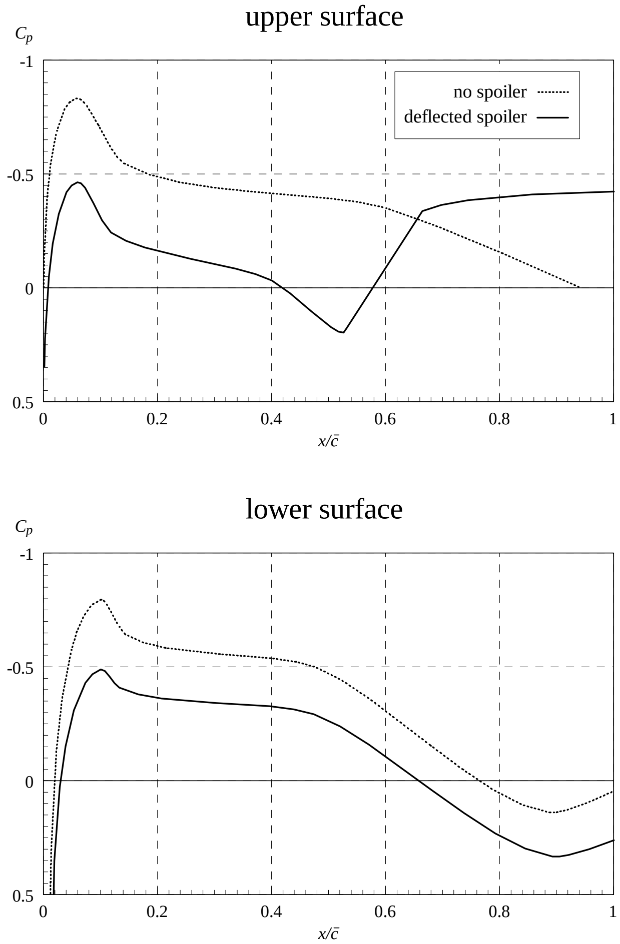

Figure 2-2: Typical pressure distribution over an airfoil with spoiler

"hinge-line separation". In addition, it is likely that the flow will reattach on the face of the spoiler, creating a turbulent bubble at the hinge. The formation of such a bubble will actually decrease the local pressure coefficient and hence, decrease the spoiler's effectiveness. Transition of the flow associated with a spoiler increasing in deflection is illustrated in Figure 2-3.

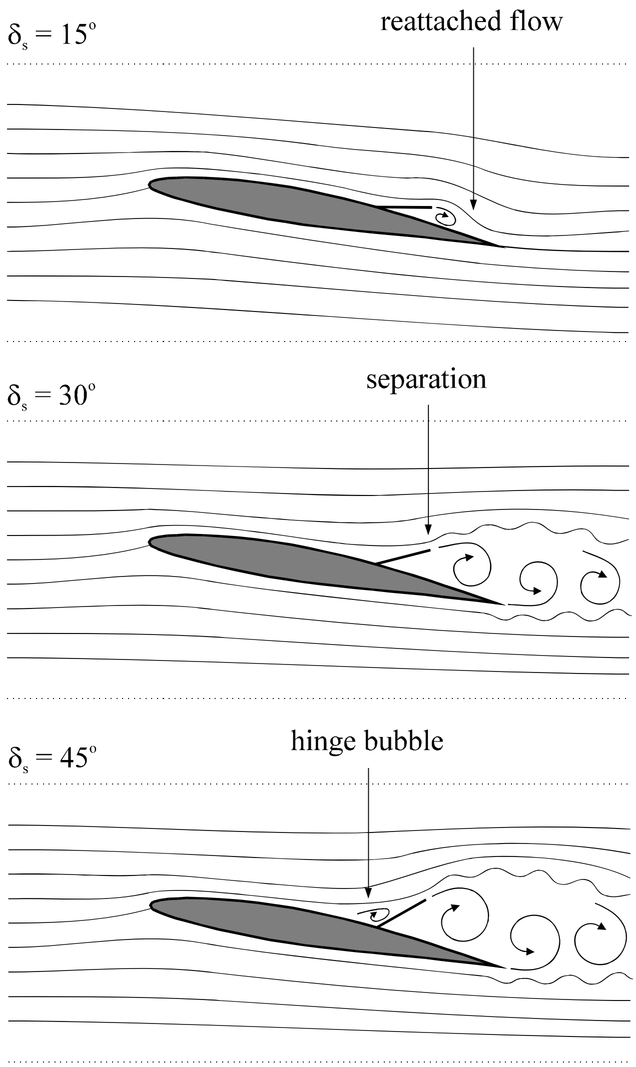

Figure 2-3: Transition of spoiler separation

The location of the hinge-bubble depends on the boundary layer characteristics. At large angles–of-attack and large spoiler deflections, a laminar hinge bubble can extend up to 25% of the chord. At high angles-of-attack, the boundary layer becomes turbulent and the hinge bubble tends to be smaller. The base pressure is also strongly affected by the spoiler's deflection. For a constant deflection, the base pressure remains relatively constant over a moderate, positive angle-of-attack range, changing rapidly outside that range.

The turbulent wake generated by the deflected spoiler is highly unsteady and complex in nature. On the other hand, the time-averaged flow field manifests a much simpler structure - a region of reversed flow forms just behind the spoiler and closes downstream of the airfoil trailing edge as depicted in Figure 2-4 (taken from Bodapati, *et al* [252]). Both the wake width and closure distance increase with spoiler deflection. Also evident from the diagram is the upper surface boundary layer development. That is, the increasing "bluffness" of the configuration as the spoiler deflects, which results in a displacement of the outer flow streamlines. It is this displacement that alters the surface pressure distribution and the resulting forces and moments.

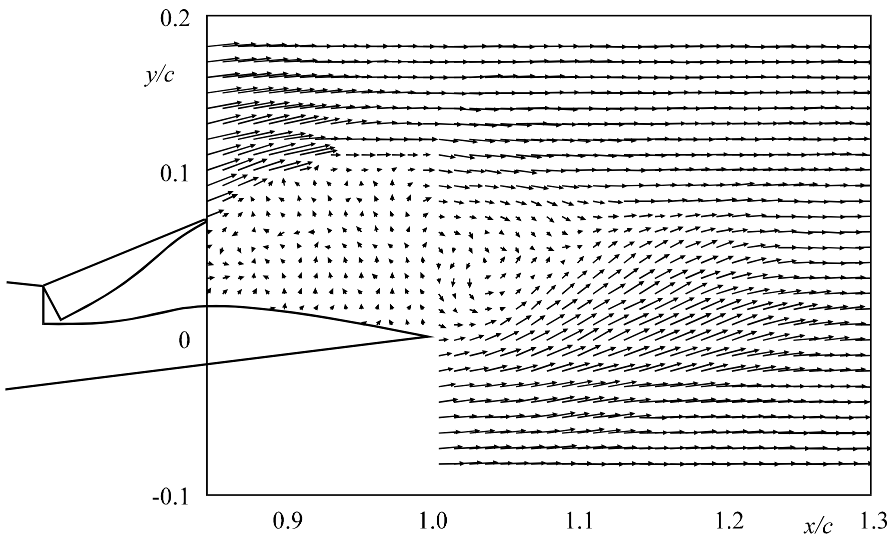

Figure 2-4: Mean velocity vector plot of the near wake

In general, it can be said that spoilers have a nonlinear control effectiveness. The lift and drag characteristics for a typical wing/spoiler combination are shown in Figure 2-5. At low angles-of-attack and spoiler deflection, the lift contribution can actually increase due to flow reattachment, although this effect is less pronounced with aft-mounted spoilers.

The corresponding drag contribution would remain relatively unchanged at zero incidence in the absence of gross separation. At moderate angles-of-attack, the lift contribution is approximately independent of α, decreasing linearly with δ_s only. The drag contribution is also approximately linear in δ_s. Unlike the lift coefficient, however, the drag coefficient generally decreases with α. As the angle-of-attack is further increased, both $\Delta C_L(\delta_s)$ and $\Delta C_D(\delta_s)$ approach zero and may even change sign. Looking at the figure, it can seen that the spoilers there have become ineffectual at 12° angle-of-attack and at 16°, have completely reversed their effect. This control reversal can be attributed to the fact that the deflected spoiler at high incidence is, in fact, keeping the flow attached to some extent and thus increasing the lift.

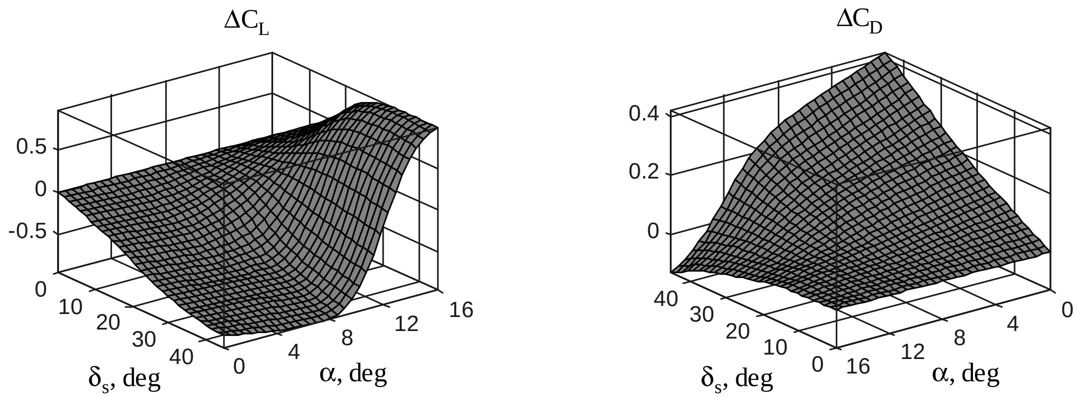

Figure 2-5: Typical lift and drag increments for a wing with spoiler

2.3.2 Unsteady Characteristics

The unsteady nature of the flow field generated by an airfoil with deflected spoiler is of interest, in view of the following:

1. The mean flow field, the determinant of the overall mean forces and moments, is itself determined by the "mixing" process of the unsteady flow field; and

2. From consideration of the previous point, it has been inferred that the nonlinear control effectiveness of spoilers is due to changes in the character of the unsteady flow field as the spoiler is deflected.

Vortex shedding characterises the turbulent wake caused by the deflected spoiler. The frequency of shedding decreases as the deflection increases and is inversely related to the width of the wake, or "bluffness" of the body. Flow visualisation of the vortex formation process has shown that vortex shedding is extremely periodic and regular at large spoiler deflections. However, as the deflection decreases, the vortex shedding becomes less regular and more intermittent. This change in the vortex shedding character with spoiler deflection manifests itself in the fluctuating wake velocity and surface pressures as a narrowband character.

The formation of vortices characterises the near wake structure of the airfoil/spoiler configuration. The vortices are formed through the interaction of two free shear layers arising from separation of the boundary layer at the spoiler tip and the airfoil trailing edge. These two shear layers are unstable and the instability creates a tendency for the shear layers to roll-up alternately into discrete vortices near the airfoil trailing edge. This formation of vortices in the spoiler wake occurs in the same manner as the formation of the vortex trail in the wake of a circular cylinder. In effect, this intense vortex interaction, particularly at small spoiler angles, can induce anomalies in the time-averaged flow field.

2.3.3 Three-Dimensional Effects

Little work on the flow characteristics about finite spoilers has been conducted in relation to either the local flow field, or the more general features of a wing/spoiler combination. McLachlan, *et al* [276] first investigated the local flow about a low aspect ratio spoiler situated on a flat floor.

For a spoiler of finite aspect ratio, the flow about the two end tips play an important role in the wake development. The flow that is swept underneath the spoiler by the vortices formed at the tips essentially pushes the separating shear flow from the spoiler upper edge, away from the airfoil. At the same time, the flow around the tips tends to reduce the reattachment length behind the spoiler as illustrated in Figure 2-6. Consequently, the curvature of the separating shear flow is increased, so the suction pressures in the separated bubble downstream of the spoiler tend to be higher for a finite spoiler than for a two-dimensional spoiler. This increased 'efficiency' of a finite spoiler means that for extremely small spoiler spans, it is possible to obtain an increase in the sectional lift, as distinct from the normal expected loss in sectional lift.

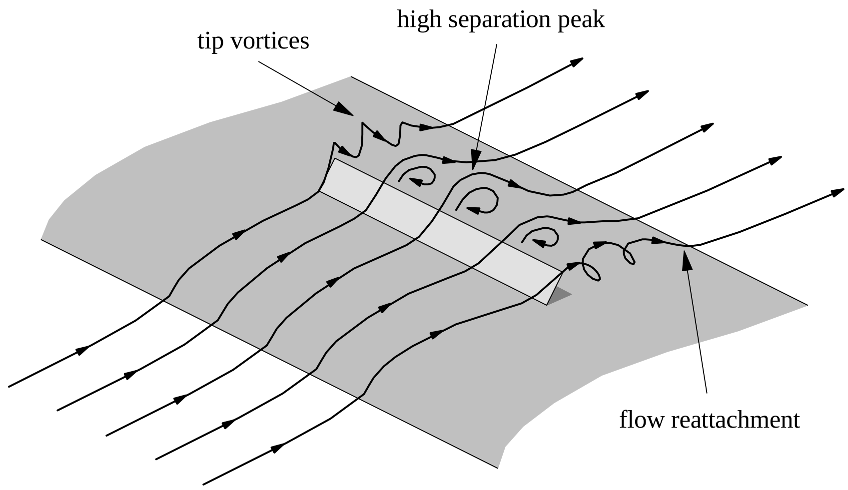

Figure 2-6: Local flow field over a deflected spoiler of finite span

The effectiveness of spoilers on sweptback wings is generally reduced at moderate incidence due to the outflow along the upper surface and may become more dependent on spoiler hinge-line sweep than on wing sweep. At high incidence, the leading-edge vortices may actually aid in the reversed effectiveness, as with the F-111C aircraft's wind-tunnel model, the coefficients of which are shown in Figures 2-7 and 2-8. It is possible to examine the lateral coefficients since the rolling and yawing moment contributions have essentially the same characteristics as the lift and drag contributions, respectively. The side force contribution, which is exactly the same as the cross-wind force on a wing, increases with sweep angle at moderate angles-of-attack since it constitutes a greater component of the total force.

2.3.4 Reynolds and Mach Number Effects

Reynolds number effects are critical in the development of the spoiler wake. The Reynolds number influences boundary layer thickness and growth and therefore also influences the spoiler effectiveness. In general, the effect is predominant at small deflections, contributing to the nonlinear behaviour and introducing uncertainty to predictions in this regime. Also,

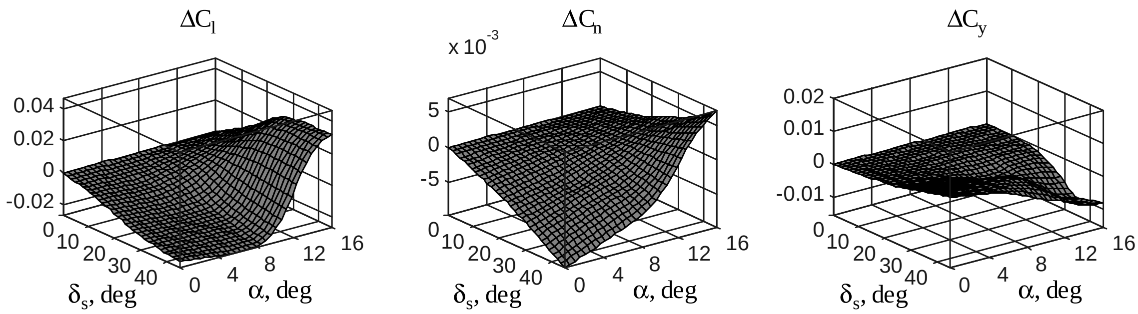

Figure 2-7: Lateral spoiler coefficients for the F-111C: $M = 0.6$; $h = 20000\,ft$; $\Lambda = 16^\circ$

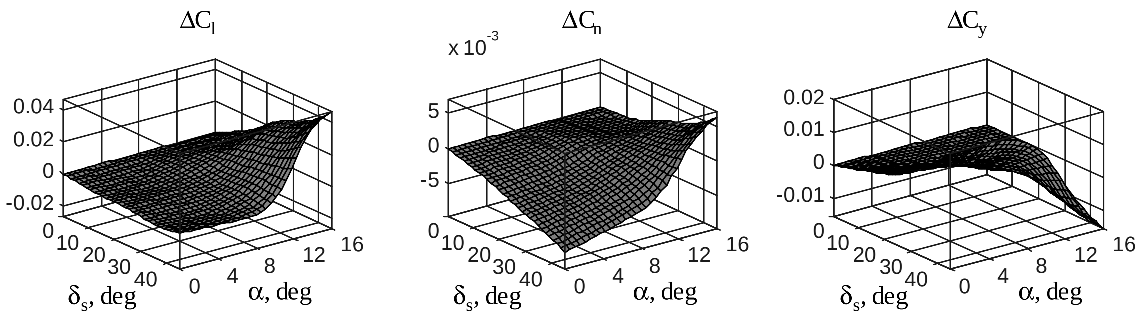

Figure 2-8: Lateral spoiler coefficients for the F-111C: $M = 0.6$; $h = 20000\,ft$; $\Lambda = 45^\circ$

as a result of the turbulent boundary layer induced at high Reynolds numbers, separation ahead of the spoiler is less likely to occur. Possibly the most important result, however, comes from the fact that Reynolds numbers in wind-tunnel tests typically only reach an order of 1×10^6, whereas actual flight Reynolds numbers may range from 20×10^6 to 40×10^6. Therefore, wind-tunnel results usually over-predict the true spoiler effectiveness. This point is highly relevant to the current research, as it introduces the issue of *scale effects* when comparing the control effectiveness as estimated from the full-scale aircraft.

Increasing the Mach number at subsonic speeds tends to increase the magnitude of the incremental loss in ΔC_L, as might be expected from simple-minded application of the Prandtl-Glauert Law. However, at transonic speeds, the loss in ΔC_L decreases and the characteristics become strongly nonlinear with respect to the airfoil incidence. That is, the spoiler loses its efficiency with increasing Mach number. Investigation of the pressure distribution has revealed the reason for this: under transonic conditions, a moderate spoiler deflection may induce a lower surface shock and possibly boundary layer separation. On the upper surface, forward of the hinge, the spoiler has only a moderate influence, although the base pressure aft of the hinge is strongly dependent. The wind-tunnel coefficients shown in the following figures, 2-9 and 2-10, generally follow these characteristics. At $M = 1.0$, for angles-of-attack greater than approximately $2°$, the spoiler effectiveness diminishes dramatically and remains relatively ineffectual above $8°$.

2.4 Moving Spoilers

Although the flowfield about a moving spoiler is somewhat different to that about a static one, the effect can often be neglected, particularly for aft-mounted spoilers with slow actuation. Work has been done with both moving (oscillating) spoilers and opening/closing ones, the results of which will now be discussed.

2.4.1 Transient Effects

One of the first characteristics of spoiler control to be noted was the significant lag between their deflection and the aircraft response [283]. During the initial part of the opening motion, the base pressure increases slightly, which is then followed by a large transient suction peak. This behaviour is associated with a "starting vortex" as it is convected downstream from the spoiler edge. In the process of convection, the pressure recovery ahead of the vortex

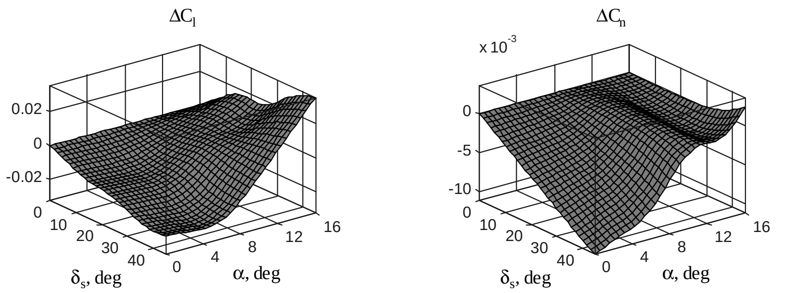

Figure 2-9: Lateral spoiler coefficients for the F-111C: $M = 0.8$; $h = 40000\,ft$; $\Lambda = 35°$

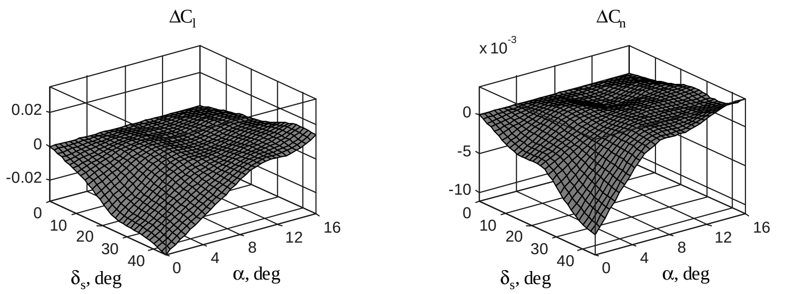

Figure 2-10: Lateral spoiler coefficients for the F-111C: $M = 1.0$; $h = 40000\,ft$; $\Lambda = 35°$

increases, while the strength of the vortex itself decreases. When the spoiler deflection is decreased, however, there are no large pressure fluctuations.

The rapid change in pressure underneath the spoiler can increase lift momentarily, resulting in a temporary reversal of effectiveness. Thus, either steady or unsteady effectiveness reversal can be encountered with spoilers. An important factor in transient aerodynamics is the reduced frequency, k, given by

$$k = \frac{\omega \bar{c}}{2V_\infty} \tag{2.1}$$

where ω is the frequency of actuation, $\bar{c}$ is the mean aerodynamic chord and V_∞ the freestream velocity. It has been found [253] that an increase in k above 0.008 or so can cause both a large reduction in spoiler effectiveness and a large increase in the phase lag.

2.5 Differentially Actuated Spoilers

There are a number of characteristics of spoilers that are specific to those used for lateral (roll) control. Perhaps the most notable is their symmetry properties, which will now be shown. Along with the preceding information on spoiler aerodynamics, the behaviour of the spoilers on the F-111C aircraft will then be examined.

2.5.1 Lateral Implications

Spoilers are often used for dumping lift or in speed-braking, in which case they are deflected simultaneously. When used differentially for roll-control, they are deflected on either one wing or the other. In this case, the sense follows that for aileron controls in roll: a positive deflection corresponds to spoiler actuation on the port wing; a negative deflection corresponds to actuation on the starboard wing. Hence, the rolling-moment-due-to-spoiler derivative, $C_{l_{\delta_s}}$ will generally be negative for moderate angles-of-attack. As previously discussed, this derivative - which is a measure of the spoiler's efficiency - decreases as the angle-of-attack is increased. The yawing-moment derivative, $C_{n_{\delta_s}}$ is also negative, or proverse, for moderate angles-of-attack. This is an important characteristic of spoilers since conventional ailerons generally produce adverse yawing moments.

Like all geometrically symmetric lateral control devices, the spoilers on an aircraft exhibit similar characteristics for positive and negative deflections. In fact, the characteristics are *anti-symmetric*, which greatly simplifies their estimation. This attribute will be explained in Chapter 5. As an example, the anti-symmetric nature of the rolling and yawing moment coefficients is illustrated in Figure 2-11.

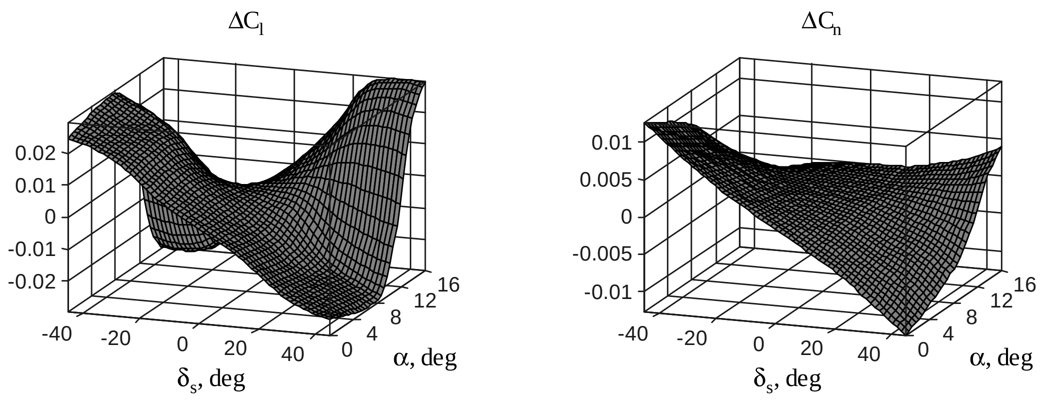

Figure 2-11: Typical anti-symmetric lateral spoiler characteristics of the F-111C

As with most roll-control devices, spoilers produce a very small side force, which may even prove negligible in some cases. Figures 2-7 and 2-8 in Section 2.3.3 show the side force coefficients for two different wing-sweep angles. It can be seen from these that the side force is more closely associated with the yawing moment than the rolling moment, which is to be expected from this type of control device. The characteristics of the spoiler side force coefficients are also anti-symmetric in spoiler deflection.

2.5.2 Spoilers on the F-111C Aircraft

The F-111C aircraft is a two-seat tactical strike and reconnaissance bomber with a variable wing-sweep angle and a wingspan of 19.2 m when fully extended. It is powered by two Pratt & Whitney TF-30-P-3 turbofans and has a maximum speed of Mach 2.5 at 40000 ft. Roll-control is achieved primarily through differentially actuated stabilators and wing-spoilers; there are no ailerons as such.

The spoilers on the wings of the F-111C are located as shown in Figure 2-12. Their positioning is similar to those examined in many past experiments, reported in references such as [273], [280] and [276].

The information discussed above will now be examined, in the context of the F-111C aircraft's spoiler characteristics. The characteristics for a scaled wind-tunnel model of the

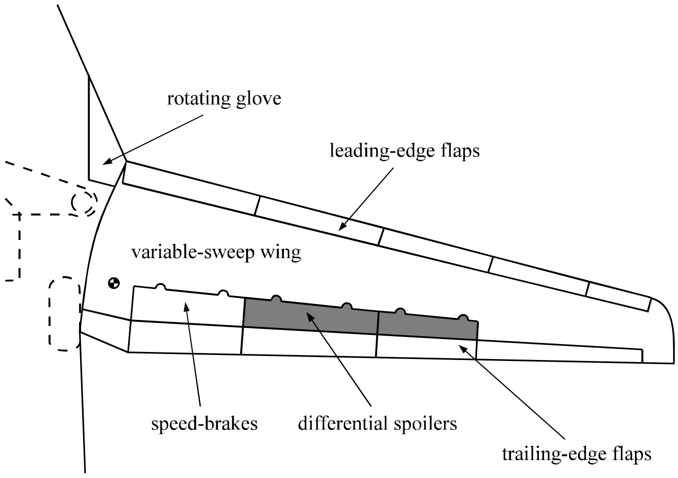

Figure 2-12: Planform showing spoiler location on the F-111C aircraft

aircraft, presented in several of the previous sections, provide a good starting point upon which the real aircraft's nature can be based.

Under nominal conditions, one would expect the general behaviour of the full-scale aircraft to follow that of the model. That is, for moderate angles-of-attack and subsonic Mach number, the aircraft's spoilers should exhibit nonlinear characteristics described by typical separated flow patterns. For very small control deflections, the flow may indeed reattach aft of the spoiler, resulting in low rolling and yawing moments. A lack of effectiveness is expected in this regime, although the spoilers are aft-mounted, so this characteristic should be small and may even be insignificant. For larger control deflections, separation ahead of the spoiler may also occur, with reattachment on the spoiler face creating a hinge-bubble. However, at typical full-scale Reynolds numbers, hinge-line separation is less likely to come about. Hence, this phenomena will also be small, if not negligible in actual flight. Certainly, another impingement on the formation of a bubble in this region would come from the flow changes induced by the hinge-line gap on the F-111C's spoilers. No substantial work has been conducted in the analysis of spoilers with hinge-line gaps and therefore, one can only make speculative assumptions concerning their effect. At high angles-of-attack, control reversal is quite possible, since the aerodynamics associated with this behaviour are fundamental in nature.

It is important at this point to re-emphasize the fact that the true spoiler effectiveness tends to be *overestimated* by scaled-model tests, due to differences in Reynolds numbers. Therefore, it is expected that a smaller spoiler contribution will be estimated from the flight-data.

The true spoiler characteristics should be affected by wing-sweep angle as discussed in Section 2.3.3 and may also exhibit a loss in efficiency in the high-subsonic/transonic regime, becoming highly nonlinear. The last aspect presented was the response lag inherent with spoiler controls. There are, however, two factors which minimise this effect on the F-111C: the first is the aft placement of the spoilers on the wing-chord, which tends to reduce the influence of the starting vortex as it is convected downstream; the second is the relatively slow actuation rate of the spoilers ($\omega = 160 \deg/s$, yielding a reduced frequency range of $0.004 < k < 0.01$ for the flight tests examined) which is generally lower than the rate at which lag effects start to become marked.

2.6 Concluding Remarks

In general, spoiler devices exhibit some intriguing characteristics since, by their very nature, they induce separated flow. This chapter has outlined the behaviour of spoilers, based largely on experimental results obtained from wind-tunnel testing. Very little research in this area has been conducted in other fields, such as computational fluid dynamics and flight testing, which is one of the primary reasons for the current study.

Essentially, the spoiler's wake and hence the pressure distribution over the aerofoil is characterised by vortex shedding. The flowfield can change dramatically with increasing spoiler deflection and is often highly dependent on the angle-of-attack as well. Such features as trailing-edge reattachment at low deflections and hinge-line separation generally lead to a nonlinear effectiveness. Moreover, the rolling and yawing contributions can actually change sign in high angle-of-attack regimes. Other important factors that affect the behaviour of spoiler devices include the Mach and Reynolds numbers. It has been found that the spoiler's effectiveness will typically become more positive (adverse) as the flow approaches sonic conditions. In addition, wind-tunnel tests conducted at Reynolds numbers lower than flight have been found to overestimate the effectiveness significantly. This last result is particularly relevant to the current study, in which the flight-identified coefficients of the F-111C aircraft are compared against wind-tunnel data.

Chapter 3

Dynamic Aircraft Model

3.1 Introduction

In this chapter, the known physical response of an aircraft to control input will be examined, as well as various errors that can arise in formulating a representative model.

Firstly, the general equations of motion will be presented, in terms of the linear and angular accelerations in each axis. The model coefficients, or stability and control derivatives, are then introduced and the question of model adequacy addressed. This constitutes a problem common to many forms of modelling and identification.

In the next section, the aerodynamic model of the F-111C aircraft is constructed. Each of the coefficients is detailed, in terms of its significance and behaviour with respect to flight variables such as the angle-of-attack. Following this general description of the aircraft model, the nonlinear coefficients are formulated using spline functions. Various properties of splines are outlined, as well as simplifications that can be made concerning their structure.

The last section covers errors, and their effect on the identified model. Three categories of errors are examined, including modelling error, systematic error and random error.

3.2 Model Formulation

This section will begin by examining the aircraft model in detail. Both linear and nonlinear terms are included, since the coefficients are basically functions of the aircraft states and control deflections. This is particularly important in the model of the F-111C aircraft, which has inherently high-order characteristics at elevated angles-of-attack.

3.2.1 Equations of Motion

In order to estimate the aerodynamic parameters from flight data, a mathematical model of the aircraft must first be postulated. The rigid-body equations of motion are presented in Appendix A. These are referred to a set of (body) axes fixed in the aircraft and positioned at its centre of gravity. In concise form, the equations are written in as:

$$\begin{aligned} \dot{x} &= f(x, u, \theta) \quad ; \quad x(0) = x_0 \\ y &= h(x, \theta) \end{aligned} \tag{3.1}$$

where x represents the states, u the input or control variables and y represents the outputs or the measurements, if there is no noise present. The dynamics of the system are governed by the functions, $f(x, u, \theta)$ and $h(x, \theta)$ which are in general, nonlinear functions of the states, controls and system parameters, θ. From Equations (A.4) and (A.5), the linear accelerations can be written:

$$\begin{aligned} a_x = \dot{u} - vr + wq + g\sin\theta &= \frac{QS}{m}C_x \\ a_y = \dot{v} + ur - wp - g\sin\phi\cos\theta &= \frac{QS}{m}C_y \\ a_z = \dot{w} - uq + vp - g\cos\phi\cos\theta &= \frac{QS}{m}C_z \end{aligned} \tag{3.2}$$

and the angular accelerations:

$$\begin{aligned} \dot{p} - \frac{I_{xz}}{I_x}(\dot{r} + pq) + \frac{I_z - I_y}{I_x}qr &= \frac{QSb}{I_x}C_l \\ \dot{q} + \frac{I_x - I_z}{I_y}pr + \frac{I_{xz}}{I_y}(p^2 - r^2) &= \frac{QS\bar{c}}{I_y}C_m \\ \dot{r} - \frac{I_{xz}}{I_z}(\dot{p} - qr) + \frac{I_y - I_x}{I_z}pq &= \frac{QSb}{I_z}C_n \end{aligned} \tag{3.3}$$

Now u, v and w denote the velocity components in body axes, p, q and r, the angular rates and ϕ and θ denote the bank and pitch angles with respect to the inertial axes. The forces and moments have been expressed in terms of their non-dimensional coefficients, C_x, C_y, C_z and C_l, C_m, C_n. Hence, the effects of dynamic pressure, $Q = \frac{1}{2}\rho V_1^2$, aircraft size, geometry, mass and inertia are removed from the aerodynamic model. Principal aerodynamic dimensions include the wing area, S, mean aerodynamic chord, $\bar{c}$ and the wingspan, b. The aircraft's mass is denoted m and the inertias about each body axis, I_x, I_y, and I_z.

It is assumed that the aerodynamic coefficients can be expressed as functions of the instantaneous state and control variables and their derivatives. The model equations are well developed and each can be formulated by taking a Taylor series expansion of the coefficients about some trim condition. They will have the general form:

$$C_{\mathrm{a}} = \sum_j \frac{\partial C_{\mathrm{a}}}{\partial z_j} z_j + \sum_i \sum_j \frac{\partial C_{\mathrm{a}}}{\partial z_i \partial z_j} z_i z_j + \ldots + \mathrm{O}(z^n) \tag{3.4}$$

where the z_j are non-dimensional perturbation quantities associated with the variables x_j and u_j. The *stability* and *control derivatives* are given as $\partial C_{\mathrm{a}} / \partial x \equiv C_{\mathrm{a}_x}$ and $\partial C_{\mathrm{a}} / \partial u \equiv C_{\mathrm{a}_u}$ respectively, for a $= x, y, z, l, m, n$. This equation represents an n^{th}-order expansion, which encompasses all high-order and coupling terms. However, a number of simplifying assumptions can be made concerning the implementation of Equation (3.4) in order to obtain a reduced model. In fact, a linear approximation of the aircraft model is completely sufficient in many practical situations. These assumptions will now be examined in detail.

The first is to consider all derivatives of second- and higher-order negligible, since the small perturbation model often provides an adequate representation. This assumption is made in the Appendix A and is appropriate for linear time-response simulation purposes. For many other purposes, such as nonlinear simulations or identification, it is necessary to retain some of these higher-order terms. The analyst is thus presented with the question of model adequacy, that is: How many terms are required to construct a model such that it will provide an *adequate* representation of the true system ? In the context of response simulation, the bounds of model size are more directly obvious. A model comprising too few terms may be unable to follow the true response sufficiently, whereas a model comprising too many terms will not only increase the computational effort required by the simulation unnecessarily, but may also prove sensitive to changes in the conditions if they were not accounted for. The problems associated with model adequacy in identification will be discussed in detail in the following section. In this application, it is not clear what the best relationship should be between model complexity and measured information. Briefly, a postulated model must first include those derivatives that are to be estimated, or some means by which they may subsequently enter the model. One must be cautious, however, since an *overmodelled* system, comprising an excessive number of terms, may induce "identifiability" problems. This means that it may be impossible to estimate the parameters with acceptable accuracy, or in more severe cases, to estimate the parameters at all. In this respect, only those higher-order terms of particular relevance to the analyses should be included - one should avoid postulating too many terms for the sake of generality.

The second assumption involves judgement on the contribution of each derivative to the system response. Many of the terms that are referred to axes which are orthogonal to the axes associated with their corresponding state or control variable can be considered negligible. Examples of this are the sideforce due to an angle-of-attack derivative, C_{y_α} and pitching moment due to a yaw-rate change, C_{m_r}. Even more than the previous assumption, this simplification requires the analyst to impose constraints based on prior knowledge of the system. However, in most flight dynamics applications, these assumptions are well established and if necessary, examination of the aircraft's characteristics should reveal any differences that need to be taken into account.

3.2.2 The F-111C Aircraft Model

When a model structure is to be determined from flight-data, the aerodynamic model must first be postulated. In the identification of the F-111C aircraft's aerodynamic characteristics, the form of the postulated model was developed under the following assumptions:

1. The instantaneous aerodynamic forces and moments are dependent on the instantaneous values of the response and input variables along with several of their derivatives.

2. There are no propulsion effects on any of the aerodynamic coefficients. The thrust is assumed constant during the manoeuvres under analysis.

3. The net longitudinal and lateral coefficients can be expressed as:

$$C_{\mathrm{a}} = C_{\mathrm{a}}(\dot{\alpha}, V, \alpha, q, \delta_h) \quad ; \quad \mathrm{a} = x,\, z,\, m$$

   and

$$C_{\mathrm{a}} = C_{\mathrm{a}}(\dot{\beta}, \beta, p, r, \delta_a, \delta_r, \delta_s, \alpha) \quad ; \quad \mathrm{a} = y,\, l,\, n$$

4. The corresponding aerodynamic coefficients are obtained as sums of contributions due to $\dot{\alpha}$, V, α, q, δ_h and $\dot{\beta}$, β, p, r, δ_a, δ_r, δ_s, respectively. Each of the aerodynamic derivatives associated with these variables are, in general, dependent on the angle-of-attack, Mach number, altitude and wing-sweep angle. The spoiler contribution is also a function of its deflection, δ_s.

Under the preceding assumptions, the aerodynamic model equations can be written:

$$
\begin{aligned}
C_x &= C_{x_0} + C_{x_{\dot\alpha}} \frac{\dot\alpha \bar c}{2V_1} + C_{x_V} \frac{V}{V_1} + C_{x_\alpha}\,\alpha + C_{x_q} \frac{q\bar c}{2V_1} + C_{x_{\delta h}}\,\delta_h \\
C_y &= C_{y_0} + C_{y_{\dot\beta}} \frac{\dot\beta b}{2V_1} + C_{y_\beta}\,\beta + C_{y_p} \frac{pb}{2V_1} + C_{y_r} \frac{rb}{2V_1} + C_{y_{\delta a}}\,\delta_a + C_{y_{\delta r}}\,\delta_r + \Delta C_{y_{\delta s}} \\
C_z &= C_{z_0} + C_{z_{\dot\alpha}} \frac{\dot\alpha \bar c}{2V_1} + C_{z_V} \frac{V}{V_1} + C_{z_\alpha}\,\alpha + C_{z_q} \frac{q\bar c}{2V_1} + C_{z_{\delta h}}\,\delta_h \\
C_l &= C_{l_0} + C_{l_{\dot\beta}} \frac{\dot\beta b}{2V_1} + C_{l_\beta}\,\beta + C_{l_p} \frac{pb}{2V_1} + C_{l_r} \frac{rb}{2V_1} + C_{l_{\delta a}}\,\delta_a + C_{l_{\delta r}}\,\delta_r + \Delta C_{l_{\delta s}} \\
C_m &= C_{m_0} + C_{m_{\dot\alpha}} \frac{\dot\alpha \bar c}{2V_1} + C_{m_V} \frac{V}{V_1} + C_{m_\alpha}\,\alpha + C_{m_q} \frac{q\bar c}{2V_1} + C_{m_{\delta h}}\,\delta_h \\
C_n &= C_{n_0} + C_{n_{\dot\beta}} \frac{\dot\beta b}{2V_1} + C_{n_\beta}\,\beta + C_{n_p} \frac{pb}{2V_1} + C_{n_r} \frac{rb}{2V_1} + C_{n_{\delta a}}\,\delta_a + C_{n_{\delta r}}\,\delta_r + \Delta C_{n_{\delta s}}
\end{aligned}
\tag{3.5}
$$

These expressions are similar to those utilised in wind-tunnel testing. In each equation, the first term represents the ‘static’ part, with controls fixed at zero deflection. The remaining terms represent contributions of the dynamic stability and control derivatives.

Up to this stage, the effect of unsteady aerodynamics has been maintained, that is, the $\dot\alpha$ and $\dot\beta$ terms have been kept in the model equations. However, this can cause identifiability problems, since these dynamic terms have a near-linear relationship with the other variables. One way to avoid the problem is to implicitly include the effects of $\dot\alpha$ and $\dot\beta$ in the equations by augmenting the remaining terms. By assuming the trim rate, $q_1 = 0$ and that all perturbations are small (*see* Appendix A.5), substituting equations (3.2) into (3.5), yields the longitudinal derivatives:

$$
\begin{aligned}
C'_{z_\mathrm{x}} &= K_{z_{\dot\alpha}} C_{z_\mathrm{x}} \qquad ; \quad \mathrm{x} = V,\, \alpha,\, \delta_h \\
C'_{z_q} &= K_{z_{\dot\alpha}} (C_{z_q} + \tfrac{1}{B}) - \tfrac{1}{B}
\end{aligned}
\tag{3.6}
$$

and

$$
\begin{aligned}
C'_{m_\mathrm{x}} &= C_{m_\mathrm{x}} + B C_{m_{\dot\alpha}} K_{z_{\dot\alpha}} C_{z_\mathrm{x}} \\
C'_{m_q} &= C_{m_q} + B C_{m_{\dot\alpha}} K_{z_{\dot\alpha}} (C_{z_q} + \tfrac{1}{B})
\end{aligned}
\tag{3.7}
$$

where the constant, $B = \frac{QS\bar c}{2mV_1^2}$ and $K_{z_{\dot\alpha}} = \frac{1}{1 - BC_{z_{\dot\alpha}}} \to 1$ if $C_{z_{\dot\alpha}}$ is small. Similarly, assuming $p_1 = r_1 = 0$ for the side-force derivatives:

$$
\begin{aligned}
C'_{y_\mathrm{x}} &= K_{y_{\dot\beta}} C_{y_\mathrm{x}} \qquad ; \quad \mathrm{x} = \beta,\, \delta_a,\, \delta_r \\
C'_{y_p} &= K_{y_{\dot\beta}} (C_{y_p} + \tfrac{\alpha_1}{B}) - \tfrac{\alpha_1}{B} \\
C'_{y_r} &= K_{y_{\dot\beta}} (C_{y_r} - \tfrac{1}{B}) + \tfrac{1}{B}
\end{aligned}
\tag{3.8}
$$

and the rolling and yawing moment derivatives:

$$
\begin{aligned}
C'_{\mathrm{a_x}} &= C_{\mathrm{a_x}} + BC_{\mathrm{a}_{\dot\beta}} K_{y_{\dot\beta}} C_{y_{\mathrm{x}}} \qquad ; \quad \mathrm{a} = l,\, n \\
C'_{\mathrm{a}_p} &= C_{\mathrm{a}_p} + BC_{\mathrm{a}_{\dot\beta}} K_{y_{\dot\beta}} (C_{y_p} + \tfrac{\alpha_1}{B}) \\
C'_{\mathrm{a}_r} &= C_{\mathrm{a}_r} + BC_{\mathrm{a}_{\dot\beta}} K_{y_{\dot\beta}} (C_{y_r} - \tfrac{1}{B})
\end{aligned} \tag{3.9}
$$

where $B = \frac{QSb}{2mV_1^2}$ now and $K_{y_{\dot\beta}} = \frac{1}{1-BC_{y_{\dot\beta}}}$. The effects of $\dot\alpha$ and $\dot\beta$ are primarily seen through the angular rate derivatives, C_{z_q}, C_{m_q} and C_{y_p}, C_{y_r}, C_{l_p}, C_{l_r}, C_{n_p} and C_{n_r}. An alternative to removing the unsteady terms from the model equations is to instead bias them in the identification procedure. Several biased estimation techniques are presented in Section 4.3, which can be used to prevent singularities from occurring, although some do require prior estimates of the derivatives for solution.

As mentioned above, most of the stability and control derivatives, or coefficients, are functions of the angle-of-attack, Mach number, altitude and wing-sweep angle. Now in manoeuvres designed for parameter estimation, the aircraft wing-sweep is kept constant and both Mach number and altitude vary relatively little. Therefore, for single manoeuvres, it is possible to reduce the number of variables that each coefficient is dependent upon. Each derivative can be approximated by functions of α only, except for the spoiler contribution, $\Delta C_{\mathrm{a}_{\delta s}}$, which becomes a function of δ_s and α. Furthermore, if the angle-of-attack remained relatively constant over the flight-data, its influence on the coefficients could also be removed, by approximating them as constants. Ideally, it would be desirable to leave all dependencies in the model, such that each coefficient was expressed by a multivariable function in M, h, α plus any other relevant variables. However, the addition of extra terms into the model would induce identification problems, as more parameters were estimated from the finite data set. There is also an increasing possibility that some of these new terms will have a near-linear relationship with those already in the model. For example, if the altitude remained relatively constant on a particular flight test, the Mach number variation would closely follow the airspeed and should therefore be kept out of the model.

The model equations, (3.5), represent a fairly general formulation of the aerodynamic coefficients. In each case, however, the postulated aerodynamic model should reflect any available *a-priori*, or previously obtained information, based on theoretical, wind-tunnel or additional flight results.

Each coefficient in the model equations not approximated by a constant can be represented by any multivariable function. Two commonly employed forms are polynomials and splines, both of which can be written in a manner that conforms to the Taylor series expansion of the coefficients. Using one of these functions for the coefficients, the model equations can be formulated as:

$$C_{\mathrm{a}} = \theta_0 + \theta_1 X_1 + \ldots + \theta_p X_p \tag{3.10}$$

where $X_1, \ldots, X_p$ are the response variables, input variables and their combinations. The coefficients, or parameters in the model are represented by $\theta_0, \theta_1, \ldots, \theta_p$. Posing the aerodynamic model equations in this way facilitates estimation of the parameters through an *equation error* technique. The Least Squares solution constitutes one form of this technique and is presented in Chapter 4.

3.2.3 Representation of Nonlinear Parameters

The aerodynamic coefficients can often be adequately represented by constants, since for small perturbations their behaviour is approximately linear. However, under conditions when the flow about the aircraft becomes complex such as in large amplitude manoeuvres or at high angles-of-attack, the behaviour of these coefficients may change substantially. A more suitable representation of the coefficients would have the form of some nonlinear function, a polynomial or spline for example. Both of these forms can be utilised to model the aerodynamic transitions that occur through these regimes [63, 64, 67, 68].

Now the characteristics in one region of, say, angle-of-attack, may be quite different from and unrelated to the characteristics in any other region. In such a case, a polynomial approximation to the aerodynamic nonlinearities might prove inadequate, because polynomials are by definition, determined everywhere from their values in any one interval - no matter how small. They can therefore, adequately follow the aerodynamic behaviour in one region, but depart from that behaviour or even oscillate erratically elsewhere. Obviously, the addition of extra terms to a polynomial model could improve the approximation over a greater region, but would also reduce the accuracy of each coefficient estimated from the finite data set. Spline functions have been shown [125, 9] to provide a better approximation while avoiding some disadvantages of polynomials. Because they are defined on pre-selected intervals, low-order terms can be used effectively to model any aerodynamic behaviour.

Spline functions are essentially a concatenation of 'piecewise' polynomials. When continuity restrictions are considered, the function values and derivatives agree at the points where the polynomials join. These points are called *knots* and are defined by their projection onto the plane or axis of independent variables. From Schumaker [207], a polynomial spline of degree m with continuous derivatives up to degree $(m-1)$ approximating some function, $f(x)$ for $x \in [x_0, x_{\max}]$, can be expressed as:

$$s_m(x) = \sum_{h=0}^{m} D_h\, |x|_+^h + \sum_{i=1}^{k} D_{i+m}(|x| - x_i)_+^m \tag{3.11}$$

where

$$(|x| - x_i)_+^m = \begin{cases} (|x| - x_i)^m & ; \quad x \geq x_i \\ 0 & ; \quad x < x_i \end{cases}$$

The knots are denoted $x_1, x_2, \ldots, x_k$ and obey the condition: $x_0 < x_1 < \ldots < x_k < x_{\max}$. The constants, D_i represent the spline coefficients. Figure 3-1 illustrates a one-dimensional spline and its polynomial constituents.

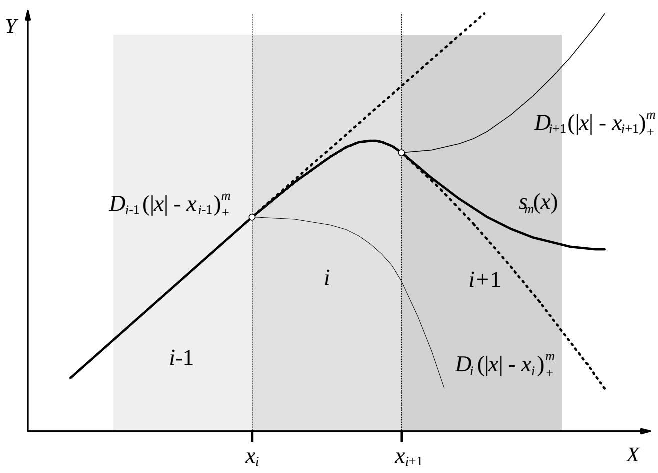

Figure 3-1: Polynomial spline function in one variable

It is practicable to construct a space of multidimensional splines by taking the tensor-product of one-dimensional spaces of polynomial splines. Many of the simple algebraic properties of ordinary polynomial splines in one dimension can be carried over, because of the tensor nature of the resulting space. For example, a tensor-product polynomial spline in two dimensions, of degree m in x and n in z, implementing continuous partial derivatives up to degree $(m-1)$ and $(n-1)$, respectively can be written:

$$\begin{aligned} s_{m,n}(x,z) = \quad & \sum_{h=0}^{m}\sum_{s=0}^{n} D_{h,s}\,|x|_+^s\,|z|_+^h & + \sum_{h=0}^{m}\sum_{j=1}^{l} D_{h,j+n}(|x|-x_j)_+^n\,|z|_+^h \; + \; \ldots \\ & \sum_{i=1}^{k}\sum_{s=0}^{n} D_{i+m,s}\,|x|_+^s\,(|z|-z_i)_+^m & + \sum_{i=1}^{k}\sum_{j=1}^{l} D_{i+m,j+n}(|x|-x_j)_+^n(|z|-z_i)_+^m \end{aligned} \tag{3.12}$$

to approximate the function, $f(x,z)$ for $x \in [x_0, x_{\max}]$ and $z \in [z_0, z_{\max}]$. In the x-axis, the variables,

$$\begin{aligned} |x|_+^m &= \begin{cases} |x|^m & ; \quad x \geq 0 \\ \textit{undefined} & ; \quad x < 0 \end{cases} \\ (|x|-x_i)_+^m &= \begin{cases} (|x|-x_i)^m & ; \quad x \geq x_i \\ 0 & ; \quad x < x_i \end{cases} \end{aligned}$$

and in the z-axis, the same rules apply. In this case, the knots in each axis obey the conditions: $x_0 < x_1 < \ldots < x_k < x_{\max}$ and $z_0 < z_1 < \ldots < z_l < z_{\max}$. One can envisage the bounds created by each knot subdividing the two-dimensional space into rectangular regions, as shown in Figure 3-2.

Since many of the aircraft parameters, particularly the lateral coefficients, exhibit symmetry of some type, it would be advantageous to make use of this property in their formulation. Only the positive space must be explicitly defined, along with the symmetry conditions, in order to evaluate the function anywhere. The lower bounds, x_0, z_0, *etc.* must also be set to zero, so that the spline is fully defined in each axis. There are three fundamental types of symmetry, defined by symmetric, non-symmetric and anti-symmetric extrapolations. These are illustrated in Figure 3-3.

By prescribing sign changes in the variables, according to the symmetry of the spline about each axis, the same set of parameters can be used to determine several (opposite) regions. For each symmetry type, these sign changes can be written as follows:

$$\begin{aligned} |x|_+^m &= \varsigma_0\,|x|^m \\ (|x|-x_i)_+^m &= \varsigma_1(|x|-x_i)_+^m \end{aligned}$$

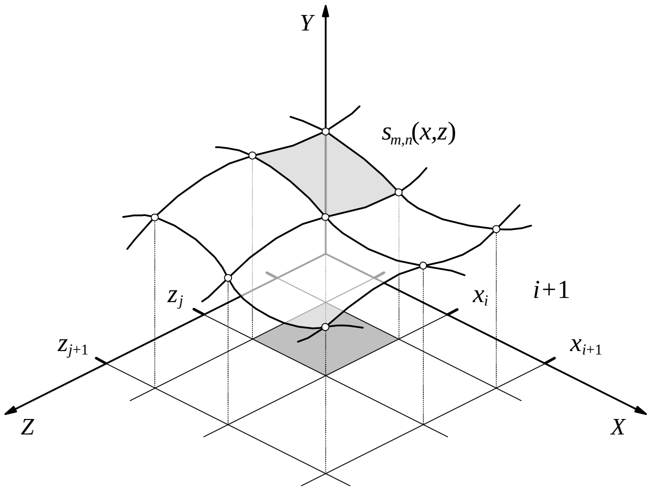

Figure 3-2: Tensor-product polynomial spline in two variables

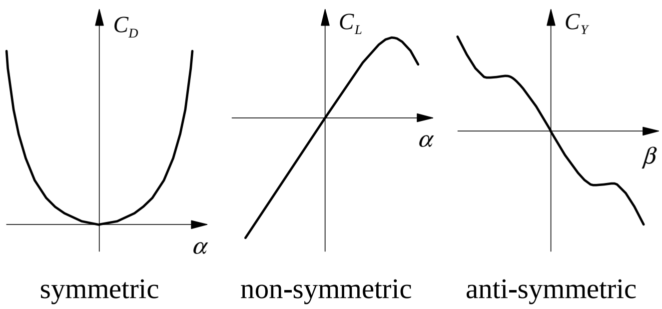

Figure 3-3: Various symmetry types of coefficients

where the flags, ς_0 and ς_1 are given by the following table,

Symmetry	ς_0		ς_1		
	$x \geq 0$	$x < 0$	$x \geq x_i$	$\lvert x \rvert < x_i$	$x < -x_i$
anti-symm.	1	-1	1	0	-1
non-symm.	1	-1	1	0	0
symmetric	1	1	1	0	1

Table 3.1: Extrapolated spline symmetry rules

By the same token, measured data lying in more than one region can be utilised for the estimation of a common set of parameters. The model is effectively reduced, leading to better estimates and, in general, making the identification more robust.

As examples of polynomial splines in the approximation of nonlinear aerodynamic functions, consider the rolling moment coefficient from Equations (3.5):

$$\begin{aligned} C_l(\alpha,\beta,p,r,\delta_a,\delta_r,\delta_s) = \quad & C_{l_0} + C_{l_\beta}(\alpha)\,\beta + C_{l_p}(\alpha)\,\frac{pb}{2V_1} + C_{l_r}(\alpha)\,\frac{rb}{2V_1} + \;\ldots \\ & C_{l_{\delta a}}(\alpha)\,\delta_a + C_{l_{\delta r}}(\alpha)\,\delta_r + \Delta C_{l_{\delta s}}(\delta_s,\alpha) \end{aligned} \tag{3.13}$$

where each nonlinear coefficient might be expressed as:

$$\begin{aligned} C_{l_\beta}(\alpha) &= D_{\beta_0} + D_{\beta_1}\,|\alpha|_+ + D_{\beta_2}\,|\alpha|_+^2 + \sum_{i=1}^{k} D_{\beta_{i+2}}(|\alpha|-\alpha_i)_+^2 \\ C_{l_p}(\alpha) &= D_{p_0} + D_{p_1}\,|\alpha|_+ + D_{p_2}\,|\alpha|_+^2 + \sum_{i=1}^{k} D_{p_{i+2}}(|\alpha|-\alpha_i)_+^2 \\ C_{l_r}(\alpha) &= D_{r_0} + \sum_{i=1}^{k} D_{r_i}\,(|\alpha|-\alpha_i)_+^0 \\ C_{l_{\delta a}}(\alpha) &= D_{\delta a_0} + D_{\delta a_1}\,|\alpha|_+ + D_{\delta a_2}\,|\alpha|_+^2 + \sum_{i=1}^{k} D_{\delta a_{i+2}}(|\alpha|-\alpha_i)_+^2 \\ C_{l_{\delta r}}(\alpha) &= D_{\delta r_0} + \sum_{i=1}^{k} D_{\delta r_i}\,(|\alpha|-\alpha_i)_+^0 \end{aligned} \tag{3.14}$$

and the spoiler contribution,

$$
\begin{aligned}
\Delta C_{l_{\delta s}}(\delta_s,\alpha) = \quad & D_{\delta s 0,0} \;+\; D_{\delta s 0,1}\,|\delta_s|_+ \;+\; \sum_{j=1}^{l} D_{\delta s 0,j+1}(|\delta_s|-\delta_{sj})_+ \;+\; \ldots \\
& D_{\delta s 1,0}\,|\alpha|_+ \;+\; D_{\delta s 1,1}\,|\delta_s|_+\,|\alpha|_+ \;+\; \sum_{j=1}^{l} D_{\delta s 1,j+1}(|\delta_s|-\delta_{sj})_+\,|\alpha|_+ \;+\; \ldots \\
& \sum_{i=1}^{k} D_{\delta s_{i+1,0}}(|\alpha|-\alpha_i)_+ \;+\; \sum_{i=1}^{k} D_{\delta s_{i+1,1}}\,|\delta_s|_+\,(|\alpha|-\alpha_i)_+ \;+\; \ldots \\
& \sum_{i=1}^{k}\sum_{j=1}^{l} D_{\delta s_{i+1,j+1}}(|\delta_s|-\delta_{sj})_+(|\alpha|-\alpha_i)_+
\end{aligned}
\tag{3.15}
$$

Equations (3.14) indicate that the derivatives, C_{l_β}, C_{l_p} and $C_{l_{\delta a}}$ have been approximated by piecewise quadratic polynomials in second-order splines, while C_{l_r} and $C_{l_{\delta r}}$ have been approximated by piecewise constants in zeroth-order splines. The spoiler contribution in Equation (3.15) has been formulated as a tensor-product polynomial spline of first-order in both δ_s and α. From the previous section, the general form of the aerodynamic model equations is given by Equation (3.10), with X_1 to X_p representing variables in the spline approximation of C_l.

Several simplifications to the aerodynamic model can now be made by considering some of the physical attributes inherent in the system. The first is to assume near-linearity about trim. In terms of the coefficients, this requires that they remain constant for small deviations about the trim state. If this linear region is defined by the knots, $\alpha \in [\alpha_0, \alpha_1]$, the coefficients, D_{β_1}, D_{β_2}, D_{p_1}, D_{p_2}, $D_{\delta a_1}$ and $D_{\delta a_2}$ can be removed. Additionally, had $\Delta C_{l_{\delta s}}$ been of higher-order, the corresponding terms could also be eliminated from the model. The second simplification concerns the spoiler contribution and comes about from the fact that $\Delta C_{l_{\delta s}}$ will be zero for zero deflection, regardless of the angle-of-attack. In Equation (3.15), this results in the removal of the spline parameters $D_{\delta s_{i,0}}$, for all i. These two simplifications can be made in any postulated model of the aircraft and do not depend on the flight data under analysis. If, however, the angle-of-attack perturbation was *small*, the α-dependance could be effectively removed from the model coefficients altogether. Subsequently, all of the coefficients above would become constant, except for the spoiler contribution which would reduce to a one-dimensional spline in δ_s only:

$$
\Delta C_{l_{\delta s}}(\delta_s) = D_{\delta s_0} + D_{\delta s_1}\,|\delta_s|_+ + \sum_{j=1}^{l} D_{\delta s_{j+1}}(|\delta_s|-\delta_{sj})_+ \tag{3.16}
$$

Clearly, the analyst must first decide exactly how small these perturbations can be before eliminating any dependence on α from the nonlinear coefficients. This is one area in which prior information, in the form of say, wind-tunnel data, can be utilised. In fact, the entire aerodynamic model can be better “structured” by taking into consideration any *a-priori* knowledge obtained from analytic, wind-tunnel and/or flight-identification results.

3.3 Errors

In any analytic model of a real system, there will always be a number of differences apparent. These differences manifest themselves as errors in the model and can be attributed to inadequate modelling, systematic effects and random noise. In all forms of system identification, these errors must be considered, so that the accuracy of any estimated models can be assessed. Some can be treated or accounted for, removing their influence on the estimates altogether. The distributive properties of others can be approximated and thus, confidence bounds placed on the resulting estimates. Inevitably though, some simply cannot be isolated and are therefore left in the data. In general, one should attempt to minimise the adverse effects of errors in the model, using prescribed methods and engineering judgement as appropriate to each particular case.

3.3.1 Modelling Errors

Many approximations have to be made in the process of building a tractable mathematical model. Generally, aircraft have a low structural weight, resulting in flexibility of the wings and fuselage. The F-111C, for example, has thin wings optimised for supersonic flight and yet can undergo very high wing-loadings during certain manoeuvres. Flexible structural modes can therefore have a significant effect on the measured responses - particularly accelerometer recordings - and should not be ignored. These modes are seldom included in the control modes identified from flight data, whereas in flutter testing the structural modes are of prime importance.

If accurate model parameters are to be identified, it is essential that the magnitude of responses attributable to the unmodelled dynamics be less than the response variations resulting from the desired tolerance in the parameters being estimated. The analyst thus has a fine line to tread in selecting a model structure that is complex enough to be realistic, but not over-parametrized so as to cause identifiability problems. For parameters in a model to be identified from flight data, each parameter must be able to produce a significant, unique change in the measured response. If two parameters produce identical effects, then only a combination of them can be identified. If their effects are very similar, but not identical, their estimates will be highly correlated and have large variances. For similar reasons, inclusion of a parameter whose effect is similar to that of a combination of others will cause the variances in all of their estimates to increase greatly. The problem of collinearity will be further discussed in Chapter 4, along with methods of dealing with it.

It is clear that errors are inherent in the modelling and identification process. Theory can provide little help in estimating their effect, since the errors must first be modelled, resulting in circular conclusions. The analyst must understand the system he or she is modelling and be able to determine whether the model they have found is adequate for its intended use.

With this understanding of the approximations inherent in modelling, it is not surprising that different analysts may deduce models of the same form, but with different parameters from the same set of flight-data. For example, the control designer would prefer a model that is most accurate at the control system crossover frequency, whereas the aerodynamicist may prefer model parameters that most closely estimate the quasi-static stability derivatives. Since users are interested in model validity in different frequency regions, their model parameters will often differ.

3.3.2 Systematic Errors

Systematic errors are usually caused by calibration or dynamic errors in the instrumentation and filtering and simplifications or coefficient errors in the measurement equations. Subtle errors such as time skewing in the A-D conversion process can also cause time errors up to one telemetry frame time, which can affect some identification algorithms seriously. A similar and frequently worse effect is produced if different sensor channels include anti-alias low-pass filters with different cutoff frequencies and consequently, different time delays.

Instrumentation usually comprises rate gyros, attitude gyros, accelerometers, airspeed indicators and wind-angle vanes. The sensors utilised in the F-111C flight test program are outlined in Chapter 5.

3.3.3 Random Errors

Flight data are often gathered via telemetry links which produce data errors. The coding seldom flags small bit errors even though large dropouts may be removed, sometimes without the analysts being aware of the time-gap.

Aircraft sensors operate in the vibration environment of the aircraft. The accelerometers in particular respond to the higher frequency noises from engines and structural resonant modes. The high frequency noise can often be removed by filtering, but all channels must be identically treated to avoid introducing time-skews or transfer function differences between channels. Sensors also have their own noise generation mechanisms and analog-to-digital conversion adds quantisation noise. For example, the NBTU probe on the F-111C was calibrated for a range of 900 kts, though in some manoeuvres, the variation in airspeed was in the order of 30 kts. In a 9-bit A-D converter, this corresponds to only 18 quantising levels - much less than would be required for analysis of the speed effects.

The term *measurement noise* is used to describe the noise associated with measurements of the aircraft response. Its effect reduces as the data length increases and some errors such as telemetry errors are easily detected. Noise or errors in the control position sensors and turbulence is called *process noise* and has a more insidious effect, since these errors disturb the states of the aircraft model used in the identification process. The errors thus only decay at rates determined by the response modes.

Figure 3-4 illustrates the general dynamic system, including external noise inputs.

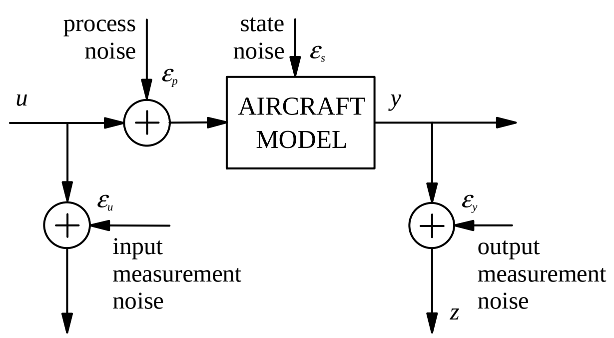

Figure 3-4: Block diagram of the dynamic aircraft model

3.4 Concluding Remarks

The postulation of an adequate model structure is a difficult step in the identification procedure. As discussed, the inclusion of too many terms in the model can lead to identifiability problems - commonly referred to as overmodelling. If too few parameters are used, however, an inadequate representation of the aircraft will result - either in the predicted response, or the model itself, or both. It was concluded that the best choice would be a conservative model, with no more terms than is needed to represent the true model sufficiently.

For the F-111C aircraft model, tensor-product polynomial splines were employed to represent the nonlinear aerodynamic coefficients. These functions have proven highly suitable for the representation of unsteady aerodynamic effects. In flights of relatively constant Mach number and altitude, the lateral derivatives could generally be expressed as functions of the angle-of-attack. The spoilers' contribution in each axis was also dependent on the deflection and was therefore modelled using two-dimensional splines in δ_s and α. Taking various aspects into consideration, the nonlinear models were able to be simplified quite substantially, thus reducing the size of the model.

In the last section, model errors and sources of systematic and random errors were discussed. The effect of these was outlined, with methods that can be used to minimise their influence.

Chapter 4

System Identification

4.1 Introduction

Experimental work often involves the measurement of a number of variables, which are either directly observed or derived, over a range of conditions. If there exists some relationship between certain variables which is to be characterised, then a model of the underlying system needs to be determined. The extent to which the model should be parametrized depends largely on its intended purpose. Generally speaking, a model should sufficiently follow the measured data, facilitate the estimation of desired system parameters and demonstrate favourable prediction qualities. System identification encompasses the first two aspects of state and parameter estimation. The third is useful as a validation of the estimated model.

Multiple linear regression is a statistical technique by which a number of parameters or coefficients in the model are estimated. In the first section, the details of the regression procedure will be explored, from estimating the coefficients to constructing confidence intervals and performing hypothesis tests. The variance of the estimates and predicted response are discussed, as well as correlation within the regression. Following appraisal of the model's significance, various criteria that can be used as indicators of the accuracy and efficiency of the regression model will be examined. Dummy variables will also be discussed, with reference to their use in categorical data samples.

The next section covers biased estimation. The motivation behind using a biased method can often be explained in terms of scaling or collinearity, which are included in the discussion. In particular, various sources of collinearity are examined and a number of measures suggested for its detection. Two biased estimation methods are then examined: Principal

Components Regression and Mixed Estimation [134]. Either of these can be employed to curtail any problems that might arise due to near-linear dependency. Restricted Estimation is also outlined, though is more appropriately used in implementing hard constraints in the model.

The topic of model structure determination is addressed in the last section. More specifically, techniques that can be used to deduce a significant model from a set of candidate variables are discussed. These include Exhaustive Search, Backward Elimination, Forward Selection and Stepwise Regression. The last of these is essentially a combination of the previous two and constitutes the most efficient algorithm for this type of procedure. In closing, the subject of model validation is reviewed, for final assessment of the estimated model.

4.2 Multiple Linear Regression

Under real conditions, measured data will unfortunately never provide an exact representation of the true model state. Additional variation due to process and measurement errors necessitates a need to find the best model, in terms of representing the variables. A common form of model consists of one dependent variable, also known as the response, and several independent variables, or the predictors. The response is assumed to have some random distribution associated with it, whilst the error in the predictors is assumed negligible. This is an important conjecture affecting the properties of any estimates subsequently obtained and will be discussed in more detail later.

An equation relating the average observed values in the response to the predictor variables, forming a mathematical model of the system, is called the regression equation. A regression curve illustrates the locus of estimated values of the dependent variable against each independent variable. This relationship may be a straight line, in the linear case, or some higher-order function. It may also have differing characteristics in neighbouring regions of certain variables. For example, the function might display a linear relationship within a small region of one variable and change dramatically above this region.

Consider the following linear model, in which the predictor variables, x_j, are related to the response, y, thus:

$$\mathbf{y} = \theta_0 + \mathbf{X}\theta + \varepsilon \tag{4.1}$$

where

$$\mathbf{y}=\begin{bmatrix} y_1 \\ y_2 \\ \vdots \\ y_n \end{bmatrix} \qquad \mathbf{X}=\begin{bmatrix} x_{11} & x_{12} & \cdots & x_{1p} \\ x_{21} & x_{22} & \cdots & x_{2p} \\ \vdots & \vdots & & \vdots \\ x_{n1} & x_{n2} & \cdots & x_{np} \end{bmatrix} \qquad \varepsilon=\begin{bmatrix} \varepsilon_1 \\ \varepsilon_2 \\ \vdots \\ \varepsilon_n \end{bmatrix} \tag{4.2}$$

and

$$\theta=\begin{bmatrix} \theta_1 & \theta_2 & \cdots & \theta_p \end{bmatrix}^T \tag{4.3}$$

Each observation equation corresponds to a separate row in the matrix formulation:

$$y_i=\theta_0+\theta_1 x_{i1}+\theta_2 x_{i2}+\ldots+\theta_p x_{ip}+\varepsilon_i \tag{4.4}$$

such that $\mathbf{y}$ defines the vector of observations, of size $[n \times 1]$. The matrix of independent variables, $\mathbf{X}\,[n \times p]$, is comprised of p regressor variables, which make up the columns. Each variable is related to a corresponding element in the parameter vector, $\theta\,[p \times 1]$. Both the parameter vector and the measurement or equation error vector, $\varepsilon\,[n \times 1]$, are generally unknown, although the latter is a random variable, so assumptions can be made concerning its distribution. This will allow for the construction of confidence intervals and implementation of various hypothesis tests.

Using the information provided by the observations, an estimate of the parameter vector, $\hat{\theta}$, can be obtained. Then,

$$\hat{\mathbf{y}}=\hat{\theta}_0+\mathbf{X}\hat{\theta} \tag{4.5}$$

is the predicted response and the residual,

$$\tilde{\mathbf{y}}=\mathbf{y}-\hat{\mathbf{y}} \tag{4.6}$$

4.2.1 Least Squares Solution

The basic assumption made concerning error in the independent variables can now be used to an advantage in the formulation of a Least Squares (LS) solution. Since the error in $\mathbf{X}$ is assumed negligible, all that is required is to minimise the difference between measured and predicted responses.

Before proceeding, the θ_0 term can be effectively removed from the regression by 'centering' the data in each variable about their respective means. This reduces the number of degrees of freedom, or independent pieces of information in the regression model to $(n-1)$, as will be explained in the following section. Equation (4.5) can then be expressed:

$$\mathbf{y} - \bar{y} = (\mathbf{X} - \mathbf{1}\bar{\mathbf{x}})\theta + \varepsilon \tag{4.7}$$

where the unit vector $\mathbf{1}$ is of size $[n \times 1]$ and $\bar{\mathbf{x}}$ is $[1 \times p]$. The mean values,

$$\bar{y} = \frac{1}{n}\sum_{i=1}^{n} y_i \qquad \bar{\mathbf{x}} = \frac{1}{n}\sum_{i=1}^{n} \mathbf{x}_i \tag{4.8}$$

For simplicity, the variables, $\mathbf{y}$ and $\mathbf{X}$ will hereafter be considered as *centred.* That is,

$$\mathbf{y} \equiv \mathbf{y} - \bar{y} \quad \text{and} \quad \mathbf{X} \equiv \mathbf{X} - \mathbf{1}\bar{\mathbf{x}}$$

reducing the regression model to:

$$\mathbf{y} = \mathbf{X}\theta + \varepsilon \tag{4.9}$$

The Least Squares estimate of θ is that which minimises the cost functional, $J(\theta)$, based on the error sum of squares:

$$\begin{aligned} J(\theta) = \varepsilon^T\varepsilon \; &= (\mathbf{y} - \mathbf{X}\theta)^T(\mathbf{y} - \mathbf{X}\theta) \\ &= \mathbf{y}^T\mathbf{y} - 2\theta^T\mathbf{X}^T\mathbf{y} + \theta^T\mathbf{X}^T\mathbf{X}\theta \end{aligned} \tag{4.10}$$

Differentiating with respect to θ and setting the result to zero,

$$\frac{\partial}{\partial\theta}\mathbf{J}(\theta) = -2\mathbf{X}^T\mathbf{y} + 2(\mathbf{X}^T\mathbf{X})\theta = \mathbf{0} \tag{4.11}$$

provides a set of *normal equations*:

$$\left(\mathbf{X}^T\mathbf{X}\right)\theta = \mathbf{X}^T\mathbf{y} \tag{4.12}$$

Providing that the p normal equations are independent, the matrix $\mathbf{X}^T\mathbf{X}$ is non-singular and its inverse exists. The least squares solution for the parameters is then solved via:

$$\hat{\theta} = (\mathbf{X}^T\mathbf{X})^{-1}\mathbf{X}^T\mathbf{y} \tag{4.13}$$

If there are fewer than p independent equations, $\mathbf{X}^T\mathbf{X}$ is singular. In this case, either the model must be reduced, or additional restrictions placed on the parameters in order for a solution to be possible. Section 4.3 deals with the situation where $\mathbf{X}^T\mathbf{X}$ is near-singular: the solution to the normal equations is obtained through the use of a biased-estimation technique.

With an estimate of the parameter vector, a corresponding estimate for the intercept term, θ_0, can be obtained from Equation (4.5):

$$\hat{\theta}_0 = \bar{y} - \bar{\mathbf{x}}\hat{\theta} \tag{4.14}$$

Now several additional assumptions concerning the independent variables and equation error can be made, which effectively govern the resulting properties of the least-squares estimates. Under the assumptions:

a) ε is stationary with zero mean, $\mu(\varepsilon) = \mathrm{E}\{\varepsilon\} = 0$;

b) ε is uncorrelated with $\mathbf{X}$, $\mathrm{E}\{\mathbf{X}^T\varepsilon\} = \mathrm{E}\{\mathbf{X}^T\}\mathrm{E}\{\varepsilon\}$; and

c) $\mathbf{X}$ is a deterministic quantity.

The estimates will be *unbiased.* Additionally, if:

d) the measurement noise, ε_i are identically distributed and independent with zero mean and variance σ^2, $\mathrm{E}\{\varepsilon\varepsilon^T\} = \mathbf{I}\sigma^2$,

then $\hat{\theta}$ will also be a *consistent* and *efficient* estimator.

Often, if the model is correct, the first two assumptions are not unreasonable. On the other hand, the predictor variables are normally corrupted by noise, violating assumption c) and consequently biasing the estimated parameters. This drawback is unavoidable, although it has been shown [112], that the LS estimates can still provide accurate values. The estimates may even be comparable to those obtained from a Maximum Likelihood (ML) technique, which are consistent and asymptotically unbiased. In fact, under assumption d), $\hat{\theta}$ is equal to the ML estimate of θ, obtained by maximising the *likelihood function*:

$$\prod_{i=1}^{n} \frac{1}{\sigma(2\pi)^{1/2}} \cdot e^{-\varepsilon_i^2/2\sigma^2} = \frac{1}{\sigma^n(2\pi)^{n/2}} \cdot e^{-\varepsilon^T\varepsilon/2\sigma^2}$$

Generally speaking, assumption d) is never met. It must however, be placed on the data if one is to go about constructing confidence intervals or performing hypothesis tests.

4.2.2 Analysis of Variance

The most common way in which the quality of the regression can be surmised is through an analysis of variance approach. This approach calls for a subdivision of the total variation in the dependent variable into meaningful components that may each be examined. By doing this, it becomes clear exactly what proportion of the variation can be attributed to the model and what proportion is due to error.

The total sum of squares (SS), corrected for mean, may be written as:

$$\sum {y_i}^2 = \sum {\widehat{y}_i}^2 + \sum (y_i - \widehat{y}_i)^2 \tag{4.15}$$

where $\sum {\widehat{y}_i}^2$ is the regression sum of squares which reflects the amount of variation explained by the model. The term, $\sum(y_i - \widehat{y}_i)^2$, is the error sum of squares and indicates the variation about the regression. In matrix form:

$$\mathbf{y}^T\mathbf{y} = \hat{\mathbf{y}}^T\hat{\mathbf{y}} + \tilde{\mathbf{y}}^T\tilde{\mathbf{y}} \tag{4.16}$$

Each sum of squares has associated with it a number of degrees of freedom (dof). These represent the number of independent pieces of information needed to compile that sum of squares. An ANOVA - Analysis of Variance - table (4.1) summarises these results for comparison:

SOURCE	dof	SS	MS
regression	p	$\hat{\mathbf{y}}^T\hat{\mathbf{y}}$	$\frac{\hat{\mathbf{y}}^T\hat{\mathbf{y}}}{p}$
residual	$n-p-1$	$\tilde{\mathbf{y}}^T\tilde{\mathbf{y}}$	$\frac{\tilde{\mathbf{y}}^T\tilde{\mathbf{y}}}{(n-p-1)}$
total	$n-1$	$\mathbf{y}^T\mathbf{y}$	$\frac{\mathbf{y}^T\mathbf{y}}{(n-1)}$

Table 4.1: Generalised ANOVA table

In the far-right column, the mean square (MS) for each entry is obtained by dividing the corresponding sum of squares by its number of degrees of freedom. One important term worth noting is the mean square about regression (residual), written:

$$s^2 = \frac{\tilde{\mathbf{y}}^T \tilde{\mathbf{y}}}{(n-p-1)} \tag{4.17}$$

This ratio provides an unbiased estimate based on $(n-p-1)$ dof, of the true variance about the regression, σ^2, which is otherwise unknown.

The analysis of variance in Equation (4.16) is often expressed in terms of the Least Squares results as:

$$\mathbf{y}^T\mathbf{y} = \widehat{\theta}^T\mathbf{X}^T\mathbf{y} + \tilde{\mathbf{y}}^T\tilde{\mathbf{y}} \tag{4.18}$$

since

$$\begin{aligned} \widehat{\mathbf{y}}^T\widehat{\mathbf{y}} &= (\mathbf{X}\widehat{\theta})^T(\mathbf{X}\widehat{\theta}) \\ &= \hat{\theta}^T(\mathbf{X}^T\mathbf{X}\hat{\theta}) = \hat{\theta}^T(\mathbf{X}^T\mathbf{y}) \end{aligned} \tag{4.19}$$

from the normal equations, (4.12). The covariance of the random variable, $\hat{\theta}$, can also be evaluated from the LS result, using the expectation:

$$\begin{aligned} \mathbf{Cov}(\widehat{\theta}) = \mathrm{E}\{\widehat{\theta}\widehat{\theta}^T\} &= \mathrm{E}\{[(\mathbf{X}^T\mathbf{X})^{-1}\mathbf{X}^T\mathbf{y}][(\mathbf{X}^T\mathbf{X})^{-1}\mathbf{X}^T\mathbf{y}]^T\} \\ &= (\mathbf{X}^T\mathbf{X})^{-1}\mathbf{X}^T\mathrm{E}\{\mathbf{y}\mathbf{y}^T\}\mathbf{X}(\mathbf{X}^T\mathbf{X})^{-1} \end{aligned} \tag{4.20}$$

Utilising assumption d) from the previous section, which implies $\mathrm{E}\{\mathbf{y}\mathbf{y}^T\} = \mathbf{I}\sigma^2$, yields:

$$\mathbf{Cov}(\widehat{\theta}) = (\mathbf{X}^T\mathbf{X})^{-1}\sigma^2 \tag{4.21}$$

From this expression, the standard deviation for each of the estimates, θ_j, may be evaluated. This is done by simply taking the square root of the variance:

$$\begin{aligned} \sigma_j &= \sqrt{Var(\theta_j)} \\ &= \sqrt{(\mathbf{X}^T\mathbf{X})^{-1}_{jj}\sigma^2} \end{aligned} \tag{4.22}$$

and the corresponding estimates,

$$s(\theta_j) = \sqrt{(\mathbf{X}^T\mathbf{X})^{-1}_{jj}s^2} \tag{4.23}$$

The last measure to be presented is the variance of the predicted response. For any single set of observations, denoted by subscript i,

$$\begin{aligned} Var(\widehat{y}_i) = \mathrm{E}\{\widehat{y}_i\widehat{y}_i^T\} &= \mathrm{E}\{[\mathbf{x}_i\widehat{\theta}][\mathbf{x}_i\widehat{\theta}]^T\} \\ &= \mathbf{x}_i\mathrm{E}\{\widehat{\theta}\widehat{\theta}^T\}\mathbf{x}_i^T = \mathbf{x}_i\mathbf{Cov}(\widehat{\theta})\mathbf{x}_i^T \end{aligned} \tag{4.24}$$

which equates to:

$$Var(\widehat{y}_i) = \mathbf{x}_i(\mathbf{X}^T\mathbf{X})^{-1}\mathbf{x}_i^T\sigma^2$$

For the entire set of observations,

$$\mathbf{Var}(\widehat{\mathbf{y}}) = [\mathbf{X}(\mathbf{X}^T\mathbf{X})^{-1} \cdot \times \mathbf{X}]\mathbf{1}\sigma^2 \tag{4.25}$$

The unit vector, $\mathbf{1}$ is $[p \times 1]$ and the operator '$\cdot\times$' represents *array*, or element-by-element multiplication. As with the previous term, it is also possible to obtain an estimate for $Var(\widehat{y}_i)$, by substituting the residual variance, s^2.

4.2.3 Correlation

The correlation between two random variables, X and Y, which follow some continuous joint bivariate probability distribution $f(X,Y)$, can be described as the reduction in variance of Y due to conditioning on X. This can be seen in the *correlation coefficient*, $\rho_{Y\,|\,X}$.

$$\rho^2_{Y\,|\,X} = \frac{\sigma^2_Y - \sigma^2_{Y\,|\,X}}{\sigma^2_Y} \quad ; \quad -1 \le \rho_{Y\,|\,X} \le 1 \tag{4.26}$$

where σ_Y is the variance of Y and $\sigma^2_{Y\,|\,X}$ the *conditional variance* of Y, given X. The correlation coefficient is an often-used statistic that not only provides a measure of how two random variables are associated in a sample, but has properties that closely relate it to a linear regression. Values of $\rho_{Y\,|\,X}$ close to -1 indicate a large negative correlation between X and Y (high $X \Leftrightarrow$ low Y), $\rho_{Y\,|\,X}$ close to $+1$ indicates a large positive correlation (high $X \Leftrightarrow$ high Y) and $\rho_{Y\,|\,X}$ close to zero corresponds to a small linear correlation, if any.

If a sample of n observations is available from the distribution, then the *sample correlation coefficient*, $r_{x,y}$, provides a measure of the linear association between x and y:

$$r^2_{x,\,y} = \frac{\mathbf{y}^T\mathbf{y} - (\mathbf{y}-\mathbf{x})^T(\mathbf{y}-\mathbf{x})}{\mathbf{y}^T\mathbf{y}} = \frac{(\mathbf{x}^T\mathbf{y})^2}{(\mathbf{x}^T\mathbf{x})(\mathbf{y}^T\mathbf{y})} \tag{4.27}$$

since (here) $\mathbf{x}^T\mathbf{x} = \mathbf{x}^T\mathbf{y}$ from Equation (4.19). This can be further generalised by stating:

$$r_{x,\,y} = \frac{Cov(x, y)}{\sqrt{Var(x)Var(y)}} \tag{4.28}$$

When more than two independent variables are involved, the essential features of regression are described not by a single correlation coefficient, but by several correlations. These include a set of zero-order correlations, such as r, plus higher-order indices called multiple, partial and multiple-partial correlations. Only the first two higher-order correlations will be presented here. For a full description of correlation in regression, refer to Kleinbaum, *et al* [110].

The *multiple correlation coefficient*, denoted as $R_{y\,|\,x_1, x_2, \ldots, x_p}$, is a measure of the overall linear association of one (dependent) variable $\mathbf{y}$ with several other (independent) variables $\mathbf{x}_1, \mathbf{x}_2, \ldots, \mathbf{x}_p$. The overall linear association actually refers to the correlation between $\mathbf{y}$ and the LS estimate using $\mathbf{x}_1, \mathbf{x}_2, \ldots, \mathbf{x}_p$. From Equation (4.27), the multiple correlation coefficient can be written in terms of $\mathbf{y}$ and $\hat{\mathbf{y}}$:

$$R_{y\,|\,x_1, x_2, \ldots, x_p} = r_{\hat{y},\,y} = \frac{\widehat{\mathbf{y}}^T\mathbf{y}}{\sqrt{(\widehat{\mathbf{y}}^T\widehat{\mathbf{y}})(\mathbf{y}^T\mathbf{y})}} \tag{4.29}$$

A more commonly used form of the statistic is the *squared multiple correlation coefficient*, denoted R^2.

$$R^2 = \frac{(\widehat{\mathbf{y}}^T\mathbf{y})^2}{(\widehat{\mathbf{y}}^T\widehat{\mathbf{y}})(\mathbf{y}^T\mathbf{y})} = \frac{\widehat{\mathbf{y}}^T\widehat{\mathbf{y}}}{\mathbf{y}^T\mathbf{y}} \quad ; \quad 0 \leq R^2 \leq 1 \tag{4.30}$$

The *partial correlation coefficient* is a measure of the strength of a linear relationship between two variables, after accounting for the effects of other variables. If the two variables are Y and X_j and the *control variables* are $X_1, \ldots, X_{j-1}, X_{j+1}, \ldots, X_p$, then the corresponding partial correlation coefficient is denoted by $\rho_{Y,\,X_j\,|\,X_R}$. The formula for the square of $\rho_{Y,\,X_j\,|\,X_R}$ can be written:

$$\rho^2_{Y,\,X_j\,|\,X_R} = \frac{\sigma^2_{Y\,|\,X_R} - \sigma^2_{Y\,|\,X_F}}{\sigma^2_{Y\,|\,X_R}} \quad ; \quad -1 \leq \rho_{Y,\,X_j\,|\,X_R} \leq 1 \tag{4.31}$$

where X_F denotes the *full* model, $X_1, X_2, \ldots, X_p$ and X_R the *reduced* model, $X_1, \ldots, X_{j-1}$, $X_{j+1}, \ldots, X_p$. The order of the partial correlation is equal to the number of variables that are being 'controlled' for: $(p-1)$ in this case. The structure of the correlation coefficient helps to relate this form of higher-order correlation to regression. It then follows that an analogous formula for the squared *sample partial correlation coefficient* is:

$$r^2_{y,\,x_j\,|\,X_R} = \frac{(\tilde{\mathbf{y}}^T\tilde{\mathbf{y}})_R - (\tilde{\mathbf{y}}^T\tilde{\mathbf{y}})_F}{(\tilde{\mathbf{y}}^T\tilde{\mathbf{y}})_R} \quad ; \quad 0 \le r^2 \le 1 \tag{4.32}$$

Here, $(\tilde{\mathbf{y}}^T\tilde{\mathbf{y}})_R$ is the residual sum of squares using the reduced model, which excludes the variable X_j. Another interpretation concerning partial correlations comes from the sample correlation of the residuals:

$$r_{y,\,x_j\,|\,X_R} = r_{y-\hat{y}_R,\,x_j-\hat{x}_j} \tag{4.33}$$

where $\hat{y}_R$ is the estimated regression of y on X_R and $\hat{x}_j$ is the estimated regression of x_j on X_R. That is,

$$\hat{\mathbf{y}}_R = \mathbf{X}_R\hat{\theta}_R \qquad \hat{\mathbf{x}}_j = \mathbf{X}_R\hat{\phi}_R \tag{4.34}$$

The parameter vectors, $\hat{\theta}_R$ and $\hat{\phi}_R$ are both Least Squares estimates for the corresponding models. Defining the residuals, $\tilde{\mathbf{y}}_R = \mathbf{y} - \hat{\mathbf{y}}_R$ and $\tilde{\mathbf{x}}_j = \mathbf{x}_j - \hat{\mathbf{x}}_j$, and substituting into Equation (4.27) yields,

$$r^2_{y-\hat{y}_R,\,x_j-\hat{x}_j} = \frac{(\tilde{\mathbf{y}}^T\tilde{\mathbf{y}})^2_R}{(\tilde{\mathbf{y}}^T\tilde{\mathbf{y}})_R(\tilde{\mathbf{x}}_j^T\tilde{\mathbf{x}}_j)} \tag{4.35}$$

By subtracting the LS estimates from both $\mathbf{y}$ and $\mathbf{x}_j$, any effects that the control variables, $\mathbf{X}_R$ have on the regression are effectively removed. This leaves two variables, $\tilde{\mathbf{y}}_R$ and $\tilde{\mathbf{x}}_j$ that are **independent** of those control variables. The resulting correlation coefficient therefore provides an indication of the importance of each independent variable, which may not yet be in the regression.

4.2.4 Confidence Intervals

Up to this point, the only assumptions made concerning the distribution of the errors have been in defining the properties of the LS estimates. In order to construct confidence intervals and test various hypotheses, these need to be extended by an assumption on the distribution of each ε_i. Measures formed under this assumption include variance estimates of the parameters and response. As there is a tendency for measurement errors that occur in most real situations to have Gaussian distributions, this is often the best assumption to follow. That is, for a large number of data points, the errors are assumed to be normally distributed as: $\varepsilon \sim N(\mathbf{0}, \mathbf{I}\sigma^2)$. The Central Limit Theorem is an important result and states this approximation formally:

Theorem 1 *If $\overline{X}$ is the mean of a random sample of size n taken from a population with mean μ and finite variance σ^2, then the limiting form of the distribution of the variable:*

$$Z = \frac{\overline{X} - \mu}{\sigma / \sqrt{n}} \tag{4.36}$$

as $n \to \infty$ is the standard normal distribution, $N(0, 1)$.

A normal random variable X, with mean μ and variance σ^2 has a *probability density function* given by

$$f(x) = \frac{1}{\sqrt{2\pi}\sigma}\, e^{-(x-\mu)/2\sigma^2} = N(\mu, \sigma^2) \quad ; \quad -\infty < x < \infty \tag{4.37}$$

Since $\widehat{\theta}$ is a linear function of independent normal variables, it will also be normally distributed according to: $\widehat{\theta} \sim N(\theta, \mathbf{Cov}(\widehat{\theta}))$. Hence the random variable, $\widehat{\theta}_j / \sigma_j$, will have the standard normal distribution. Additionally, the statistic, s^2, will have a normal distribution about the true variance and therefore, under the normality assumption, it may be derived that $\nu_2 s^2 / \sigma^2$ is a chi-squared variable with $\nu_2 = (n - p - 1)$ degrees of freedom, independent of θ_j. It then follows that the statistic,

$$\begin{aligned} t &= \frac{(\theta_j - \widehat{\theta}_j) \,/\, \sigma_j}{\sqrt{s^2 \,/\, \sigma^2}} \\ &= \frac{(\theta_j - \widehat{\theta}_j)}{s\sqrt{(\mathbf{X}^T\mathbf{X})^{-1}_{jj}}} \end{aligned} \tag{4.38}$$

has a t-distribution with ν_2 degrees of freedom. This may be utilised in obtaining individual confidence intervals for each parameter, by substituting a tabulated value of t which is based on a pre-determined significance level, α_p.

$$|\theta_j - \widehat{\theta}_j| < t(\nu_2, 1 - \tfrac{\alpha_p}{2}) s \sqrt{(\mathbf{X}^T\mathbf{X})^{-1}_{jj}} \tag{4.39}$$

In formulating the individual confidence intervals, an implicit assumption was made that the parameters are uncorrelated. Consequently, the t-distribution may be utilised for obtaining confidence intervals on single parameters only and neglects any influence from other parameters. In order to look at all of the parameters simultaneously, the joint confidence region must be considered. Now the variable, $(\widehat{\theta}\,\widehat{\theta}^T) \cdot / \,\mathbf{Cov}(\widehat{\theta})$, also has a chi-squared distribution, so a joint confidence region can be defined by the statistic:

$$\begin{aligned}\mathbf{f} &= \frac{(\theta-\widehat{\theta})(\theta-\widehat{\theta})^T \cdot / \, \mathbf{Cov}(\widehat{\theta})}{ps^2 \, / \, \sigma^2} \\ &= \frac{(\theta-\widehat{\theta})(\theta-\widehat{\theta})^T}{(\mathbf{X}^T\mathbf{X})^{-1}ps^2}\end{aligned} \tag{4.40}$$

which has an F-distribution with $\nu_1 = p$ and $\nu_2 = (n-p-1)$ dof, respectively. The confidence region for a significance level of α_p is therefore expressed:

$$(\theta-\widehat{\theta})\mathbf{X}^T\mathbf{X}(\theta-\widehat{\theta})^T < F(\nu_1, \nu_2, 1-\alpha_p)ps^2 \tag{4.41}$$

This equation circumscribes a region in the parameter space bounded by a multi-dimensional ellipse, which can become difficult to interpret for any number of parameters greater than three. It is possible, however, to examine the confidence ellipse resulting from a model with two parameters and note some important aspects that will be relevant to any model. Figure 4-1 illustrates an example of this simple case. Both individual and joint confidence bounds are shown centered about the parameter estimates.

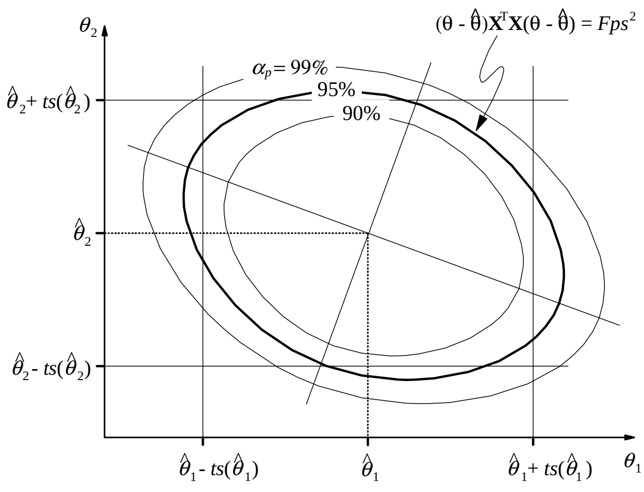

Figure 4-1: Two-parameter confidence ellipse

As the confidence level, $100(1-\alpha_p)\%$, is increased, the ellipse expands forming contours of similar shape. Any point (θ_1, θ_2) within a chosen confidence region will be regarded as being jointly reasonable, according to the data.

Now if $\widehat{\theta}_1$ and $\widehat{\theta}_2$ have variances of different size the ellipse will be stretched accordingly. If there exists a significant correlation between parameters, the major axes of the ellipse will be skewed by some amount. In order to formulate the correlation coefficient for the two parameters, $\widehat{\theta}_1$ and $\widehat{\theta}_2$, based on the sampled data, the covariance,

$$Cov(\widehat{\theta}_1, \widehat{\theta}_2) = \mathbf{Cov}(\widehat{\theta})_{12} = (\mathbf{X}^T\mathbf{X})^{-1}_{12}\sigma^2 \tag{4.42}$$

and variance,

$$Var(\widehat{\theta}_j) = \mathbf{Cov}(\widehat{\theta})_{jj} = (\mathbf{X}^T\mathbf{X})^{-1}_{jj}\sigma^2 \quad ; \quad j = 1, 2$$

are substituted into Equation (4.28). The *sample correlation coefficient* can then be written:

$$r_{12} = \frac{(\mathbf{X}^T\mathbf{X})^{-1}_{12}}{\sqrt{(\mathbf{X}^T\mathbf{X})^{-1}_{11}(\mathbf{X}^T\mathbf{X})^{-1}_{22}}} \tag{4.43}$$

When one of these situations occurs, there are no serious consequences. However, if the estimates have both different variances and a high correlation, a special case emerges where the individual confidence intervals regarded simultaneously, do not sufficiently represent the joint confidence region. As demonstrated in Figure 4-2, a large area may exist in which any point, (θ_1, θ_2), will not fall within the joint confidence ellipse. Hence, care must be taken when comparing LS estimates with others obtained from highly correlated data.

The confidence ellipse may also be expressed in terms of the *Hessian matrix*, since,

$$\begin{aligned} \mathbf{HES} &= (\nabla_\theta \tilde{\mathbf{y}})^T \frac{1}{\sigma^2} (\nabla_\theta \tilde{\mathbf{y}}) \\ &= \frac{1}{\sigma^2} \mathbf{X}^T\mathbf{X} \end{aligned} \tag{4.44}$$

Consequently, the bound is described by:

$$(\theta - \widehat{\theta})\, \mathbf{HES}\, (\theta - \widehat{\theta})^T = F(\nu_1, \nu_2, 1 - \alpha_p)\, p \tag{4.45}$$

The Hessian is commonly used in output error methods which employ gradient-type optimisation techniques. Eccentricity of the ellipsoid is measured by examining two geometric relationships, which are also used in these methods.

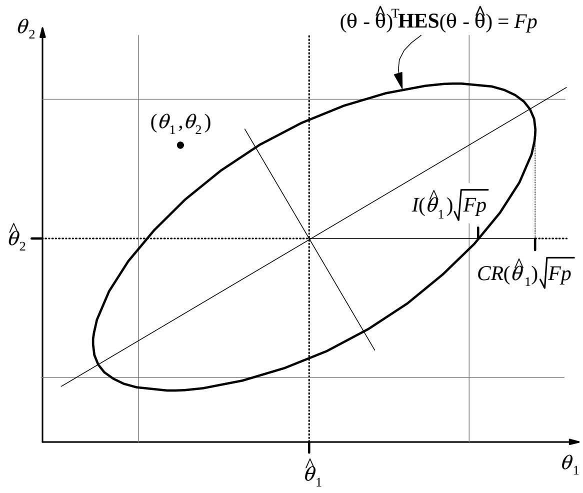

Figure 4-2: Skewed confidence ellipse

These are the *Cramer-Rao* bounds, given by:

$$CR_j = \sqrt{(\mathbf{HES})^{-1}_{jj}} \tag{4.46}$$

and the *Insensitivities*,

$$I_j = \frac{1}{\sqrt{(\mathbf{HES})_{jj}}} \tag{4.47}$$

both of which are also indicated in Figure 4-2.

The Cramer-Rao bound is equivalent to the standard deviation of each parameter estimate, $\hat{\theta}_j$. If this is multiplied by $\sqrt{Fp}$, the result defines the furthest projection of the confidence ellipse on to the θ_j axis. The change required in θ_j alone, to move from the LS estimate to the ellipsoid, is equal to the Insensitivity multiplied by $\sqrt{Fp}$. By evaluating the ratio of these parameters, one can gain a better idea of the ellipsoid's eccentricity. This ratio has been given the name *Geometric Dilution of Precision*, following analogous use in satellite navigation literature.

$$GDOP_j = \frac{CR_j}{I_j} \geq 1 \tag{4.48}$$

Obviously, large *GDOP*'s will indicate that the ellipsoid is stretched and skewed in those axes and hence the parameter estimates less reliable.

In the same way by which the t-distribution was used to construct confidence intervals on the individual parameters, confidence bounds can be constructed for the response. Each observation, y_i, is normally distributed, so the statistic,

$$\begin{aligned} t &= \frac{(y_i - \widehat{y}_i)/s(\widehat{y}_i)}{s/\sigma} \\ &= \frac{(y_i - \widehat{y}_i)}{s\sqrt{x_i(\mathbf{X}^T\mathbf{X})^{-1}x_i}} \end{aligned} \tag{4.49}$$

also has a t-distribution with $\nu_2 = (n - p - 1)$ dof A $100(1 - \alpha_p)\%$ confidence interval on the mean response may then be calculated:

$$|\, y_i - \widehat{y}_i| < t(\nu_2, 1 - \tfrac{\alpha_p}{2}) s\sqrt{x_i(\mathbf{X}^T\mathbf{X})^{-1}x_i} \tag{4.50}$$

Utilising Equation (4.25) for the vector representation, this becomes:

$$|\, \mathbf{y} - \widehat{\mathbf{y}}| < t(\nu_2, 1 - \tfrac{\alpha_p}{2}) s\sqrt{[\mathbf{X}(\mathbf{X}^T\mathbf{X})^{-1} \cdot \times \mathbf{X}]\mathbf{1}} \tag{4.51}$$

The confidence intervals in each axis, X_j define hyperbolic loci, illustrated in Figure 4-3 for the simple linear case.

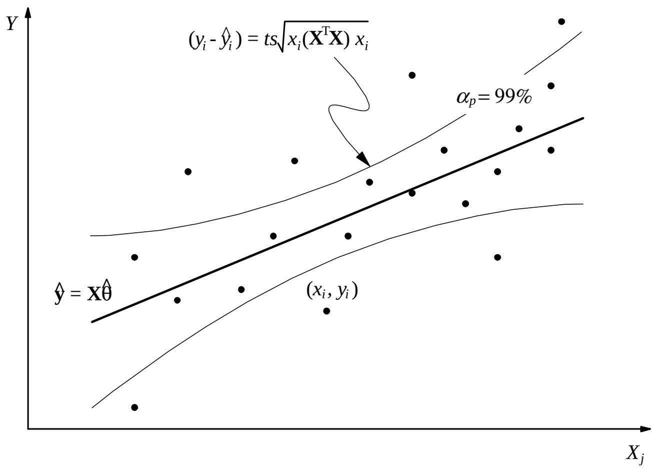

Figure 4-3: Confidence bands for the true response

4.2.5 Hypothesis Tests

Having fitted a multiple regression model and obtained estimates for the various parameters of interest, it is now appropriate to assess the contribution of each variable to the prediction of the response. This is typically done by performing statistical tests of hypotheses. The *null hypothesis* for these tests can be stated in terms of the unknown parameters in the model to determine their significance. There are essentially two types of hypothesis tests that can be performed to achieve this, both of which fall under the heading of F tests. A key feature of F tests is that they all involve a ratio of two independent estimates of variance. For these, consider the model containing p variables:

$$\mathbf{y} = \theta_0 + \mathbf{x}_1\theta_1 + \mathbf{x}_1\theta_2 + \ldots + \mathbf{x}_p\theta_p + \varepsilon \tag{4.52}$$

The first hypothesis test is for significance of overall regression. In this test, it established whether the entire set of independent variables, taken collectively, contribute significantly to the prediction. The *null* and *alternative* hypotheses may be generally stated as:

$$\begin{aligned} H_0 &: \theta_1 = \theta_2 = \ldots = \theta_p = 0 \\ H_1 &: \text{not all } \theta_j = 0 \end{aligned}$$

In other words, the null hypothesis states:

> *"The postulated model, comprising all p variables does not explain a significant amount of variation in the response"*

To perform this test, the mean square values previously compiled in the ANOVA table (4.1) are utilised. Recall that the residual mean square, s^2, provides an unbiased estimate of the true variance about the regression, σ^2, so the ratio, $\nu_2\, s^2/\sigma^2$, will have a chi-squared distribution. The regression mean square, $\hat{\mathbf{y}}^T\hat{\mathbf{y}}/p$, also provides an independent estimate of σ^2, though **only under the conditions of the null hypothesis**. Therefore, the ratio of mean squares will have an F-distribution as

$$f = \frac{\hat{\mathbf{y}}^T\hat{\mathbf{y}}}{ps^2} \tag{4.53}$$

which can be compared against the critical point, $F(\nu_1, \nu_2, 1 - \alpha_p)$. The null hypothesis is rejected if the calculated value of f exceeds this critical value, indicating that $\hat{\mathbf{y}}^T\hat{\mathbf{y}}/p$ has overestimated the variance, σ^2. The rejection of H_0 means that the proportion of variation observed in the data, which has been accounted for by the model, is greater than would be expected by chance in $100(1-\alpha_p)\,\%$ similar sets of data.

It is of interest to note that f can also be expressed in terms of the squared multiple correlation coefficient (Equation (4.30)):

$$f = \frac{(n-p-1)}{p} \cdot \frac{R^2}{(1-R^2)} \tag{4.54}$$

As a consequence, the same hypothesis test for overall regression can be performed by comparing a calculated value of R^2 against a beta $\beta(\frac{\nu_1}{2}, \frac{\nu_1}{2}, 1-\alpha_p)$ distribution. This however, is much less commonly employed than the F test.

The second hypothesis test is for significance of individual variables. In order to determine whether the addition of a variable to the existing regression model has significantly contributed to the prediction of the response, a *partial-F* test must be conducted. This test is critical for statistical model selection, as it identifies any non-significant terms, which can be subsequently eliminated from the regression. Stating this test formally, the following hypotheses are written:

$$\begin{aligned} H_0 &: \theta_j = 0 \\ H_1 &: \theta_j \neq 0 \end{aligned}$$

The test procedure basically compares two models. The *full* model contains all independent variables $\mathbf{x}_1,\mathbf{x}_2,\ldots,\mathbf{x}_p$, whereas the *reduced* model contains only $\mathbf{x}_1,\ldots,\mathbf{x}_{j-1},\mathbf{x}_{j+1},\ldots,\mathbf{x}_p$ (excluding $\mathbf{x}_j$). The goal is to evaluate which model is more appropriate, based on the amount of additional information $\mathbf{x}_j$ provides about $\mathbf{y}$, over that already provided by the existing regressors. This requires the 'extra sum of squares' principle:

$$SS(\mathbf{x}_j|\mathbf{x}_1,\ldots,\mathbf{x}_{j-1},\mathbf{x}_{j+1},\ldots,\mathbf{x}_p) = SS(\mathbf{x}_1,\mathbf{x}_2,\ldots,\mathbf{x}_p) - SS(\mathbf{x}_1,\ldots,\mathbf{x}_{j-1},\mathbf{x}_{j+1},\ldots,\mathbf{x}_p) \tag{4.55}$$

Which means the *extra sum of squares* from the addition of $\mathbf{x}_j$, given $\mathbf{x}_1,\ldots,\mathbf{x}_{j-1},\mathbf{x}_{j+1},\ldots,\mathbf{x}_p$ is equal to the difference between the regression sum of squares for $\mathbf{x}_1,\mathbf{x}_2,\ldots,\mathbf{x}_p$ and the regression sum of squares for $\mathbf{x}_1,\ldots,\mathbf{x}_{j-1},\mathbf{x}_{j+1},\ldots,\mathbf{x}_p$.

Rewriting the equation:

$$\begin{aligned} SS(\mathbf{x}_j|\mathbf{X}_R) &= (\hat{\mathbf{y}}^T\hat{\mathbf{y}})_F - (\hat{\mathbf{y}}^T\hat{\mathbf{y}})_R \\ &= (\theta^T\mathbf{X}^T\mathbf{X}\theta)_F - (\theta^T\mathbf{X}^T\mathbf{X}\theta)_R \\ &= \theta_j(\mathbf{X}^T\mathbf{X})_{jj}\theta_j \end{aligned} \tag{4.56}$$

Again, F denotes the full model and R, the reduced model. As with the F test for overall significance then, the mean square ratio,

$$\begin{aligned} f_p &= \frac{SS(\mathbf{x}_j|\mathbf{X}_R)/1}{s^2} \\ &= \frac{\theta_j^2}{s^2(\theta_j)} \end{aligned} \tag{4.57}$$

will also have an F-distribution with $\nu_1 = 1$ and $\nu_2 = (n-p-1)$ dof Hence, by comparing this with the critical point, $F(\nu_1, \nu_2, 1-\alpha_p)$, it can be ascertained if the contribution of the variable, $\mathbf{x}_j$, is significant to the regression. If the calculated value of f exceeds its critical value, H_0 is rejected, since the change in variance due to the addition of $\mathbf{x}_j$ is greater than would be expected.

It is also possible to use the t-distribution for comparison, since the numerator in Equation (4.57) has only 1 dof,

$$t_p = f_p^{1/2} = \frac{\theta_j}{s(\theta_j)} \tag{4.58}$$

and the critical point, $t(\nu_2, 1-\frac{\alpha_p}{2}) = F^{1/2}(1, \nu_2, 1-\alpha_p)$, for a pre-selected significance level, α_p.

Note that the partial-F statistic is related to the partial correlation in the corresponding variable, through Equation (4.32):

$$f_p = \frac{(n-p-1)}{1} \cdot \frac{r^2_{y,x_j\,|\,X_R}}{(1-r^2_{y,x_j\,|\,X_R})} \tag{4.59}$$

4.2.6 Accuracy of the Estimated Model

The accuracy of the model can be assessed by comparing the predicted response with the actual data, comparing the estimated parameters with other results, or examining their variances. The model's efficiency is evaluated by examining its accuracy against the number of parameters used. An efficient model should therefore have a high accuracy and minimal number of terms. Obviously, a more complex structure will often better represent the true system, since it is only a mathematical approximation at best. In parameter identification, however, it becomes much more difficult to estimate a large number of terms from a finite amount of data. As the parameter set increases, the number of degrees of freedom decreases by the same amount. This loss of orthogonality in the parameter space can lead to a near-singular $\mathbf{X}^T\mathbf{X}$ matrix, resulting in grossly inaccurate estimates. If the square matrix does become singular, then it will be impossible to obtain any estimates using the Least Squares technique.

There exist a number of criteria by which the estimated regression can be assessed in terms of its accuracy and efficiency. These criteria can be divided into two groups according to their requirement for any distributional assumptions in the measurement error. The first four that will be discussed do not require any assumptions regarding distribution of the errors. These include:

1. Residual sum of squares
2. Squared multiple correlation coefficient
3. Prediction sum of squares
4. Autocorrelation coefficient

Now looking at these criteria in detail:

1. The *residual sum of squares* is a simple measure of the accuracy of the estimated regression, based on the difference between measured and predicted responses:

$$RSS = \tilde{\mathbf{y}}^T\tilde{\mathbf{y}} \tag{4.60}$$

   Clearly, RSS will approach a minimum as the prediction accuracy improves.

2. The *squared multiple correlation coefficient* measures the proportion of total variation about the mean explained by the regression. Recall from Equation (4.30),

$$R^2 = \frac{\widehat{\mathbf{y}}^T\widehat{\mathbf{y}}}{\mathbf{y}^T\mathbf{y}} \quad ; \quad 0 \le R \le 1 \tag{4.61}$$

   In other words, the squared multiple correlation coefficient measures the usefulness of terms, other than θ_0, in the model. However, R^2 can increase simply from the addition of new terms to the model and hence, is no real reflection on its efficiency. This is particularly important when the number of degrees of freedom is small.

3. More recently, the *prediction sum of squares* has been proposed [3] for the selection of a parsimonious model. The principle of *parsimony* can be utilised in choosing a model that will be a good predictor. It states:

> *"Given two models fitted to the same data with residual variances which are close to each other, choose the model which involves the smaller number of parameters."*

For the effective implementation of this principle, the $PRESS$ criterion, based upon the mean square prediction error, $\mathrm{E}\{\mathbf{y} - \widehat{\mathbf{y}}\}$, is used. In this way, the accuracy to which the estimated model is able to predict the response values that **were not used in building the model** may be assessed. This is also known as *cross validation*. $PRESS$ is evaluated as follows:

$$PRESS = \delta^T \delta \tag{4.62}$$

where

$$\delta_i = y_i - \widehat{y}(i \,|\, 1, 2, \ldots, i-1, i+1, \ldots, n)$$

The term, $\widehat{y}(i \,|\, 1, 2, \ldots, i-1, i+1, \ldots, n)$, is the estimate of $\mathrm{E}\{y_i\}$ using a subset which excludes the i^{th} observation. A more efficient computing scheme for formulation of the $PRESS$ residuals utilises the variance of the predicted response:

$$\delta_i = \frac{\tilde{y}_i}{\sqrt{1 - Var(\widehat{y}_i)/\sigma^2}} \tag{4.63}$$

In matrix terms then, the prediction sum of squares may be written:

$$PRESS = \mathbf{1}^T[(\tilde{\mathbf{y}} \cdot \times \tilde{\mathbf{y}}) \cdot / \, (\mathbf{1} - \mathbf{Var}(\widehat{\mathbf{y}})/\sigma^2)] \tag{4.64}$$

where the vector, $\mathbf{1}$, is of length $[n \times 1]$.

$PRESS$ is sensitive to small numbers of large values and can focus attention on influential data points. It should be intuitively obvious that as the number of data points increases, $PRESS$ will approach RSS. As with the other criteria, a major disadvantage of $PRESS$ is that it does not provide any indication of the efficiency of the estimated model.

4. A basic descriptor of a stationary random process is the *autocorrelation coefficient*, $R_X(\tau)$ [20]. The autocorrelation coefficient calculated for an estimated model should ideally follow that for the measured data. Since the true coefficient cannot be determined from experimental data, one must consider two factors when evaluating an approximation. First, the data sample must have sufficient length and second, the sample must exhibit ergodicity. In other words, the sample must be representative of all possible samples. Hence, the autocorrelation coefficient should be treated cautiously when it has been evaluated for a small number of data points. $R_X(\tau)$ may be approximated by multiplying the time function, $X_T(t)$, by itself shifted τ units in time and then averaging:

$$\begin{aligned} R_X(\tau) &= \mathrm{E}\{V_X(\tau)\} \\ &= \mathrm{E}\{\frac{1}{T-\tau}\int_0^{T-\tau} X_T(t)\, X_T(t+\tau)dt\} \end{aligned} \tag{4.65}$$

For the discrete process with constant sampling rate, this can be estimated using:

$$\hat{R}_y(h) = \frac{1}{n-h}\sum_{i=1}^{n-h} y(i)\, y(i+h) \tag{4.66}$$

where h is the lag index. This formulation becomes cumbersome for large n though. Calculation of the autocorrelation coefficient is often more easily done using Fast Fourier Transforms (FFT's) via the relation:

$$\mathcal{F}\{R_X(\tau)\} = \mathrm{E}\{\frac{1}{T}\,|\mathcal{F}\{X_T(t)\}|^2\} \quad ; \quad T \to \infty \tag{4.67}$$

A convenient measure of the model's adequacy is the normalised representation, based on the residuals,

$$\frac{\hat{R}_{\tilde{y}}(h)}{\hat{R}_{\tilde{y}}(0)} = \frac{\sum_i\, \tilde{y}(i)\, \tilde{y}(i+h)}{\sum_i\, \tilde{y}(i)\, \tilde{y}(i)} \tag{4.68}$$

Assuming that the model is correct, this function should approach that for white noise with values of $\hat{R}_{\tilde{y}}(h)\,/\hat{R}_{\tilde{y}}(0) = 0$ for $h > 0$. It is therefore possible to utilise the point estimate, $\hat{R}_{\tilde{y}}(1)\,/\hat{R}_{\tilde{y}}(0)$, as a reflection of the colouring in the error, ε.

Several additional measures of accuracy, which require distributional assumptions, can also be utilised in the determination of a parsimonious model . These include:

5. F-statistic
6. Partial-F statistic

Both statistics were used in the previous Section in conducting various hypothesis tests on the model.

5. The computed value of the F statistic, which is equal to the ratio of the regression mean square to the residual mean square, should ideally have a maximum value. From Equation (4.53),
$$f = \frac{(n-p-1)}{p} \cdot \frac{\hat{\mathbf{y}}^T \hat{\mathbf{y}}}{\tilde{\mathbf{y}}^T \tilde{\mathbf{y}}} \tag{4.69}$$
This statistic has been recommended [67] for the selection of the "best" model from a set of data, since it takes into account not only the fit of the estimated response to the data, but also the number of terms in the model.

6. The *partial-F* statistic(s), which should also reach maximum values for an adequate model, are expressed:
$$f_p = (n-p-1) \cdot \frac{(\mathbf{X}^T\mathbf{X})_{jj}\theta_j^2}{\tilde{\mathbf{y}}^T \tilde{\mathbf{y}}} \tag{4.70}$$
Here, f_p is simply the inverse of the relative variance estimate for each parameter and as such, should reflect all significant contributions to the regression.

The last group of criteria involve direct examination of the residuals, $\tilde{y}(i)$. These reflect the amount of discrepancy between observed and predicted values, still present after having fitted the LS model. In other words, the residuals correspond to that variation which the regression has not been able to explain. Each $\tilde{y}(i)$ therefore represents an estimate of the corresponding error, $\varepsilon(i)$. Recall the assumptions made in Sections 4.2.1 and 4.2.4, concerning the unobserved error terms for regression analysis, requiring that they be independent, have zero mean, common variance, σ^2 and follow a normal distribution. If the model is indeed appropriate for the data under analysis, it is reasonable to expect that the observed residuals, $\tilde{y}(i)$, should exhibit properties that do not conflict with these assumptions. After examining the residuals, it should be possible to decide if the assumptions have been violated or not. The latter does not mean that the assumptions are correct; it merely means that, on the basis of the data seen, there is no reason to believe that they are incorrect. The basic strategy underlying the statistical procedure, generally referred to as *residual analysis*, is to assess the appropriateness of a model according to the behaviour of the residuals.

The following measures can be used in a residual analysis:

7. Residual mean and variance

8. Normal quantile-quantile plot

Expanding on these:

7. The residual mean is given by:

$$\bar{\tilde{y}} = \frac{1}{n}\tilde{\mathbf{y}} \tag{4.71}$$

and the residual variance, $s^2(\varepsilon)$, can be taken from the residual sum of squares:

$$s^2(\varepsilon) = \frac{\tilde{\mathbf{y}}^T\tilde{\mathbf{y}}}{(n-p-1)} \tag{4.72}$$

Each should be compared to independent unbiased estimates of the mean and variance, $\mu(\varepsilon) = 0$ and $\sigma^2(\varepsilon)$, respectively.

8. The normality of the residuals can be assessed through examination of a *normal quantile-quantile* plot. From the Central Limit Theorem, if the number of data points under analysis is large and the model is correct, then these residuals should approximate a Gaussian distribution. By plotting the distribution of residuals against a normal distribution, any errors will show up as deviations from the mean, indicating either a lack of data or an inadequate model. The normal quantile-quantile is also useful for identifying outliers and other irregularities in the data. Furthermore, the normality assumption made, in order to construct confidence intervals and test hypotheses, may be unjustified if this deviation is substantial. The main drawback of this criterion is that it involves subjective decision and should therefore be used only in conjunction with other criteria for determination of the model's accuracy.

The area under the normal distribution, $N(\mu, \sigma)$, from $-\infty$ to some point x_i is given by the *cumulative normal density function*. From Equation (4.12),

$$\Phi(x_i) = \frac{1}{\sqrt{2\pi}\sigma}\int_{-\infty}^{x_i} e^{-(1/2)\,[(x-\mu)\,/\sigma]^2}\,dx \tag{4.73}$$

which is equal to the probability that the variable, x will be less than x_i, $P(x < x_i)$. It immediately follows that:

$$P(x_i < x < x_{i+1}) = \Phi(x_{i+1}) - \Phi(x_i) \quad ; \quad \Phi(-\infty) = 0\,,\ \Phi(\infty) = 1 \qquad (4.74)$$

Now if there were n samples of the normal random variable, X available and the area under the normal density function was divided into the same number of equal areas, one might 'expect' that one observation would lie in each section so marked out. In order to compile a sequence of expected values from the distribution, the values of x defining the midpoint of each area must be evaluated. If each midpoint is denoted by x_i, for $i = 1, 2, \ldots, n$ then,

$$\Phi(x_{i+1}) - \Phi(x_i) = \frac{1}{n} \quad \text{and} \quad \Phi(x_1) = \frac{1}{2n} \qquad (4.75)$$

Consequently, the sequence of normally distributed values can be evaluated from the inverse of:

$$\Phi(x_i) = \frac{i - \frac{1}{2}}{n} \qquad (4.76)$$

That is,

$$x_i = \Phi^{-1}(\frac{i - \frac{1}{2}}{n}) \qquad (4.77)$$

for each section bounded by $\{x_i - \Phi^{-1}(\frac{i-1}{n}), x_i + \Phi^{-1}(\frac{i-1}{n})\}$, where Φ^{-1} is the inverse operator of the cumulative density function. Figure 4-4 illustrates the normal density functions and division of sections.

A plot of the estimated x_i against an ordered sequence of the residuals, $\tilde{y}_i$, will reveal a scatter of points which, for a normal distribution, should approximate a straight line. The intercept and slope of this line are equal to the sample mean and standard deviation of the observed errors, respectively. Any deviation from the linear trend can be easily identified and assessed.

Equipped with this collection of criteria, it should now be possible to examine the regression in detail and make informed decisions regarding its structure. The measures detailed above will provide indications of the estimated model's accuracy and significance. Moreover, they will reflect the accuracy and significance of each individual term in the model, enabling effective removal or addition as required.

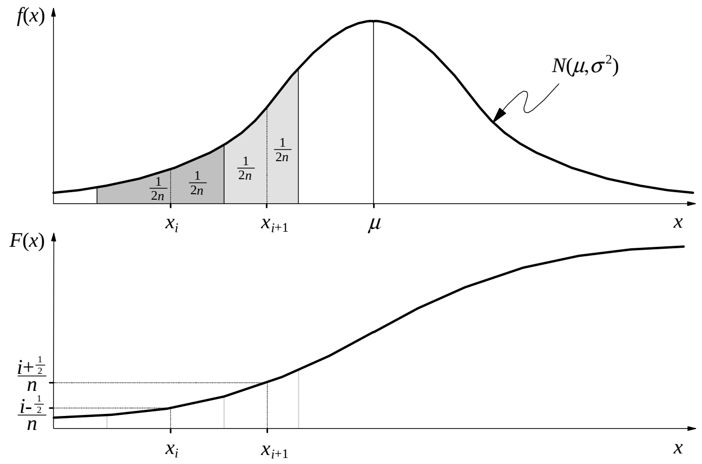

Figure 4-4: Division of normal distribution for quantile comparison

4.2.7 Dummy Variables

Up to this point, only continuous variables have been considered as predictors. However, regression analysis can be generalized to treat categorical predictors as well. This generalisation is based entirely on the use of *dummy variables*. A dummy variable is any variable that takes on a finite number of values so that different categories of nominal values can be identified. The values taken on by the dummy variable indicate no meaningful measurement, but rather the categories of interest.

One example of a dummy variable can be found in the attachment of the unit variable, X_0 to θ_0 in the original regression model. The X_0 is unnecessary, but provides a notational convenience at times. The linear model would then be expressed:

$$\mathbf{y} = \mathbf{X}\theta + \varepsilon \tag{4.78}$$

where

$$\mathbf{X} = \begin{bmatrix} 1 & x_{11} & x_{12} & \cdots & x_{1p} \\ 1 & x_{21} & x_{22} & \cdots & x_{2p} \\ \vdots & \vdots & \vdots & & \vdots \\ 1 & x_{n1} & x_{n2} & \cdots & x_{np} \end{bmatrix} \quad \text{and} \quad \theta = \begin{bmatrix} \theta_0 & \theta_1 & \theta_2 & \cdots & \theta_p \end{bmatrix}^T \tag{4.79}$$

Perhaps a more important use though, is in the analysis of categorical data. If a common model is to be identified, using blocks of data from several experiments, the matrix of independent variables can be augmented by dummy variables, $Z_1, Z_2, \ldots, Z_N$. For the i^{th} observation then, the regression model becomes:

$$y_i = \theta_{01} z_{i1} + \ldots + \theta_{0N}\ z_{iN} + \theta_1 x_{i1} + \ldots + \theta_p x_{ip} + \varepsilon_i \tag{4.80}$$

where

$$z_{ik} = \begin{cases} 1 & \text{if} \quad i \in \text{BLOCK } k \\ 0 & \text{otherwise} \end{cases} \tag{4.81}$$

and N is the number of data blocks. In matrix form, $\mathbf{Z}$ is of size $[n \times N]$ and θ_0, $[N \times 1]$.

$$\mathbf{Z} = \left[\begin{array}{ccccc} 1 & 0 & \cdots & \cdots & 0 \\ \vdots & \vdots & & & \vdots \\ 0 & 1 & 0 & \cdots & 0 \\ \vdots & \vdots & \vdots & & \vdots \\ 0 & \cdots & \cdots & 0 & 1 \\ \vdots & & & \vdots & \vdots \end{array} \right] \begin{array}{l} \left.\vphantom{\begin{array}{c}1\\ \vdots\end{array}}\right\} \text{BLOCK } 1 \\ \left.\vphantom{\begin{array}{c}1\\ \vdots\end{array}}\right\} \text{BLOCK } 2 \\ \qquad \vdots \\ \left.\vphantom{\begin{array}{c}1\\ \vdots\end{array}}\right\} \text{BLOCK } N \end{array} \quad \text{and} \quad \theta_0 = \left[\begin{array}{cccc} \theta_{01} & \theta_{02} & \cdots & \theta_{0N} \end{array} \right]^T \tag{4.82}$$

Augmenting the regression:

$$\mathbf{X} = \left[\begin{array}{cc} \mathbf{Z} & \mathbf{X} \end{array} \right] \quad \text{and} \quad \theta = \left[\begin{array}{c} \theta_0 \\ \theta \end{array} \right] \tag{4.83}$$

There are a number of alternative representations for the dummy matrix. The important thing to consider when choosing a particular representation, is that all categories in the model must be uniquely represented, without making the $\mathbf{X}^T\mathbf{X}$ matrix singular. Another application of this type of categorical estimation exists is in the determination of several models with similar characteristics, but differing offsets. In this situation, it may be advantageous to utilise various interaction terms, involving the dummy variables and then formulate appropriate hypothesis tests for comparison of the different models. The ease by which this can be performed is, perhaps, the biggest advantage in using dummy variables.

In many practical situations, notable trends occur in the response data. These may come about through variation with the predictors in the parameters, or the response itself.

That is, either $\theta(x)$ or $\mathbf{y}(x)$ may be categorised with respect to the predictors, $\mathbf{x}_i$. Generally speaking, these trends can be accounted for by using one or more suitably defined dummy variables. Appropriate model terms for these dummy variables are then added to the basic regression and the entire model is then fitted in a similar manner to that above.

When there are a number of trends in the model, a unique dummy variable must be set up for each. The problem may then be then divided, according to prior information concerning the model structure. There are essentially two cases:

i. When it is known which points lie on which trends and ;

ii. When it is *not* known.

The first case will now be examined in detail. Assuming that it is known not only which data points lie on which trends, but also where the trends intersect, then a composite model may be formulated. Substituting the dummy variables, $X_{1+}, X_{2+}, \ldots, X_{p+}$, for the usual independent variables, $X_1, X_2, \ldots, X_p$, yields the model:

$$y_i = \theta_0 + \theta_1 x_{i1+} + \ldots + \theta_p \, x_{ip+} + \varepsilon_i \tag{4.84}$$

for the i^{th} observation, where

$$x_{i\,j+} = \begin{cases} x_{i\,j} & \text{if} \quad i \in \text{BLOCK } j \\ 0 & \text{otherwise} \end{cases} \tag{4.85}$$

The matrix of regressors, $\mathbf{X}_+$, now has size $[n \times p]$:

$$\mathbf{X}_+ = \begin{bmatrix} x_{i1} & 0 & \cdots & \cdots & 0 \\ \vdots & \vdots & & & \vdots \\ 0 & x_{i2} & 0 & \cdots & 0 \\ \vdots & \vdots & \vdots & & \vdots \\ 0 & \cdots & \cdots & 0 & x_{ip} \\ \vdots & & & \vdots & \vdots \end{bmatrix} \begin{array}{l} \left.\vphantom{\begin{matrix} x \\ \vdots \end{matrix}}\right\} \text{BLOCK } 1 \\ \\ \left.\vphantom{\begin{matrix} x \\ \vdots \end{matrix}}\right\} \text{BLOCK } 2 \\ \qquad \vdots \\ \left.\vphantom{\begin{matrix} x \\ \vdots \end{matrix}}\right\} \text{BLOCK } p \end{array} \quad \text{and} \quad \theta = \begin{bmatrix} \theta_1 & \theta_2 & \cdots & \theta_p \end{bmatrix}^T \tag{4.86}$$

If instead, a set of parameters given by the vector, ψ, have been categorised with respect to one of the predictors, $\mathbf{x}_j$, the model becomes:

$$y_i = \theta_0 + \theta_1 x_{i1} + \ldots + (\psi_{1+} + \ldots + \psi_{N+})\, x_{i\,j} + \ldots + \theta_p x_{ip} + \varepsilon_i \tag{4.87}$$

where

$$\psi_{k+} = \begin{cases} \psi_k & \text{if} \quad i \in \textsc{block}\ k \\ 0 & \text{otherwise} \end{cases} \tag{4.88}$$

This can be effected by augmenting the matrix of regressors with another matrix, $\mathbf{X}_+$, of similar form to Equation (4.86) above, encompassing N blocks.

$$\mathbf{X} = \begin{bmatrix} \mathbf{X}_+ & \mathbf{X} \end{bmatrix} \quad \text{and} \quad \theta = \begin{bmatrix} \psi \\ \theta \end{bmatrix} \tag{4.89}$$

Figure 4-5 illustrates the response as estimated from a composite model in the variable $\mathbf{x}_j$. Three defining regions in this sub-model have been shown, each with a unique linear variation in x_j. Note that the intercepts, $x_{(1)}, x_{(2)} \ldots, x_{(N)}$, **must be pre-defined** before identification of the corresponding model can take place. If the exact location of the intercepts were not known, an additional set of dummy variables identical to those in Equation (4.81) would be needed, to account for the extra degrees of freedom introduced. However, the definition of each region in terms of the data infers that the location of each intercepts is approximately known and so, unless the exact locations are of interest, this further addition is unnecessary.

An alternative model representation can be utilised to produce the same fit:

$$y_i = \theta_0 + \theta_1 x_{i1} + \ldots + \sum_{k=1}^{N} \psi_{k+}\, \Delta x_{ik} + \ldots + \theta_p x_{ip} + \varepsilon_i \tag{4.90}$$

where the dummy variables,

$$\Delta x_{ik} = (x_{i\,j} - x_{(k)}) \tag{4.91}$$

and the parameters,

$$\psi_{k+} = \begin{cases} \psi_k & \text{if} \quad i \geq \textsc{block}\ k \\ 0 & \text{otherwise} \end{cases} \tag{4.92}$$

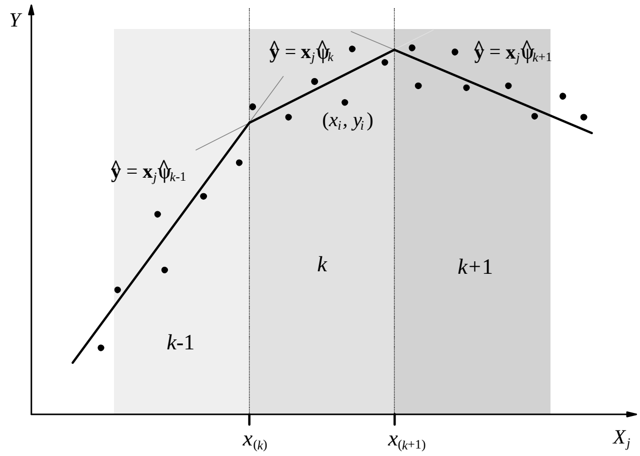

Figure 4-5: LS solution for a composite model using dummy variables

Subsequently, the matrix, $\mathbf{X}_+$ can be expressed:

$$\mathbf{X}_+ = \left[\begin{array}{ccccc} \Delta x_{i1} & 0 & \cdots & \cdots & 0 \\ \vdots & \vdots & & & \vdots \\ \vdots & \Delta x_{i2} & 0 & \cdots & 0 \\ \vdots & \vdots & \vdots & & \vdots \\ \vdots & \vdots & \vdots & & \Delta x_{iN} \\ \vdots & \vdots & \vdots & & \vdots \end{array} \right] \begin{array}{l} \left.\right\} \text{BLOCK } 1 \\ \\ \left.\right\} \text{BLOCK } 2 \\ \quad \vdots \\ \left.\right\} \text{BLOCK } N \end{array} \quad \text{and} \quad \psi = \left[\begin{array}{cccc} \psi_1 & \psi_2 & \cdots & \psi_N \end{array} \right]^T \tag{4.93}$$

When it is not known which points lie on which trends, a solution could be obtained by examining models constructed from every possible division of the points. However, for a composite model with trends in more than one variable, or with a large number of trends (or data points), this approach would be extremely difficult. In fact, unless the space of possible models were reduced substantially, an exhaustive search like this would be impossible in most cases. A far more efficient way of casting the problem would be to perform some nonlinear optimisation of the estimated model, based on a cost function which reflects the accuracy of the model, such as the residual error. Ultimately, one would like to achieve a result that is optimal not only with respect to the model's accuracy, but also in terms of the parsimony of the model structure.

4.3 Biased Estimation

Certain features of a regression analysis can result in numerical problems, which in turn lead to inaccurate estimates of the regression coefficients and their variance. These problems can be loosely grouped into one of two types: *scaling* and *collinearity.* Scaling pertains to the units in which the variables under study are measured and their means. Collinearity concerns the relationship between independent variables. Certain types of collinearity problems can be expressed as scaling problems and therefore easily resolved. These concepts will be expanded below and methods for dealing with these problems will be discussed in the following sections.

There are several ways in which the problem of data collinearity can be resolved. Some of these include the acquisition of more data, redesign of the experiment, model respecification and the use of alternative estimation techniques. For the purpose of this section, the discussion will be restricted to the latter two.

Application of the ordinary Least Squares technique to data which has some amount of collinearity among the independent variables will normally result in inaccurate estimates with large variances. The Least Squares technique provides an unbiased linear estimator which, according to Gauss-Markov theorem, has a minimum variance in the class of unbiased estimators. This variance need not be small, however, as illustrated in Figure 4-6. The unbiased estimate has a large variance, which infers a large confidence interval on θ. The biased estimate, in contrast, has a much smaller variance, though has been offset by some bias error, $(\mathrm{E}\{\hat{\theta}\} - \theta\,)$. The resulting mean square error of the biased estimate is:

$$\mathrm{E}\{\hat{\theta}_b - \theta\}^2 = \sigma^2(\hat{\theta}_b) + [\mathrm{E}\{\hat{\theta}_b\} - \theta\,]^2 \tag{4.94}$$

which may, in fact, be smaller than the Least Squares variance estimate, $\mathrm{E}\{\hat{\theta}\} = \sigma^2(\hat{\theta})$, if the error term is small. This property has motivated the development of various biased estimation techniques [61].

4.3.1 Scaling

A general class of problems in regression analysis may arise due to improper scaling of the predictors and/or the response variable. Specifically, such problems concern the loss of computational accuracy. The resulting inaccuracy can even be so great as to cause gross

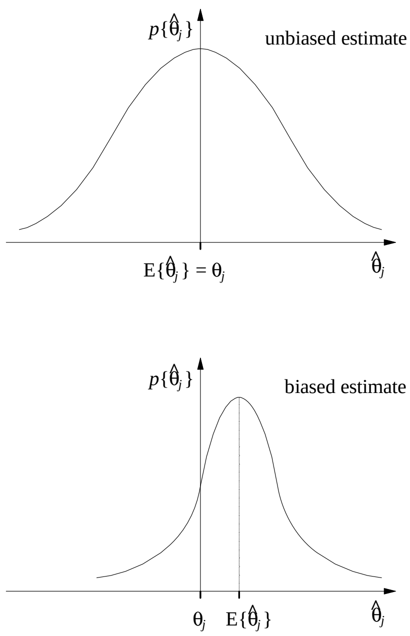

Figure 4-6: Distributions for typical unbiased and biased estimates

errors in the coefficient estimates. A scaling problem may also occur if a predictor has too wide a range of values. Most scaling problems can be avoided, however, by proper data validation and rescaling before performing regression analysis.

Often, scaling just refers to the multiplication of a variable by a constant, rather than multiplication and addition of constants. One important case of adding a constant - a form of scaling - is *centring*. Centring simply involves subtracting the mean, as in Equation (4.7):

$$\mathbf{X} \equiv \mathbf{X} - \mathbf{1}\bar{\mathbf{x}} \tag{4.95}$$

where the unit vector, $\mathbf{1}$, is of size $[n \times 1]$ and $\bar{\mathbf{x}}$ is $[1 \times p]$.

$$\bar{\mathbf{x}} = \frac{1}{n}\sum_{i=1}^{n}\mathbf{x}_i \tag{4.96}$$

Variables which have been *standardised*, are centred and scaled to unit length. 'Scaling to unit length' means adjusting the variables such that their sample variances equal 1.

Denoting the standardised matrix, $\mathbf{X}^*$, each variable is given by:

$$\mathbf{x}_j^* = \frac{\mathbf{x}_j}{s(\mathbf{x}_j)} \tag{4.97}$$

where the variance,

$$s^2(\mathbf{x}_j) = \frac{(\mathbf{X}^T\mathbf{X})_{jj}}{p} \tag{4.98}$$

One may then go about obtaining estimates from the standardised regression model:

$$\mathbf{y} = \mathbf{X}^*\theta^* + \varepsilon \tag{4.99}$$

Now if ${\mathbf{X}_j^*}^T \mathbf{X}_k^* = 0$ for $j \neq k$, the regressors are orthogonal and the matrix, ${\mathbf{X}^*}^T\mathbf{X}^*$, is diagonal. If the variables, $\mathbf{x}_j^*$, are linearly independent, then from Equation (4.13), the LS solution can be formulated:

$$\hat{\theta}^* = ({\mathbf{X}^*}^T\mathbf{X}^*)^{-1}\, {\mathbf{X}^*}^T\, \mathbf{y} \tag{4.100}$$

where ${\mathbf{X}^*}^T\mathbf{X}^*$ is the matrix of correlations with elements,

$$({\mathbf{X}^*}^T\mathbf{X}^*)_{jk} = \frac{\mathbf{x}_j^T\mathbf{x}_k}{\sqrt{(\mathbf{X}^T\mathbf{X})_{jj}(\mathbf{X}^T\mathbf{X})_{kk}}} \tag{4.101}$$

The original parameters are related to their standardised counterparts by:

$$\hat{\theta} = \frac{\hat{\theta}^*}{s(\mathbf{x}_j)} \tag{4.102}$$

4.3.2 Data Collinearity

For the general regression model, the variables, $\mathbf{x}_j$, are linearly independent only if the constants, k_j, do not exist, whereby:

$$\sum_{j=1}^{p} k_j\mathbf{x}_j = \mathbf{0} \tag{4.103}$$

If, however, Equation (4.103) does hold for some k, the rank of $\mathbf{X}^T\mathbf{X}$ will be less than p and $(\mathbf{X}^T\mathbf{X})^{-1}$ will not exist. In many practical applications of statistical regression, the assumption of linear independence is only approximately true, indicating that the problem of collinearity exists. In such a case, $\mathbf{X}^T\mathbf{X}$ is *ill-conditioned*, which can cause computational problems and reduce the accuracy of the estimates.

Some common sources of collinearity are:

- design of the experiment;
- constraints in the data; and
- model specification.

If the model is designed in such a way that the resulting data lies on a subspace close to the region defined by Equation (4.103), then collinearity might occur. This situation can arise if one or more of the variables, corresponding to those parameters being identified, were not sufficiently excited. Constraints in the data might come about through properties inherent in the system under observation. For example, a system in which various controls are activated in concert may be difficult to identify, since those controls will have a (near) linear dependence. Furthermore, an *over-parametrized* model can lead to collinearity problems. That is, a model comprising an excessive number of coefficients, in comparison to one that adequately describes the system response, based on the data available.

There are a number of procedures for the detection of collinearity. These include:

- examination of the correlation between variables; and
- eigensystem analysis and singular value decomposition

The response variable does not have any effect on collinearity and as such, one informative way to examine the problem is to regress the predictor variables on to one another. Consider p distinct models, each consisting of one predictor variable, acting as the response, and the remaining predictors as independent variables of the regression. That is, for the model:

$$\mathbf{y} = \theta_0 + \theta_1 \mathbf{x}_1 + \theta_2 \mathbf{x}_2 + \ldots + \theta_p \mathbf{x}_p + \varepsilon \tag{4.104}$$

the p models would be fitted as follows:

$$\begin{array}{lllllll}
\mathbf{x}_1 = \phi_{01} & & + \phi_{21}\mathbf{x}_2 & + \ldots & + \phi_{p1}\mathbf{x}_p & + \eta_1 \\
\mathbf{x}_2 = \phi_{02} & + \phi_{12}\mathbf{x}_1 & & + \ldots & + \phi_{p2}\mathbf{x}_p & + \eta_2 \\
\quad \vdots & \quad \vdots & \quad \vdots & & \quad \vdots & \quad \vdots \\
\mathbf{x}_p = \phi_{0p} & + \phi_{1p}\mathbf{x}_1 & + \phi_{2p}\mathbf{x}_2 & + \ldots & & + \eta_p
\end{array} \tag{4.105}$$

To assess collinearity, the correlation coefficients based on these models are needed - namely $R^2(\mathbf{x}_j|\mathbf{X}_R)$, where the reduced model, $\mathbf{X}_R = \begin{bmatrix} \mathbf{x}_1 & \cdots & \mathbf{x}_{j-1} & \mathbf{x}_{j+1} & \cdots & \mathbf{x}_p \end{bmatrix}$. Generalising Equations (4.105):

$$\mathbf{x}_j = \phi_{0j} + \mathbf{X}_R\phi_R + \eta_j \tag{4.106}$$

where the reduced parameter vector is denoted ϕ_R and the error in each predictor variable, η_j. If any of these multiple R^2 values equals unity, then a perfect collinearity is said to exist among the set of predictors. The term *collinearity* is used to indicate that one of the predictors is an exact linear combination of the others. Perhaps a more relevant concept though, is that of *near-collinearity*, which arises if one of the multiple R^2 values is close to unity. The *variance inflation factor, VIF*, is often used to measure collinearity in a multiple regression analysis. It may be computed for each variable as:

$$VIF_j = \frac{1}{1 - R_j^2} \tag{4.107}$$

where the squared multiple correlation coefficient,

$$R_j^2 = \frac{\widehat{\mathbf{x}}_j^T\widehat{\mathbf{x}}_j}{\mathbf{x}_j^T\mathbf{x}_j} \quad ; \quad 0 \leq R_j \leq 1 \tag{4.108}$$

The larger the value of VIF_j, the more highly correlated the variable X_j. A rule-of-thumb to keep in mind when examining the variance inflation factor is that a value exceeding 10 will generally indicate collinearity. This corresponds to R_j^2 equal to 0.9. In fact, the multiple R^2 coefficients can be used in place of VIF, since both hold exactly the same information.

Now if the predictor variables have been standardised, the variance inflation factors will be equal to the diagonal elements in the inverse correlation matrix, $(\mathbf{X}^{*T}\mathbf{X}^*)^{-1}$. Since the correlation matrix is unable to reveal the presence of several coexisting near dependencies among the regressors, though, its usefulness is limited. Moreover, its inverse and the variance inflation factor are similarly restricted in that they can only measure the correlation between individual regressors. One further drawback in employing VIF to detect collinearity is the lack of meaningful boundaries with which it can be compared. The value of 10, given above is only a rough guide to measure the strength of correlation and should not be used blindly.

A second way to avoid the impasse created by collinearity and near-collinearity is to use alternate computational methods in diagnosis. In particular, a popular method for characterising collinearities among the predictors involves an *Eigensystem analysis* of the correlation matrix. The eigenvalues and vectors are connected with the biased estimation technique described as *Principal Components* regression. This will be discussed in detail in the next section. The principal components of the predictors are a set of new variables that are linear combinations of the original predictors.

These components have the following properties:

a) they are uncorrelated with each other; and

b) each has a maximum variance, given that all are mutually uncorrelated.

The principal components provide idealised predictor variables that still retain all of the same information as the original variables. The eigenvalues correspond to the variances of these components. The larger the eigenvalue, the more important is the associated principal component in representing the information in the predictors. As an eigenvalue approaches zero, the presence of near-collinearity among the original predictors is indicated.

If a set of k predictor variables does not involve an *exact* collinearity, then k principal components are needed to exactly reproduce all of the information contained in the original variables. If one of the predictors is a perfect linear combination of the others, then only $(k-1)$ principal components are needed to provide all of the information in the original variables. The number of zero (or near-zero) eigenvalues is the number of collinearities (or near-collinearities) among the predictors.

In using the eigensystem to determine the presence of near-collinearity, three statistics are usually employed:

i. Condition number

ii. Condition index

iii. Parameter variance-decomposition proportions

Evaluation of the *condition number* requires decomposition of the correlation matrix as:

$$\mathbf{X}^T\mathbf{X} = \mathbf{T}\boldsymbol{\Lambda}\mathbf{T}^T \tag{4.109}$$

where $\boldsymbol{\Lambda}$ is a $[p \times p]$ matrix, whose diagonal elements are the eigenvalues, λ_j, of $\mathbf{X}^T\mathbf{X}$ and $\mathbf{T}$ is a $[p \times p]$ orthogonal matrix whose columns are the eigenvectors of $\mathbf{X}^T\mathbf{X}$. Now collinearity can be measured by the presence of small eigenvalues. Unfortunately, there is no specification of exactly what ‘small’ is. A relative measure such as the condition number often provides a more sound indication, however. This is defined as:

$$\kappa_j = \frac{\lambda_{\max}}{\lambda_j} \quad ; \quad j = 1, 2, \ldots, p \tag{4.110}$$

It has been recommended [175] that a value for κ_j of 1×10^3 or more reflects moderate to severe collinearity, worthy of further investigation.

An approach using singular-value decomposition (SVD) for diagnosing collinearity has also been proposed. This is based on the decomposition of the matrix $\mathbf{X}$ as:

$$\mathbf{X} = \mathbf{U}\,\mathbf{D}\,\mathbf{T}^T \tag{4.111}$$

where $\mathbf{U}$ is of size $[n \times p]$ and $\mathbf{U}^T\mathbf{U} = \mathbf{T}^T\mathbf{T} = \mathbf{I}$. The matrix $\mathbf{D}$ is a $[p \times p]$ diagonal matrix with non-zero diagonal elements, μ_j, which are called the *singular values* of $\mathbf{X}$. The singular-value decomposition is closely related to the concept of eigenvalues and eigenvectors, since by Equations (4.109) and (4.111),

$$\mathbf{X}^T\mathbf{X} = \mathbf{T}\,\mathbf{D}^2\mathbf{T}^T \tag{4.112}$$

The diagonal elements of $\mathbf{D}^2$ are therefore the eigenvalues of $\mathbf{X}^T\mathbf{X}$ and the columns of $\mathbf{U}$ are the eigenvectors. The degree of ill-conditioning depends on how small the singular value is, relative to the maximum singular value. In this context, a condition index of the matrix $\mathbf{X}$ has been proposed as:

$$\eta_j = \frac{\mu_{\max}}{\mu_j} \quad ; \quad j = 1, 2, \ldots, p \tag{4.113}$$

It was further suggested considering a value for μ_j of 30 to 100 as evidence of moderate to strongly collinear data. The SVD of the matrix $\mathbf{X}$ provides similar information to that given by the eigensystem of $\mathbf{X}^T\mathbf{X}$. The use of SVD is, however, preferred by many authors, mainly because of the greater numerical stability in its computing, compared to that of the eigensystem of $\mathbf{X}^T\mathbf{X}$. This may be especially relevant when $\mathbf{X}^T\mathbf{X}$ is ill-conditioned. On the other hand, computing problems associated with SVD may arise when the number of data points is large.

The *Parameter Variance Decomposition* approach utilises the variance proportions of the estimated regression coefficients to signify collinearity. From the covariance matrix of parameter estimates in Equation (4.21), it follows that

$$\mathbf{Cov}(\widehat{\theta}) = (\mathbf{X}^T\mathbf{X})^{-1}\sigma^2 = (\mathbf{T}\mathbf{D}^{-2}\mathbf{T}^T)\sigma^2 \tag{4.114}$$

Now the variance for each parameter may be expressed:

$$\sigma_j^2 = \phi_j\sigma^2 \tag{4.115}$$

where the variance ratio is simply the sum of each component:

$$\phi_j = \sum_{k=1}^{p} \phi_{jk} \tag{4.116}$$

and the k^{th} component of the variance decomposition for the j^{th} parameter,

$$\phi_{jk} = \frac{t_{jk}^2}{\mu_j^2} \tag{4.117}$$

Here, t_{jk} represents the elements of the eigenvector, $\mathbf{t}_j$, associated with λ_j. Equation (4.117) decomposes the variance of each parameter into a sum of components, each corresponding to one of the p singular values, μ_j. The singular values appear in the denominator, so one or more small singular values can substantially increase the variance of θ_j. This means that an unusually high proportion of the variance of two or more coefficients, for the same small singular value, can provide evidence that the corresponding near-dependency may cause problems. The k, j^{th} variance-decomposition proportion is given as:

$$\pi_{kj} = \frac{\phi_{jk}}{\phi_j} \quad ; \quad j = 1, 2, \ldots, p \tag{4.118}$$

Since two or more predictors are required to create near dependency, then two or more variances will be adversely affected by high variance-decomposition proportions, associated with each singular value. Variance-decomposition proportions greater than 0.5 have been recommended [15] as a guide for possible collinearity problems.

4.3.3 Principal Components Regression

The Principal Components (PC) approach [4] utilises a transformation of the original regressors, $\mathbf{x}_j$, on to the space of orthogonal variables, $\mathbf{z}_j$, in a Least Squares solution. These transforms are obtained from the eigenvalues and eigenvectors of the matrix, $\mathbf{X}^T\mathbf{X}$, yielding an orthogonal matrix:

$$\mathbf{Z} = \mathbf{X}\mathbf{T} \tag{4.119}$$

where $\mathbf{T}$ is obtained from Equation (4.109). The parameter vector must also be transformed via:

$$\gamma = \mathbf{T}^T\theta \tag{4.120}$$

and γ constitute the new model parameters. The regression model then becomes:

$$\mathbf{Y} = \mathbf{Z}\gamma + \varepsilon \tag{4.121}$$

with an LS solution given by:

$$\begin{aligned} \hat{\gamma} &= (\mathbf{Z}^T\mathbf{Z})^{-1}\mathbf{Z}^T\mathbf{y} \\ &= \mathbf{\Lambda}^{-1}\mathbf{Z}^T\mathbf{y} \end{aligned} \tag{4.122}$$

since the matrix of eigenvalues, $\mathbf{\Lambda} = \mathbf{T}^T\mathbf{X}^T\mathbf{X}\mathbf{T}$. The columns of $\mathbf{Z}$ defining a new set of orthogonal variables are referred to as principal components. In order to formulate a principal components estimator, only the r terms corresponding to the **largest eigenvalues** are included. Therefore, if each matrix in the transformed model is arranged according to the decreasing order of eigenvalues and the last $(p-r)$ columns are eliminated, the parameter vector becomes:

$$\gamma_R = \begin{bmatrix} \gamma_1 & \gamma_2 & \cdots & \gamma_r \end{bmatrix}^T \quad \text{where} \quad \lambda_1 \geq \lambda_2 \geq \ldots \geq \lambda_r \geq \ldots \geq \lambda_p \tag{4.123}$$

which is estimated by:

$$\hat{\gamma}_R = \mathbf{\Lambda}_R^{-1}\mathbf{T}_R^T\mathbf{X}^T\mathbf{y} \tag{4.124}$$

The subscript, R, denotes the reduced model comprising variables $\mathbf{z}_1, \mathbf{z}_2, \ldots, \mathbf{z}_r$. By removing the trailing $(p-r)$ terms from the model, the rank of the original regressor matrix, $\mathbf{X}$, has been effectively reduced to r. The original set of parameters can now be evaluated through a linear combination of the transformed parameters:

$$\hat{\theta}_{PC} = \mathbf{T}_R \hat{\gamma}_R \tag{4.125}$$

In fact, the model need not be reduced until this final step, since the variables are orthogonal and so, the presence of less terms has no bearing on the estimates. Denoting the eliminated sub-model by the subscript S , it can be shown that the amount by which the PC parameter estimates have been biased is equal to $\mathbf{T}_S \gamma_S$. That is,

$$\mathrm{E}\{\hat{\theta}_{PC}\} = \theta - \mathbf{T}_S \gamma_S \tag{4.126}$$

where the eliminated parameter vector,

$$\gamma_S = \begin{bmatrix} \gamma_{r+1} & \cdots & \gamma_p \end{bmatrix}^T \tag{4.127}$$

If the error, ε, is assumed to have zero mean and variance, σ^2, then the covariance matrix for the LS estimates of θ are:

$$\begin{aligned} \mathbf{Cov}(\widehat{\theta}_{LS}) &= (\mathbf{T}\mathbf{\Lambda}^{-1}\mathbf{T}^T)\sigma^2 \\ &= (\mathbf{T}_R\mathbf{\Lambda}_R^{-1}\mathbf{T}_R^T + \mathbf{T}_S\mathbf{\Lambda}_S^{-1}\mathbf{T}_S^T)\sigma^2 \end{aligned} \tag{4.128}$$

from Equation (4.21). Comparing this with the covariance matrix for the PC estimates:

$$\mathbf{Cov}(\widehat{\theta}_{PC}) = (\mathbf{T}_R\mathbf{\Lambda}_R^{-1}\mathbf{T}_R^T)\sigma^2 \tag{4.129}$$

confirms that this biased technique will result in a decrease in the variance of the parameter estimates. The diagonal elements of the matrix, $\mathbf{T}_S\mathbf{\Lambda}_S^{-1}\mathbf{T}_S^T$, can be considered as weighted sums of the inverse of the eigenvalues associated with the eliminated principal components. If these eigenvalues are small, a substantial reduction in the variance of the PC estimates can be expected.

In practical application of this technique, the problem of deciding how many principal components should be eliminated may arise. This could be answered by using one of the diagnostic measures discussed in the Section 4.3.2, or by examination of commonly used Least Squares criteria, such as s^2, R^2 and others. Another possibility is to apply a *backward* *elimination* procedure (*see* Section 4.4.3) to the transformed regression. This procedure sequentially reduces the model by eliminating variables with non-significant partial-F values, until a satisfactory form is reached. Recall that f_p is based on the inverse of the parameters' estimated variance. Hence, those transformed variables corresponding to small eigenvalues (and large variances) will tend to be eliminated from the regression. Once again, the assumption of normality must be made in order to formulate the F statistic and perform the hypothesis tests. This may be a more desirable approach, though, since the reduced model is ultimately based on the statistical significance of each of the principal components.

4.3.4 Mixed Estimation

Mixed Estimation (ME) is a Bayes-like technique which uses prior information concerning the parameters to augment the measured data. Starting from the usual regression model, Equation (4.9),

$$\mathbf{y} = \mathbf{X}\theta + \varepsilon \tag{4.130}$$

it is assumed that the errors follow $\mathrm{E}\{\varepsilon\} = 0$ and $\mathrm{E}\{\varepsilon\varepsilon^T\} = \mathbf{I}\sigma^2$. It is further assumed that the set of prior conditions on θ can be written:

$$\mathbf{a} = \mathbf{P}\theta + \zeta \tag{4.131}$$

where $\mathbf{a}$ is a $[p \times 1]$ vector of specified values, $\mathbf{P}$ is a square matrix, $[p \times p]$, of known constants and ζ is a conforming vector of random variables with $\mathrm{E}\{\zeta\} = 0$ and $\mathrm{E}\{\zeta\zeta^T\} = \mathbf{S}$. The weighting matrix, $\mathbf{S}$, can be formed as a diagonal, with its nonzero elements expressing the uncertainty in the prior values.

The new model is obtained by combining Equations (4.130) and (4.131):

$$\begin{bmatrix} \mathbf{y} \\ \mathbf{a} \end{bmatrix} = \begin{bmatrix} \mathbf{X} \\ \mathbf{P} \end{bmatrix} \theta + \begin{bmatrix} \varepsilon \\ \zeta \end{bmatrix} \tag{4.132}$$

Applying Least Squares to the augmented model yields the mixed estimate:

$$\hat{\theta}_{ME} = [\frac{1}{\sigma^2}\mathbf{X}^T\mathbf{X} + \mathbf{P}^T\mathbf{S}^{-1}\mathbf{P}]^{-1}[\frac{1}{\sigma^2}\mathbf{X}^T\mathbf{Y} + \mathbf{P}^T\mathbf{S}^{-1}\mathbf{a}] \tag{4.133}$$

which, if the exact form of Equation (4.131) is known, will be optimal and unbiased.

In real application of the mixed estimation, however, the prior information is usually not known exactly. In this case,

$$\mathbf{a} = p_0 + \mathbf{P}\theta + \zeta \tag{4.134}$$

where p_0 is some unknown vector. The expected value of $\hat{\theta}$ is then obtained by substituting Equations (4.130) and (4.134) into (4.133):

$$\mathrm{E}\{\hat{\theta}_{ME}\} = \theta + [\frac{1}{\sigma^2}\mathbf{X}^T\mathbf{X} + \mathbf{P}^T\mathbf{S}^{-1}\mathbf{P}]^{-1}[\mathbf{P}^T\mathbf{S}^{-1}p_0] \tag{4.135}$$

defining the quantity by which the mixed estimate is biased. The covariance matrix for the mixed estimates is:

$$\mathbf{Cov}(\widehat{\theta}_{ME}) = [\frac{1}{\sigma^2}\mathbf{X}^T\mathbf{X} + \mathbf{P}^T\mathbf{S}^{-1}\mathbf{P}]^{-1} \tag{4.136}$$

and the covariance of the LS estimate can also be expressed:

$$\mathbf{Cov}(\widehat{\theta}_{LS}) = [\frac{1}{\sigma^2}\mathbf{X}^T\mathbf{X}]^{-1} \tag{4.137}$$

Therefore, since the matrix, $\mathbf{P}^T\mathbf{S}^{-1}\mathbf{P}$, is non-negative definite, the addition of prior information to the ordinary regression will result in a reduction of variance in the LS estimates. As with the Principal Components technique, this reduction in variance will affect any confidence intervals and hypothesis tests made on the variables. Considering the partial-F statistic, for example, the value calculated for a biased variable would be larger than that if the variable was unbiased, according to the ratio $\theta_j/s^2(\theta_j)$. Subsequent hypothesis tests conducted using this statistic would therefore favour the alternative result, $\theta_j \neq 0$, thus retaining the corresponding parameter in the model. This is an important influence and should be kept in mind, particularly when using model selection procedures, such as *stepwise regression*, as described in Section 4.4.

The restrictions on the parameters given by Equation (4.131) can take several forms. One of the most common is expressed in terms of a separate estimate,

$$\theta_0 = \theta + \zeta \tag{4.138}$$

in which case, the vector, $\mathbf{a} = \theta_0$ and $\mathbf{P} = \mathbf{I}$.

A more difficult entity to quantify is the weighting matrix. For the above restriction,

$\mathbf{S} = \mathrm{E}\{\zeta\zeta^T\}$ should reflect the expected covariance of θ_0. One formulation utilises the LS covariance estimate:

$$\mathbf{S} = \mathbf{V}\,(\mathbf{X}^T\mathbf{X})^{-1}\mathbf{V}\,\sigma^2 \quad ; \quad 0 \leq \mathbf{V}_{jj} \leq 1 \tag{4.139}$$

Here, $\mathbf{V}^2$ is a $[p \times p]$ diagonal matrix, with non-zero elements equal to the fraction of each LS parameter variance estimate that the ME parameter variances are expected to have. If the parameters are to be biased equally, $\mathbf{V}^2$ will just be the identity multiplied by some constant. Obviously, this formulation should not be used if the mixed estimation procedure is being used to alleviate collinearity problems, since it employs the inverse of the matrix, $\mathbf{X}^T\mathbf{X}$. In this case, it would be best to first standardise the predictors and use a standard weighting matrix,

$$\mathbf{S} = \mathbf{V}^2\sigma^2 \tag{4.140}$$

4.3.5 Restricted Estimation

In some situations, the model will have inherent restrictions on its parameters, which must be accounted for in any estimation procedure. This (additional) prior information can also be used in a regression analysis of collinear data to improve the estimates obtained. Suppose the constraints are of the form:

$$\mathbf{C}\theta = \mathbf{d} \tag{4.141}$$

where $\mathbf{C}\,[q \times p]$ and $\mathbf{d}\,[q \times 1]$ are both specified. Then it is possible to use *Lagrange Multipliers* to minimise the function:

$$\begin{aligned} \mathbf{f}(\theta, \lambda) &= (\mathbf{y} - \mathbf{X}\theta)^T(\mathbf{y} - \mathbf{X}\theta) + \lambda^T(\mathbf{d} - \mathbf{C}\theta) \qquad (4.142) \\ &= \mathbf{y}^T\mathbf{y} - 2\theta^T\mathbf{X}^T\mathbf{y} + \theta^T\mathbf{X}^T\mathbf{X}\theta + \lambda^T\mathbf{d} - \theta^T\mathbf{C}^T\lambda \end{aligned}$$

in which the vector, $\lambda\,[q \times 1]$, is unknown. Differentiating partially with respect to θ and setting the results to zero provides p equations:

$$\frac{\partial}{\partial\theta}\,\mathbf{f}(\theta, \lambda) = -2\mathbf{X}^T\mathbf{y} + 2(\mathbf{X}^T\mathbf{X})\theta - \mathbf{C}^T\lambda = \mathbf{0} \tag{4.143}$$

These, along with an additional q equations:

$$\mathbf{d} - \mathbf{C}\hat{\theta}_C = \mathbf{0} \tag{4.144}$$

provide $(p+q)$ equations, which can be solved for the unknowns, θ and λ. Rearranging Equation (4.143):

$$\hat{\theta}_C = (\mathbf{X}^T\mathbf{X})^{-1}[\mathbf{X}^T\mathbf{y} + \frac{1}{2}\mathbf{C}^T\lambda] \tag{4.145}$$

and substituting into Equation (4.144) gives:

$$\mathbf{d} - \mathbf{C}[(\mathbf{X}^T\mathbf{X})^{-1}\mathbf{X}^T\mathbf{y} + (\mathbf{X}^T\mathbf{X})^{-1}\frac{1}{2}\mathbf{C}^T\lambda] = \mathbf{0}$$

$$\lambda = 2[\mathbf{C}(\mathbf{X}^T\mathbf{X})^{-1}\mathbf{C}^T]^{-1}(\mathbf{d} - \mathbf{C}\hat{\theta}_{LS}) \tag{4.146}$$

where $\hat{\theta}_{LS} = (\mathbf{X}^T\mathbf{X})^{-1}\mathbf{X}^T\mathbf{y}$ is the usual unrestricted estimate. The solution for $\hat{\theta}_C$ is then obtained through Equation (4.145):

$$\hat{\theta}_C = \hat{\theta}_{LS} + (\mathbf{X}^T\mathbf{X})^{-1}\mathbf{C}^T[\mathbf{C}(\mathbf{X}^T\mathbf{X})^{-1}\mathbf{C}^T]^{-1}(\mathbf{d} - \mathbf{C}\hat{\theta}_{LS}) \tag{4.147}$$

If instead, the constraints have a simpler form, given by

$$\begin{bmatrix} \mathbf{C}^T & \mathbf{0} \end{bmatrix} \theta = \theta \tag{4.148}$$

where $\mathbf{C}\,[q \times p : q < p]$ is non-trivial and $\mathbf{0}$ is a $[p \times (p-q)]$ matrix of zeros, a solution can be obtained from the reduced model:

$$\mathbf{y} = \mathbf{X}_C\,\theta + \varepsilon \tag{4.149}$$

This is achieved by substituting the regressor matrix, $\mathbf{X}_C = \mathbf{X}\mathbf{C}^T$ into the Least Squares formulation:

$$\begin{aligned} \hat{\theta}_C &= \mathbf{C}^T(\mathbf{X}_C^T\mathbf{X}_C)^{-1}\mathbf{X}_C^T\mathbf{y} \\ &= \mathbf{C}^T[\mathbf{C}(\mathbf{X}^T\mathbf{X})\mathbf{C}^T]^{-1}\mathbf{C}(\mathbf{X}^T\mathbf{X})\hat{\theta}_{LS} \end{aligned} \tag{4.150}$$

The matrix, $\mathbf{X}_C$, is of size $[n \times q]$ and effectively reduces the number of degrees of freedom in the regression by $(p-q)$. By constraining the parameters corresponding to collinear variables, any linear dependencies can be removed from the normal equations. However, as with Mixed Estimation, the drawback in using this method to alleviate the effects of problematic data is the requirement for prior information, which may not be available. Restricted Estimation is most often used to implement *hard* constraints in the model, derived from known properties of the system under analysis.

4.4 Model Structure Determination

The general problem of model selection in the context of regression analysis can be stated as follows:

> *"Given a response variable, Y and a set of k predictor variables, $X_1, X_2, \ldots, X_k$, we wish to determine the 'best' subset of the k predictors and the corresponding best-fitting regression model for describing the relationship between Y and the variables, X_j."*

What exactly is meant by "best" depends, in part, on the overall goal for modelling. One goal is to find a model that gives the best prediction of Y, given X_j for some new set of observations. Using this goal, one might say that the best model is *reliable* if it predicts well in a new sample. The details of the model may be of little or no consequence, such as the inclusion of any particular variable or the even magnitude or sign of its regression coefficient.

In addition to the question of prediction is that of validity. That is, obtaining accurate estimates for one or more regression coefficients in a model and then making inferences concerning the parameters of interest. The goal here is to quantify the relationship between one or more independent variables of interest and the dependent variable, after accounting for the other variables.

In this section, strategies for selecting the best model will be dealt with, when the primary goal of analysis is prediction.

4.4.1 Selecting the Best Regression

In selecting the best regression equation, the following steps should be taken:

1. Postulate a set of *candidate variables*
2. Specify a number of criteria for the selection of a model
3. Define a strategy for model structure determination

4. Conduct the analysis

5. Validate the model chosen

All possible models can be formed from the set of candidate predictor variables. The *maximum model* is defined to be the largest model considered at any point in the process of model selection, with k parameters ($p \leq k$). However, the largest model may not necessarily be the best with respect to the accuracy criteria of step 2.

There are many reasons for choosing a large number of candidate variables. The most important one is to avoid making a Type II (false negative) error. In regression analysis, a Type II error corresponds to omitting a predictor that has a significant regression coefficient in the population. Another reason for considering a large candidate variable set is to include all conceivable basic and higher-order predictors, transformations and interactions among the predictors.

Now *overfitting* a model, or including terms in the model that are nonsignificant, will not introduce bias when estimating the regression coefficients if the usual LS assumptions are met. However, the analyst must be careful that overfitting does not introduce harmful collinearity. On the other hand, *underfitting* (leaving important predictors out of the final model) **will** introduce bias in the estimated coefficients.

There are also several reasons for working with a conservative number of candidates. If the goal is prediction, the need for reliability strongly argues for a small model and with a validity goal, usually only a few important variables are of interest. In either case, it is advisable to avoid a Type I (false positive) error. A Type I error in a regression analysis corresponds to the inclusion of a predictor that has a nonsignificant regression coefficient. The desire for *parsimony* is another valid reason for choosing a conservative model. Largely unimportant but statistically significant predictors can greatly confuse the interpretation of regression results; complex interaction terms are particularly troublesome in this regard.

The sample of data to be analysed imposes certain constraints on the choice of a candidate variable set. In general, the smaller the sample size, the smaller the number of candidates should be. A larger number of independent observations are needed to reliably estimate a larger number of regression coefficients. The most basic constraint is that the number of error degrees of freedom be positive, requiring $(n-p-1) > 0$ for n observations and $(p+1)$ predictors, including the intercept. One reasonable suggestion is to have at least 10 observations per predictor, namely, require that $n \geq 10p$.

Another constraint on the set of candidate variables concerns the amount of variability present in the predictor values, considered either individually or jointly. If a predictor has a constant value (excluding the error) for all observations, then it obviously cannot be used in any model.

Lastly, polynomial terms and other transformations merit particular consideration, since near collinearities can lead to unstable and often uninterpretable results when attempting to find the best model. Consequently, one should make an effort to reduce such collinearity if possible. Standardising the predictors, if applicable, almost always helps to increase numerical accuracy.

If the collinearity problem cannot be dealt with effectively, then one should either:

- conduct separate analyses for each form of the regression;
- eliminate troublesome variables; or
- impose some structure on the model.

The second step in selecting the best model is to specify the selection criterion. A *selection criterion* is an index that can be computed for each postulated model and subsequently used for comparison. Thus, given one particular selection criterion, candidate models can be ordered according to their accuracy. This helps to automate the process of choosing the "best" model. This selection-specific process may not find the best model in a global sense, however, it can substantially reduce the work involved in finding an *adequate* model.

Many selection criteria for choosing the best model have been successfully employed. Three of these will now be examined:

1. The sample squared multiple correlation coefficient, R^2 is a natural choice for deciding which model is best. Unfortunately, R^2 has some potentially misleading characteristics. First, it tends to overestimate the true correlation, ρ^2. Second, adding predictors, even useless ones, can never decrease R^2. In fact, adding regression terms will invariably increase its value. Hence, R^2 will always be largest for the maximum model, even though a better model may be obtained by deleting some variables. Such a reduced model may indeed be better, because it may sacrifice only a negligible amount of predictive strength while simplifying the model structure substantially.

2. A much better criterion for selecting the best model is the F statistic, since it conveys the same information as the squared multiple correlation coefficient, as well as accounting for the size of the model. Therefore, an increase in R^2 resulting from the addition of a variable to the regression, will not necessarily lead to an increase in F. This can be illustrated by the fact that, for $n \gg p$, the F statistic is approximately proportional to some function of R^2, divided by the number of parameters. From Equation 4.54:
$$F = \frac{(n-p-1)}{p} \cdot f\left(R^2\right) \tag{4.151}$$

3. If all regressions are done on a large problem, an assessment of the average magnitude of the residual mean square, s^2, as the number of variables in the regression increases sometimes indicates the best cutoff point. The fitting of regression equations that involve more predictor variables than are necessary to obtain a satisfactory model has been described as overfitting. As more predictor variables are added to the already overfitted model, the residual mean square will tend to stabilise and approach the true value of σ^2, provided that all important variables have been included and the number of observations greatly exceeds the number of variables in the fitted equation. This situation is illustrated in Figure 4-7.

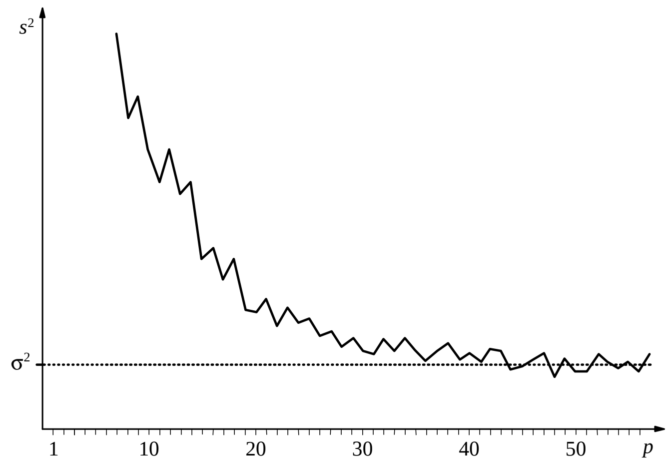

Figure 4-7: Overfitting as the number of model parameters is increased

For small sets of data one cannot expect this idea to work as effectively, of course, but it may provide a helpful first guideline. The procedure basically gives an asymptotic estimate of σ^2 with which a model can be chosen, whose residual variance is acceptable, containing the fewest predictor variables needed to achieve that.

4. An alternative statistic which has gained popularity in recent years is the C_p statistic, initially suggested by C.L. Mallows [28]. This has the form:

$$C_p = \frac{\tilde{\mathbf{y}}^T\tilde{\mathbf{y}}}{s_k^2} - [n - 2(p+1)] \tag{4.152}$$

where $\tilde{\mathbf{y}}^T\tilde{\mathbf{y}}$ is the residual sum of squares for a model containing $(p+1)$ parameters, including θ_0 and s_k^2 is the residual mean square for the maximum model, presumed to be a reliable unbiased estimate of the error variance, σ^2. C_p is closely related to the R^2 coefficient through

$$C_p = (n-k-1)\cdot\frac{(1-R^2)}{(1-R_k^2)} - [n - 2(p+1)] \tag{4.153}$$

Now, if a model with p parameters is adequate, that is, does not suffer from a lack of fit, then $\mathrm{E}\{\tilde{\mathbf{y}}^T\tilde{\mathbf{y}}\} = (n-p-1)\,\sigma^2$. Since it is also assumed that $\mathrm{E}\{s_k^2\} = \sigma^2$ is approximately true, then the ratio, $\tilde{\mathbf{y}}^T\tilde{\mathbf{y}}/s_k^2$, has an expected value of $(n-p-1)$ and ultimately,

$$\mathrm{E}\{C_p\} = (p+1) \tag{4.154}$$

for an adequate model. It follows that a plot of C_p versus $(p+1)$ will show up any adequate models. Conversely, the quantity, $(C_p - p - 1)$ should approach zero under the same conditions above. One quotation from an article of Mallows stated:

> *"The C_p coefficient cannot be expected to provide a single best equation when the data are intrinsically inadequate to support such an inference."*

Nor, for that matter, can *any* of the other selection criteria. All selection procedures are essentially methods for the orderly display and review of the data. Applied with common sense, they can produce useful results; applied thoughtlessly and/or mechanically, they may be useless or even misleading.

The third step in choosing the best model is to specify a strategy for selecting the variables. Such a strategy is concerned with determining how many variables and also, which particular variables, should be in the final model. Traditionally, such strategies have focused on deciding whether a single variable should be added to the current model, or if one should be removed.

4.4.2 Exhaustive Search

Whenever practical, an *Exhaustive Search* - a procedure involving all-possible regressions - should be preferred over any other variable selection strategy. It is the only method guaranteed to find the model with the largest R^2, the smallest s^2 and so on. This strategy is not always used, because the amount of calculation necessary becomes impractical if the number of variables, k, in the maximum model is large. The exhaustive search requires that each regression equation be fit with every possible combination of the k independent variables. Hence, the total number of equations that must be examined is equal to $(2^k - 1)$.

Once all models have been fitted, they may be assembled into sets of equal model size and then ordered within each set, according to some criterion: F_p, for example. The partial-F values are based on the mean square error for each model as if the corresponding variable were added to the regression last. Tests employing such statistics should be treated with some caution, however. Any test based on a model with fewer terms than the correct model will be biased - perhaps seriously - because the test involves the use of biased terms. Overall F tests are also affected by the estimate of the error variance used. In variable selection, this estimate is important, because biased tests conducted early in a selection algorithm may stop the procedure prematurely and miss important predictors.

The all-possible regressions procedure has the distinction of being the only method guaranteed to find the best model, in the sense that any selection criteria will be numerically optimised for the particular sample under study. Naturally, this does not guarantee that the *correct* model has been found. In fact, in many situations, several reasonable candidates for the best model can be found, with different selection criteria suggesting different models. Furthermore, such criteria may vary from sample to sample, even though all the samples are chosen from the same population. Consequently, the choice for the best model can also vary from sample to sample.

As mentioned above, the exhaustive search algorithm is often impractical, since $(2^k - 1)$

models must be fitted when k candidate predictors are being evaluated. As computationally feasible alternatives, many methods have been suggested to approximate the all-possible regressions procedure. These methods are not guaranteed to find the best model. Nevertheless, they can glean essentially all of the information in the data needed to choose one.

4.4.3 Backward Elimination

In the *Backward Elimination* procedure, the following steps are taken:

Step 1. Determine the fitted regression equation containing all independent variables.

Step 2. Calculate the partial-F statistic for every variable in the regression, as though it were the last variable to enter.

Step 3. Compare the value of the *lowest* observed partial-F value, say f_L, with a preselected critical value of the F-distribution. That is, test for the significance of the corresponding independent variable.

a) If $f_L < F(1, \nu_2, 1-\alpha_p)$, remove the variable under consideration from the model, compute the regression equation for the remaining variables and return to *Step 2*.

b) If $f_L > F(1, \nu_2, 1-\alpha_p)$, adopt the complete regression equation as calculated.

This is a satisfactory procedure - much more economical of computer time than the *Exhaustive Search* method. However, if the input data yields an $\mathbf{X}^T\mathbf{X}$ matrix that is ill-conditioned, then the overfitting equation may be meaningless due to rounding errors. Another drawback of this procedure is that once a variable has been eliminated from the model, it will not be used again. Thus, all alternative models using the eliminated variables are never encountered.

4.4.4 Forward Selection

The *Forward Selection* procedure acts in reverse to the previous method. The basic steps include:

Step 1. Select as the first variable to enter the model, that most highly correlated with the response and then fit the resulting regression equation.

Step 2. Evaluate the importance of those variables not yet in the regression via their partial correlations with the response, or their partial-F statistics. If no candidate variables remain, terminate the process with the current model.

Step 3. Test for the significance of the partial-F statistic associated with the variable deemed most important (with highest partial correlation or partial-F) in *Step 2.*, f_H.

a) If $f_H < F(1, \nu_2, 1-\alpha_p)$, terminate the process with the current model.

b) If $f_H > F(1, \nu_2, 1-\alpha_p)$, add the respective variable to the regression equation and return to *Step 2.*

It is possible to use the partial-F statistics in *Step 2.* to determine the importance of the remaining variables since, from Equation (4.59),

$$f_p = \frac{(n-p-1)}{1} \cdot \frac{r_j^2}{(1-r_j^2)} \tag{4.155}$$

where $r_j^2 \equiv r^2_{y,x_j \,|\, X_R}$, the partial correlation of $\mathbf{x}_j$, given the *reduced* model, X_R. This avoids the need to compute the partial correlations - the partial-F values are used to determine both the insertion order and each variable's significance. However, the use of Equation (4.57) to calculate f_p in *Step 2.* is impractical, because each variable is effectively added to the model in order to determine which variable should be added to the model first! Perhaps a more efficient way is to first calculate the partial correlations via Equation (4.35) and then use the above expression in partial-F tests for the most highly correlated variables(s) to evaluate their significance. It is only necessary to test the variable with the highest partial correlation in *Step 3.*, since for $0 \leq r_j^2 \leq 1$, the function for f_p is monotonically increasing. So if f_H proves non-significant, any partial-F values based on smaller partial correlations will also be non-significant.

4.4.5 Stepwise Regression

Stepwise Regression [30] is a modified version of the Forward Selection procedure that permits re-examination, at every step, of the variables incorporated in the model from previous steps. A variable that entered at an early stage may become superfluous at a later stage because of its relationship with other variables subsequently introduced. To check on this possibility, at each step a partial-F test for every variable already in the model is made as though it were the most recent variable introduced, regardless of its actual entry point into the model. If any variables are found to have non-significant partial-F values, they are removed from the regression. If the model is fully significant, partial correlations for each remaining candidate variable are obtained and examined - the most important being added to the regression. The new model is then refitted and the process is repeated until no more variables are entered or removed.

By placing less restriction on the rejection level, that is, by increasing α_p, the stepwise program will accept several additional variables beyond what would be accepted with more conservative schemes. This allows the investigation of additional variables that would not have otherwise been included and hence, alternative models with similar predictive characteristics.

The stepwise procedure can be initialised with any model; there is no requirement to begin with the one independent variable most highly correlated with the response. By the same token, however, the use of different initial models in the procedure will not necessarily lead to the same final model. In other words, the model resulting from a stepwise procedure depends, in part, on the starting point in the iteration. For this reason, a good model to start with is one in which the analyst has a high confidence. The assumption being that the final model will basically be a reduction or extension of the initial model, rather than an entirely different one. In any case, the final model will have a higher probability of obtaining a certain state if the initial model is chosen near that state, than if the initial model is chosen as otherwise. One should be careful not to include too many terms in the initial model since a fully non-significant model, using all candidate variables, will terminate the selection process unless appropriate measures have been implemented.

A flowchart of the Stepwise Regression procedure is illustrated in Figure 4-8.

4.4.6 Analysis and Validation

Having specified the candidate variables, the criterion for selecting variables and a strategy for applying that criterion, the analysis must then be conducted as planned.

It has been shown that a model based exclusively on the statistical significance of individual parameters can still include too many terms [115]. Therefore, it is recommended that a number of quantities and their variations be looked at, for the selection of an adequate model. For each model in the selection procedure, several criteria including those presented

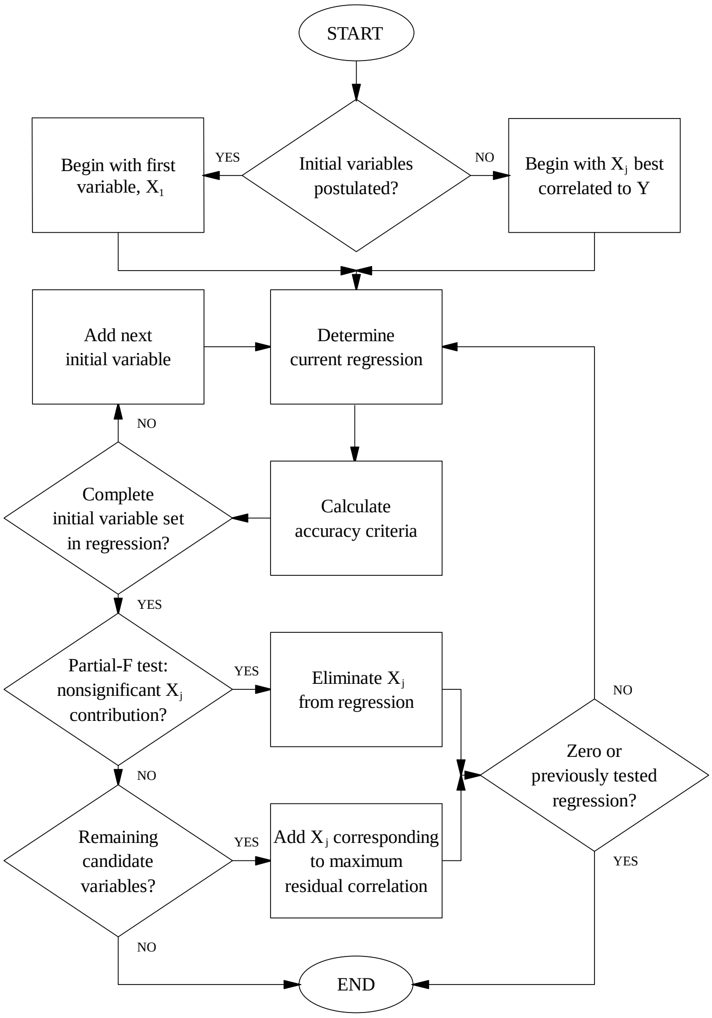

Figure 4-8: Flowchart of the Modified Stepwise Regression procedure

in Section 4.2.6, can be calculated and stored for examination at the procedure's conclusion. As with all of the approaches discussed, shrewd judgement is still required in the initial selection of variables and in the critical appraisal of the model through examination of the residuals.

The most compelling way to assess the reliability of a chosen model is to conduct a new study and test the fit of that model to the new data. However, this approach is often expensive and sometimes intractable. The question then arises as to whether a single study can achieve the two goals of finding the best model and assessing its reliability. A *split-sample analysis* provides a means of achieving this by dividing the sample data into two groups: the first is utilised for identification and is called the *training* group; the second is for verification, called the *holdout* group. Various methods for dividing the population into groups exist and can be either randomly or deterministically assigned. It is also viable to swap the two groups and perform a second identification/verification, comparing the estimated models. Typically, any difference in the predictor variables chosen by the two selection processes is taken as an indication of unreliability. In practice, the two models will almost always differ by some amount, which is the primary reason that model selection methods have a reputation for being unreliable.

The above approach for assessing reliability is far too stringent when prediction is the goal. More realistically, a good predictive model should:

- predict as well in any new sample as it does in the sample at hand; and
- pass all regression diagnostic tests for model adequacy applied to any new sample.

In order to address the more modest goal of prediction, the squared multiple correlation coefficients, R^2_T and R^2_H, can be compared, where T denotes the training group and H the holdout group. Both R^2 statistics are based on correlations between the true response and estimated response, using the model estimated in the training region only. R^2_H is referred to as the *cross-validation correlation.*

Depending upon the situation, using only half of the data for the training sample analysis may be inadvisable. A useful rule is to increase the relative size of the training sample as the total sample size decreases and to decrease the relative training size as the total sample size increases. In general, the splitting proportion should be tailored to the problem under study.

Another statistic which provides a good indication of the model's predictive capacity is the *prediction sum of squares*, described earlier in Section 4.2.6. This measure sums the single-point residuals predicted by n unique models; each model being estimated from training groups of $n-1$ observations and the remaining observation constituting the holdout group.

4.5 Concluding Remarks

In this chapter, a number of aspects of the identification process have been addressed, starting with the standard multiple linear regression. Using an analysis of variance approach, it was possible to examine the regression equation in detail and derive several useful quantities. The multiple and partial correlation coefficients were also evaluated, for subsequent use in correlation analysis and parameter selection, respectively.

In order to construct confidence bounds, the assumption of normally distributed errors was imposed. Using statistical t and F distributions, the individual and joint confidence regions were formulated and the problem of collinearity addressed. A useful measure of the 'skewness' of the joint confidence ellipsoid was introduced from previous use in output error methods. The normality assumption also allowed two hypothesis tests to be devised: the F test, for assessing the significance of overall regression; and the partial-F test, which provides judgment on the significance of individual terms.

A collection of accuracy and significance criteria were then outlined to aid in the assessment of the estimated model. These included a number of measures, such as the prediction sum of squares and autocorrelation coefficient, as well as the F statistic and partial-F statistic mentioned above. In addition, the normal quantile-quantile plot was described for illustration of the prediction error's normality.

Various uses of dummy variables in the regression were explored, including the implementation of a simple unit variable in order to concurrently estimate the offset term in the equation. Also, dummy variables defined by *blocks* were presented for the analysis of categorical data. As alluded to in this section, the regression model can be expressed in a form similar to that of a spline function and may therefore be utilised for the estimation of coefficients represented in this way.

Collinearity can prove a major problem in any type of identification. Highly correlated variables can be difficult for the estimator to discern between and consequently, can lead to near-singularities in the solution. In the section on collinearity, several methods for its detection were outlined. One such method used an eigen-system analysis to reveal small eigenvalues and possibly problematic data. The Principal Components regression was based on a similar decomposition and therefore able to reduce the adverse effect of collinear variables. In this procedure, the regressors are transformed into orthogonal components and the smallest eigenvalue removed before estimation takes place.

Another biased technique examined was the Mixed Estimation procedure. Unlike the previous method, this technique can be employed to bias specific coefficients in the model, regardless of their contribution. The main drawback of using this, however, is that prior estimates of the coefficients and a weighting matrix must first be supplied.

The last main section covered model structure determination. That is, determining the "best" model from a set of candidate variables. In defining the problem, the concepts of undermodelling and overmodelling were considered, similar to the simplifying assumptions of the last chapter. Several of the parameters outlined above were also suggested as possible selection criteria from which an adequate model could be resolved.

Of the determination procedures examined, the Stepwise Regression was found to be the most efficient. Essentially, it involves an iterative process in which variables are sequentially added to, or removed from the regression. The order of insertion is governed by their partial correlations, while the criterion for elimination is the partial-F value for each. Clearly a better procedure than either Backward Elimination or Forward Selection techniques, Stepwise Regression augmented with additional criteria has been used successfully in many different applications. The Exhaustive Search procedure was also examined and although it proved more burdensome, it was able to provide an extensive coverage of the model space.

Chapter 5

Analysis of Flight Data

5.1 Introduction

Before identification of the F-111C aircraft model could take place, the flight-data required a considerable amount of pre-processing. The purpose of this chapter is to outline the flight-testing and data processing undertaken, as well as formulate various procedures for determination of the model structure.

The first section covers the testing program and preliminary analysis, conducted prior to the current research. A number of corrections were made to the data in this analysis, before a linear model was estimated using an output error technique.

In the second section, all data pre-processing and examination that was performed in the current research is detailed. This incorporated:

- Extraction and conversion of the stability and control derivatives from the F-111C aerodynamic database;
- Frequency analysis of the flight-data and subsequent estimation of the measurement noise variance;
- Removal (replacement) of outliers;
- Correction for phase lags unaccounted for in the preliminary analysis; and
- Assessment of collinearity amongst the variables.

Much of the initialisation was done in MATLAB using the script, `F111_INI.M`.

Since the data were to be partitioned in order to estimate a nonlinear model for each case, a partitioning scheme and corresponding identification strategy were required. The various schemes examined are detailed in the last section and have been divided into two cases: when it is known which data points lie in which regions; and when it is not known. One way in which the knots can be positioned is to manually place them at critical points, as defined by previously obtained models. Another is to place a number of knots in the model and then examine the significance of the parameters associated with each piecewise region. Lastly, three nonlinear optimisation techniques are trialed, with both simulated and real flight-data and their relative performance assessed.

5.2 F-111C Flight Testing and Preliminary Analysis

In 1987, a series of flight tests were performed on the F-111C aircraft at the RAAF's Aircraft Research and Development Unit. In a general examination of the aircraft's flight characteristics, the data obtained from the tests were processed and analysed at the Aeronautical Research Laboratory (ARL), as detailed in reference [26]. This report described all data handling procedures, pre-analysis flight data processing as well as the methods used to make corrections to the air-sensor measurements.

The resulting aerodynamic coefficients were used to validate a comprehensive flight dynamic model of the F-111C, developed at ARL.

5.2.1 Test Aircraft and Instrumentation

The F-111C aircraft was extensively modified with flight test quality instrumentation and data recording equipment. On-board digital magnetic-tape recording was complemented by data telemetry for real-time flight test monitoring. The instrumentation was developed for flight-dynamic measurements and was capable of recording up to 200 signals at a sampling frequency of 60 Hz. A Nose Boom Transducing Unit (NBTU) used in the second phase of the trials was designed to provide high quality measurements of pitot pressure, angle-of-attack, sideslip angle and linear accelerations. General details of the acquisition units, including their ranges and accuracies are provided in Table B.1.

5.2.2 Flight Test Program

The flight test program was carried out in two phases. The matrix of test points examined from *phase 1* and *phase 2* is given in Table B.3. The first phase covered 75 test conditions of varying wing-sweep, altitude and Mach number. At each test point, two longitudinal and two lateral manoeuvres were performed. The flow angles in this phase were obtained from transducers in the aircraft's Central Air Data System (CADS). For the second phase of the program, the NBTU was available for these measurements. A number of test points were repeated in order to compare measurements from the CADS and NBTU systems. The remaining tests were made at Mach numbers between those tested in *phase 1* to provide a more comprehensive data coverage.

The manoeuvres were designed to produce optimal responses for the determination of the linear stability and control derivatives, using a Maximum Likelihood technique (*see next section*). Advice provided by NASA Dryden personnel indicated that large, rapid control inputs were necessary to provide large amplitude excitation of the aircraft's natural modes with the automatic flight control system engaged. The Dryden Flight Research Center had previously conducted their own investigation [86] of the F-111A aircraft's flight characteristics under the Transonic Aircraft Technology (TACT) program.

Several manoeuvres were also flown with the aircraft in landing and takeoff (flaps deployed) configurations. The current research was restricted to clean-wing configurations, however, so these cases were not examined.

5.2.3 Flight Data Processing

Prior to analysis, the input data required additional processing in the form of various measurement corrections and appropriate formatting. The calculations included:

- Compensation of airspeed, Mach number and altitude for pressure errors and compressibility effects at the pitot-static sensor locations;
- Application of time-shifts to the time history records to account for instrument signal conditioning and recording lags;
- Evaluation of the pitch and roll control (elevator and aileron equivalent) deflections from the measured differential-stabilator deflections; and

- Calculation of the weight, centre of gravity (cg) position and moments of inertia from the fuel tank contents data.

An approach utilised for identifying the relative time lags between instrumentation channels was developed at ARL and documented in reference [18]. The data compatibility procedure was applied to a number of selected cases to determine the lag parameters, which are summarised in Table B.2. According to the results, the NBTU angle-of-attack signal lead the control deflection signals by 2 sample periods, indicating that this unit had a smaller delay than the *phase 1* instrumentation.

In addition to determining the pressure error corrections for airspeed and altitude, it was necessary to calculate the position errors, or calibration constants, for the angle-of-attack and sideslip angle transducers. In particular, the aircraft CADS transducers, mounted close to the forward fuselage, were affected by the local flow. A flight path reconstruction method, based on an extended Kalman filter [157, 158], was used to determine the calibration constants. The CADS sideslip angle sensor, used in *phase 1*, overestimated the true value by 50 to 60%, indicating strong cross flow in that region. As expected, however, the NBTU gave a more accurate estimate of the sideslip angle, overreading by only 10 to 20%. The errors were subsequently corrected for, prior to estimation of the aerodynamic coefficients. While some small variations were found to occur in the angle-of-attack scale-factor with Mach number and sweep angle, they were not well defined within the accuracy of the data, so constant values were used with differences of no more than 10% for both phases.

5.2.4 Parameter Estimation

For analysis of the F-111C data, a Maximum Likelihood technique was used [150]. *A-priori* information for the technique was obtained using the ARL six degree-of-freedom flight dynamic model.

Within the range of flight conditions tested, it was assumed that the aircraft motion would be adequately represented by separate linear flight dynamic models for the longitudinal and lateral motion. Both longitudinal and lateral flight dynamic models used for this purpose were derived assuming small disturbance motion and linear aerodynamic characteristics.

The Maximum Likelihood program used a Newton-Raphson search algorithm to iterate to a converged solution. To assist the identification procedure, particularly for those derivatives which made only a small contribution to the aircraft motion, *a-priori* information was used. A facility was also implemented to constrain selected parameters to either their prior values or other model parameters.

A comprehensive set of results was compiled in reports [31] and [32]. Later, modifications were made [37] to the flight dynamic model in a validation of its properties. The main objective of this was to combine the modified aerodynamic database with the existing model of the flight control system to give a better representation of the measured flight behaviour.

Generally, a good correlation between calculated and measured responses was obtained. In some cases, however, discrepancies appeared in the estimated parameters, resulting in poor response predictions. This was especially prominent in the yawing moment derivatives and several of the rolling moment derivatives. Unfortunately, these reports were classified as RESTRICTED and hence, a critical review of the estimates presented was not possible.

5.3 Data Pre-processing

5.3.1 Conversion of the Model Coefficients

The first step in preparing the coefficient data was to convert it from the form in which it was stored, to one suitable for analysis and comparison in MATLAB. For each flight case, the wing-sweep, cg position and flight-identified derivatives were initially read from file. Trim variables including the altitude, Mach number, angle-of-attack and control deflections were also read, in order to define each particular flight condition. With this information, it was then possible to extract the relevant coefficients from the F-111C wind-tunnel model database.

The database comprises rigid-body stability and control derivatives, along with "flexibility factors" for a range in each control deflection, angle-of-attack, Mach number, altitude and wing-sweep. The flexibility factors, which can be effectively added to the corresponding derivatives, account for aeroelastic deformation of the airframe. They are the only coefficients affected by dynamic pressure and thus, if removed, a rigid model independent of altitude would result. At any flight condition, the coefficients may be evaluated via an n^{th} order linear interpolation on the database, where the order varies according to the number of associated variables. Thus, a linear model can be constructed with the derivatives obtained for one set of trim conditions and a nonlinear model can be constructed using the derivatives from a range of conditions.

In Chapter 3, the general form of the F-111C aircraft model was presented. Each coefficient, apart from the spoiler contribution, was initially represented by a polynomial spline function of the angle-of-attack. The lateral spoiler contribution terms were represented by tensor-product splines in spoiler deflection and angle-of-attack. Adopting this formulation in the construction of a base wind-tunnel model, the derivatives were all evaluated over a range of angle-of-attack: $\alpha = [0, 4, 8, 12, 16]^\circ$. The spoiler contribution was also evaluated over a range of spoiler deflection, given by $\delta_s = [0, 10, 20, 30, 45]^\circ$, resulting in 25 explicitly defined points.

Each of the coefficients in the wind-tunnel database was referred to a centre of gravity located at 45 % MAC, 117.5 in.WL. Consequently, the next step in initialising the data entailed adjusting those coefficients to their flight cg values. By doing this, the wind-tunnel coefficients could be compared directly with those identified from flight data.

Lastly, the aircraft weight and inertias for each case were read from file, completing the set of data that defined the corresponding model. This information was saved in a binary format `.MAT` file for effective use in MATLAB.

5.3.2 Frequency Analysis

When ascertaining information about a system from measured data, it is always a good idea to examine the data content in the frequency domain as well as the time domain. High-frequency dynamics can often go unnoticed and consequently, are not implemented in the time-based dynamic model. More importantly, unwanted noise can sometimes contaminate the signals to the point that no cohesive model can be identified. In aircraft, external disturbances such as turbulence and engine noise occur frequently and their influence, if significant, may distort the estimated model.

A rudimentary frequency analysis was conducted on the F-111C flight data, as an important step in the processing prior to identification. For the majority of the following procedures, various functions included in the MATLAB *Signal Processing Toolbox* [144] were utilised.

All of the flight data sequences recorded on the F-111C were examined with regard to their frequency content and any notable features accounted. A plot of the power spectrum, estimated for each channel, revealed the natural frequencies associated with characteristic modes of the aircraft. For example, the power spectral density of the sideslip angle in

Figure 5-1 indicates a low-frequency narrowband signal, corresponding to the dutch-roll mode, in a background of wide-band noise. The peak occurs close to 0 Hz - the actual dominant frequency is about 0.22 Hz - with a smaller, almost indistinguishable peak at approximately 13 Hz. This secondary peak is caused by the fluctuating pressure of the local flow and is considerably more prominent in the angle-of-attack reading. Obviously, the CADS instrumentation employed in this flight case has been affected by local flow disturbances. However, the effect on β is small enough to be neglected, since it is of the same order as that due to the wideband noise. The Nyquist rate, equal to 30 Hz, represents the highest frequency of information that can be extracted from the sequence.

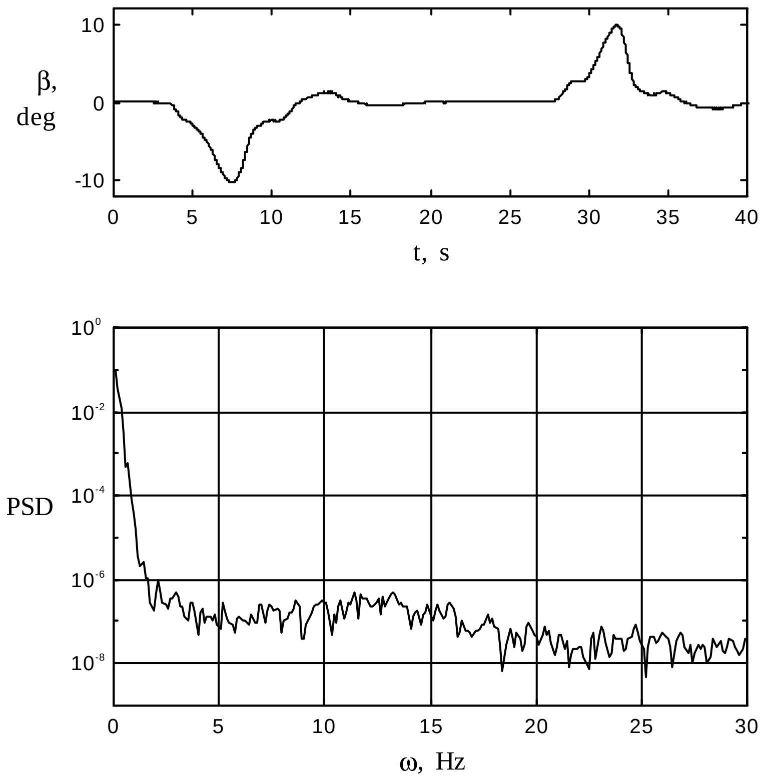

Figure 5-1: Time-history and spectra of the sideslip angle signal

The F-111C flight data were not filtered since, among other reasons, filtering necessarily involves the loss of information from the data [228]. A number of factors, which might have prompted filtering include:

- one or more corruptive disturbances produced by sources of known behaviour;

- an excessive level of noise in the data (In the equation-error model, those signals to be utilised as independent variables are of particular importance); and
- the need for a lower sampling rate, thus reducing the number of data points to a manageable size.

There was no serious amount of noise in the flight data, nor was there any need to reduce the sampling rate and so the data were left unaltered. A filtered copy of the data was used, however, for two purposes. The first was to replace any data that had been removed because of inconsistencies (drop-outs, spikes, etc.) and the second, to provide an initial estimate of the error variance. Data outliers and their removal will be discussed in the next Section. In this section, the characteristics of the filter employed will be looked at, as well as the formulation of the error variance.

Filtering, in general, does not require any information concerning the underlying structure of the system that has been measured. In order to remove all variation in the data which is not associated with the rigid-body aircraft response, the spectral content must first be assessed. From examination of the frequency spectrum in various F-111C flight data cases, it became clear that the aircraft response had a narrow bandwidth, with an upper limit of approximately 3 Hz. It was therefore decided that the filter to be applied should remove any noise *above* this frequency. Since the required specifications were somewhat "loose", a Butterworth IIR filter, which is often used in similar circumstances, was deemed sufficient. The filter order was chosen by close examination of the filtered response and corresponding spectral density. In summary, a 4^{th} order lowpass Butterworth filter with 3 Hz cutoff frequency was chosen and applied through the function, `BUTTER.M`, in MATLAB.

The main disadvantage in using standard causal filtering, such as type IIR filters, is their inherent phase distortion which can be highly nonlinear. There is a well known trick in signal processing, though, which can be used to eliminate this problem. Since the data is not being filtered in real-time, access is available to the entire sequence. It can therefore be filtered twice - first in the forward direction and then in the reverse - producing a sequence with exactly zero phase and the square of the filter's magnitude effects. `FILTFILT.M` performs this function satisfactorily, whilst also minimising any filter start-up transients.

As a demonstration of the Butterworth filter, applied to flight data, the raw and filtered yaw-acceleration signals from one test case are illustrated in Figure 5-2.

It can be deduced from these plots that there is a large proportion of moderate- to

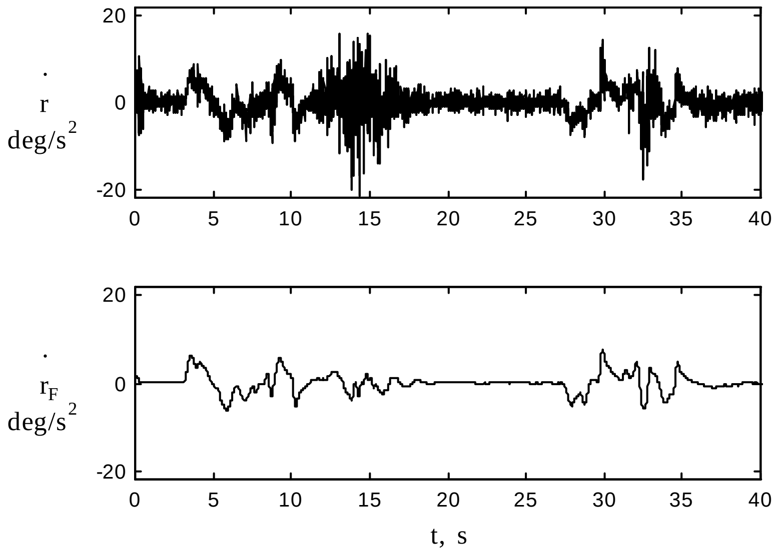

Figure 5-2: Yaw acceleration signal filtered at 3 Hz

high-frequency noise resident in the yaw-acceleration signal. This proportion will now be evaluated, using variance estimates of the response and error for several relevant channels. The estimate of the error covariance is obtained by

$$\mathbf{g}^T\mathbf{g} = \frac{(\mathbf{x} - \mathbf{x}_F)^T(\mathbf{x} - \mathbf{x}_F)}{n-1} \tag{5.1}$$

where $\mathbf{x}$ and $\mathbf{x}_F$ represent the raw and filtered signals, respectively. Dividing each diagonal element of $\mathbf{g}^T\mathbf{g}$ - the variance estimates - by the corresponding filtered response variance estimates yields the noise-to-signal ratios shown in Table 5.1.

The high variance ratio for $\dot{r}$ confirms the level of noise seen in its response and far exceeds that for any of the other channels considered. This should not have any significant effect on the identification of linear model parameters, as long as a substantial length of data is utilised. In fact, it is only in the dependent variables, a_y, $\dot{p}$ and $\dot{r}$, that any serious amount of noise exists and consequently, all LS estimates should have very little bias. However, if the data is subdivided or shortened in any way, the estimates may become quite inaccurate. This may become evident in the determination of a nonlinear model from partitioned data subsets.

Channel	Variance Ratio,%
α	0.05
β	0.00
p	0.01
r	0.02
ϕ	0.01
a_y	1.69
$\dot{p}$	2.36
$\dot{r}$	176.74

Table 5.1: Noise-to-signal variance estimates

5.3.3 Outliers

The next step in pre-processing the flight data entailed the removal of any outliers, which might otherwise affect the identification adversely. The term "outliers" covers any anomalies in the data which generally lie outside the expected range of variation. These include gross errors such as spikes and drop-outs as well as more subtle deviations. Outliers can be caused by external disturbances, faults in the instrumentation or errors in the acquisition and storage of data.

In the preparation of the F-111C data for identification, any discrepancies in the recordings were not removed as such. Rather, they were replaced by their corresponding filtered response values, thus maintaining a constant sampling rate. This is actually not a requirement for identification using the equation error approach, as time is not taken into account. It is critical, though, in other approaches that utilise the system dynamics, such as the Maximum Likelihood technique. It is also desirable to have a complete run of data for subsequent comparison of the identified model response.

Firstly, any gross errors lying outside each sensor's range, summarised in Table B.1, were replaced. The same was then done to any *extraneous* points in the data. It is actually quite difficult, however, to define exactly what extraneous points are. A good starting point can be found in the limiting form of a normally distributed finite data sequence.

From Section 4.2.6, the extreme points in such a sequence will most probably lie at:

$$x_n = \pm F^{-1}(\frac{n - \frac{1}{2}}{n}) \tag{5.2}$$

where F^{-1} is the inverse of the cumulative normal distribution function:

$$F(x_i) = \frac{1}{\sqrt{2\pi}\sigma} \int_{-\infty}^{x_i} e^{-(x-\mu)/2\sigma^2}\, dx \tag{5.3}$$

It is important to remember that this value only provides an *estimate* of the extreme points, under the assumption of normality. In reality, they may well exceed this and therefore, a buffer of some form should be added. After a number of trials, an additional space of two standard deviations was decided upon, which typically excluded 1 % of the data. That is, approximately 1 % of the points in each data set, comprising 16 channels, were considered to be outliers.

5.3.4 Phase Shifts

In the initial data-processing program conducted at ARL, a number of channels were corrected for time lags induced by the instrumentation. Some important channels which were not examined, such as the roll- and yaw-accelerations, were subsequently found to have significant lags.

A simple compatibility check was performed for these accelerations in each flight case by comparing their integrals against the corresponding angular rates. The phase shift, restricted to a discrete number of time samples, was estimated via a minimisation of the cost function:

$$J(h, n) = \frac{1}{n-1}\, \xi^T \xi \tag{5.4}$$

In continuous form, the error in the roll-acceleration, for example, may be expressed:

$$\xi(t, h) = \int_0^t \dot{p}(\tau)\, \mathrm{d}\tau - p(t + h.\Delta t) \quad ; \quad h = \ldots -1, 0, 1, 2, \ldots \tag{5.5}$$

which is a function of the integer, h. If a phase difference was identified, the length of the entire data set was reduced accordingly. On average, the angular accelerations lagged the rates by the number of samples shown in Table 5.2.

No further compatibility checks [40, 42, 43, 118] were undertaken on the flight data,

Channel	*phase 1*	*phase 2*
$\dot{p}$	5	5
$\dot{q}$	3	–
$\dot{r}$	4	3

Table 5.2: Angular accelerometer time lags

because the procedure is essentially an identification in itself, which would invariably result in manipulation of the data. Data compatibility checks in general, tend to be extremely difficult, requiring simplifications and often subjective input to the problem at hand. The estimation of states, along with bias and offset terms, can easily involve as much effort in tailoring the problem as the model identification. Any errors then, brought about by the compatibility check, would manifest themselves in later estimates, possibly misleading the analyst. In summary, such checks need only be performed if significant bias or scale factor errors in the data are suspected. It was therefore decided to leave the F-111C flight data unmodified in this respect.

5.3.5 Collinearity

Prior to identification analysis, the flight data were also checked for possible sources of collinearity, which might affect the results adversely. The (mostly) lateral variables to be used as regressors in the equation-error model were examined using several measures, as described in Section 4.3.2. These included the correlation matrix, variance inflation factors, condition indices and variance-decomposition proportions.

Several cases exhibited an extremely high collinearity between the independent variables, though most had only a moderate amount of collinearity. An example from one of the more highly correlated cases will now be discussed in more detail.

Flight P1F7E21 ($\Lambda = 35°$, 10000 ft, Mach 0.4) consisted of combined inputs in differential-stabilator and rudder, as did the majority of flight tests performed for estimation of the lateral model. Figure 5-3 illustrates the lateral response and control inputs.

The number of data points acquired was around 1200, taken over 20 seconds. For an assessment of direct collinearity between the variables, the correlation matrix, R, and its determinant were evaluated using standardised regressors. These are shown in Table 5.3.

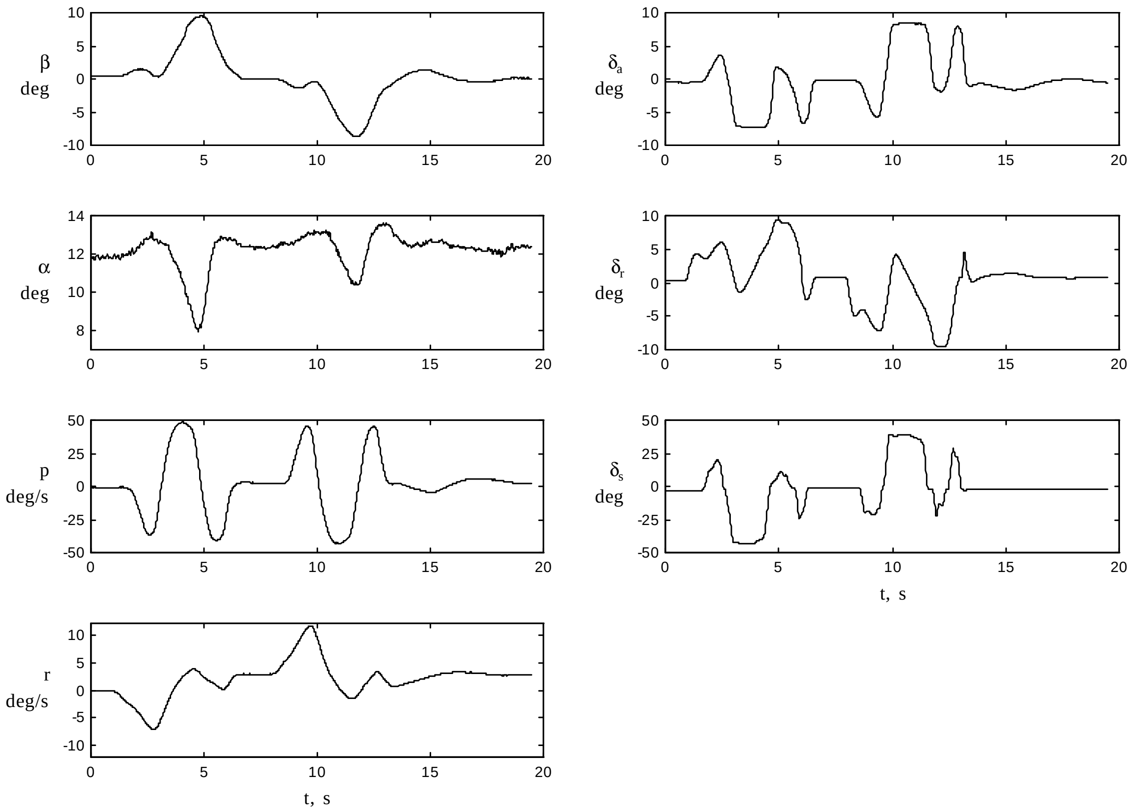

Figure 5-3: Flight P1F7E21 lateral state and control variables

Correlation Matrix : det = 0.0039							
	β	α	$pb/2V_1$	$rb/2V_1$	δ_a	δ_r	δ_s
β	1.0000	−0.2847	0.1933	0.3355	−0.4553	0.7453	−0.3249
α		1.0000	−0.1617	−0.0915	0.1193	−0.1663	0.1325
$pb/2V_1$			1.0000	0.5051	−0.5739	−0.3502	−0.5366
$rb/2V_1$				1.0000	−0.2107	−0.0823	0.0157
δ_a					1.0000	0.0622	0.9038
δ_r						1.0000	0.0943
δ_s							1.0000
Variance Inflation Factors							
	11.3290	1.1382	2.9273	2.7528	9.7073	9.0000	8.4884

Table 5.3: Correlation matrix of lateral variables

The matrix is dominated by a simple correlation of 0.9038 between differential-stabilator and spoiler deflections, (δ_a, δ_s), indicating a high amount of collinearity. An additional source of collinearity, though not as prominent, can also be seen between the sideslip and rudder deflection. The low value for the correlation matrix determinant reinforces the fact that there could be a possible problem with collinearity. Generally speaking, large variance inflation factors point to collinearity, although there are no meaningful boundaries, so it is difficult to use as a diagnostic measure. The values shown in Table 5.3 for β, δ_a, δ_r and δ_s are however, relatively high compared to the others, suggesting that there is at least a *greater* degree of correlation between them. This can be seen in the response plots of Figure 5-3, particularly the differential-stabilator and spoiler deflections.

As well as examining the correlation matrix and its inverse, an Eigensystem analysis was conducted on the lateral flight variables. Table 5.4 summarises the results for each Eigen-vector, in decreasing order.

Referring to the first column of Eigen-values of the unscaled $\mathbf{X}^T\mathbf{X}$ matrix, one extremely small entry of 0.0058 can be seen, pointing to a near-linear dependency in the data. This is also reflected in the large condition index of 141 - well above that suggested for highly collinear data. One might even suspect some amount of linear dependency in the sixth and even the fifth Eigen-vectors, which yield condition indices of 25 and 21, respectively.

In order to ascertain exactly which regressors were affected by collinearity, the variance-

Eigen-Value	Condition Index	Variance Proportions						
		β	α	$pb/2V_1$	$rb/2V_1$	δ_a	δ_r	δ_s
115.9291	1	0.0000	0.0000	0.0000	0.3594	0.0000	0.0000	0.0000
8.3663	4	0.0000	0.8610	0.0006	0.0059	0.0000	0.0000	0.0000
1.5372	9	0.0000	0.0196	0.3514	0.1061	0.0023	0.0011	0.0000
0.5548	14	0.0347	0.0751	0.0005	0.0185	0.0069	0.0169	0.0000
0.2613	21	0.0017	0.0177	0.4494	0.0393	0.1374	0.0295	0.0002
0.1822	25	0.9555	0.0181	0.0830	0.2507	0.1481	0.9463	0.0006
0.0058	141	0.0080	0.0084	0.1151	0.2202	0.7054	0.0062	0.9991

Table 5.4: Eigensystem analysis of lateral variables

decomposition proportions were also computed. Recall from Section 4.3.2, that a high proportion of the variance of two or more coefficients, concentrated in components associated with the same singular value, will provide evidence that the corresponding singular value may cause problems. The variance proportions associated with the largest condition index highlight a strong dependency in δ_s and δ_a terms, as previously indicated by the correlation matrix. In addition, the proportions associated with the second largest condition index reveal a moderate dependency in β and δ_r. The third largest condition index has only one significant variance proportion associated with it and is therefore *not* an indication of collinearity.

5.4 Data Partitioning

In Section 4.2.7, the use of dummy variables to represent composite regression models was introduced. This formulation required the positioning of intercepts, which defined regions of unique variation in the model. With regard to estimating a model from measured data then, the analyst is left with the problem of first postulating its structure in terms of these intercepts. This means that both the model's complexity (i.e. the number of intercepts) and structure (the placement of those intercepts) must be given, prior to identification.

For the analysis of the F-111C flight data, the model utilised incorporated splines to represent nonlinear coefficients. Section 3.2.1 presented the aircraft rigid-body equations of motion, in which each coefficient was expressed as a function of the angle-of-attack, except for the spoiler contribution, which was also dependent on the spoiler deflection. Now the form of a regression model that includes spline variables is the same as the composite model described previously and so, each spline parameter may be estimated by partitioning the data accordingly. It is also important to note that, because the lateral spoiler derivatives are anti-symmetric, the spoiler deflection data can be partitioned with respect to their *absolute* value (*see* Section 3.2.3).

The problem of composite-model identification was divided into two cases, according to whether or not it is known which data points lie in each region. In this situation, it is known beforehand that distinct regions exist and therefore, simply a matter of finding the exact position of the corresponding knots. There is a subtle difference, however, when determining the structure of a nonlinear model based on splines, since it is essentially up to the analyst to define those regions in the first place. The problem is, more specifically, to find a combination of knots, such that the resulting model will best fulfill its purpose. That is, to either follow the data closely, or give an accurate representation of the coefficients, or both.

There are a number of approaches that can be used to determine a model's structure from measured data. Three such approaches were investigated [223] using flight data from the F-111C aircraft and are discussed below.

5.4.1 Utilising Prior Knowledge

The simplest approach for model structure determination is to first postulate a model based on prior knowledge and then estimate the constituent parameters. Knots in each coefficient, represented by splines, should ideally be placed at critical points defining specific regions. For example, the second knot can usually be placed so as to bound the linear region where small-perturbation theory holds (recall that the first knot is set to zero). Remaining knots might then be placed at points corresponding to critical gradient changes in the prior model.

Obviously, the biggest drawback associated with this procedure is the requirement for *a-priori* information. In the absence of such information, or if a prior model of low integrity is employed, the knots may be positioned detrimentally. One runs the risk of under-, or even over-modelling. Even with an accurate prior model, the approach will typically involve a small amount of trial and error in the search for a satisfactory estimate.

Another aspect, central to any form of identification through data-partitioning, is the fact that each region must also contain a sufficient number of points for reliable estimation. This means that the analyst must, in this case, ensure that each knot not only defines a distinct region, but also bounds a reasonable amount of data. As a consequence, the estimated model will often vary and may be compromised, according to the spread of data under examination.

Some of the advantages in using this approach include the ability to produce a model of conservative size, with correspondingly small standard errors. The approach is generally robust, as with linear identification, since sufficiently large data sets can be used to estimate each group of parameters. Hence, the resulting model should approximate the true model well, although it may not capture some of the more intricate details.

It is expected that most, if not all of the model parameters, will have significant estimates as determined by statistical hypothesis tests, such as the partial-F test. Usually, a nonsignificant parameter will result if the knots have been poorly situated to begin with. One example of the estimated sideforce coefficient in Figure 5-4 illustrates this point. Here, the second and third knots have been badly placed, resulting in a slight overshoot of the true model. Note also the small standard error of the estimated coefficient function.

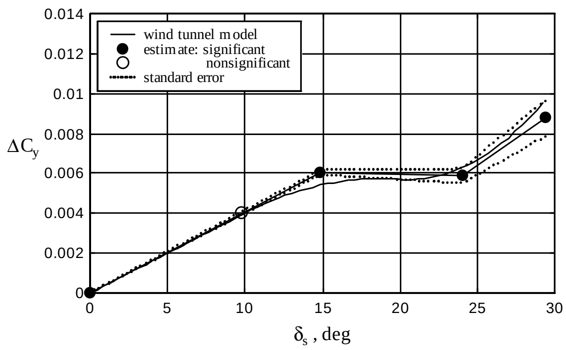

Figure 5-4: Conservative knot placement utilising prior information

Because the second parameter has been deemed nonsignificant, the second knot is inconsequential and may be removed, thus reducing the model size by one. This idea of utilising the significance of each parameter in the model to determine its structure leads to the next approach.

5.4.2 Significant Regions

By initially postulating a model with an excessive number of knots across each spline function axis and then applying some selection procedure, such as stepwise regression, a (fully) significant model can be determined [14]. Ideally, the remaining knots will be arranged in a manner such that the true spline function is represented adequately. In a first-order approximation, this means they will be concentrated around regions of large curvature, or high nonlinearity. The resulting model should also be greatly reduced in size. As explained above, however, the accuracy of the estimated model also depends on the spread of data and in particular, the amount of data lying in each partitioned region. One must therefore be especially cautious when employing this method, since many of the data subsets could contain extremely small numbers of points, leading to dubious estimates.

The estimation of model parameters from subsets of partitioned data can be approached in one of two ways: The first is to sequentially estimate the parameters from each subset, subtracting their contribution from the response after each step; the second involves compiling a global model from those subsets and then performing a single identification on that. Now because spline functions were utilised for representation of the nonlinear coefficients, the two approaches can produce two, quite different models. If the parameters are to be estimated sequentially, only the data lying *within* each region can be used for identification of the corresponding local models. This approach is therefore prone to large errors in regions containing small data subsets. Additionally, any bias error arising from an identification in one region will be accumulated in the response, thus affecting all subsequent estimates. The effect is oscillatory - since each estimate will tend to account for errors induced in the previous step - and often divergent, as those errors compound. Figure 5-5 illustrates this phenomena for an example of the sideforce model, as the number of postulated knots is increased.

Neither of these problems occur when a single, global model is estimated. Columns of the global regression matrix, pertaining to nonlinear coefficients, will comprise variables of the form:

$$(|x| - x_i)_+^m = \begin{cases} (|x| - x_i)^m & ; \quad x \geq x_i \\ 0 & ; \quad x < x_i \end{cases}$$

from Section 3.2.3. Hence, the data lying *above* each knot is utilised for estimation of the associated set of parameters - a far greater amount than the data in each region bounded by

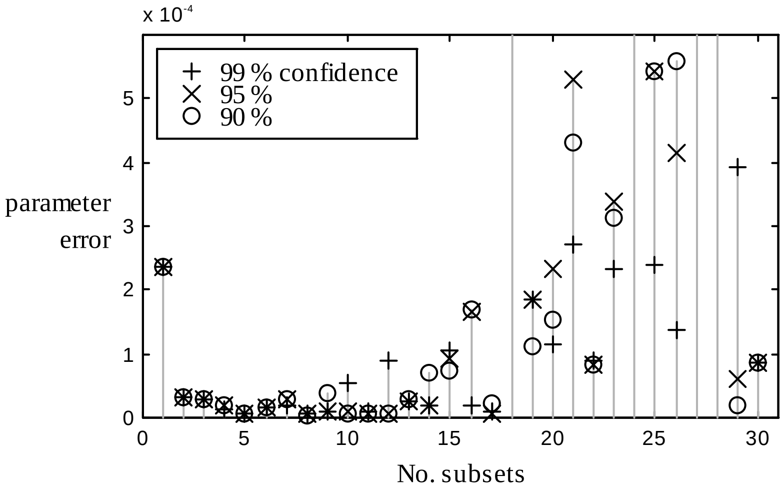

Figure 5-5: Parameter error increase with model size

knots. It is important to note that no new information has been extracted from the data; it has simply been used more efficiently in formulating the approach. Since all of the spline variables 'overlap' to some extent, the data is actually shared between regressors. Now, instead of identifiability problems arising in small data sets, it is more likely that collinearity problems will be encountered, among variables whose knots are close. Nonetheless, this is generally less serious and can be dealt with via biased estimation methods (or avoided through better partitioning !) if necessary. Another advantage of sharing the information in this way is that bias errors induced in successive regions will not compound as with the first approach. Because each regressor, and therefore each parameter, is associated with the other regressors and parameters, the estimates from one region will affect estimates in the higher regions accordingly. More importantly, though, the estimates in those higher regions will also affect the estimates from that one region - producing a more accurate model overall. Comparing exemplary model estimates using these two approaches, as in Figure 5-6, reveals their difference.

As with the previous example, the standard error bounds shown are based on their actual values - not their effect on the parameters, or gradients, of the model - and are therefore much larger for illustration purposes. For the same preselected significance level, this approach will generally produce a smaller model (i.e. less significant parameters) than

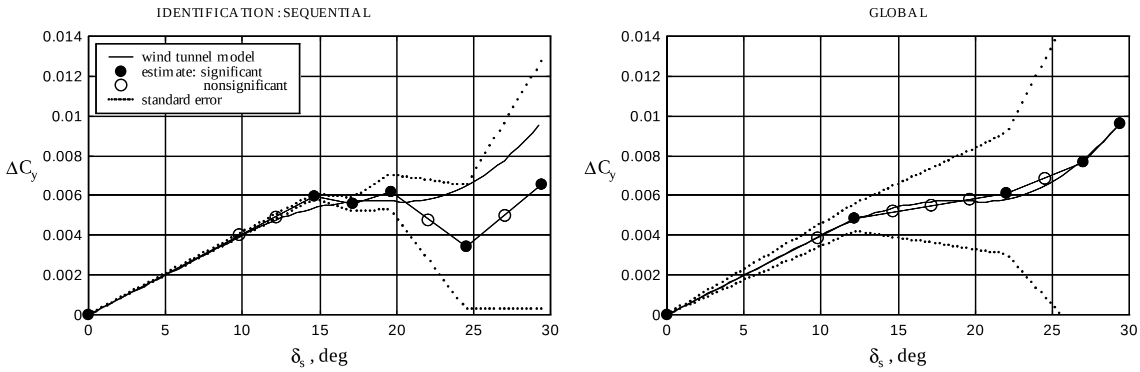

Figure 5-6: Estimated models obtained through sequential and global identification

the first approach. This is due to the fact that the cumulative error induced in each region using the first approach is seen as a change - possibly a significant one - in the following regions.

Instead of obtaining a reduced model by eliminating nonsignificant parameters, an alternative method can be used, whereby only significant parameters are added to the model in the first place. This is accomplished through an iterative addition and placement of knots in the spline model, based on the significance of the estimates. At each step in the iteration, the sequence of events proceeds as follows:

First, perform a regression using data *only* in the local region, bounded by knots and calculate the partial-F statistic for the appropriate coefficient; if that exceeds its critical value for a significance level, α_p, add a new knot spaced Δx from the present one and continue, otherwise; expand the current region by adding some small amount, δx and perform a new regression.

Writing this in algorithm form:

```
if  F_p(i) > F(ν_1, ν_2, 1 − α_p)
    x_{i+1} = x_i + Δx  ;  i = i + 1        % add new knot
else
    x_i = x_i + δx                          % expand current region
end
```

The expanded region will gradually encompass more data points over a greater range and thus, will eventually become significant, assuming the model is sufficiently nonlinear. Consequently, a fully significant model will result, as shown in Figure 5-7.

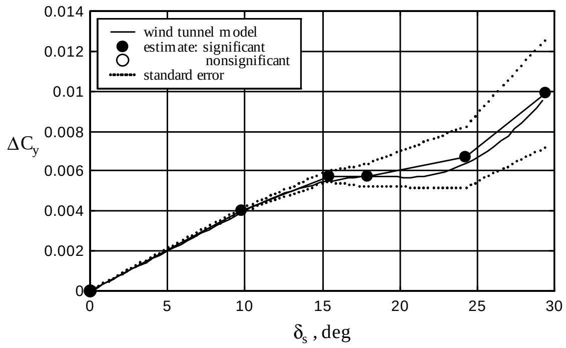

Figure 5-7: Model obtained through iterative knot placement

One should be aware, however, that the model parameters are only significant as determined by a sequential identification approach. They may not all be significant if the same model is estimated via the second approach, which performs a global regression.

Although this method can be used to provide a relatively efficient model, it works on a crude iteration scheme and still requires several constraints, including the significance level, α_p and knot-increments, Δx and δx. For simple models, the identification would require just as much user-input as one of the preceding methods. Furthermore, the iterative method can really only be used for models incorporating one-dimensional splines, since it only provides feedback on the significance of the current region.

5.4.3 Nonlinear Optimisation

Common to most optimisation schemes is some error-based cost function, which is minimised with respect to the system parameters and constraints. In model structure determination, as with any output-error approach, a good choice for this cost function is the mean square error, MSE, since it provides a direct indication of the estimated model's accuracy.

For a model implementing spline function coefficients, the optimum arrangement of knots is desired, assuming the spline order and number of knots are known. These must be fixed in the optimisation procedure, so as to avoid large discrete changes in the underlying model. Models of varying order and/or size can be compared later on the basis of their efficiency, via criteria such as the F or C_p statistics.

Now since the model structure is to be estimated from a finite data sequence, the parameter space, described by knots, is actually discrete. That is, only a finite number of solutions exist - each spanning some range in the parameters. Any optimisation performed on the partitioning scheme must therefore take this into account, by either working within a pre-defined set of solutions, or enforcing a minimum-step size constraint. These constitute the two approaches examined:

1. Discrete algorithms
   - exhaustive search
   - fixed-step solution
2. Continuous approximation methods
   - unconstrained optimisation

The discrete approach initially entails compilation of a candidate variable set, corresponding to a set of knots, and then selection from those variables to reach some final model. One could perform a naive Exhaustive Search of *all* possible locations for the knots, with a recalculation of the regression and resulting error at each stage. Such a search however, even for relatively small samples, would prove extremely costly. In order to find the global minimum MSE for a model with up to k segments, and sample size n, the required number of calculations (regression-solutions) is of the order, $\mathrm{O}(n^k/(k-1)!)$. Typically, this would correspond to approximately 2×10^9 calculations on a data set of length 2300, for a model employing only 3 partitions !

A far more efficient approach can be employed by searching through a reduced set of candidate variables, or knot locations, defined prior to selection. For the same example as that above, setting the number of candidate locations to 12 would mean that only 220 regression equations need be calculated. Once again utilising the sideforce model, described in the previous sections, an exhaustive search was conducted for 2, 3 and 4 knots, chosen from 12 uniformly spaced locations. The plots in Figure 5-8 illustrate the variation of F and MSE statistics for the different partitioning schemes trialed.

The value of F is seen to generally increase (and MSE to decrease), simply because the algorithm first utilises the higher, less important parameters and then gradually introduces

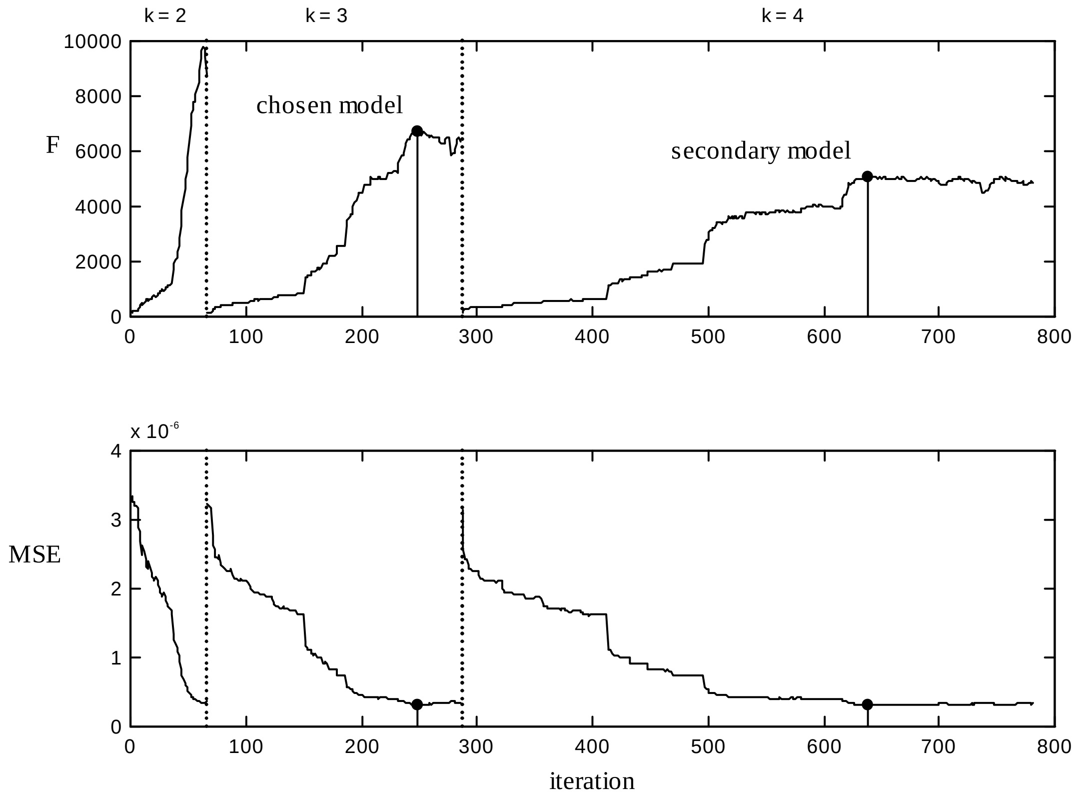

Figure 5-8: F statistic and mean-square error variation for an Exhaustive Search

the lower parameters. In this case, a model comprising 3 segments has been chosen, since it has a large significance and low mean-square error. A secondary, alternative model with 4 segments also managed to capture the coefficient's nonlinear characteristics adequately, as shown in Figure 5-9.

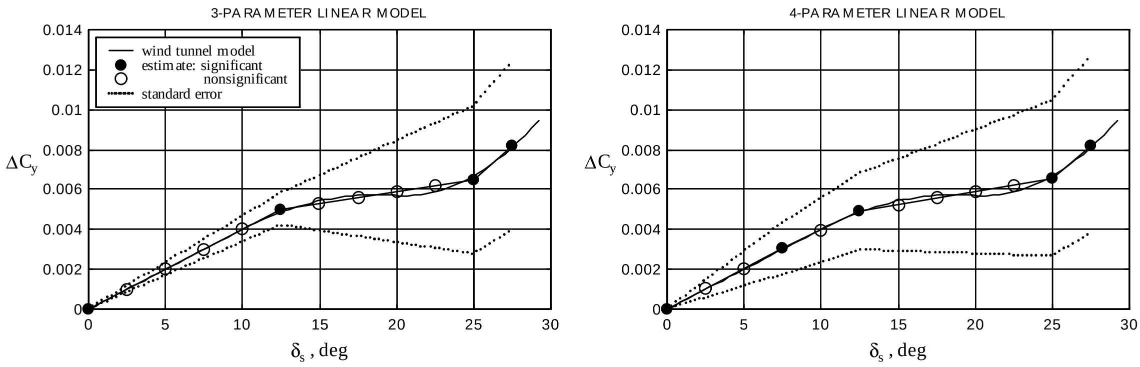

Figure 5-9: Models obtained through exhaustive selection

Although the exhaustive search procedure is able to locate the global minimum, it is still a very rough-handed approach, requiring a large amount of computation. Even if the parameter space is reduced substantially, the procedure can become extremely burdensome for splines of dimension greater than one.

In 1974, Guthery [66] used an optimality concept from dynamic programming to develop a piecewise linear regression algorithm, which produced the global minimum MSE for models with up to k segments and required only $O(n^2k)$ calculations. McGee and Carleton [164] also devised an algorithm for piecewise linear regression, based on hierarchical clustering. Their algorithm reduced the number of calculations to $O(n)$, but did not seek to produce a global minimum MSE. In fact, the algorithm did not seek to produce even a local minimum MSE.

A similar non-exhaustive technique was later presented in reference [33], which successfully located minima in partitioned data. This technique is based on the selection of an initial partition with k segments, followed by iterative refinement of the partition. At each step of the iteration, the neighbouring partition that produces the smallest error is chosen. "Neighbouring partitions" are defined as those partitioning schemes which alter the data-subsets of adjacent regions by one unit. The process is continued until no further improvement in the MSE is possible, at which point, the k segments may be collapsed to form $(k-1)$ segments. In order to arrive at a solution for the reduced model, pairs of adjacent segments are combined to produce $(k-1)$ different partitions. Each of these partitions is then considered as a starting value for the next sequence of iterations. The solution for the $(k-1)$ segment partition is then taken to be the minimum of these local minima and further reduction can be performed in the same way. As with the clustering algorithm, the number of calculations necessary to produce a local minimum is $\mathrm{O}(n)$.

Again, this approach is still far from optimal, since the step size does not take into account the relative error produced at each stage. That is, the partitioned subsets are changed by only one data point (or a fixed number of points) each iteration, regardless of the level of improvement in the MSE. Another drawback is the "steepest-descent" nature of the optimisation's search direction. This approach is actually quite inefficient, particularly in cases where the parameters have not been suitably scaled, producing narrow valleys in the error-surface.

The last approach involves performing an optimisation on some continuous approximation of the error function. Hudson [77] first introduced the approach, though devoted little attention to the problem of achieving a solution. Later, Gallant, *et al* [52] proposed a reparametrized model in order to facilitate a modified Gauss-Newton optimisation.

Many different types of algorithms exist for the multi-dimensional optimisation of nonlinear functions: Simplex Search and quasi-Newton methods, as well as various nonlinear Least-Squares techniques to name just a few. Because these algorithms require continuous functions, the data must be approximated as such, or measures taken to ensure that the discontinuities between data points in the sequence are never seen. The former option is undesirable since, like filtering, information is removed from the data in order to obtain a continuous model. Therefore, a minimum step-size must be imposed on each spline-variable, equal to the largest difference between data points in those variables.

Another peculiarity of partition-optimisation stems from the fact that the knot locations must be bounded. Recall from Section 3.2.3 that the set of knots must obey the condition: $x_0 < x_1 < \ldots < x_k < x_{\max}$. In order to implement this constraint into the optimisation, one of two things can be done:

a) perform a constrained optimisation or;

b) transform the variables onto a continuous space.

At first, one might consider the constrained optimisation to be the natural choice. However, the constrained approach is actually much more difficult to perform effectively. This is because, even for constrained optimisation, the error function **must** be defined for all values of the parameters. A common procedure employed to account for this is to replace the error function by some penalty function outside the feasible range of values. The penalty function should return a large (undesirable) value for the error and should also be smooth and continuous for gradient calculations. Consequently, the real difficulty lies in formulating a suitable penalty function.

The second choice involves transforming the parameters into continuous ones and then performing an unconstrained optimisation with respect to those. In order that each knot be bounded between its upper and lower neighbours, the transformation function should be defined only in that region. A number of functions exist that will satisfy this requirement adequately. Ideally, it would be smooth, continuous and relatively linear about the midpoint. This last property is desirable, since the knot positions should vary most "predictably" when they are near-evenly spaced. Figure 5-10 illustrates an example of the relationship between the unbounded parameters and the resulting spline function.

The transformation for each of the unconstrained variables, x_i', can be expressed in terms of the corresponding and neighbouring knots, x_i and $[x_{i-1}, x_{i+1}]$, respectively:

$$x_i' = f\left(x_{i-1}, x_i, x_{i+1}\right) \quad ; \quad x_{i-1} \leq x_i \leq x_{i+1} \tag{5.6}$$

One such function is based on the inverse hyperbolic tangent:

$$x_i' = \frac{(x_{i+1} - x_{i-1})}{2} \tanh^{-1}\left(\frac{2\left(x_i - (x_{i-1} + x_{i+1})/2\right)}{(x_{i+1} - x_{i-1})}\right) \tag{5.7}$$

For the selection of an efficient optimisation algorithm, one flight-test case of the F-111C was analysed using several different approaches. Flight P3F1E48 was conducted with a wing-sweep angle of 16°, trimmed at 30000 ft and Mach 0.6. The combined manoeuvre was primarily induced through differential-stabilator/spoiler and rudder input, with a small amount of coupled-stabilator (elevator) movement. The spoiler deflection ranged from −32° to 25° and the angle-of-attack, from 4° to 12°, which was well into the expected nonlinear

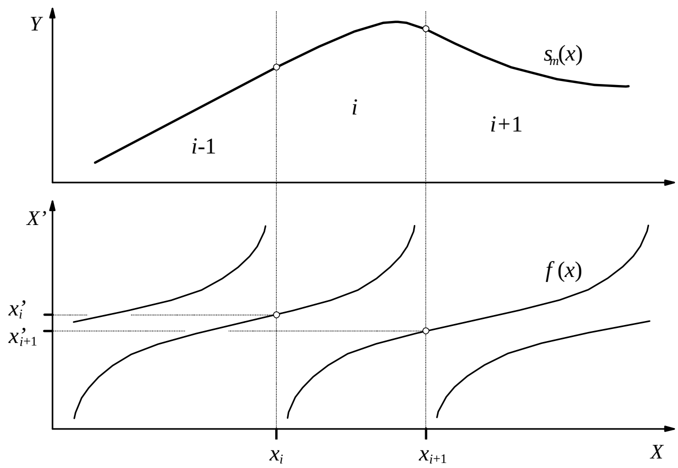

Figure 5-10: Spline function as constructed using unbounded parameters

regime. Figure 5-11 displays the manoeuvre history for the (absolute) spoiler deflection and angle-of-attack.

To begin with, two equivalent responses were simulated, using models constructed with previously estimated linear terms and nonlinear terms from wind-tunnel data. All control deflections utilised to create the responses were taken directly from the flight data, as were the trim states. In addition, measurement noise of similar variance to that found in the real flight data was added to both sets of simulated data. A model structure determination analysis with partition optimisation was then conducted on the simulated response data, using four different optimisation algorithms. The algorithms, outlined in Appendix C, included a Simplex Search, a quasi-Newton method, a nonlinear Least-Squares and a constrained optimisation procedure.

The only difference between the two models was their spoiler coefficient functions - one was created using 1 knot in each δ_s and α, while the other had 2 knots in each. Both tensor-splines were formulated as first order approximations, shown in Figure 5-12.

In the first model, intermediate knots were placed at 10° in δ_s and 8° in α. In the second model, two sets of intermediate knots were placed at $[3, 7]^\circ$ and $[10, 20]^\circ$ in δ_s and α, respectively. The spline-function values were also modified by a small amount in the second model in order to accentuate the nonlinearity above 10° spoiler deflection and consequently,

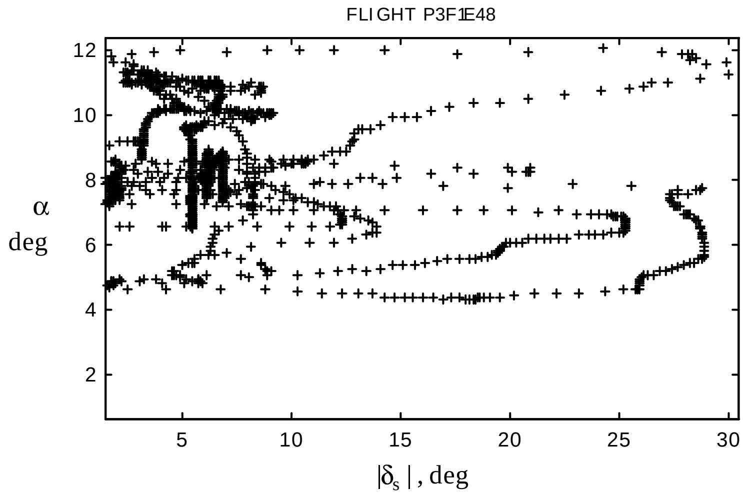

Figure 5-11: Flight P3F1E48 data spread in δ_s and α

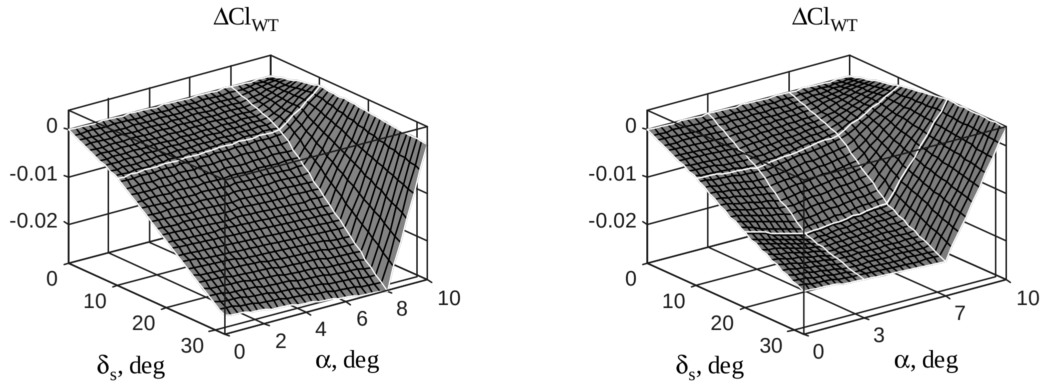

Figure 5-12: Two-knot and four-knot spline models (first-order)

make those knots more significant. Both models clearly demonstrate the characteristic decrease in spoiler roll-effectiveness at elevated angles-of-attack $\{\alpha : 7^\circ \leq \alpha \leq 10^\circ\}$.

Subsequent analysis of the data highlighted differences in each of the optimisation algorithms. For the data corresponding to the two-knot model, both Simplex and Least Squares algorithms found the optimum (modelled) partitioning scheme successfully. The quasi-Newton algorithm, however, performed poorly and did not converge to a minimum solution. Of the two unconstrained methods, the nonlinear Least Squares converged much more rapidly, as expected. The number of iterations for this method, excluding gradient calculations, totalled 40, whereas the Simplex Search took 84 iterations. Figure 5-13 illustrates the sequence of iterations for each method, superimposed over a contour plot of the error surface.

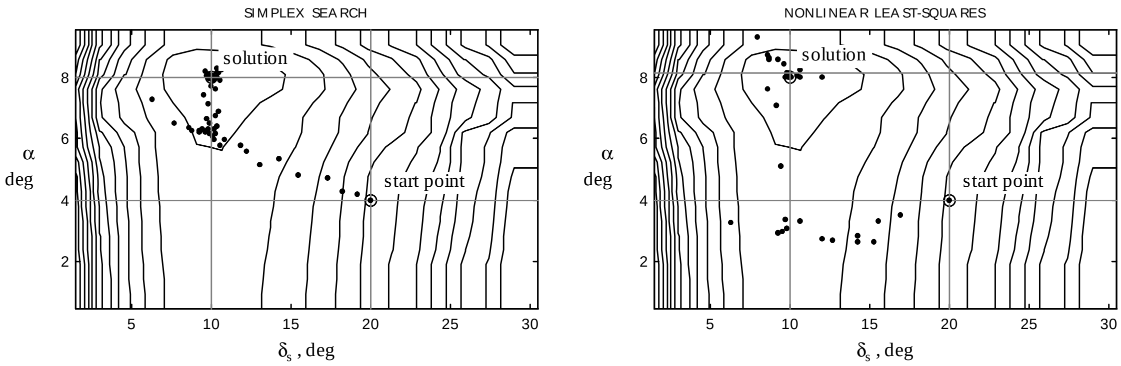

Figure 5-13: Two-knot spline optimisation on simulated data

The error, or cost surface, is characterised by a large valley along $\delta_s = 10^\circ$ and a less significant valley along $\alpha = 8^\circ$. Looking at the spoiler coefficients (Figure 5-12), one might have expected the valley along α to be more significant. However, because of the *arrangement* of data points, the opposite is in fact true. Since most of the data - approximately 85% - is concentrated below 10° spoiler deflection, the error caused by the estimated model will be highly dependent on the partitioning in δ_s around that region. The angle-of-attack data is quite evenly spread over its range and so, partitioning in α will have much less effect on the resulting error.

This is an aspect worth keeping in mind when performing this type of model structure optimisation. Moreover, it has important ramifications on the integrity of the estimated model, when that model has a different structure to the true one.

Corollary 2 *In the determination of an optimally partitioned model structure from a data set of finite length, the* spread *of data can influence the resulting model, as well as the data content. Hence, assuming that the partitioned model is an approximation of the true system, the minimum-error model will not only be optimum with respect to the parameters, but also with respect to the data itself.*

Returning to the optimisation results, the initial partitions, from which the algorithms began, were positioned at 20° in δ_s and 4° in α. The Simplex Search stepped in directions not unlike those which would be expected from a steepest-descent algorithm and therefore, required a large number of iterations to achieve convergence. The nonlinear Least Squares algorithm, on the other hand, uses gradient information and was thus able to proceed far more efficiently toward the minimum. A Levenberg-Marquardt method was used in the algorithm, as it provided a robust means of determining the search direction.

For the data simulated with the four-knot model, each of the various algorithms was tested, including a Constrained optimisation. Again, the Simplex Search and nonlinear LS algorithms performed better than the quasi-Newton algorithm, which did not converge to the correct solution. The constrained method also experienced convergence problems. However, since the algorithm uses a quasi-Newton technique for approximating the Hessian, this was not surprising.

The Simplex Search found the (approximate) minimum in 353 iterations, as shown in Figure 5-14. The nonlinear LS algorithm converged to a solution in only 132 iterations, confirming its advantage over the other optimisation methods.

The contour plot on both axes was created using the *local* errors for each of the knot-intersections independently and is therefore not a true global error surface. (It is impossible to generate a global error surface for more than two knots.) It does illustrate the local minima though, and gives an indication of their relative importance.

After analysing simulated data, the real flight case was examined in a similar manner. Both Simplex Search and nonlinear LS algorithms were trialed. Convergence was achieved in 69 and 35 iterations, respectively.

The error surface and optimisation steps are illustrated in Figure 5-15. Of note is the presence of several minima and, in particular, the trough near $(21, 9)^\circ$. For the optimisation shown, the starting position for the knots in (δ_s, α) was chosen at $(12, 6)^\circ$. If, however,

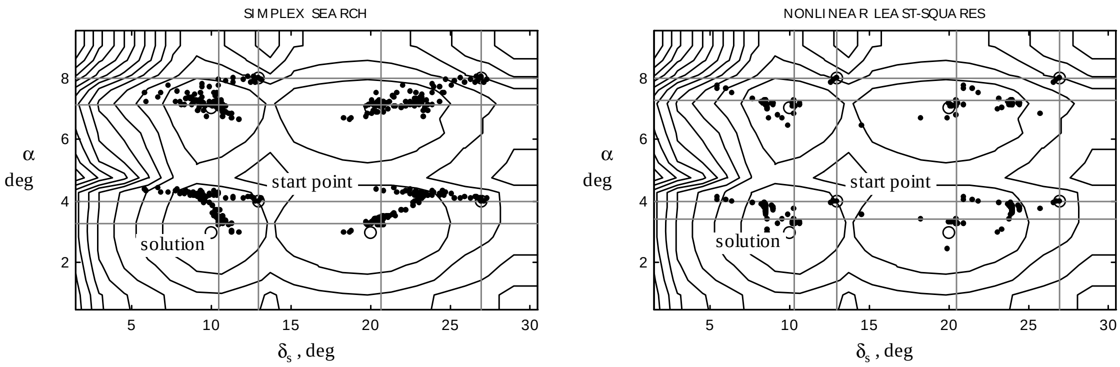

Figure 5-14: Four-knot spline optimisation on simulated data

the initial knot placed in δ_s had been greater than 14° or so, the algorithms would have converged to this other minima. With any type of multidimensional optimisation, it is always wise to initialise the algorithm from a number of different states, should there be more than one local minima.

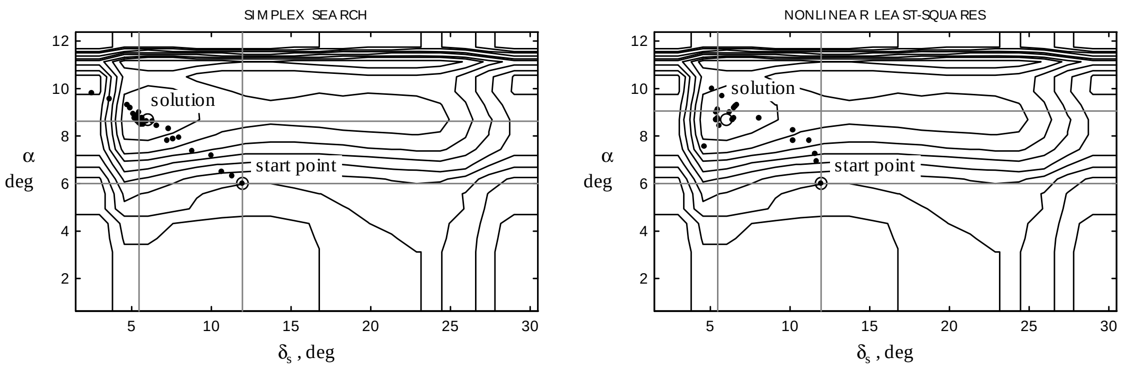

Figure 5-15: Two-knot spline optimisation on real flight data

From the diagram, it becomes clear that the resulting error is highly dependent on the partitioning in α. Since the data is more or less evenly spread in angle-of-attack, it can be deduced that a critical change exists around 9°. The error surface has also been moderately influenced by the data. Several features, such as the secondary trough along $\alpha = 16°$ can be seen to correspond with trends in the data sequence (Figure 5-11, p.126).

In summary, the nonlinear Least Squares technique generally proved to be the most efficient for optimisation of the partitions in segmented models. The algorithm used was able to provide a robust solution in significantly fewer iterations than the Simplex Search. Neither the quasi-Newton nor the Constrained optimisation algorithms were able to converge to a satisfactory solution, most likely because of the discontinuous nature of the problem.

5.5 Concluding Remarks

In the initial investigation of the F-111C aircraft's dynamic model, a number of corrections were made to the data recorded during flight testing. These included corrections for pressure errors, the recording lags in several channels and the errors inherent in the α and β vanes. Following initial pre-processing of the data, a linear model was estimated from each flight case using a Maximum Likelihood technique. The results generally correlated well, although some discrepancies appeared in the yawing-moment and rolling-moment derivatives, which were left unexplained.

The data were processed for a second time in the current research. This time, all outliers were removed and appropriate time-shifts applied to the channels not accounted for previously. An initial frequency analysis of the data allowed outliers to be found and also provided a valuable insight into the spectrum of each signal. Apart from the dominant response frequency, a smaller peak at 13 Hz was found in the sideslip recording, arising from local flow disturbances in the air data system. A significantly high level of noise in the yaw acceleration signal was also noted in all of the cases examined.

In addition to the frequency analysis, a correlation analysis was conducted on the data prior to identification. Many of the flight cases exhibited only a moderate level of collinearity, although the correlation between the differential-stabilator and spoiler deflections was generally quite high. The sideslip and rudder deflection also exhibited a significant level of correlation.

The last section covered the subject of data-partitioning, including various approaches for its implementation. Perhaps the most efficient scheme was that which utilised prior knowledge, in the form of a wind-tunnel model for example, to position the knots manually. This should result in a fully significant model, assuming an adequate number of data points exists in each region.

If no prior information was available, an alternative scheme would be required. One such scheme comprised postulating a large number of possible knot-locations and then employing some selection procedure, such as Stepwise Regression, to determine a significant combination. Unfortunately, the problem of ensuring a sufficient number of data points for each region became more critical.

Another solution without *a-priori* information was achieved through a nonlinear optimisation of the knots, based on some error of the model. This was investigated in the final section and focussed on continuous techniques including Simplex Search, nonlinear Least Squares and Constrained optimisation. In order to implement the various optimisation routines, the knot locations were transformed onto a continuous space. It was found that the first two algorithms were well suited to this type of problem, whereas the last was not. The nonlinear Least Squares algorithm proved to be the most efficient, however, the Simplex Search algorithm was generally very robust.

Chapter 6

Identification Results

6.1 Introduction

Results obtained from identification of the flight data will now be examined. The main purpose of the analysis was to determine the F-111C aircraft's spoiler model in as much detail as possible.

In the first section, the data from a simulated response with added measurement noise is analysed. The general identification details for each real flight case are then discussed. A common identification approach was adopted for the majority of cases - only the partitioning scheme differed, to suit the data. The tests were grouped into wing-sweep angles of 16°, 26°, 35° and 45° and for each, a range of flights with Mach numbers from 0.4 to 1.1 were examined.

Based on the summary of results given for each wing-sweep, as well as other pertinent aspects of the analysis, the overall results are then explained in terms of their aerodynamic relevance. This section provides some insight into the similarities and differences seen, when compared against corresponding wind-tunnel results.

The last section examines the significance of various parameters in the generic spoiler model utilised in the identification stage. To achieve this, a Stepwise Regression procedure was applied to a number of flight cases, resulting in a parsimonious model structure. By assessing the significance of the spoiler parameters, it was possible to gain a better understanding of the aerodynamics involved, since each term corresponded to a distinct feature of the model.

6.2 Simulated Data

Prior to examination of the real flight test data, a number of simulated cases were analysed in order to locate any possible problems that might occur and determine the expected accuracy of the identification procedure. The aircraft models were composed largely of linear coefficients that had been previously estimated from flight (*see* Section 5.2.4). Only the spoiler coefficients were given nonlinear variations, as found from wind-tunnel testing.

To make the resulting output more realistic, normally distributed measurement noise was added. An estimate of the true noise variance was obtained by filtering the data, as detailed in Section 5.3.2. For the lateral variables, these variances were typically of the order of those shown in Table 6.1.

VARIABLE	VARIANCE
α	1.47×10^{-3} deg
β	3.70×10^{-4} deg
p	2.83×10^{-2} deg /s
r	5.62×10^{-4} deg /s
ϕ	4.87×10^{-3} deg
a_y	4.13×10^{-5} /g
$\dot{p}$	3.26×10^{1} deg /s^2
$\dot{r}$	1.12×10^{1} deg /s^2

Table 6.1: Estimated noise variance for flight P3F1E48E

The same model structure was utilised in the identification so as to allow direct comparison of the parameters. This also meant that the data had to be partitioned according to the original knots in the model. An unbiased linear regression was performed on each of the lateral coefficients - sideforce, rolling- and yawing-moment - the results of which are compiled in Table 6.2. Only the first few terms in each tensor-spline function have been included, since the remaining terms have little physical relevance unless cumulatively added. Of these terms, all C_{a_α} $(\delta_s = 0)$; $\mathrm{a} = y, l, n$ coefficients were constrained to zero.

First, examine the sideforce coefficients. Most of the true model values fall close to or within the standard error bounds around each estimate. As expected, C_{y_β} provided the best estimate with a relatively small (0.5 %) standard deviation. The estimate of $C_{y_{\delta r}}$

	Coefficient							
	C_{y_β}	C_{y_p}	C_{y_r}	$C_{y_{\delta a}}$	$C_{y_{\delta r}}$	$C_{y_{\delta s}}$	C_{y_α}	$C_{y_{\delta s\alpha}}$
Model	-0.7219	0.0691	0.3105	0.0195	0.2097	0.0036	0.0000	-0.0574
Estimate	-0.7175	0.0777	0.3488	0.0261	0.2068	0.0060	0.0000	-0.0624
Std error	0.0039	0.0101	0.0571	0.0046	0.0043	0.0198	0.0000	0.2946
	C_{l_β}	C_{l_p}	C_{l_r}	$C_{l_{\delta a}}$	$C_{l_{\delta r}}$	$C_{l_{\delta s}}$	C_{l_α}	$C_{l_{\delta s\alpha}}$
Model	-0.0945	-0.3057	0.1243	-0.0739	0.0069	-0.0315	0.0000	-0.1008
Estimate	-0.0952	-0.3076	0.1254	-0.0755	0.0064	-0.0308	0.0000	-0.1130
Std error	0.0009	0.0023	0.0127	0.0010	0.0010	0.0044	0.0000	0.0658
	C_{n_β}	C_{n_p}	C_{n_r}	$C_{n_{\delta a}}$	$C_{n_{\delta r}}$	$C_{n_{\delta s}}$	C_{n_α}	$C_{n_{\delta s\alpha}}$
Model	0.0613	-0.0254	-0.1048	-0.0040	-0.0647	-0.0137	0.0000	0.0602
Estimate	0.0611	-0.0141	-0.1214	-0.0038	-0.0623	-0.0250	0.0000	0.2317
Std error	0.0028	0.0073	0.0413	0.0033	0.0031	0.0143	0.0000	0.2134

Table 6.2: Coefficient estimates from simulated data

also compared closely with its model value and produced a small error bound. Among the spoiler coefficients, the standard errors of $C_{y_{\delta s}}$ and in particular, $C_{y_{\delta s\alpha}}$ are extremely large - suggesting that it may be difficult to estimate them with any degree of confidence. This will improve as the sweep angle is increased. However the sideforce coefficients are, in general, less important to the aircraft dynamics and therefore the spoiler contribution should be sufficiently modelled by one linear derivative in δ_s only.

The rolling-moment coefficients were estimated with a greater accuracy overall - the best estimates being C_{l_p}, C_{l_β} and $C_{l_{\delta a}}$, all with relative errors less than 2 %. Interestingly, the estimates and standard errors of $C_{l_{\delta r}}$ and $C_{l_{\delta s}}$ are of similar proportions, indicating that they have a comparable effect on the lateral motion of the aircraft. The cross-product term, $C_{l_{\delta s\alpha}}$ again has a large standard error, though the relative magnitude is much less than in the corresponding sideforce term. As this term has a significant influence in the model, it should be possible to estimate its value with reasonable accuracy.

From the yawing-moment coefficient entries in the table, it can be seen that both C_{n_β} and $C_{n_{\delta r}}$ hold the lowest relative standard errors of approximately 5 %. The standard deviation of C_{n_r} is actually quite large, considering that it plays a primary role in the aircraft's directional response. In fact, all of the estimated standard deviations are significantly large, because of excessive noise in the yaw acceleration signal. The two most prominent coefficients in this respect are $C_{n_{\delta a}}$ and $C_{n_{\delta s \alpha}}$, which both have standard errors of magnitude approximately equal to the coefficients themselves. However, it is the two crucial spoiler coefficients, $C_{n_{\delta s}}$ and $C_{n_{\delta s \alpha}}$ that have been severely overestimated. This suggests that the yawing-moment contribution due to spoiler deflection may be extremely difficult to estimate accurately, in the presence of such noise. Moreover, it may actually be impossible to identify any significant nonlinearity in the yawing-moment coefficients.

6.3 Flight Results

6.3.1 Identification details

In order to examine the F-111C aircraft's spoiler characteristics for varying wing-sweep angle, Mach number and altitude, a range of test cases were investigated [224]. Section B.2 in the Appendices summarises the flight cases considered.

Since a large number of test cases were to be compared against each other, a common approach for the identification of each model had to be formulated. On the other hand, however, each case demanded individual attention because of the varying data structure and associated aerodynamics. It was therefore decided to customise the partitioning scheme to suit each aerodynamic model, within the bounds of the data and keep all other identification parameters the same. This approach would make use of prior wind-tunnel results to position the knots within each identification model and thus provide the regression with the correct variables for an unbiased solution (with respect to each model). The premise for this is that the wind-tunnel model itself provides an adequate representation of the nonlinear aerodynamics, or at least the *location* of critical points within the model. However, in most cases, additional degrees of freedom were integrated - via additional parameters or even extra partitions - and even if the true representation was undermodelled, a fair approximation could be expected.

Initially, Restricted Estimation was used to avoid collinearity problems in estimating the unsteady derivatives. The results for this analysis was not documented, however, as other, more efficient biased techniques, were later used instead.

The remaining details, common to each identification were as follows:

- The Mixed Estimation procedure was employed in most of the cases, with the bias weightings set such that the resulting standard errors would be 10 % of their expected unbiased values. This was found to bias the relevant terms sufficiently, without placing too much restriction on their estimates. In certain cases that exhibited a large amount of collinearity, a Principal Components Regression was used. The eigenvectors were removed, according to their condition number and variance-decomposition proportions.

- Rather than including them implicitly in the model equations, the dynamic terms, $C_{y_{\dot\beta}}$, $C_{l_{\dot\beta}}$ and $C_{n_{\dot\beta}}$ were all biased toward their wind-tunnel values to avoid any associated data collinearity problems.

- The 'weaker' linear derivatives were also biased, but instead, toward the corresponding estimates obtained from previous Maximum Likelihood identification. These *a-priori* estimates were unbiased with respect to any noise measured in the state variables (regressors) and were considered closer to the true coefficients than the wind-tunnel values were. Included in this set were the sideforce derivatives, C_{y_p}, C_{y_r}, $C_{y_{\delta a}}$, $C_{y_{\delta r}}$, $C_{y_{\delta s}}$; the rolling moment derivatives, C_{l_r}, $C_{l_{\delta r}}$; and the yawing moment derivatives, C_{n_p}, $C_{n_{\delta a}}$. The remaining unbiased linear derivatives included C_{y_β}, $C_{l_{\delta a}}$ and $C_{n_{\delta r}}$.

- Since several of the stability coefficients displayed significantly nonlinear variations with the angle-of-attack, according to the wind-tunnel results, they were approximated by first-order splines. Unlike the previous set of derivatives, these could not be adequately represented by linear terms, particularly in the high-α regime. The coefficients were unbiased and consisted of $C_{l_\beta}(\alpha)$, $C_{l_p}(\alpha)$, $C_{n_\beta}(\alpha)$ and $C_{n_r}(\alpha)$.

- Both rolling and yawing moment spoiler coefficients were represented by first-order tensor spline functions in spoiler deflection and angle-of-attack. Formulated as moment-contributions, they took the form: $\Delta C_l(\delta_s, \alpha)$ and $\Delta C_n(\delta_s, \alpha)$. As explained in Section 3.2.3, their contribution at zero deflection was fixed to zero. That is, $\Delta C_l = \Delta C_n = 0$ at $\delta_s = 0$ for all α.

- If there was significant variation in any of the nonlinear *a-priori* models *below* the $\{\delta_s, \alpha\}$ region being investigated, the corresponding lower set of spline coefficients were set to values interpolated from those models. For the coefficients approximated by splines in α only, the wind-tunnel models, modified by the corresponding ML estimates, were utilised for prior representation. For the spoiler contributions, the wind-tunnel models alone, specific to each flight condition, were used.

The primary objective in the analysis of the F-111C flight data was to identify the nonlinear aerodynamic model, focusing on the spoilers' contribution, for a range of conditions. Since the significance of each model was of no concern in the first stage, a standard regression scheme was employed, as opposed to some stepwise procedure. The general model structure was examined more closely in the following stage, with particular attention to the significance of each term.

For each of the flight cases considered, the resulting estimates are compared against their *a-priori* values. The linear derivatives and the derivatives represented by splines in α are both examined with the corresponding wind-tunnel and ML estimates. Rather than displaying the spline functions, which are of little interest, their mean values (in α) have been evaluated and compared alongside the linear coefficients. Confidence bounds were constructed for each using a critical level of 95 % and all biased terms have been highlighted.

The estimated rolling and yawing spoiler coefficients are compared against the wind-tunnel models - each plot extending to the flight-data limits in δ_s and α. In addition, the interpolated standard error variation has been superimposed on to each surface using colour shading. For model axes comprising more than one partition, the standard error was based on the cross-product parameter, $C_{\mathrm{a}_{\delta s \alpha}}$; $\mathrm{a} = y, l, n$.

A brief discussion of the results for each case is presented in the following sections. The cases have been divided according to their wing-sweep angle and the pertinent aspects summarised. For several flight tests, comparable (lateral) dynamic responses were simulated using the nonlinear model estimates. The actual control inputs were utilised, as well as the angle-of-attack signal, in place of a full longitudinal model.

6.3.2 16° wing-sweep

For the majority of flight cases examined over the Mach number range, the estimated side-force coefficient, $C_{y_{\delta s}}$, generally compared well with the wind-tunnel results. The coefficient was very small, however, often yielding a magnitude less than $C_{y_{\delta a}}$. On average, C_{y_β} was estimated to be 8 % smaller than the wind-tunnel derivative, as given by Table 6.3.

At low Mach numbers around 0.4, the spoilers' rolling contribution decreased with increasing α by a negligible amount. Contrary to the wind-tunnel model, the sudden loss in $\Delta C_l(\delta_s)$ was not identified. The estimated yawing contribution compared reasonably with the wind-tunnel model, indicating a general decrease with increasing α. At higher Mach numbers of 0.5 to 0.6, an initial increase in the rolling effectiveness occurred with increasing angle-of-attack, followed by a rapid decrease near 8°. Although significant, the change was not as prominent as that displayed in the wind-tunnel model. Another characteristic identified in this high-α regime was the increase in the local effectiveness $|C_{l_{\delta s}}|$, with spoiler deflection. The yawing contribution was again estimated to decrease uniformly with increasing α. The flight cases examined at Mach numbers in the range 0.7 to 0.8 produced a strong change in the spoilers' rolling contribution model at approximately 4° angle-of-attack. As a consequence of the limited α-range, only a small portion of each nonlinear model was identified. On the basis of these estimated sub-models though, it would not be unreasonable to expect control reversal at $\alpha > 9^\circ$. The estimated decrease in $|C_{n_{\delta s}}|$ with increasing angle-of-attack was much less than expected, from the wind-tunnel model. In fact, C_{n_α} was near-constant with α and unlikely to decrease significantly, which might have lead to an adverse yawing moment.

In general, the spoilers' estimated rolling contribution was slightly smaller than the wind-tunnel result by 4 %. The estimated yawing contribution was markedly smaller on average, as were all of the primary yawing derivatives. They were, however, estimated to within 10 % of the Maximum Likelihood values, thereby lending reassurance as to their integrity.

	Coefficient								
	C_{y_β}	C_{l_β}	C_{l_p}	$C_{l_{\delta a}}$	$C_{l_{\delta s}}$	C_{n_β}	C_{n_r}	$C_{n_{\delta r}}$	$C_{n_{\delta s}}$
Wind-Tunnel	-0.08	-0.03	0.00	-0.04	-0.04	-0.52	-0.39	-0.36	-0.25
Flight(ML)	0.00	0.02	0.17	0.07	-	0.09	-0.06	0.10	-

Table 6.3: Mean fractional differences between estimates - $\Lambda = 16^\circ$

P1F7E41 (10000 ft, Mach 0.4, $\delta_s[0, 44.8]^\circ$, $\alpha[5.6, 11.6]^\circ$)

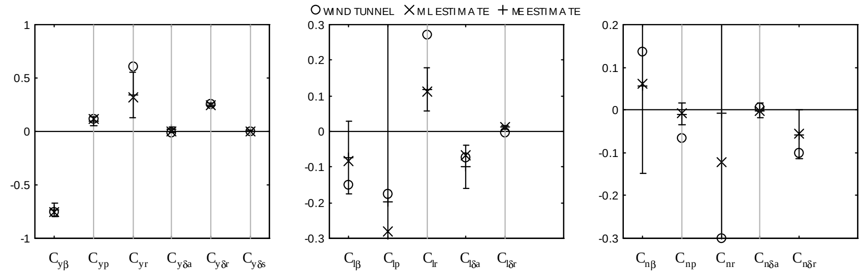

Figure 6-1: P1F7E41 Linear coefficient estimates

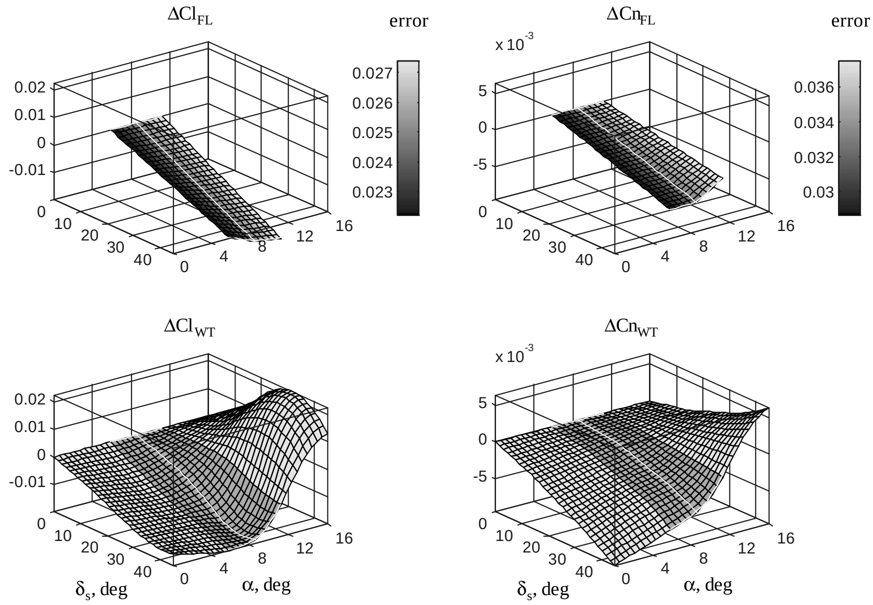

Figure 6-2: P1F7E41 Nonlinear spoiler coefficient estimates

Of the unbiased linear derivatives, C_{y_β} compared well against both wind-tunnel and Maximum Likelihood estimates. C_{l_p} matched the wind-tunnel value more closely and $C_{l_{\delta a}}$ was marginally larger. The estimate of C_{n_r} was approximately zero. In fact, all of the flight-estimated yawing-moment derivatives were less than their wind-tunnel counterparts. For identification of the nonlinear spoiler contribution, one knot was placed in α at 8.5°. Both $C_{l_{\delta_s}}$ and $C_{n_{\delta_s}}$ parameters compared well, however $C_{l_{\delta s \alpha}}$ and $C_{n_{\delta s \alpha}}$ were more negative than the wind-tunnel values. No sudden loss in the roll-effectiveness with increasing angle-of-attack was detected.

P1F7E13 (20000 ft, Mach 0.4, $\delta_s[0, 43.2]°$, $\alpha[5.4, 13.0]°$)

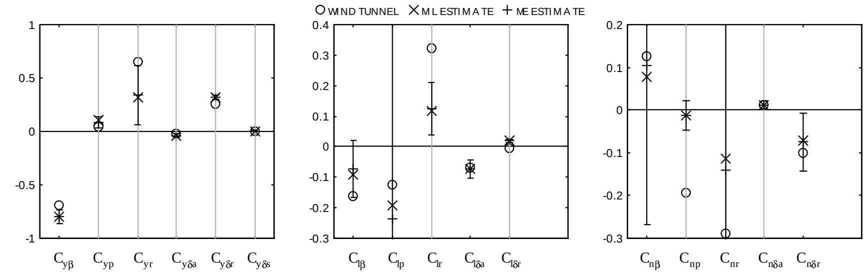

Figure 6-3: P1F7E13 Linear coefficient estimates

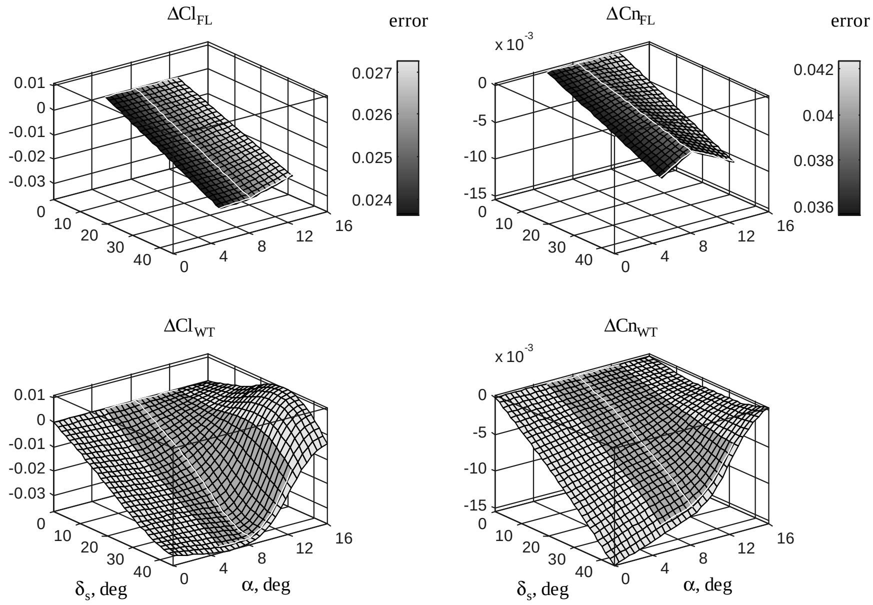

Figure 6-4: P1F7E13 Nonlinear spoiler coefficient estimates

The estimated linear sideforce coefficient, C_{y_β}, compared well with wind-tunnel and ML estimates. C_{l_β} for both flight estimates was approximately 50 % of the wind-tunnel value. As with the previous case, the confidence intervals for C_{l_p}, C_{n_β} and C_{n_r} were quite large. The coefficients themselves, however, agreed well with the other flight estimated coefficients. The nonlinear model was partitioned by one knot at 8.5° to capture an expected nonlinearity in α. Both $C_{l_{\delta s}}$ and $C_{n_{\delta s}}$ terms underestimated the wind-tunnel values by as much as 80 %, although the cross-product terms for the first region were much closer. Little change in the roll-effectiveness with α was identified. The change identified in $C_{n_{\delta s \alpha}}$ was more likely due to (poor) partitioning than actual aerodynamic transition.

P3F6E101 (20000 ft, Mach 0.5, $\delta_s[0, 34.1]°$, $\alpha[4.0, 10.6]°$)

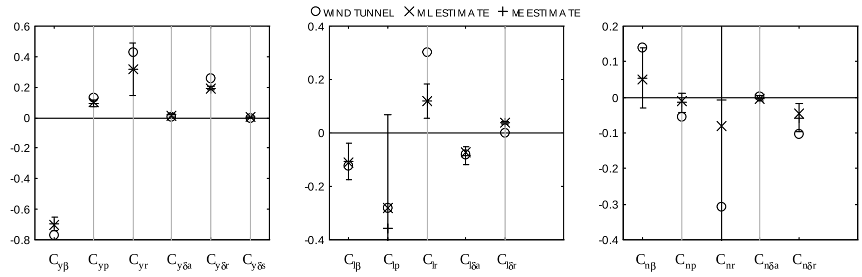

Figure 6-5: P3F6E101 Linear coefficient estimates

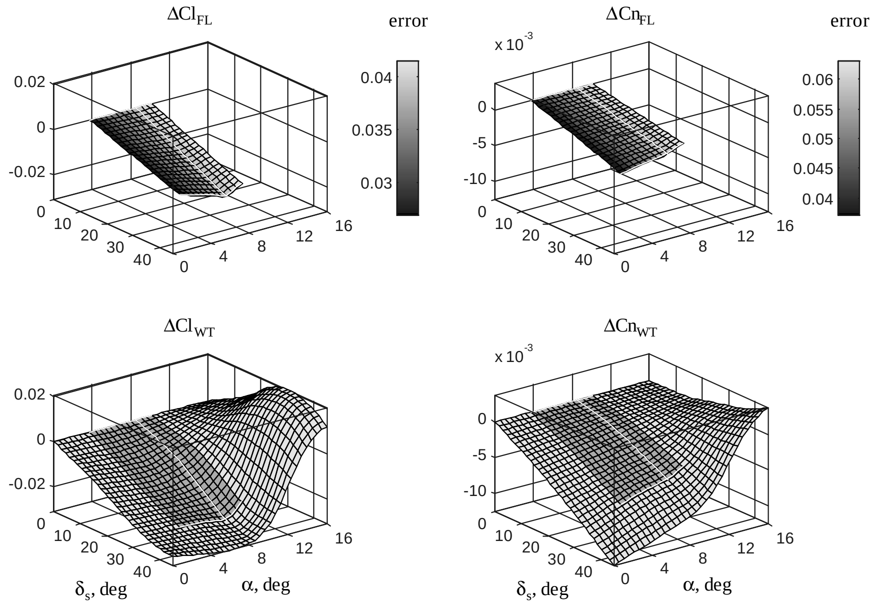

Figure 6-6: P3F6E101 Nonlinear spoiler coefficient estimates

In general, all of the unbiased linear estimates correlated well with the wind-tunnel results and ML estimates. The estimated value of C_{l_p} was slightly larger than the wind-tunnel value and ML estimate. C_{n_β} and C_{n_r} were again, much smaller than the wind-tunnel coefficients. The single partition in α at 8.5° in this case successfully facilitated the identification of a nonlinear characteristic in the spoilers' rolling contribution. In the first region, the estimated slope of ΔC_l with respect to δ_s followed that of the wind-tunnel model closely. A distinct change in the $C_{l_{\delta s \alpha}}$ parameter was detected across the partition - corresponding to a sudden loss in effectiveness. For the spoilers' yawing contribution, the wind-tunnel model was followed closely; no sudden change was identified.

P1F4E50 (10000 ft, Mach 0.6, $\delta_s[0, 33.9]^\circ$, $\alpha[2.5, 6.7]^\circ$)

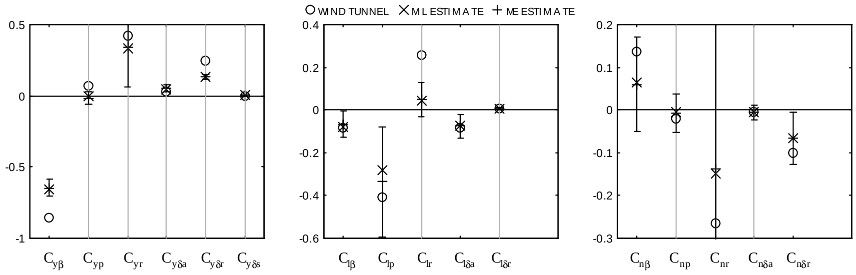

Figure 6-7: P1F4E50 Linear coefficient estimates

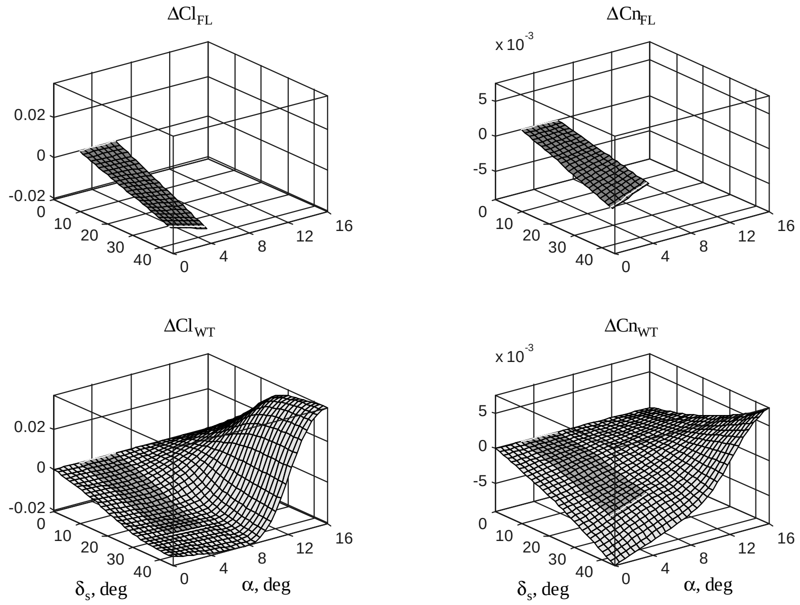

Figure 6-8: P1F4E50 Nonlinear spoiler coefficient estimates

Both flight estimates of C_{y_β} were less than the wind-tunnel derivative. The estimated C_{l_β} and $C_{l_{\delta a}}$ coefficients compared well with both wind-tunnel and ML results. In yaw, the unbiased estimates C_{n_β}, C_{n_r} and $C_{n_{\delta r}}$ were all close to their corresponding ML estimates, but smaller than those found in wind-tunnel testing. Because of the small range in α and the proximity of the data to any (expected) nonlinearity, no knots were implemented in the identification model. Estimates of both rolling and yawing spoiler contributions, however, were able to produce a good correlation with the wind-tunnel models. Only one discrepancy was found in the $C_{l_{\delta s \alpha}}$ term, which was more negative than the prior model.

P1F4E42, P3F6E93 (20000 ft, Mach 0.6, $\delta_s[0, 35.3]^\circ$, $\alpha[2.3, 10.2]^\circ$)

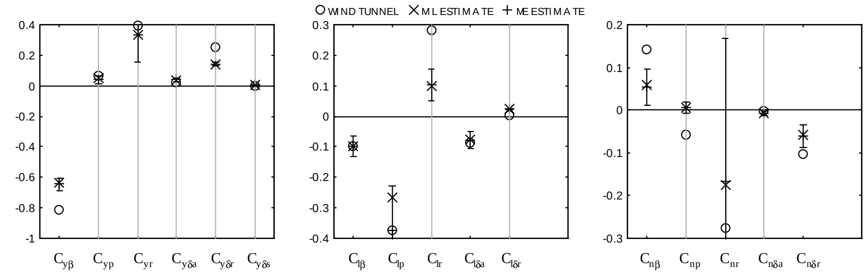

Figure 6-9: P1F4E42 Linear coefficient estimates

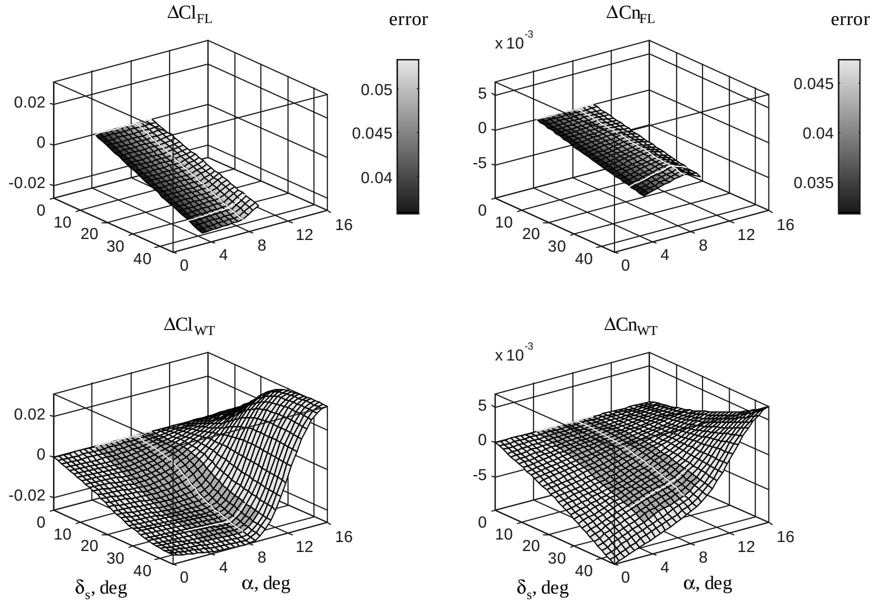

Figure 6-10: P1F4E42 Nonlinear spoiler coefficient estimates

As with the previous flight at Mach 0.6, the flight-estimated values for C_{y_β} were both smaller than the wind-tunnel result. The estimated C_{l_β} and $C_{l_{\delta a}}$ terms agreed well with previous estimates, though C_{l_p} in this case favoured the wind-tunnel coefficient. From flight data, the C_{n_β} estimates again proved smaller than the wind-tunnel prediction. C_{n_r} took on a significant, non-zero value. One knot in α was positioned at 8.5°, to allow identification of the expected change in spoiler effectiveness. This rapid change was indeed captured, though the extent was less than predicted by wind-tunnel results. In the first region, both rolling and yawing spoiler contributions compared extremely well with the wind-tunnel model. Furthermore, changes in both $C_{l_{\delta s \alpha}}$ and $C_{n_{\delta s \alpha}}$ were identified in the second (higher in α) region. The latter result may have come about because of noise in the yaw acceleration signal.

P1F5E97, P3F1E48 (30000 ft, Mach 0.6, $\delta_s[0, 43.9]^\circ$, $\alpha[4.3, 12.2]^\circ$)

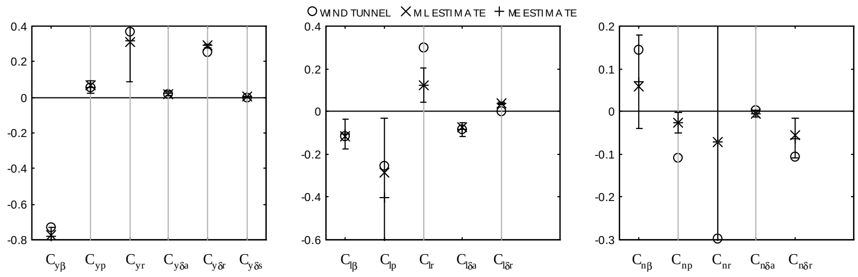

Figure 6-11: P1F5E97 Linear coefficient estimates

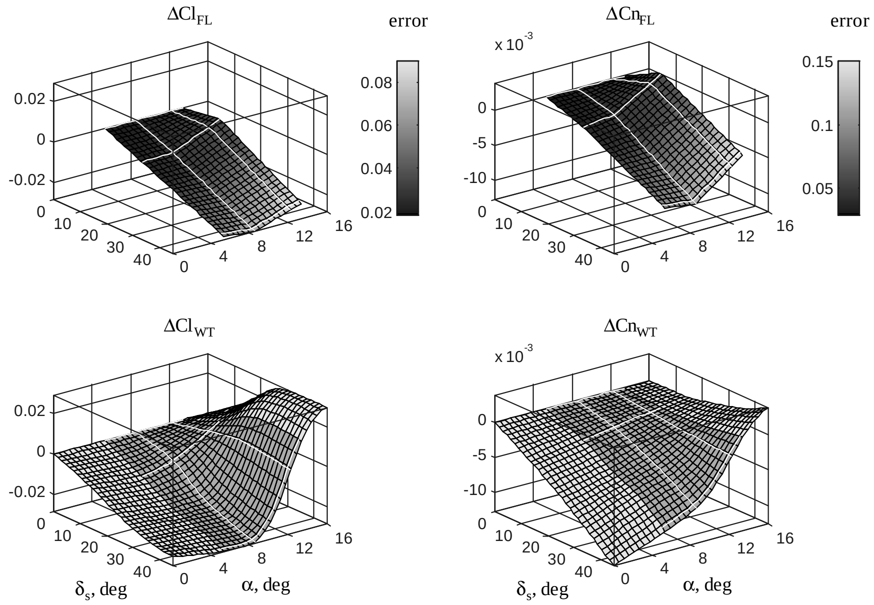

Figure 6-12: P1F5E97 Nonlinear spoiler coefficient estimates

Of the estimated sideforce coefficients, C_{y_β} proved very close to the prior results. C_{l_β} and $C_{l_{\delta a}}$ also correlated well with both wind-tunnel and Maximum Likelihood estimates. Other linear terms which followed the ML coefficients included C_{n_β}, C_{n_r} and $C_{n_{\delta r}}$. Since the data from two flights was used in this identification, covering a reasonably large range in both δ_s and α, a more complex model was postulated. One knot was placed in δ_s at 14.0° and one was placed in α at 8.5° to identify two possible nonlinearities in the model. The $C_{l_{\delta s}}$ parameters compared well with the wind-tunnel values, as did the $C_{l_{\delta s \alpha}}$ terms in all but the outermost region. Variation in this region could be attributed to the effect of unoptimally partitioned data.

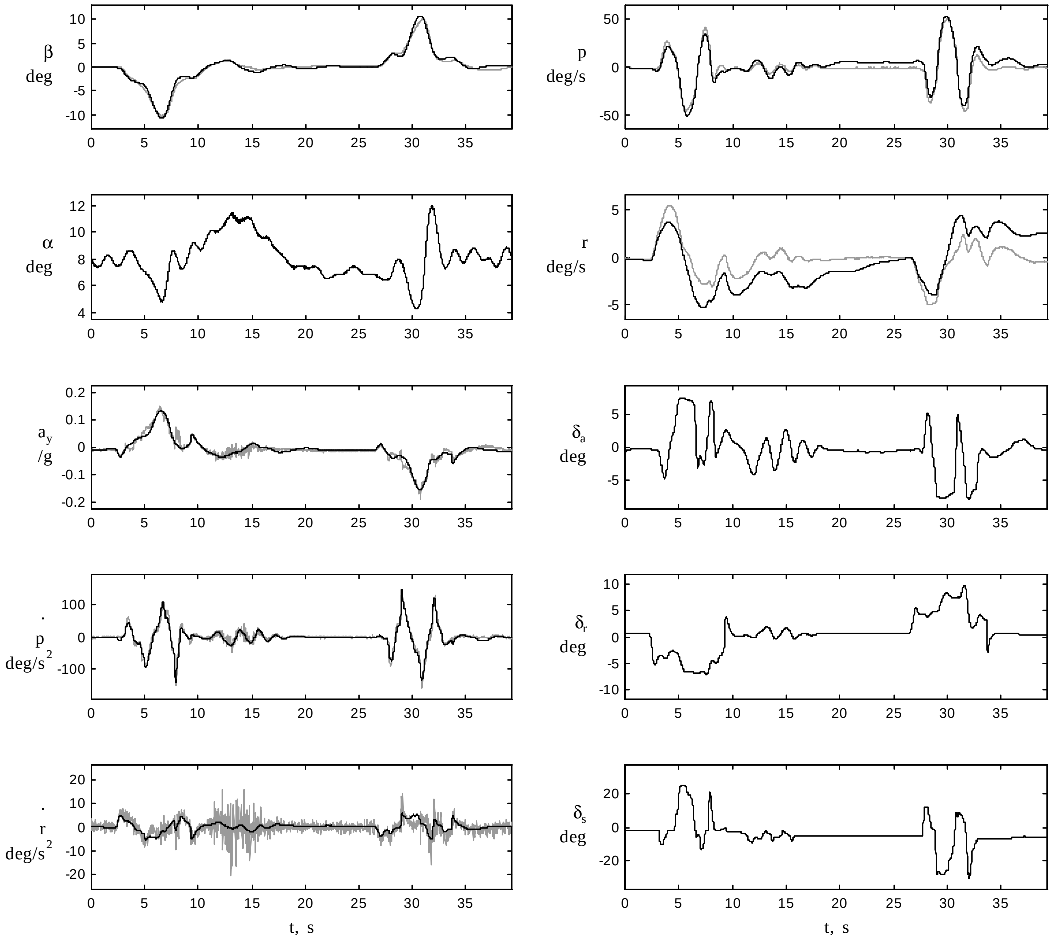

Figure 6-13: P3F1E48 Simulated response comparison

Using the nonlinear model estimated from flight, an equivalent dynamic response was simulated for comparison with the real flight data. The resulting signals followed the measured data quite closely, particularly the angular accelerations, $\dot{p}$ and $\dot{r}$. A discrepancy did appear, however, in the lateral acceleration between 12 and 23 seconds, most likely arising as a result of the biased sideforce coefficients. The sideslip and angular velocities also deviated around this interval, possibly due to the noise in the yawing acceleration coupled with the model uncertainty at high angle-of-attack.

At this point, it is important to remember that the LS solution to the equation error model minimises the response (acceleration) error and not the error in the independent (state and control) variables.

P3F6E45 (30000 ft, Mach 0.7, $\delta_s[0, 33.2]^\circ$, $\alpha[2.5, 9.3]^\circ$)

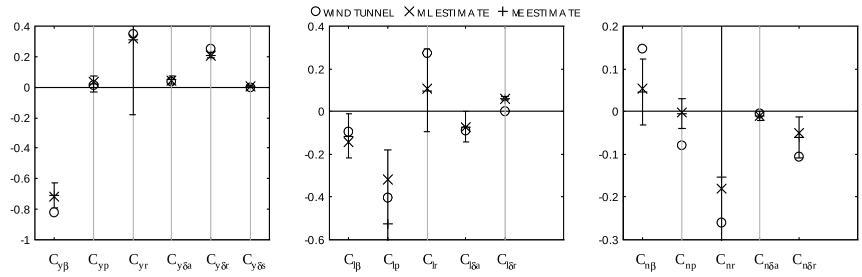

Figure 6-14: P3F6E45 Linear coefficient estimates

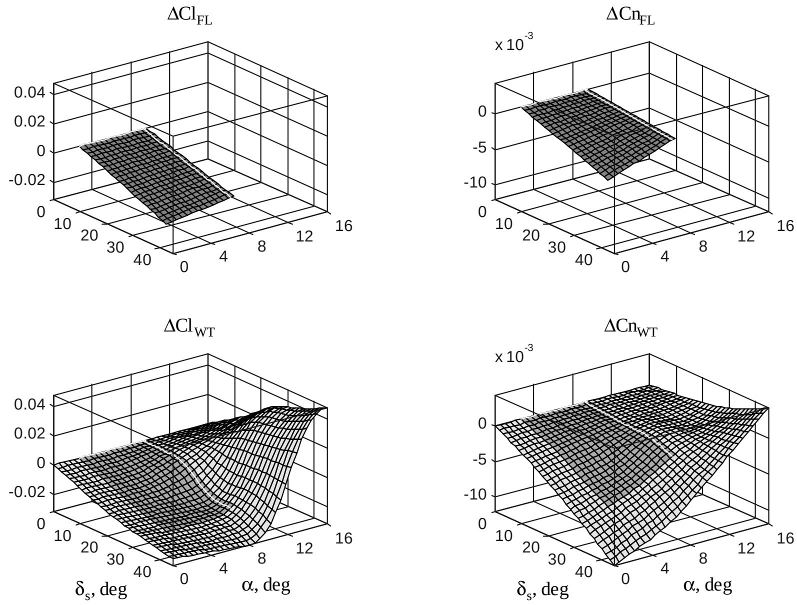

Figure 6-15: P3F6E45 Nonlinear spoiler coefficient estimates

The flight estimates of C_{y_β} were both smaller than the predicted wind-tunnel value. C_{l_p} was found to be markedly larger than both wind-tunnel and ML estimates. The yawing moment estimates, C_{n_β} and C_{n_r} reached smaller values than the wind-tunnel results, as with many previous cases. Restricted by the spread of data to only moderate angles-of-attack, the identification was performed on an unpartitioned model, since the expected (wind-tunnel) variation was approximately linear in this region. The spoilers' estimated rolling contribution compared extremely well with the wind-tunnel model. The estimated yawing contribution also compared well, though $C_{n_{\delta s \alpha}}$ was notably smaller.

P1F5E73 (30000 ft, Mach 0.8, $\delta_s[0, 42.2]^\circ$, $\alpha[1.9, 7.2]^\circ$)

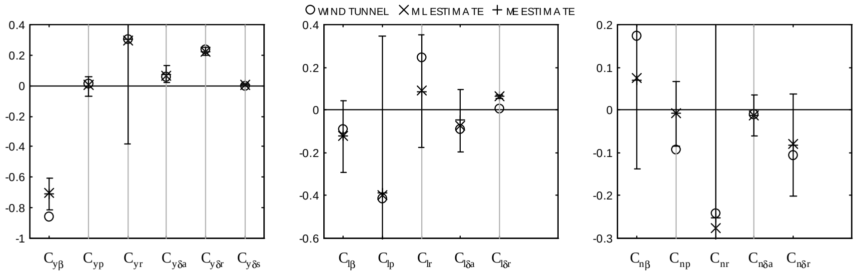

Figure 6-16: P1F5E73 Linear coefficient estimates

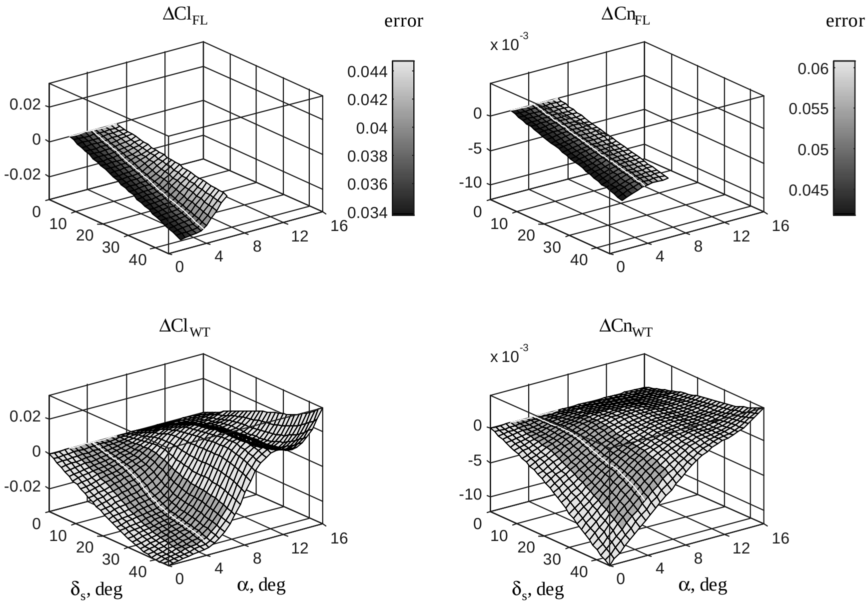

Figure 6-17: P1F5E73 Nonlinear spoiler coefficient estimates

Both flight estimates of C_{y_β} were again, smaller than the wind-tunnel value. All of the unbiased rolling moment derivatives correlated well with wind-tunnel and ML estimates, including C_{l_p}. The linear yawing moment term, C_{n_β}, was estimated to be smaller than the wind-tunnel coefficient, however, C_{n_r} and $C_{n_{\delta r}}$ both compared well. The highly nonlinear spoiler contribution at this elevated Mach number justified partitioning in α, so one knot was placed at 4.5°. The estimated rolling contribution compared remarkably well with the wind-tunnel model and successfully identified the rapid change near 4.5°. The estimated yawing contribution compared reasonably well, but with only a first-order polynomial and no partitioning in δ_s, was unable to capture the increasing drag (with spoiler deflection) effect.

6.3.3 26° wing-sweep

The low Mach numbers of 0.4 and below revealed a small loss estimated in the spoilers' rolling moment contribution with increasing α. In the region of low to moderate angle-of-attack, the local yawing effectiveness, $|C_{n_{\delta s}}|$, increased with δ_s.

At Mach numbers between 0.5 and 0.6, a small but significant change in the rolling contribution was identified at approximately 8° angle-of-attack. Similar to the previous configuration ($\Lambda = 16°$), this rapid decrease was less marked than that exhibited in the wind-tunnel model. The decrease in the spoilers' yawing moment coefficient was also very modest. Investigations on the characteristic high-α nonlinearities were not possible for the two flights at Mach 0.7 and 0.8 due to the small data-range. At Mach 0.7, the spoilers' rolling effectiveness remained near-constant for $\alpha < 8°$; the yawing contribution diminished slightly with increasing α. At Mach 0.8, $|C_{l_{\delta s}}|$ decreased significantly with increasing α above 4° ; the decrease in $|C_{n_{\delta s}}|$ was also found to be significant.

Table 6.4 summarises the *average* differences between the estimates and previous wind-tunnel and Maximum Likelihood results. As with the lower sweep-angle, the spoilers' estimated rolling contribution, $C_{l_{\delta s}}$, was marginally lower than the wind-tunnel value. In addition, both flight-obtained estimates of the yawing moment derivatives followed lower values than the wind-tunnel results. The estimates of C_{n_β} incurred the most significant difference, with values approximately 50 % lower on average.

	Coefficient								
	C_{y_β}	C_{l_β}	C_{l_p}	$C_{l_{\delta a}}$	$C_{l_{\delta s}}$	C_{n_β}	C_{n_r}	$C_{n_{\delta r}}$	$C_{n_{\delta s}}$
Wind-Tunnel	-0.06	-0.01	0.10	-0.01	-0.07	-0.49	-0.13	-0.36	-0.21
Flight(ML)	-0.02	0.12	0.17	0.13	-	0.06	0.07	0.06	-

Table 6.4: Mean fractional differences between estimates - $\Lambda = 26°$

P3F1E68, P3F6E141 (5000 ft, Mach 0.4, $\delta_s[0, 36.8]°$, $\alpha[4.8, 11.3]°$)

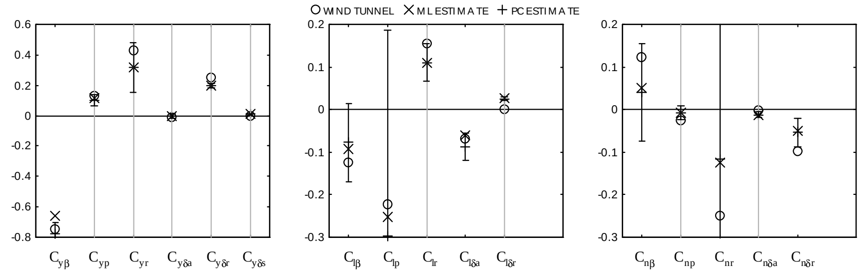

Figure 6-18: P3F1E68 Linear coefficient estimates

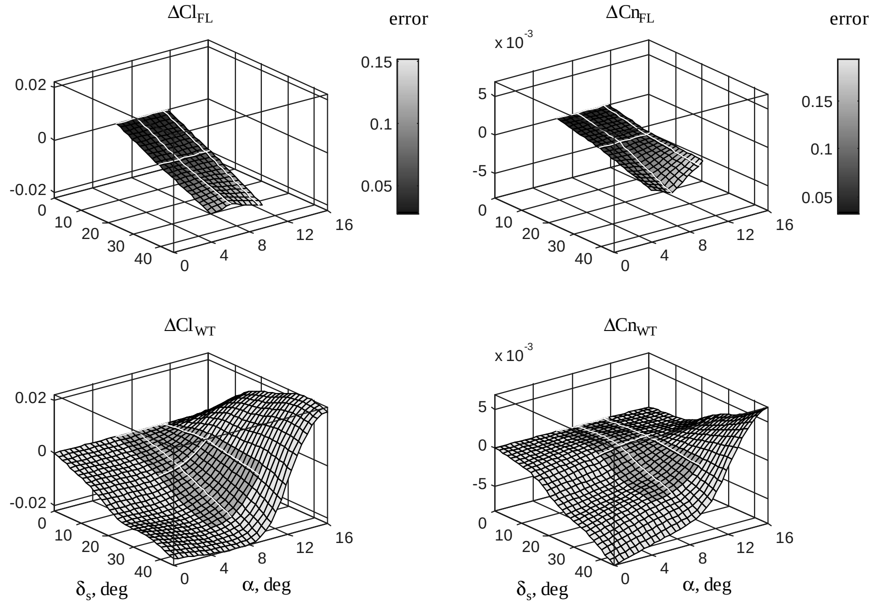

Figure 6-19: P3F1E68 Nonlinear spoiler coefficient estimates

The estimated sideforce coefficient, C_{y_β}, compared well with both wind-tunnel and ML estimates. C_{l_β}, C_{l_p} and $C_{l_{\delta a}}$ also compared well. The flight estimates of C_{n_β}, C_{n_r} and $C_{n_{\delta r}}$ were generally much smaller than the wind-tunnel values. A reasonably large range in δ_s and α with an ample number of data points in this case prompted partitioning in both axes. One knot was placed in each δ_s and α at 16.0° and 8.5°, respectively. The estimated rolling contribution for the spoilers followed the wind-tunnel model closely in the lower regions of α. However, in the higher regions, the cross-product $C_{l_{\delta s\alpha}}$ terms were closer to zero. The estimated yawing contribution followed the wind-tunnel model well, particularly with respect to the spoiler deflection.

P1F7E29 (10000 ft, Mach 0.4, $\delta_s[0, 42.7]^\circ$, $\alpha[6.1, 12.5]^\circ$)

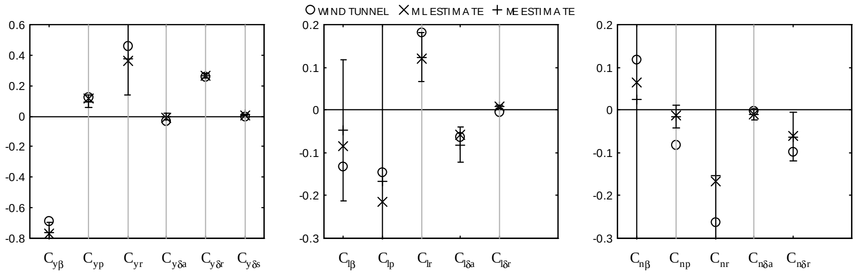

Figure 6-20: P1F7E29 Linear coefficient estimates

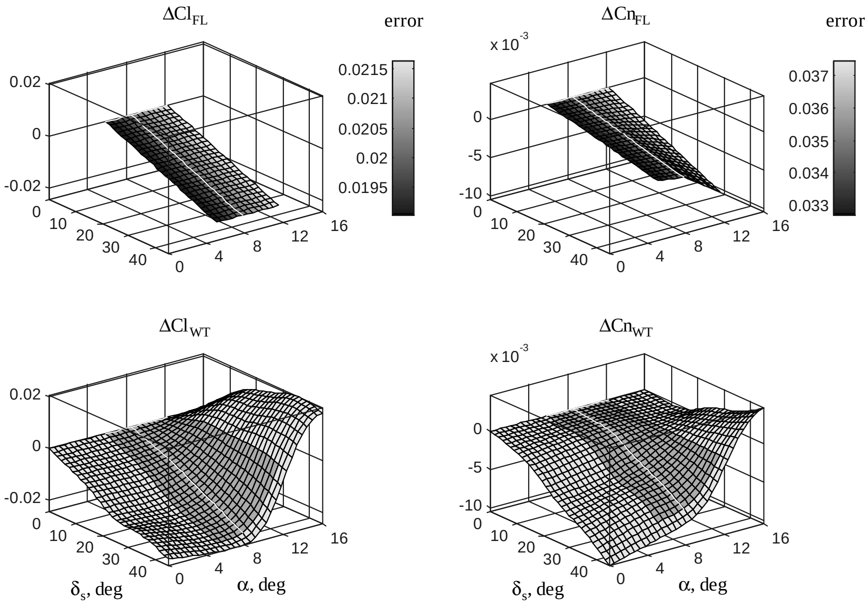

Figure 6-21: P1F7E29 Nonlinear spoiler coefficient estimates

C_{y_β} was again estimated favourably, with a small standard error. The estimate of C_{l_β} was, however, lower than both prior estimates, as was C_{n_β}. The other linear estimates generally compared well. In the postulated spoiler model, one knot was positioned at 8.5° in α. Contrary to the wind-tunnel results, though, no significant change in the rolling contribution was detected near this point. That is, $C_{l_{\delta s\alpha}}$ was approximately zero for both regions. The estimated yawing contribution parameter, $C_{n_{\delta s}}$ was significantly smaller than the wind-tunnel value and $C_{n_{\delta s}}$ indicated an (absolute) increase in the contribution with α, rather than a decrease.

P1F7E5 (20000 ft, Mach 0.4, $\delta_s[0, 40.3]^\circ$, $\alpha[6.5, 13.8]^\circ$)

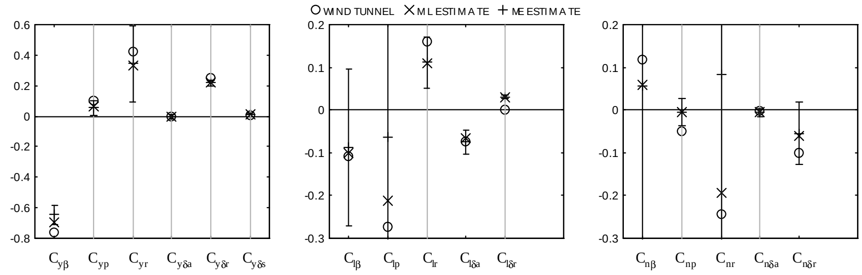

Figure 6-22: P1F7E5 Linear coefficient estimates

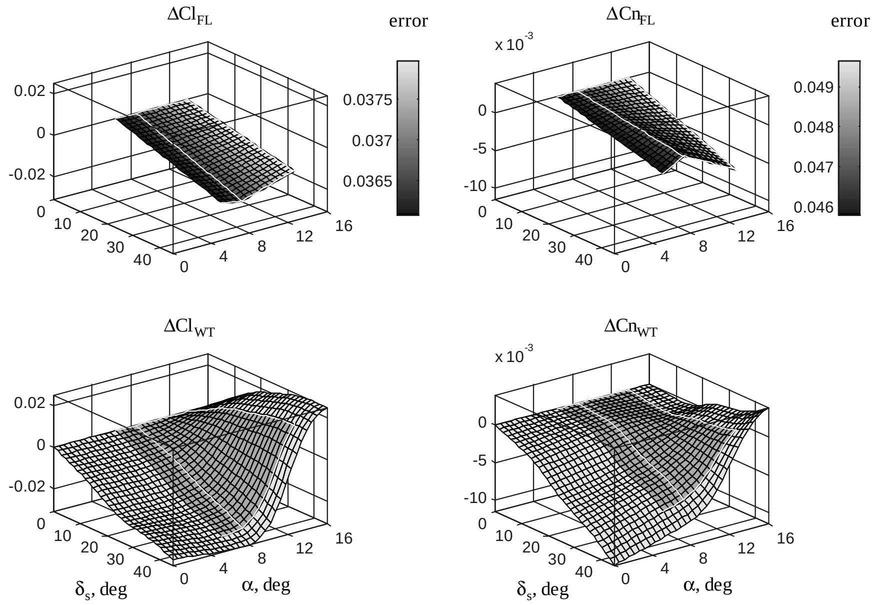

Figure 6-23: P1F7E5 Nonlinear spoiler coefficient estimates

Of the linear derivatives, all estimates of C_{y_β} and C_{l_β} compared well. The estimated roll-damping term, C_{l_p}, was much lower than the wind-tunnel or ML results. Additionally, the yaw-damping term, C_{n_r} was found to have a positive sign. The large standard error associated with this estimate, however, makes its value questionable. The spoiler model was given one knot in α at 8.5° to facilitate identification of the characteristic change in $C_{l_{\delta_s}}$ with increasing angle-of-attack. Such a change was detected, although it was not as prominent as in the wind-tunnel model. As in the previous case, the estimated $C_{n_{\delta_s}}$ parameter was less than that for the wind-tunnel. Furthermore, a dubious $C_{n_{\delta_s\alpha}}$ variation was apparent in the higher region, possibly due to data effects.

P3F1E36 (20000 ft, Mach 0.5, $\delta_s[0, 30.8]°$, $\alpha[6.7, 11.9]°$)

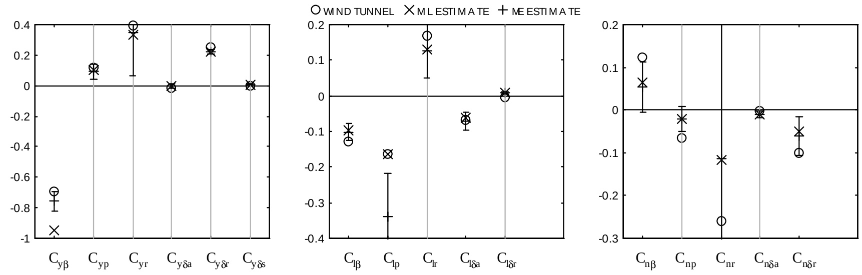

Figure 6-24: P3F1E36 Linear coefficient estimates

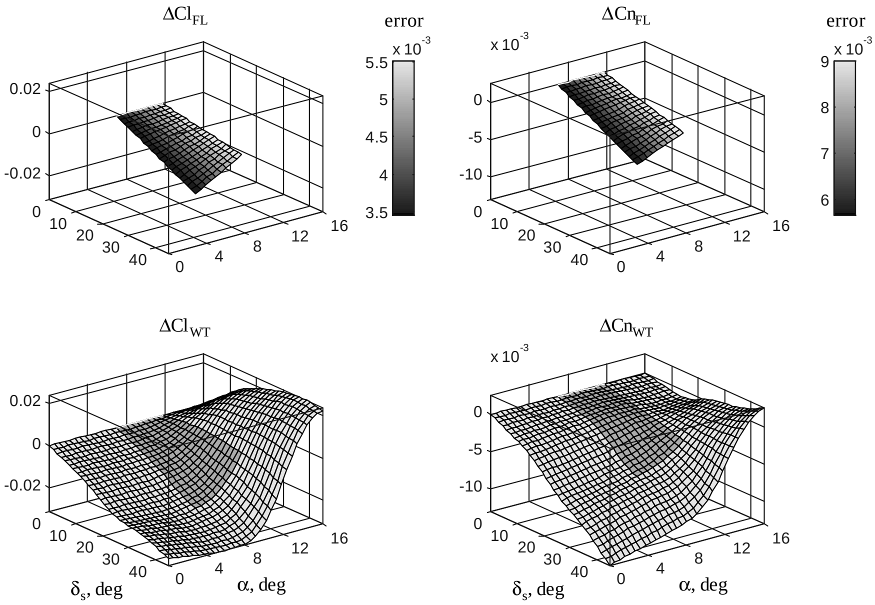

Figure 6-25: P3F1E36 Nonlinear spoiler coefficient estimates

The estimated value of C_{y_β} was closer to the wind-tunnel coefficient in this case. C_{l_p} was estimated to have a far larger value than either wind-tunnel or ML results, though both C_{l_β} and $C_{l_{\delta a}}$ compared well. All unbiased yawing moment derivatives, identified from flight, were less than those obtained from wind-tunnel testing. Since the data was spread high in the angle-of-attack range, one knot was positioned at 6.6° and the first set of coefficients were fixed at their interpolated wind-tunnel values. Both estimated $C_{l_{\delta s\alpha}}$ and $C_{n_{\delta s\alpha}}$ terms compared very well, though the same extent of rolling-control loss as exhibited in the wind-tunnel model was not seen.

P1F4E99 (5000 ft, Mach 0.6, $\delta_s[0, 38.4]°$, $\alpha[2.3, 6.1]°$)

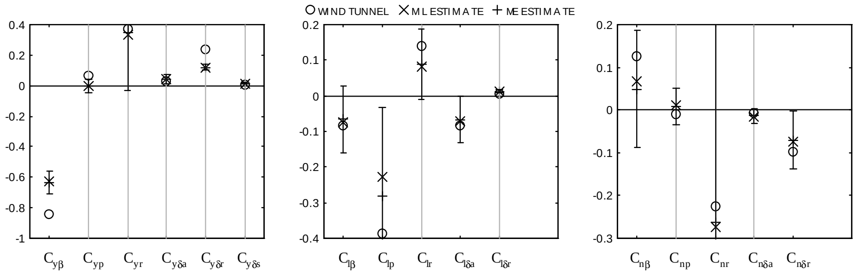

Figure 6-26: P1F4E99 Linear coefficient estimates

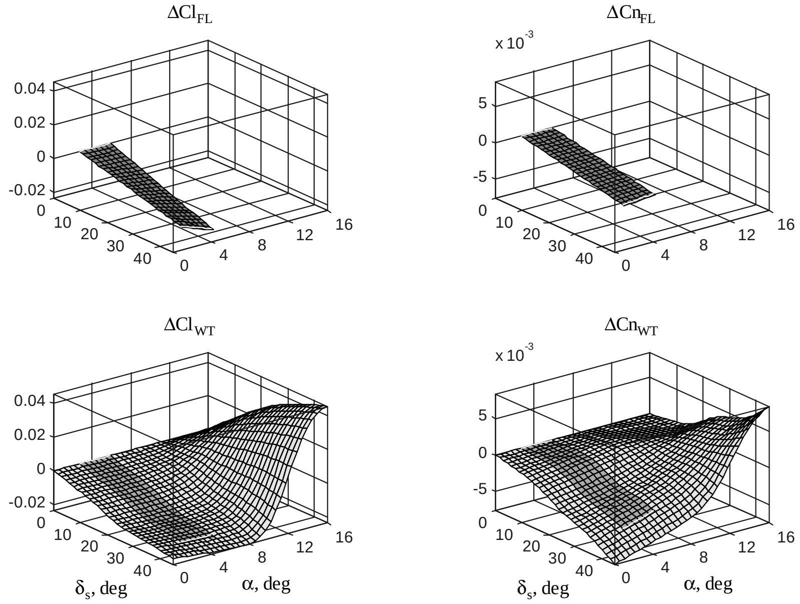

Figure 6-27: P1F4E99 Nonlinear spoiler coefficient estimates

Again, the flight-estimates of C_{y_β} were smaller than the wind-tunnel coefficients. Of the rolling-moment coefficients, C_{l_β} and $C_{l_{\delta a}}$ compared well with both prior estimates. Of the yawing-moment coefficients, C_{n_β} and $C_{n_{\delta r}}$ compared best. The α-range was low and very narrow for this flight case and therefore, no knots were utilised in the spoiler model. The estimated $C_{l_{\delta s}}$ parameter closely matched the wind-tunnel value, however, the estimate of $C_{l_{\delta s \alpha}}$ suggested an increase in the spoilers' effectiveness with α. The yawing contribution estimated from flight correlated reasonably well with the wind-tunnel model.

P1F5E89 (30000 ft, Mach 0.6, $\delta_s[0, 42.2]^\circ$, $\alpha[5.4, 13.8]^\circ$)

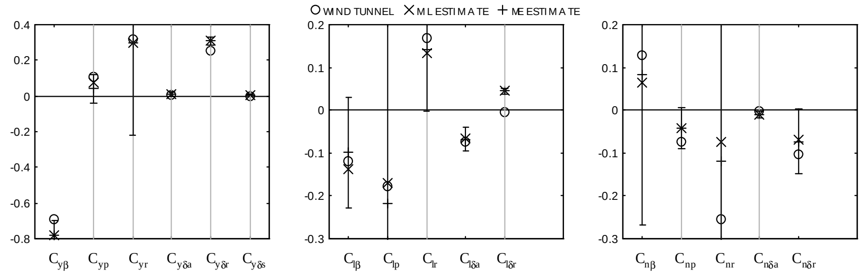

Figure 6-28: P1F5E89 Linear coefficient estimates

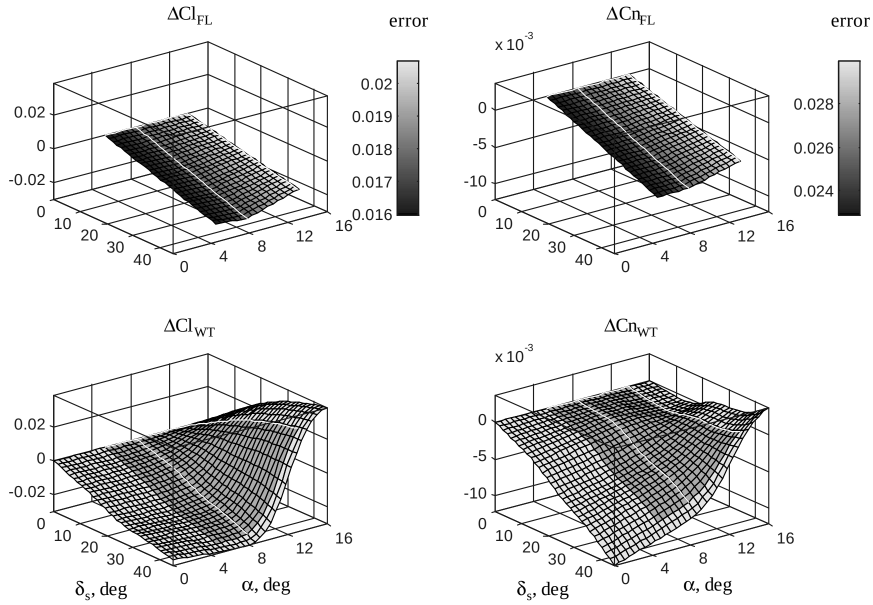

Figure 6-29: P1F5E89 Nonlinear spoiler coefficient estimates

The estimates of Cl_β, Cl_p and $Cl_{\delta a}$ all followed their wind-tunnel values very closely. The yawing moment coefficients, Cn_β, Cn_r and $Cn_{\delta r}$ favoured the ML estimates, however. The angle-of-attack range was relatively large for this flight case and so, in order to capture the expected change at 8.5°, the data was partitioned accordingly. For the lower region, the estimated rolling contribution compared agreeably with the wind-tunnel model. Across the partition though, the same difference in $Cl_{\delta s \alpha}$ did not result. The yawing contribution was estimated similarly - yielding a near constant variation with increasing α.

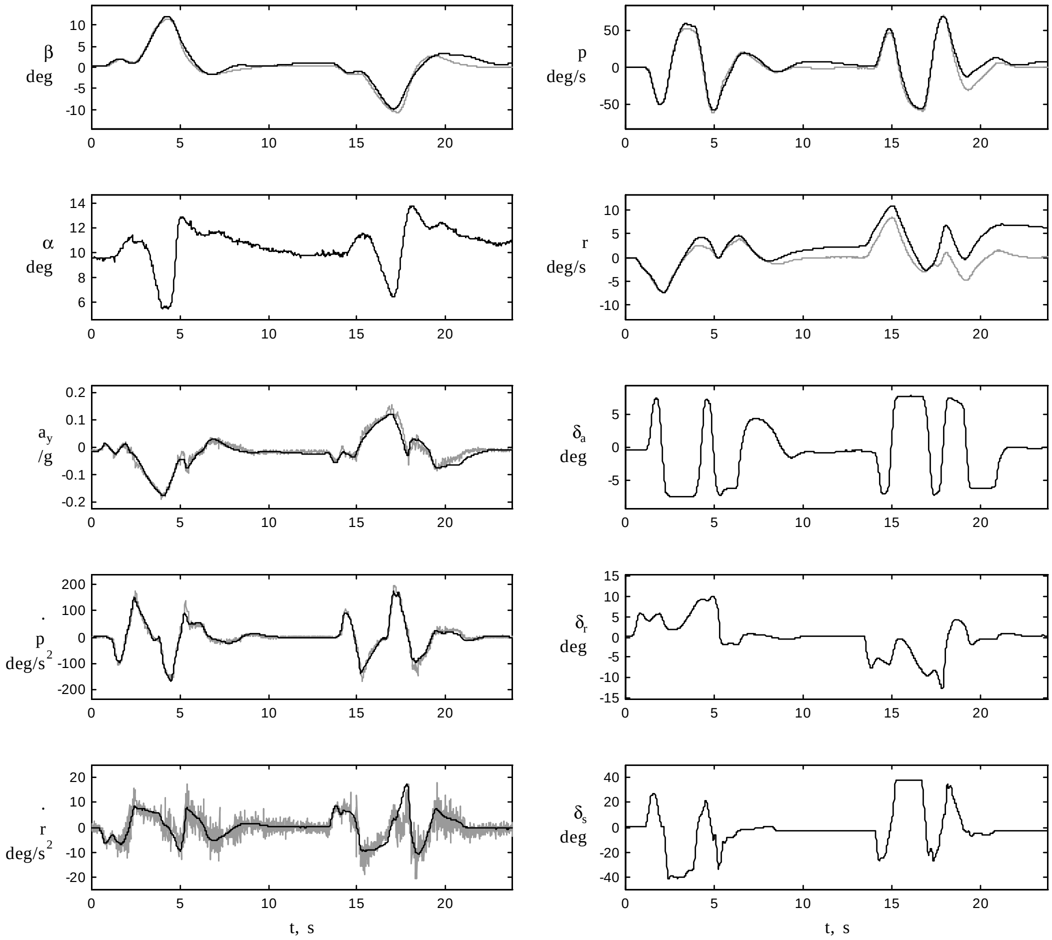

Figure 6-30: P1F5E89 Simulated response comparison

A dynamic response was simulated with the resulting identification model, as shown in the above figure (6-30). As with many of the flight cases examined, the manoeuvre was executed using a combined spoiler and rudder input. Aerodynamic complexities have arisen because of the high attitude at which the aircraft has been trimmed. Both linear and angular accelerations followed the measured data well. The level of measurement noise in the sensor data is clearly discernible against the computed signals, especially in the lateral and yawing accelerations. Of the state variables, the sideslip and roll rate compared generally well; the yaw rate exhibited some drift with respect to its measured path.

P3F6E53 (30000 ft, Mach 0.7, $\delta_s[0, 35.8]°$, $\alpha[2.9, 8.9]°$)

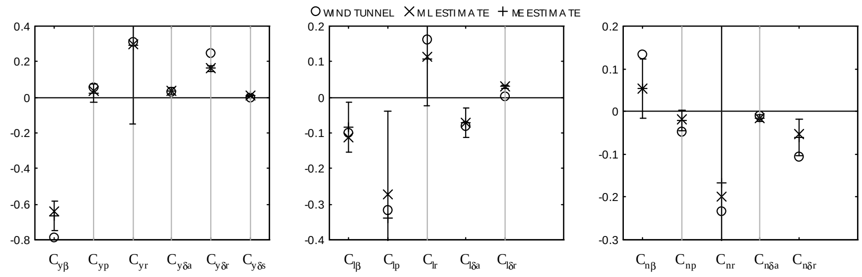

Figure 6-31: P3F6E53 Linear coefficient estimates

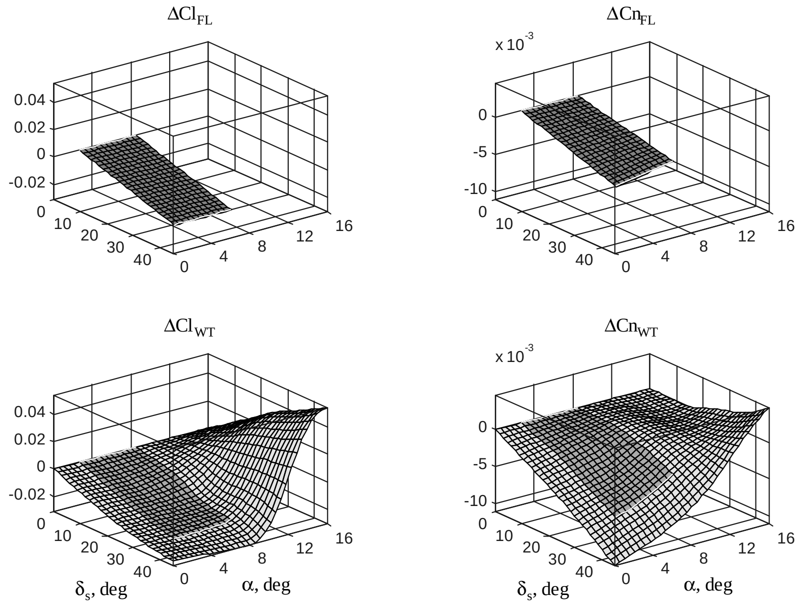

Figure 6-32: P3F6E53 Nonlinear spoiler coefficient estimates

The estimates of C_{y_β} for both flight identification analyses correlated well. Estimates obtained for both C_{l_β} and $C_{l_{\delta a}}$ also compared well; C_{l_p} was marginally larger. As in many of the previous cases, the yawing moment derivatives followed their ML estimates more closely than the wind-tunnel values. No knots were used in the identification model, since it was not expected to account for any significant aerodynamic nonlinearity. Consequently, the estimated rolling contribution compared extremely well with the wind-tunnel model. The estimated yawing contribution compared reasonably well, but did not decrease as sharply with α.

P1F5E65 (30000 ft, Mach 0.8, $\delta_s[0, 39.1]^\circ$, $\alpha[3.1, 7.2]^\circ$)

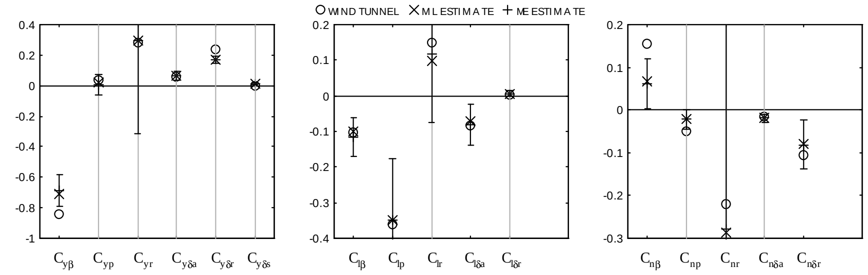

Figure 6-33: P1F5E65 Linear coefficient estimates

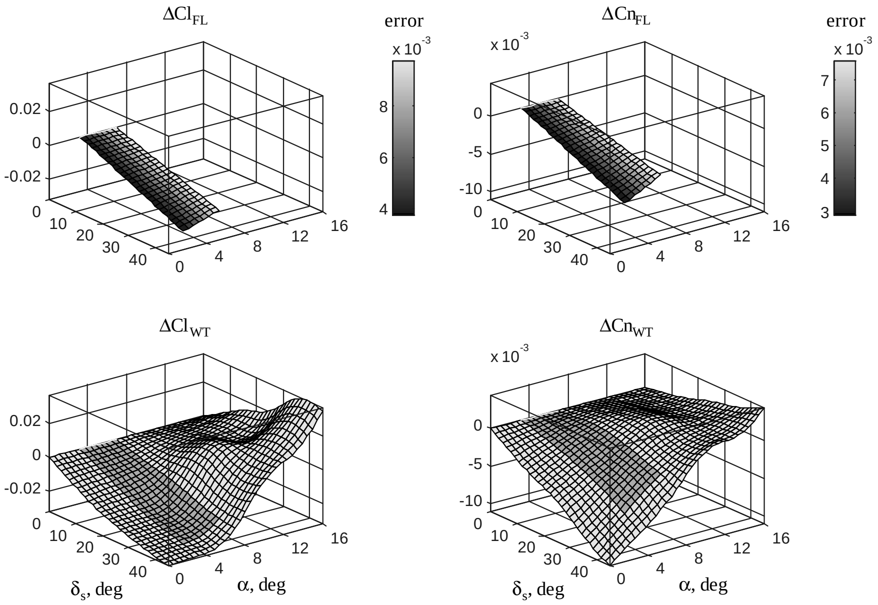

Figure 6-34: P1F5E65 Nonlinear spoiler coefficient estimates

C_{y_β} compared well with both wind-tunnel and ML results, as did all of the unbiased rolling moment coefficients, C_{l_β}, C_{l_p} and $C_{l_{\delta a}}$. The flight-identified derivatives, C_{n_β}, were approximately 50 % of the wind-tunnel value, whereas the C_{n_r} derivatives were significantly larger. As with the model of flight P3F1E36, the first set of parameters were fixed, since no data lay in the corresponding region. The partition dividing the two regions was placed in α at 3.0°. Both rolling and yawing contribution estimates compared agreeably with the wind-tunnel models, although the cross-product terms were somewhat smaller.

6.3.4 35° wing-sweep

For the range of Mach numbers examined, the estimated spoiler sideforce coefficient $C_{y_{\delta s}}$, followed the wind-tunnel results to within 3 %. As noted previously, however, the magnitude of this coefficient was very small in comparison with the remaining terms.

At the low Mach number of 0.4, a rapid loss in the spoilers' rolling moment contribution was detected near an angle-of-attack of 7°. The change was somewhat smaller than expected from the wind-tunnel model though, and control reversal was not established. A similar decrease in the yawing moment coefficient was also estimated in the high angle-of-attack regime. The loss in rolling effectiveness at approximately 8° angle-of-attack was maintained at the higher Mach numbers of 0.5 to 0.6. Above 14°, control reversal, in both roll and yaw was detected. This effect was still not as marked as in the wind-tunnel models, however, which predicted reversal above 12°. Below 8°, the spoilers' rolling contribution increased steadily with α. From the results for Mach numbers between 0.7 and 0.8, a possible delay in the spoilers' rolling loss characteristic was identified. That is, the rapid change in $\Delta C_l(\delta_s)$ was occurring at a higher angle-of-attack. The yawing contribution was generally more negative than the wind-tunnel model at Mach 0.8. Furthermore, a gentle decrease in the slope, $C_{n_{\delta s}}$, was found near $\alpha = 10°$. The higher sweep angle allowed investigations at several very high Mach numbers of 0.9 to 1.0. A marked nonlinear change (increase) in the spoilers' rolling and yawing contributions with δ_s was identified at moderate angles-of-attack. This characteristic diminished with increasing α and although the rolling effectiveness did not change sign, the yawing contribution became adverse.

Referring to Table 6.5, it can be seen that the difference between flight estimated and wind-tunnel $C_{l_{\delta s}}$ coefficients has increased from the previous wing-sweep results. Also of note is the significantly large difference exhibited between the flight estimates of C_{l_p} and $C_{l_{\delta a}}$. The remaining estimates obtained from the flight data compared agreeably.

	Coefficient								
	C_{y_β}	C_{l_β}	C_{l_p}	$C_{l_{\delta a}}$	$C_{l_{\delta s}}$	C_{n_β}	C_{n_r}	$C_{n_{\delta r}}$	$C_{n_{\delta s}}$
Wind-Tunnel	-0.03	0.06	0.01	0.06	-0.10	-0.47	-0.11	-0.30	-0.15
Flight(ML)	0.00	0.11	0.32	0.20	-	0.05	0.04	0.07	-

Table 6.5: Mean fractional differences between estimates - $\Lambda = 35°$

P1F7E49 (5000 ft, Mach 0.4, $\delta_s[0, 42.3]°$, $\alpha[6.4, 12.0]°$)

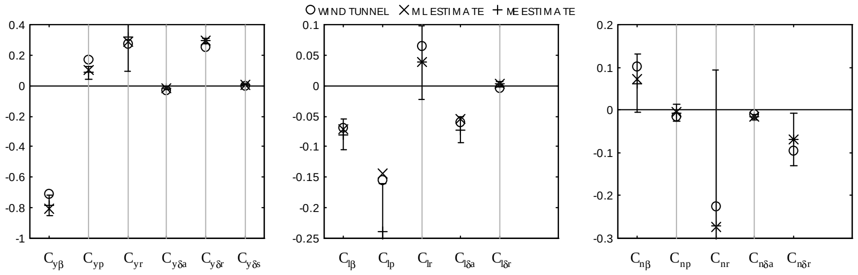

Figure 6-35: P1F7E49 Linear coefficient estimates

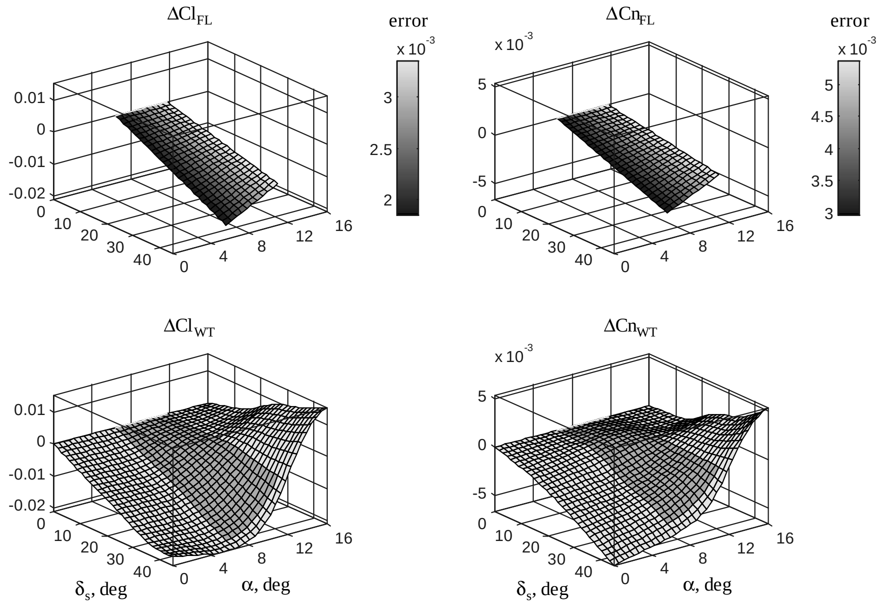

Figure 6-36: P1F7E49 Nonlinear spoiler coefficient estimates

The unbiased estimate of the sideforce derivative, C_{y_β}, compared well with both wind-tunnel and ML coefficients. C_{l_β} and $C_{l_{\delta a}}$ also compared well, though the estimate of the roll damping term, C_{l_p}, was larger than both previous results. The yawing moment coefficients generally followed their ML estimates. Since a significant change in the spoilers' rolling contribution was expected near the lower data limit of 6.3° in α, one knot was positioned there and the first set of parameters were fixed. The resulting variation decreased with angle-of-attack, however, the change was less than that seen in the wind-tunnel model. The estimated yawing moment contribution compared similarly.

P1F7E21 (10000 ft, Mach 0.4, $\delta_s[0, 44.0]^\circ$, $\alpha[8.0, 13.3]^\circ$)

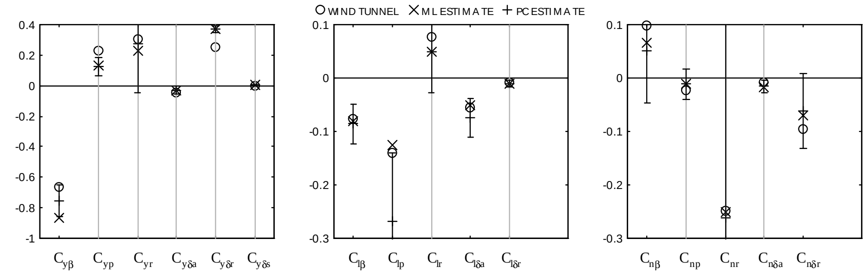

Figure 6-37: P1F7E21 Linear coefficient estimates

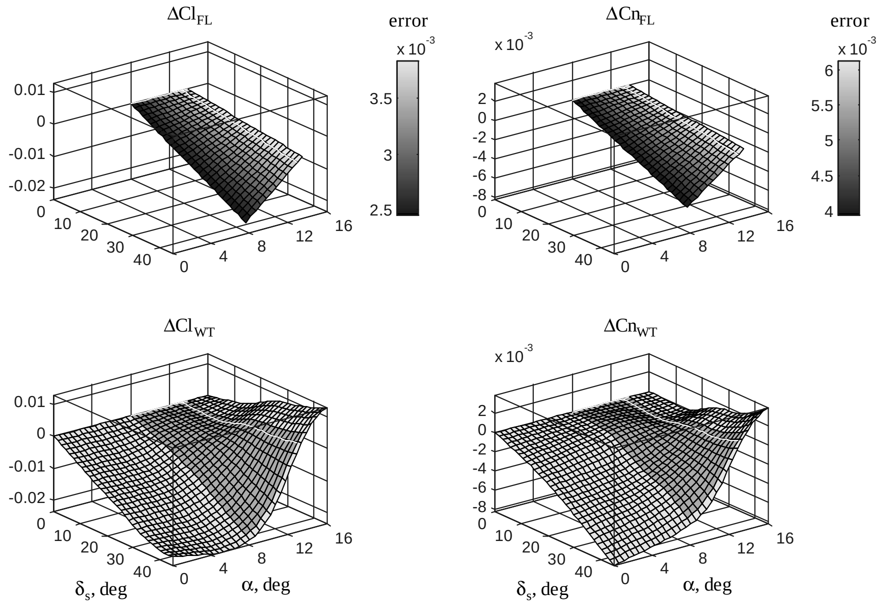

Figure 6-38: P1F7E21 Nonlinear spoiler coefficient estimates

C_{y_β} again compared well with both wind-tunnel and ML estimates. The linear rolling moment terms also compared as in the last case, with C_{l_p} estimated to be larger than the previous results. Estimates of C_{n_β} and $C_{n_{\delta r}}$ were smaller than the wind-tunnel coefficients. The same partitioning scheme as used in the last case was employed, placing one knot in α at 7.9°, and fixing the parameters below that. An abrupt loss in the rolling contribution with angle-of-attack was identified, although it was less than the wind-tunnel characteristic and did not develop into control reversal. The estimated yawing contribution also correlated well, though its reduction with α was less significant.

P3F6E117 (10000 ft, Mach 0.5, $\delta_s[0, 33.2]°$, $\alpha[3.5, 9.8]°$)

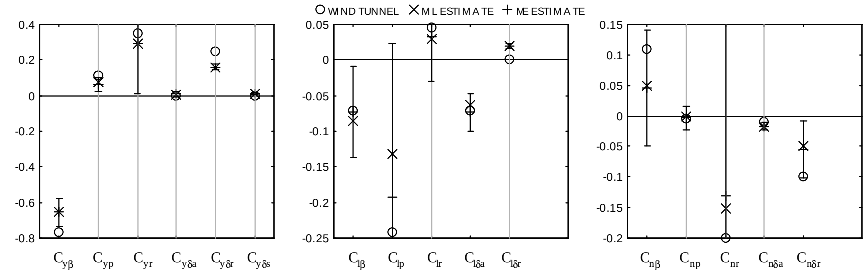

Figure 6-39: P3F6E117 Linear coefficient estimates

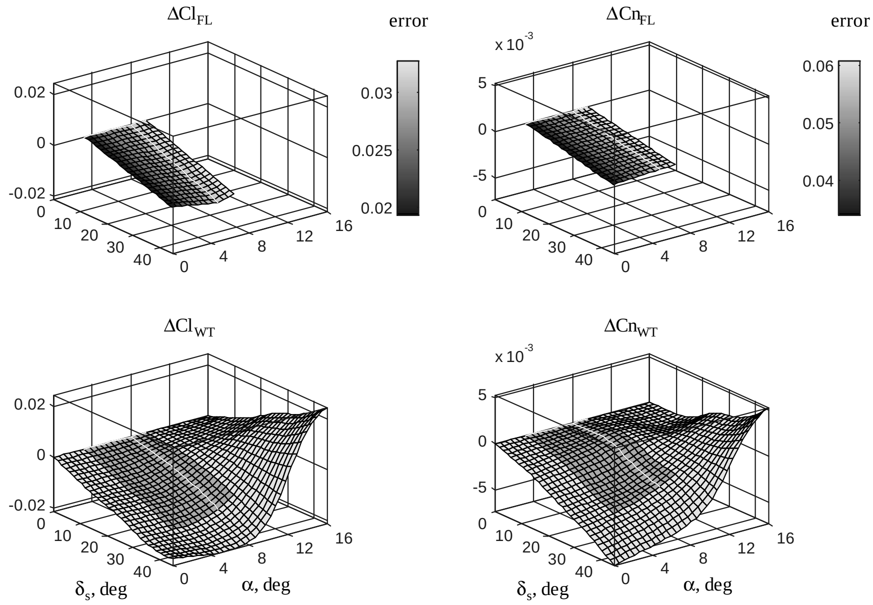

Figure 6-40: P3F6E117 Nonlinear spoiler coefficient estimates

The estimates of C_{y_β}, C_{l_β} and $C_{l_{\delta a}}$ all compared well with the wind-tunnel and ML coefficients. C_{l_p} was estimated mid-way between its previous estimates. The estimated yawing moment derivatives generally correlated with the ML estimates. For this flight case, one knot was placed in α at 8.0°, to facilitate detection of the sudden loss in spoiler rolling contribution. The estimate of the parameter, $C_{l_{\delta s}}$ closely matched the corresponding wind-tunnel term, however, $C_{l_{\delta s\alpha}}$ in the first region was more negative. The estimate of $C_{l_{\delta s\alpha}}$ in the second region was also lower than expected. The spoilers yawing contribution showed a near-constant variation with α.

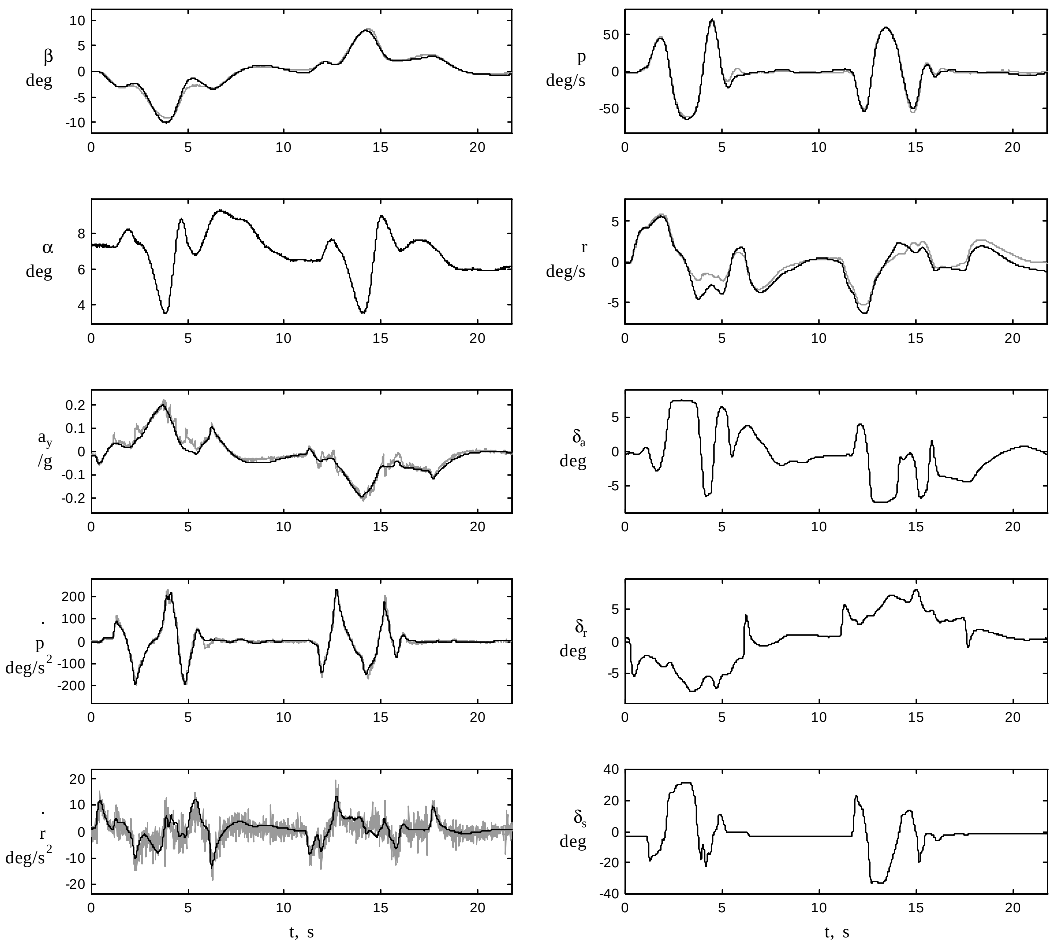

Figure 6-41: P3F6E117 Simulated response comparison

For verification of the estimated model, an equivalent response was computed and compared against the real flight data. The accelerations, a_y, $\dot{p}$ and $\dot{r}$ all compared very well, as did most of the lateral state variables. One of the more notable differences appeared in the roll rate signal. This may be due to the noise in the roll acceleration and its inherent effect on the estimated model. It may also be due to cross-coupling errors, since the longitudinal model estimated was much less accurate.

P3F1E27 (20000 ft, Mach 0.5, $\delta_s[0, 45.4]^\circ$, $\alpha[9.1, 14.2]^\circ$)

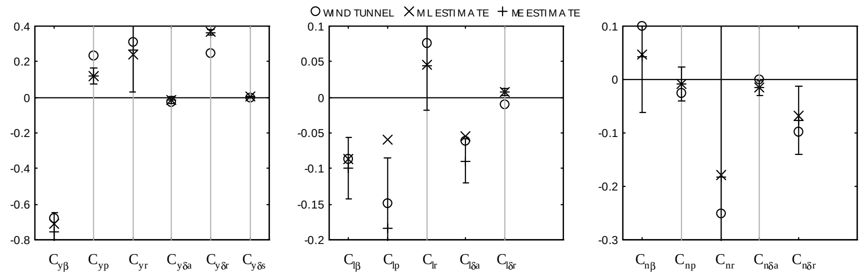

Figure 6-42: P3F1E27 Linear coefficient estimates

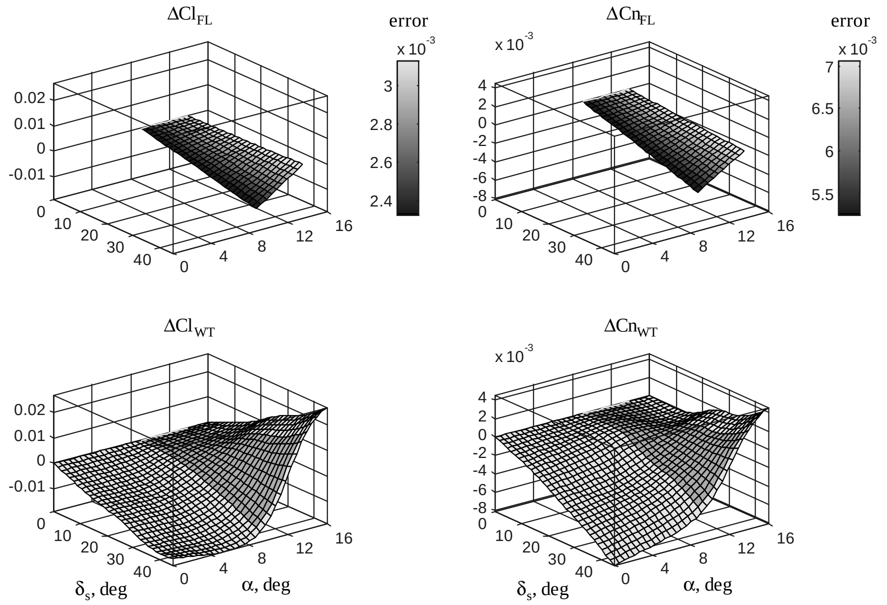

Figure 6-43: P3F1E27 Nonlinear spoiler coefficient estimates

The estimate of C_{y_β} was slightly larger than the previous estimates considered. Among the rolling moment derivatives, C_{l_β} compared well, although C_{l_p} and $C_{l_{\delta a}}$ were more negative than both the wind-tunnel and ML estimates. As expected, the estimated yawing moment derivatives were generally lower than the wind-tunnel coefficients. One knot was placed at the minimum angle-of-attack point of 9.0°, which created a region in which a rapid control loss was anticipated. The parameters in the lower region were fixed and the remaining parameters unbiased. The resulting estimated models for rolling and yawing contributions compared reasonably with the wind-tunnel models, though an expected sign reversal was not seen.

P1F4E91 (5000 ft, Mach 0.6, $\delta_s[0, 34.5]^\circ$, $\alpha[2.9, 6.8]^\circ$)

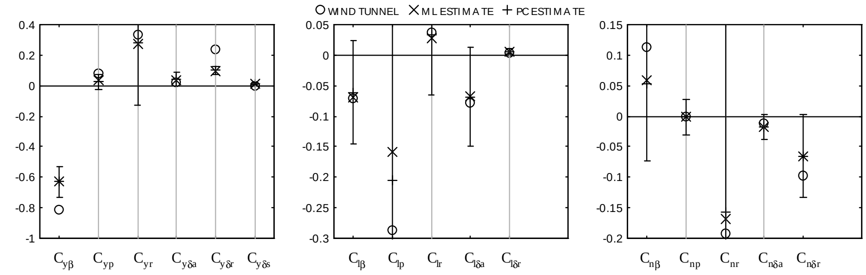

Figure 6-44: P1F4E91 Linear coefficient estimates

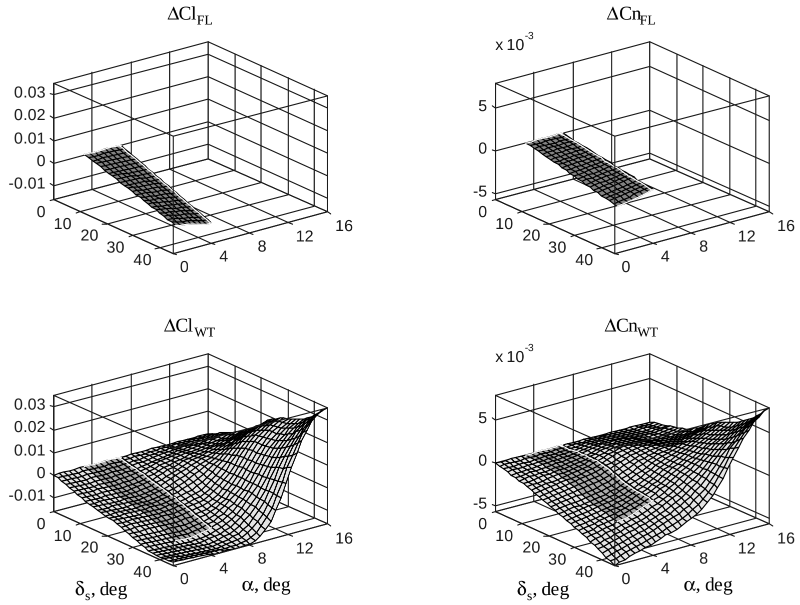

Figure 6-45: P1F4E91 Nonlinear spoiler coefficient estimates

Both flight-estimates of C_{y_β} were marginally smaller than the wind-tunnel coefficient. The estimated derivatives, C_{l_β} and $C_{l_{\delta a}}$ compared well, however. The flight-estimates of C_{n_β}, C_{n_r} and $C_{n_{\delta r}}$ generally exhibited lower values than the wind-tunnel coefficients. There were no knots utilised in the identification model, due to the narrow α-range in the data. The estimated $C_{l_{\delta s}}$ term closely matched that in the wind-tunnel model, although the cross-product term, $C_{l_{\delta s \alpha}}$, indicated an increase in the rolling contribution with α. In contrast, both $C_{n_{\delta s}}$ and $C_{n_{\delta s \alpha}}$ terms correlated well.

P1F4E22 (20000 ft, Mach 0.6, $\delta_s[0, 41.9]°$, $\alpha[5.6, 11.2]°$)

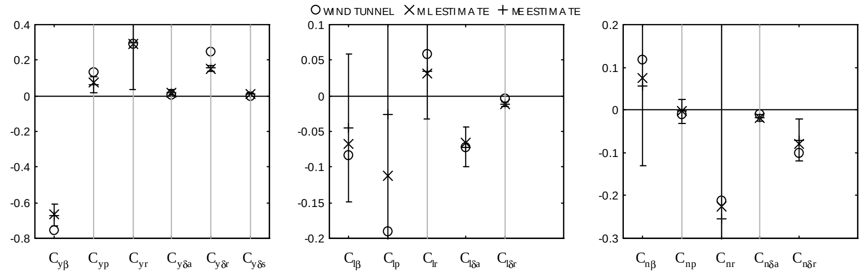

Figure 6-46: P1F4E22 Linear coefficient estimates

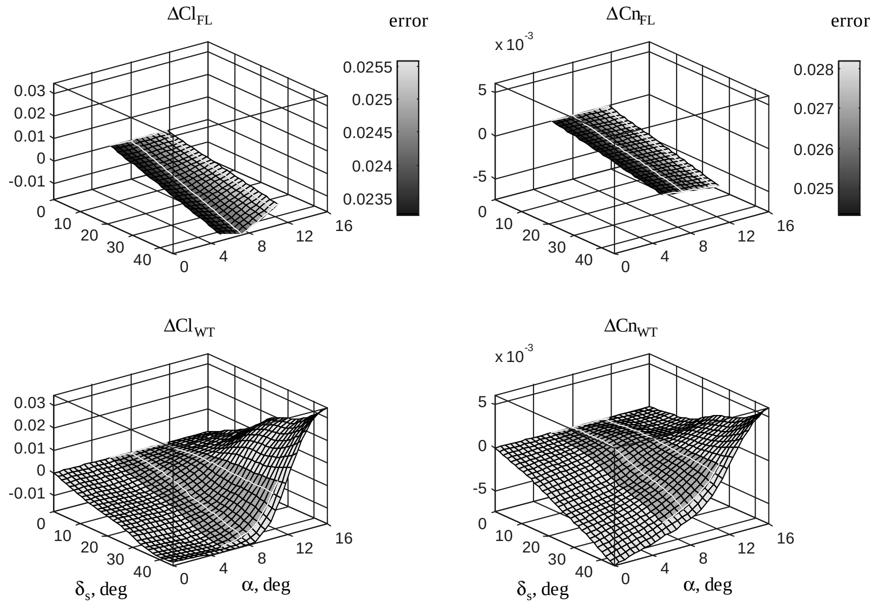

Figure 6-47: P1F4E22 Nonlinear spoiler coefficient estimates

The sideforce estimate, C_{y_β} compared well with both wind-tunnel and ML results. C_{l_β} and $C_{l_{\delta a}}$ also compared well and C_{l_p} was estimated midway between the two previous results. All of the estimates for the yawing moment derivatives generally agreed with each other. A single knot was positioned in α at 8.0°, to allow identification of the expected change in the spoilers' rolling effectiveness. Although the estimated $C_{l_{\delta s}}$ parameter compared well with the interpolated wind-tunnel value, $C_{l_{\delta s \alpha}}$ for the first region was more negative and for the second region, less positive. The yawing contribution actually increased with α, contrary to the wind-tunnel model variation.

P1F5E81 (30000 ft, Mach 0.6, $\delta_s[0, 46.8]^\circ$, $\alpha[9.3, 16.1]^\circ$)

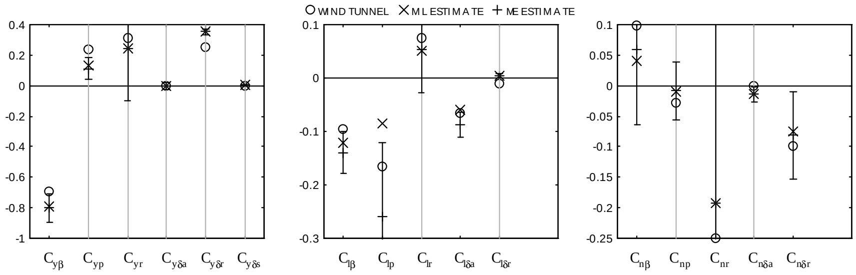

Figure 6-48: P1F5E81 Linear coefficient estimates

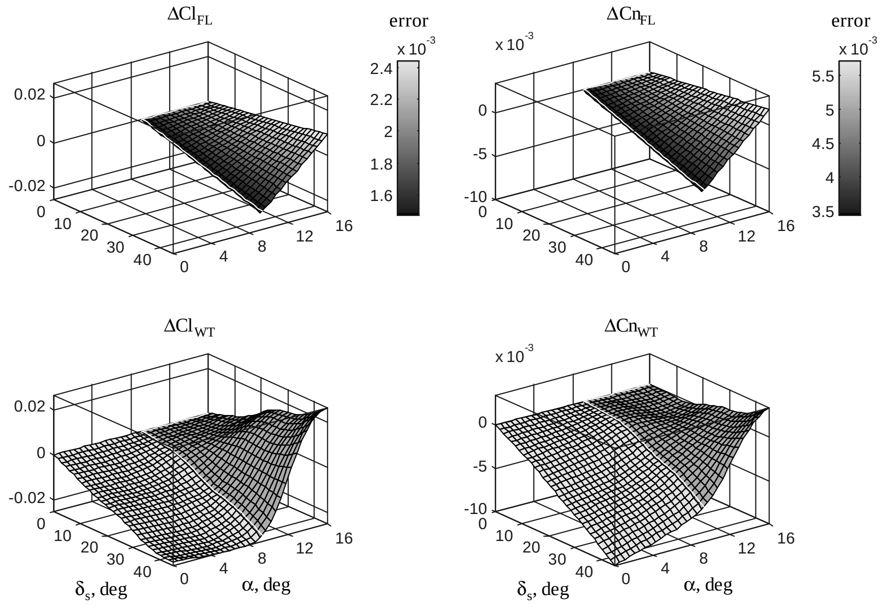

Figure 6-49: P1F5E81 Nonlinear spoiler coefficient estimates

The estimate of C_{y_β} compared well with the ML estimate. Of the linear rolling moment coefficients, C_{l_β}, $C_{l_{\delta a}}$ and in particular, C_{l_p}, were all estimated larger than their wind-tunnel or ML values. The yawing moment coefficients again correlated more closely with the ML estimates. The spoilers' rolling contribution in the high angle-of-attack regime was successfully estimated, using one partition at 9.2°. Fixing the lower model parameters, the remaining coefficients were estimated from the data and compared reasonably with the wind-tunnel model. Control reversal was identified in the $C_{l_{\delta s \alpha}}$ term, though it was less prominent. The estimated yawing contribution compared very well with its wind-tunnel model.

P3F6E61 (30000 ft, Mach 0.7, $\delta_s[0, 33.2]^\circ$, $\alpha[3.8, 10.1]^\circ$)

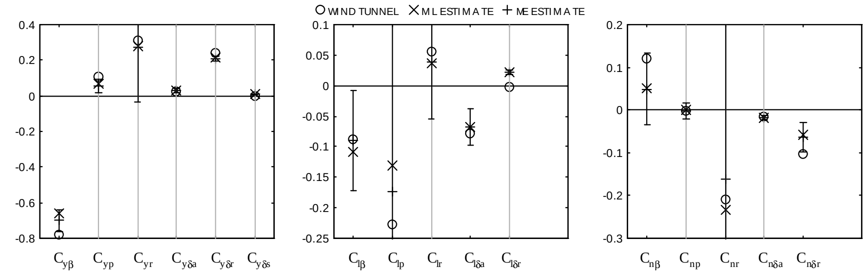

Figure 6-50: P3F6E61 Linear coefficient estimates

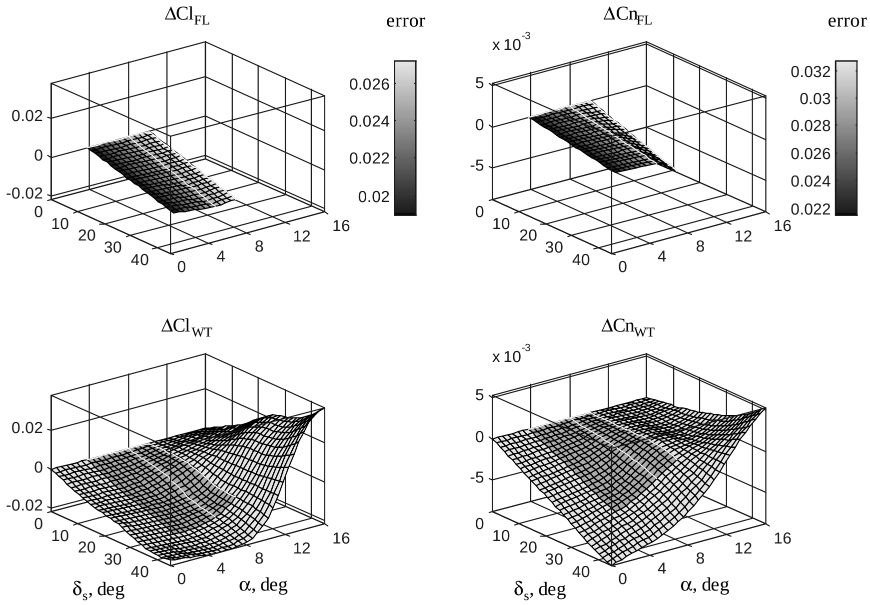

Figure 6-51: P3F6E61 Nonlinear spoiler coefficient estimates

Estimates of the unbiased derivatives, C_{y_β}, C_{l_β}, $C_{l_{\delta a}}$ and $C_{n_{\delta r}}$ all compared well against both wind-tunnel and ML results. C_{l_p}, C_{n_β} and C_{n_r} compared reasonably well, although their standard errors were relatively large. In the spoilers' nonlinear model, one knot at 8.0° angle-of-attack was implemented. The resulting estimated rolling contribution did produce a change across this partition, though it was far less significant than in the wind-tunnel model. The estimated yawing moment contribution remained relatively constant with α.

P1F5E57 (30000 ft, Mach 0.8, $\delta_s[0, 41.9]^\circ$, $\alpha[2.6, 8.8]^\circ$)

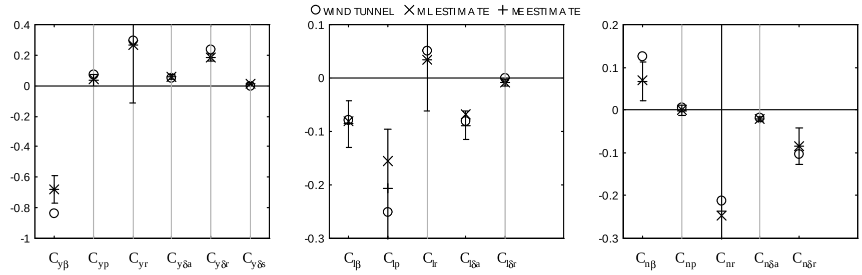

Figure 6-52: P1F5E57 Linear coefficient estimates

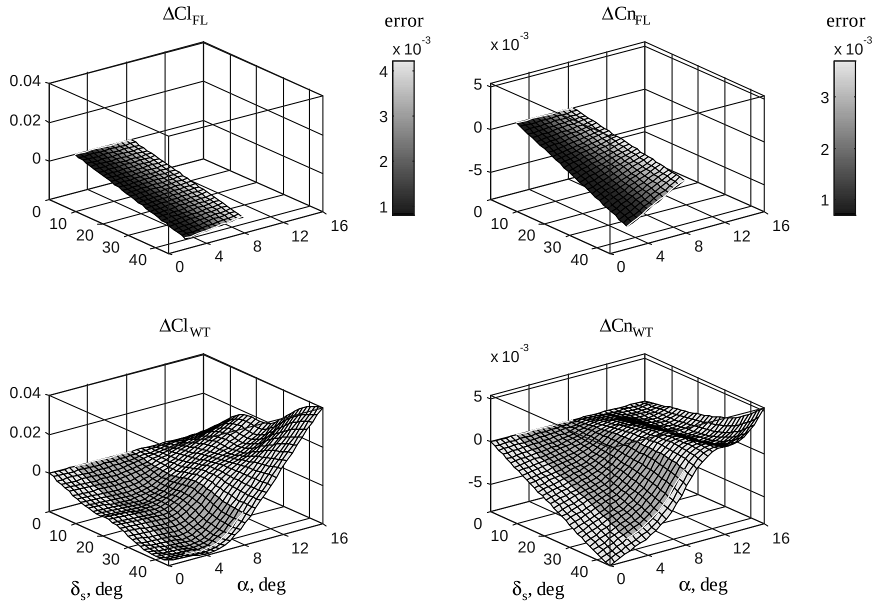

Figure 6-53: P1F5E57 Nonlinear spoiler coefficient estimates

The estimate of C_{y_β} matched the ML estimate closely, though both were smaller than the wind-tunnel coefficient. The rolling moment coefficient estimates of C_{l_β} and $C_{l_{\delta a}}$ again compared well. C_{n_r} and $C_{n_{\delta r}}$ also compared well with both wind-tunnel and ML estimates. Only one partition was utilised in α at 2.5° - the minimum data point - and the first set of spoiler parameters were fixed. The estimated rolling contribution model did not exhibit degradation with α to the same extent as the wind-tunnel model. The estimated yawing contribution model was likewise, less sensitive with respect to the angle-of-attack.

P1F5E21 (40000 ft, Mach 0.8, $\delta_s[0, 46.7]^\circ$, $\alpha[8.0, 12.4]^\circ$)

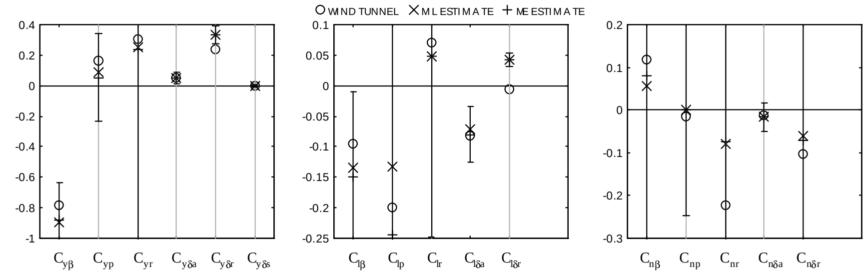

Figure 6-54: P1F5E21 Linear coefficient estimates

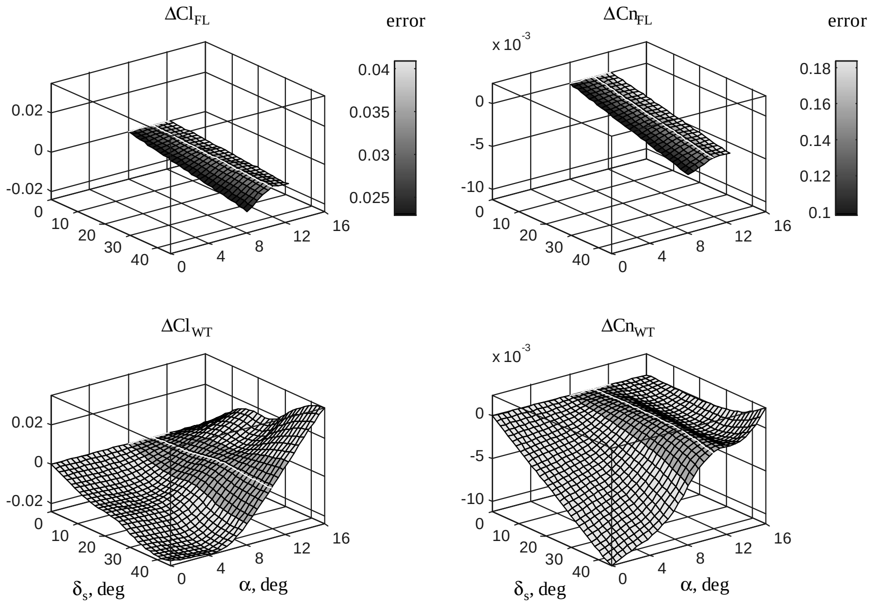

Figure 6-55: P1F5E21 Nonlinear spoiler coefficient estimates

As with many of the previous cases, the flight estimates of C_{y_β} were significantly different to the wind-tunnel coefficient. The same situation occurred with C_{l_β} and all of the unbiased yawing moment derivatives, C_{n_β}, $C_{n_{\delta r}}$ and especially C_{n_r}. For this flight case, the range in α was quite high and covered an interesting region on the spoilers' yawing contribution model. Therefore, two knots were implemented in the identification model at 7.9° and 10.5° in angle-of-attack and the lower parameters were fixed. The resulting rolling contribution model showed an initial decrease in $C_{l_{\delta_s}}$ and in the higher region, actually increased by a small amount. A reasonable correlation was achieved in the yawing contribution, although the $C_{n_{\delta_s}}$ parameter was estimated less than the wind-tunnel equivalent.

P3F2E93 (40000 ft, Mach 0.9, $\delta_s[0, 35.2]^\circ$, $\alpha[4.8, 8.9]^\circ$)

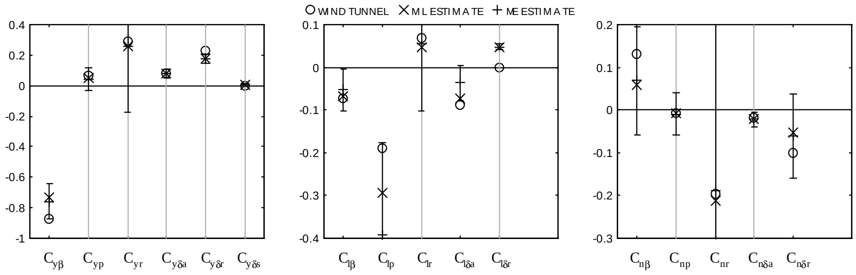

Figure 6-56: P3F2E93 Linear coefficient estimates

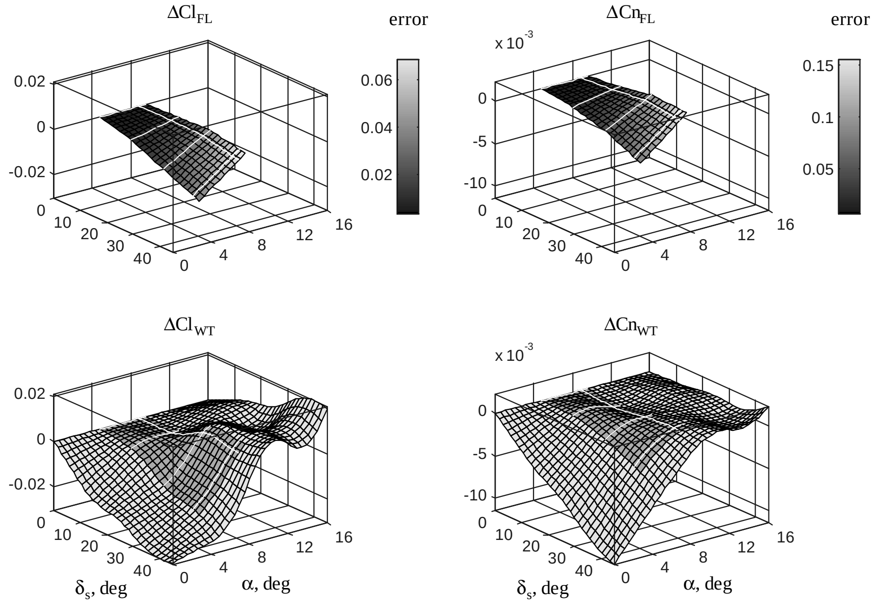

Figure 6-57: P3F2E93 Nonlinear spoiler coefficient estimates

The estimated C_{y_β} coefficient compared well, as did the rolling moment coefficient, C_{l_β}. On the other hand, C_{l_p} was estimated larger than both wind-tunnel and ML results and $C_{l_{\delta a}}$ was estimated smaller. The estimated yawing moment coefficient, C_{n_r}, correlated extremely well with both previous results. A predominantly nonlinear variation with spoiler deflection was apparent in the wind-tunnel model corresponding to this flight case. In order to capture this characteristic, two knots were positioned in δ_s at 12.0° and 24.0°. Additionally, one knot was placed in α at 4.7° and the lower parameters were fixed. The resulting estimates of both rolling and yawing contributions compared reasonably, although their variation with δ_s was more subtle.

P3F6E37 (40000 ft, Mach 1.0, $\delta_s[0, 32.6]^\circ$, $\alpha[4.9, 7.8]^\circ$)

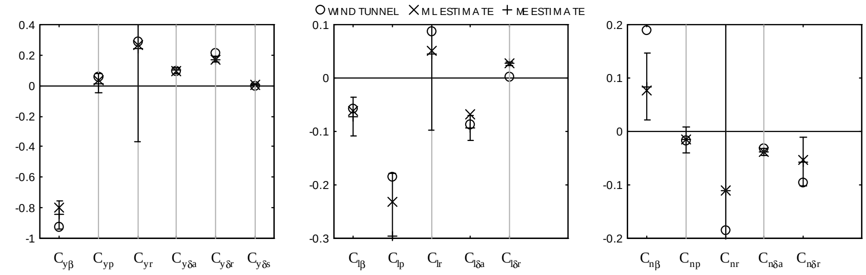

Figure 6-58: P3F6E37 Linear coefficient estimates

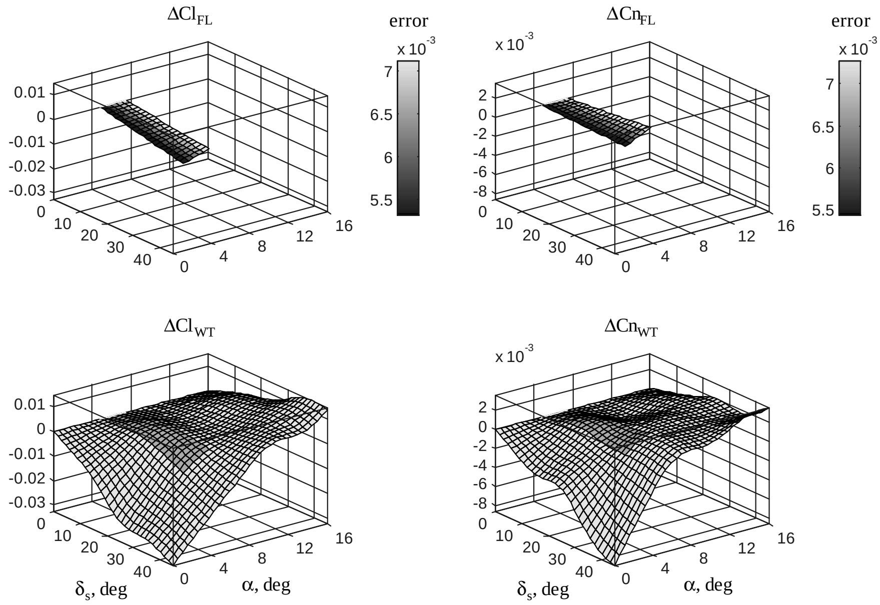

Figure 6-59: P3F6E37 Nonlinear spoiler coefficient estimates

The estimate of C_{y_β} compared reasonably well with the previous results considered. Estimates of C_{l_β} and $C_{l_{\delta a}}$ also compared well, however, the roll damping, C_{l_p} was marginally larger. The flight-estimated yawing moment derivatives were generally smaller than their wind-tunnel values. The last identification model was constructed without any knots in α, as the data range in angle-of-attack was small. One knot was also placed in δ_s at 14.0°, for identification of the increasing rolling contribution. The estimated spoiler contribution for both rolling and yawing moments compared reasonably with the wind-tunnel models. A significant change in the rolling contribution at 14.0° was detected, although $C_{l_{\delta s}}$ in the lower region was larger. In the yawing contribution model, a greater decrease with α was estimated.

6.3.5 45° wing-sweep

The most notable aspect of the spoiler coefficients estimated from flight at 45° sweep was their significantly lower magnitude, compared to those for preceding configurations. This phenomena was also seen in the wind-tunnel results and was particularly obvious at moderate angles-of-attack.

For Mach numbers ranging between 0.5 and 0.7, the spoiler characteristics were generally unchanging. At low to moderate angles-of-attack, $C_{l_{\delta s}}$ was approximately linear and exhibited little or no change with respect to α. At much higher angles of attack above 8°, a possible decrease in the rolling contribution was identified. This loss was marginal, however, and no sign of reversal was seen. The yawing contribution was also near-constant with α, even for angles up to 12°. Additionally, an increasing trend with the spoiler deflection was found, in the low angle-of-attack regime below 8°. At Mach 0.8, a small nonlinearity with respect to δ_s in the spoilers' rolling contribution was identified at low angles-of-attack. The increasing angle-of-attack revealed a small decrease in the rolling contribution and a large decrease in the yawing contribution. At Mach 0.9, the nonlinearity in $\Delta C_l(\delta_s)$ became more prominent (*see* **P1F5E123**) and reflected a greater decrease with α. The yawing contribution also exhibited a significant decrease, corresponding to a lower angle-of-attack than the previous Mach number. A decrease in both rolling and yawing contributions with α was estimated in the sonic/supersonic regime of Mach 1.0 to 1.1. For each coefficient, the loss tapered off to a value close to zero as the angle-of-attack approached 8°, following the wind-tunnel results.

The mean differences resulting between various estimates, shown in Table 6.6, were quite pronounced for this wing-sweep. In particular, the spoilers' estimated rolling contribution was around 19 % smaller than its wind-tunnel value. A significant difference was also exhibited between the yawing moment terms and their wind-tunnel estimates.

	Coefficient								
	C_{y_β}	C_{l_β}	C_{l_p}	$C_{l_{\delta a}}$	$C_{l_{\delta s}}$	C_{n_β}	C_{n_r}	$C_{n_{\delta r}}$	$C_{n_{\delta s}}$
Wind-Tunnel	-0.15	-0.05	-0.16	0.00	-0.19	-0.51	-0.11	-0.32	-0.24
Flight(ML)	0.00	0.13	0.28	0.17	-	0.05	-0.01	0.04	-

Table 6.6: Mean fractional differences between estimates - $\Lambda = 45°$

P3F3E173 (5000 ft, Mach 0.5, $\delta_s[0, 35.1]^\circ$, $\alpha[3.8, 8.1]^\circ$)

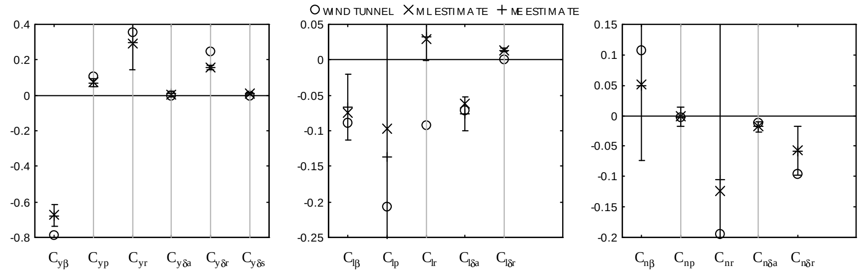

Figure 6-60: P3F3E173 Linear coefficient estimates

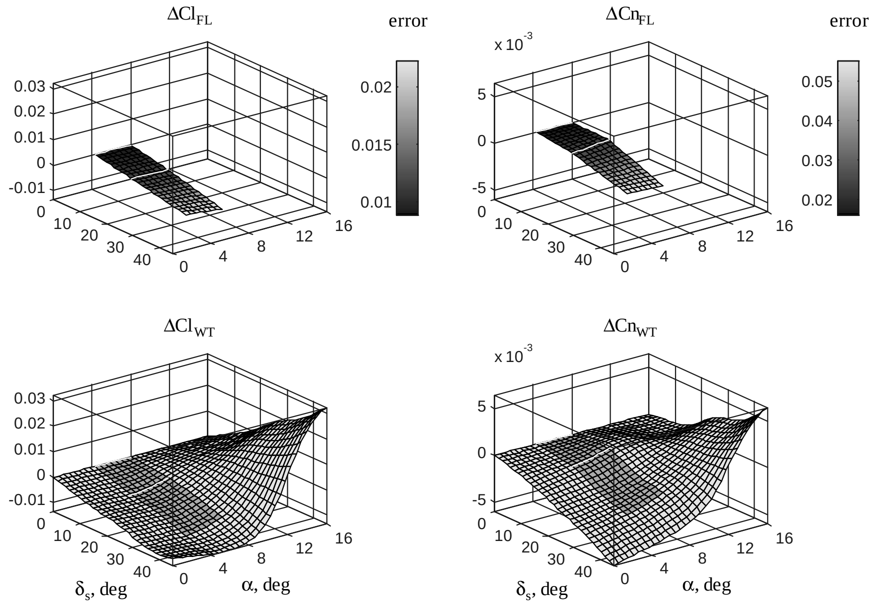

Figure 6-61: P3F3E173 Nonlinear spoiler coefficient estimates

C_{y_β} was the only unbiased sideforce derivative and was estimated lower than the wind-tunnel result. The estimates of C_{l_β} and $C_{l_{\delta a}}$ compared well with both wind-tunnel and ML coefficients, while the estimate of C_{l_p} incurred a large standard error. Generally, the yawing moment coefficient estimates followed the previous ML estimates, which were smaller than the wind-tunnel values.

In order to identify a possible change in the yawing effectiveness with δ_s, one knot was positioned at 14.0°, corresponding to a ridge on the wind-tunnel model surface. The increase was detected and both $C_{n_{\delta s}}$ and $C_{l_{\delta s}}$ terms compared well. An anticipated decrease in the rolling and yawing contributions with α was not produced, however.

P3F3E104 (10000 ft, Mach 0.5, $\delta_s[0, 27.4]°$, $\alpha[5.5, 10.5]°$)

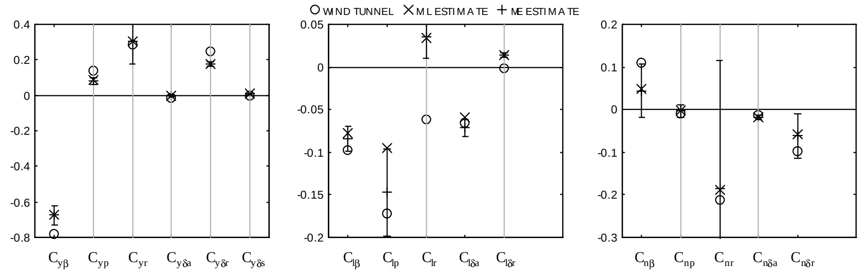

Figure 6-62: P3F3E104 Linear coefficient estimates

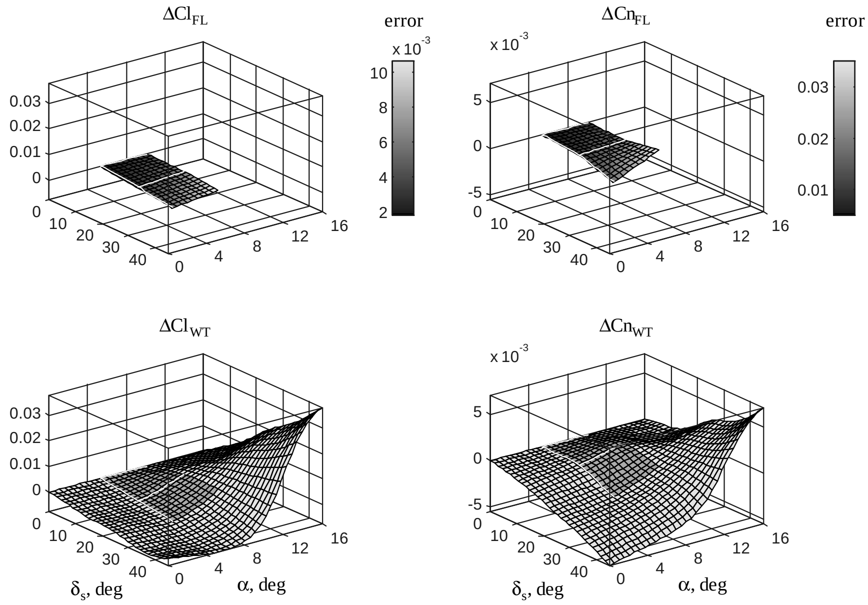

Figure 6-63: P3F3E104 Nonlinear spoiler coefficient estimates

The linear coefficients were estimated much the same as the previous case, with the exception that C_{l_p} and C_{n_r} seemed to match the wind-tunnel terms more closely. Again, one knot was placed in δ_s at 14.0° to identify a possible increase in the yawing contribution. Data limitations also required a knot to be placed in α at 5.4° and the lower coefficients to be fixed. The estimated rolling and yawing moment contributions compared reasonably well, though their variations with α were less significant.

P1F4E82 (5000 ft, Mach 0.6, $\delta_s[0, 36.7]°$, $\alpha[2.8, 7.8]°$)

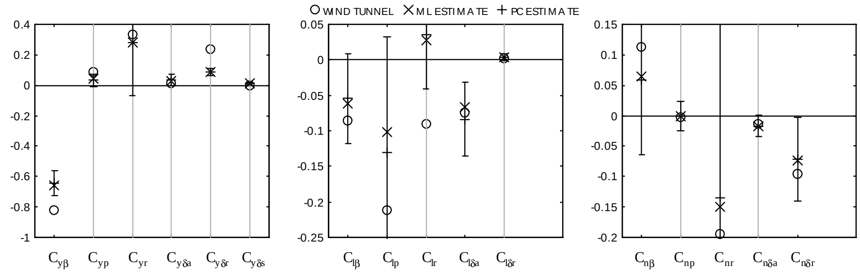

Figure 6-64: P1F4E82 Linear coefficient estimates

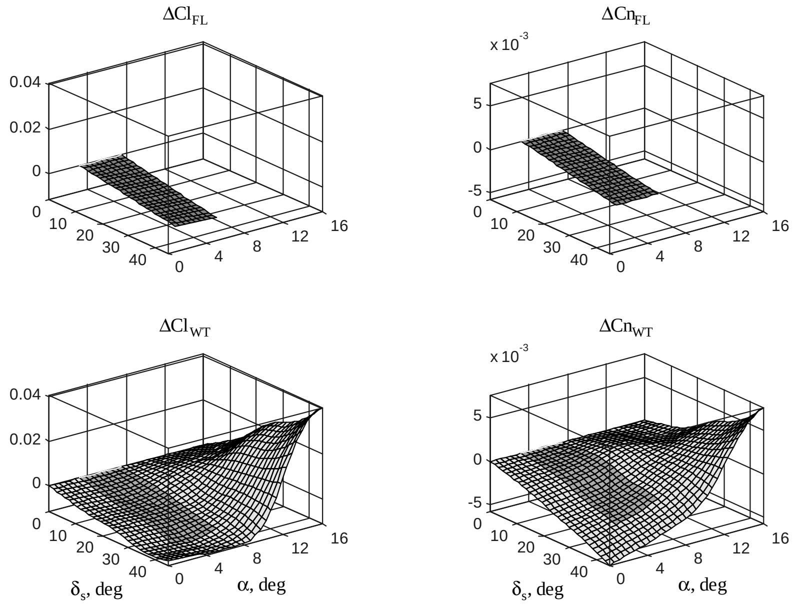

Figure 6-65: P1F4E82 Nonlinear spoiler coefficient estimates

The flight estimates of C_{y_β} compared well, as did the estimates of C_{l_β} and the yawing moment coefficients, C_{n_β}, C_{n_r} and $C_{n_{\delta r}}$. The remaining unbiased derivatives, C_{l_p} and $C_{l_{\delta a}}$, produced slightly larger values than their ML equivalents. Since the flight data lay in a predominantly linear regime, it was not partitioned with respect to the spoiler deflection or angle-of-attack. The resulting estimated models for both rolling and yawing moment contributions approximated the wind-tunnel models reasonably well. Once again, however, the expected decrease with α was not realised.

P3F2E161 (10000 ft, Mach 0.6, $\delta_s[0, 36.6]^\circ$, $\alpha[2.8, 7.4]^\circ$)

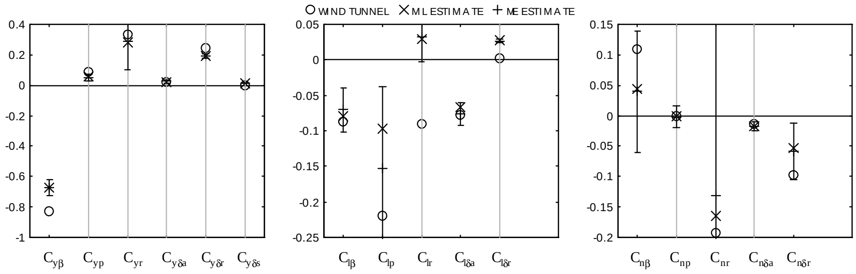

Figure 6-66: P3F2E161 Linear coefficient estimates

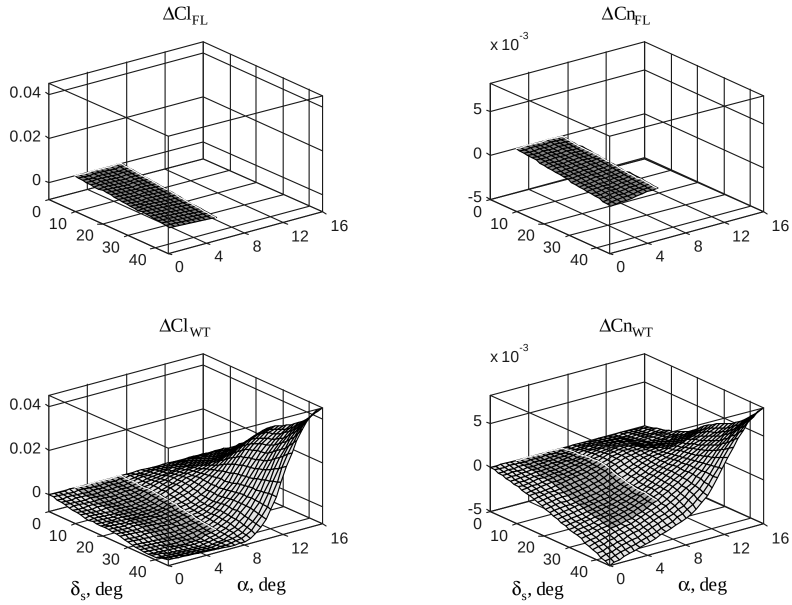

Figure 6-67: P3F2E161 Nonlinear spoiler coefficient estimates

The sideforce coefficient, C_{y_β}, was estimated more positive than the wind-tunnel result. C_{l_β} and $C_{l_{\delta a}}$ compared well with both previous estimates, though C_{n_β} and $C_{n_{\delta r}}$ favoured the ML results. As with the previous case, no knots were implemented in the spoilers' identification models. The estimated rolling contribution compared well with the wind-tunnel model. The estimated yawing contribution compared reasonably, with a significantly lower $C_{n_{\delta s \alpha}}$ characteristic.

P1F4E15 (20000 ft, Mach 0.6, $\delta_s[0, 48.3]^\circ$, $\alpha[6.0, 12.8]^\circ$)

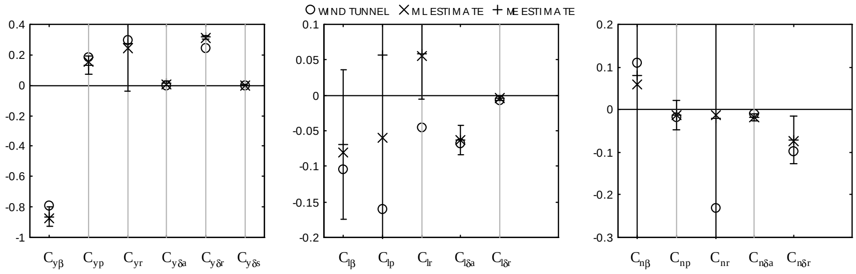

Figure 6-68: P1F4E15 Linear coefficient estimates

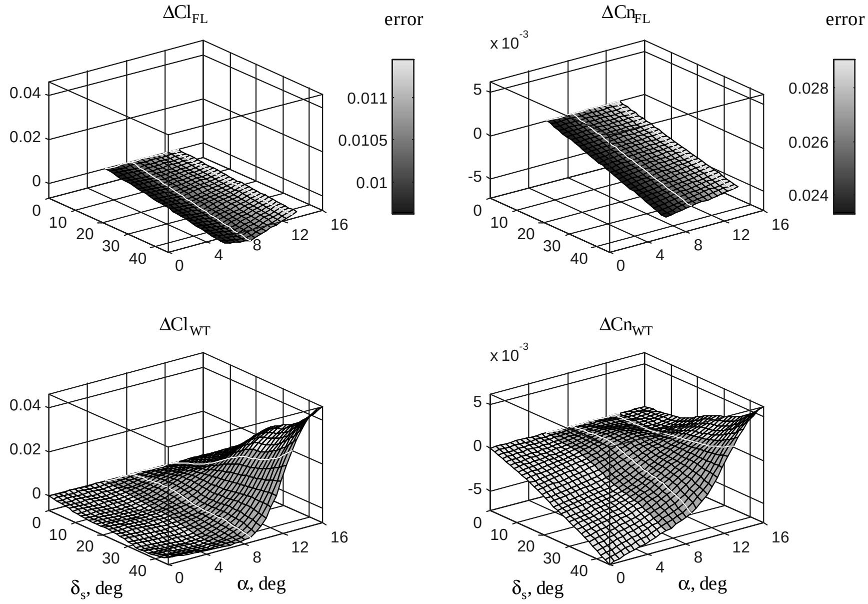

Figure 6-69: P1F4E15 Nonlinear spoiler coefficient estimates

For this flight case, the estimate of C_{y_β} compared well with both wind-tunnel and ML coefficients. The rolling moment terms, C_{l_β} and $C_{l_{\delta a}}$ also compared well, however, C_{l_p} was estimated positive with an extremely large confidence bound. The yawing moment terms compared agreeably, with C_{n_r} approaching zero. One knot in α was integrated in the spoilers' rolling and yawing contribution models, so that the expected change in $C_{l_{\delta s}}$ at 8.5° could be identified. Although the estimated rolling effectiveness compared reasonably in the lower region, there was a significantly smaller change with α in the higher region. Similarly, the estimated yawing contribution remained near-constant with respect to the angle-of-attack.

P3F3E33 (20000 ft, Mach 0.7, $\delta_s[0, 35.1]°$, $\alpha[3.0, 8.6]°$)

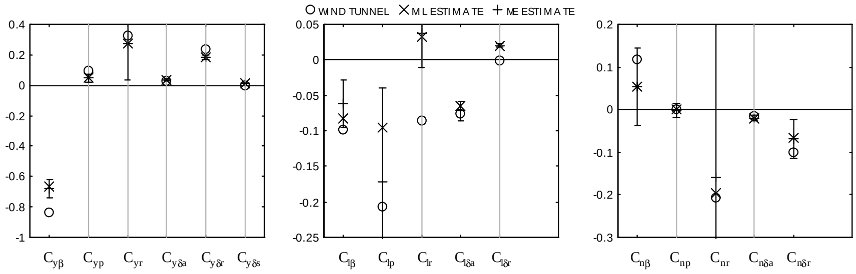

Figure 6-70: P3F3E33 Linear coefficient estimates

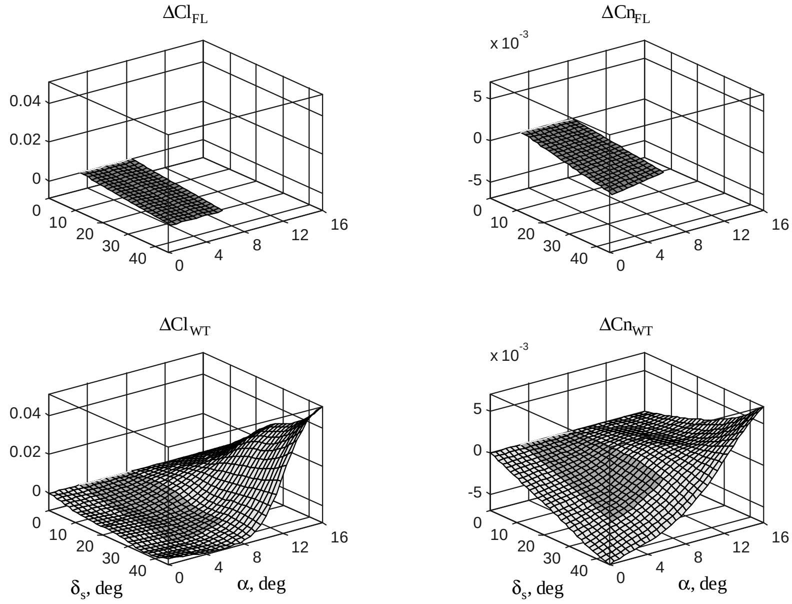

Figure 6-71: P3F3E33 Nonlinear spoiler coefficient estimates

In the set of unbiased rolling moment derivatives: C_{l_β} was estimated significantly lower than either wind-tunnel or ML values; C_{l_p} favoured its wind-tunnel estimate; and $C_{l_{\delta a}}$ compared well for all three estimates. The yawing moment derivatives, C_{n_β} and $C_{n_{\delta r}}$, followed their ML estimates, while C_{n_r} matched both previous results. Employing rolling and yawing spoiler models without any knots, the flight-identification and wind-tunnel estimates generally correlated well. One discrepancy, common to many of the flight cases examined was the invariance of each contribution with α, particularly ΔC_n.

P3F2E53 (30000 ft, Mach 0.7, $\delta_s[0, 48.3]^\circ$, $\alpha[6.7, 11.4]^\circ$)

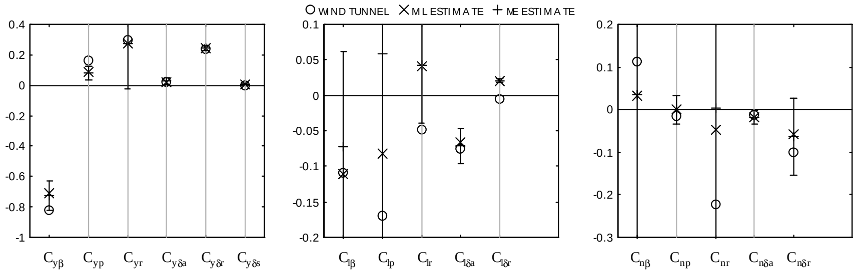

Figure 6-72: P3F2E53 Linear coefficient estimates

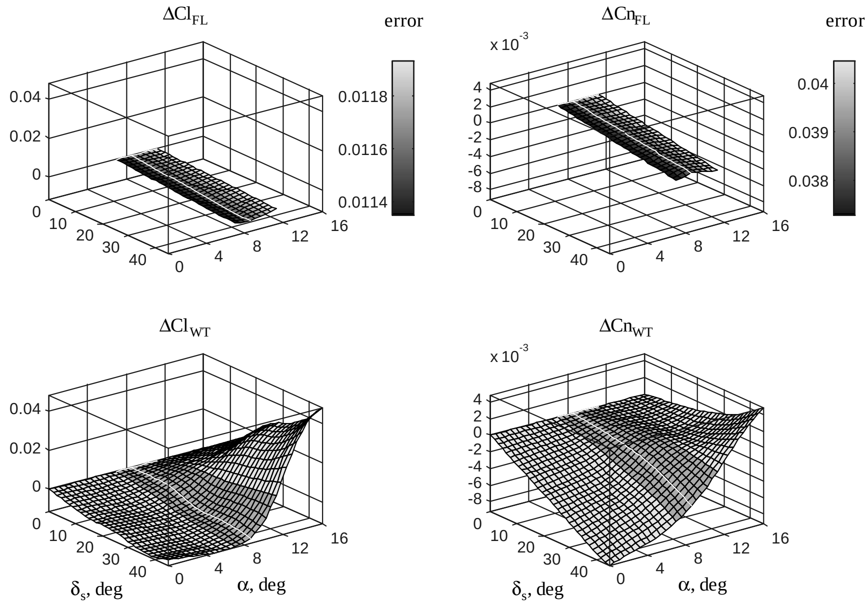

Figure 6-73: P3F2E53 Nonlinear spoiler coefficient estimates

The estimate of C_{y_β} compared well to the previous results. C_{l_β} was significantly smaller than both wind-tunnel and ML estimates and C_{l_p} was again estimated positive. The estimated yawing moment derivatives generally followed the ML coefficients and C_{n_r} was close to zero. One knot was positioned in α at 8.5° to capture the anticipated rapid loss (and reversal) in spoiler rolling effectiveness. A change was identified, though it was much less significant than exhibited in the wind-tunnel model. The yawing moment contribution was also estimated to have little variation with respect to the angle-of-attack.

P3F2E21 (10000 ft, Mach 0.8, $\delta_s[0, 33.7]°$, $\alpha[2.1, 5.4]°$)

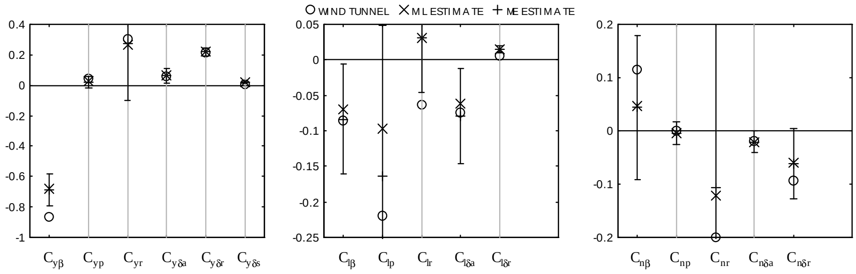

Figure 6-74: P3F2E21 Linear coefficient estimates

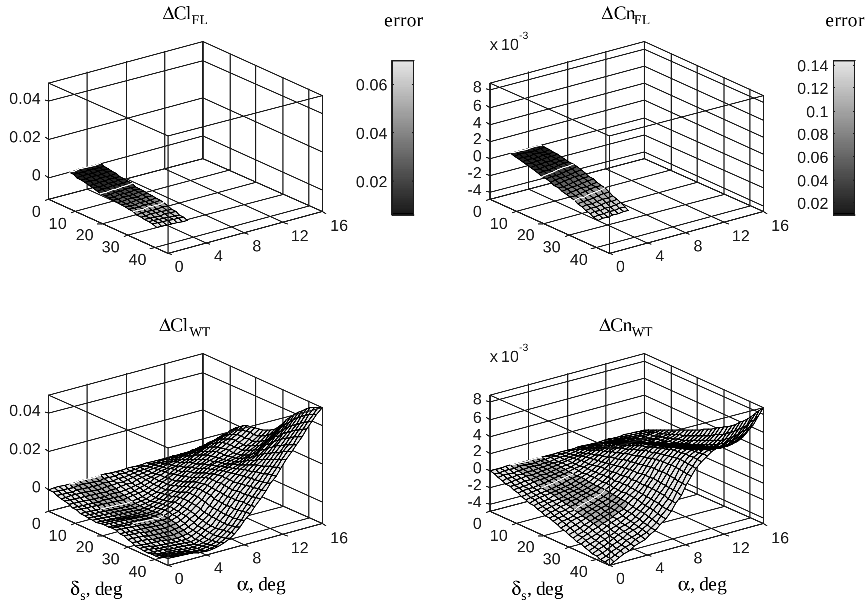

Figure 6-75: P3F2E21 Nonlinear spoiler coefficient estimates

Both flight estimates of C_{y_β} were less than the wind-tunnel coefficient. C_{l_β} and $C_{l_{\delta a}}$ compared well with the previous estimates. On the other hand, C_{n_β}, C_{n_r} and $C_{n_{\delta r}}$ were generally smaller than the wind-tunnel coefficients. In this unique case, the range in α was small enough such that partitioning was not required in that variable. Two partitions in δ_s at 12.0° and 24.0°, however, allowed a nonlinear characteristic of the spoilers' wind-tunnel model to be successfully approximated. The yawing contribution also compared relatively well.

P1F5E49 (30000 ft, Mach 0.8, $\delta_s[0, 43.4]°$, $\alpha[3.4, 9.4]°$)

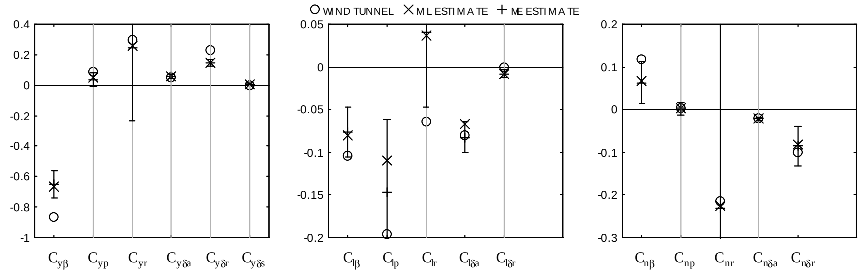

Figure 6-76: P1F5E49 Linear coefficient estimates

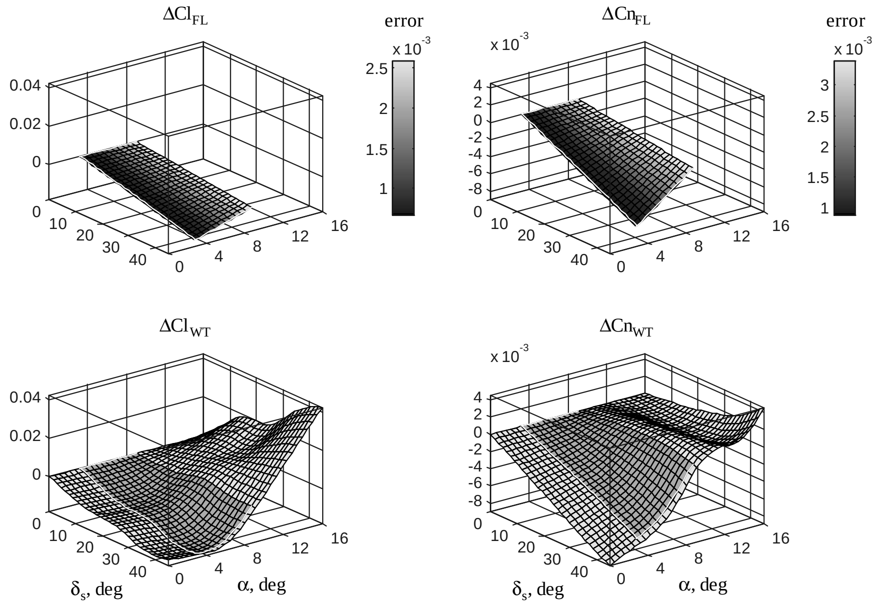

Figure 6-77: P1F5E49 Nonlinear spoiler coefficient estimates

The estimate of C_{y_β} was significantly smaller than its wind-tunnel value, as were the estimates of C_{l_β}, C_{l_p}, C_{n_β} and $C_{n_{\delta r}}$. The remaining unbiased terms compared reasonably well. Since the spoilers' rolling contribution underwent a substantial change below the region covered by the flight data, one knot was placed at the minimum point of 3.3°. In addition, the parameters corresponding to that lower region were fixed. The change in ΔC_l was identified, but its magnitude was much less than that indicated by the wind-tunnel model. ΔC_n compared closely with its wind-tunnel model.

P1F5E123, P3F1E9 (20000 ft, Mach 0.9, $\delta_s[0, 40.8]^\circ$, $\alpha[2.3, 5.8]^\circ$)

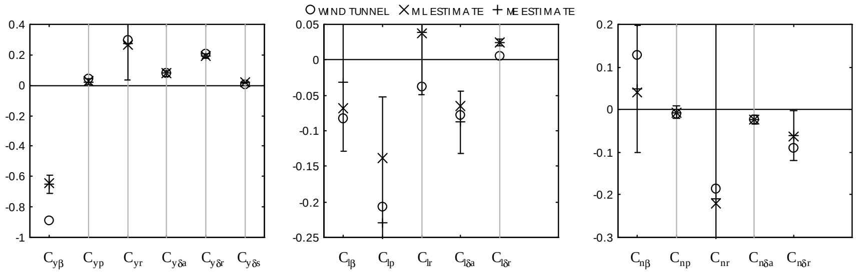

Figure 6-78: P1F5E123 Linear coefficient estimates

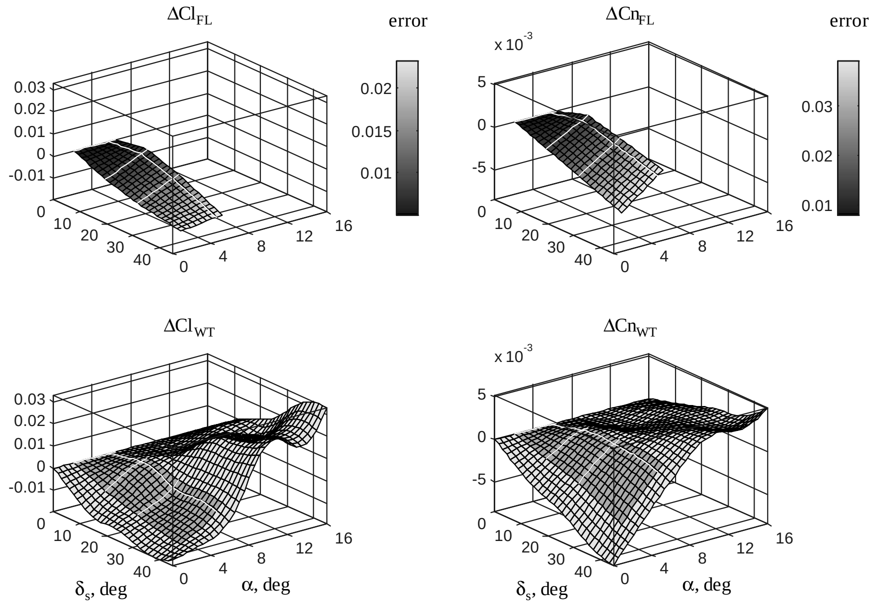

Figure 6-79: P1F5E123 Nonlinear spoiler coefficient estimates

C_{y_β} was again estimated significantly smaller than the wind-tunnel result. The rolling moment coefficient, C_{l_β} was also less than previously estimated. $C_{l_{\delta a}}$ compared reasonably with both wind-tunnel and ML estimates, as did C_{n_r} and $C_{n_{\delta r}}$. Because two flight cases were combined in this identification and the expected spoiler contribution was significantly nonlinear, two knots were positioned in δ_s at 12.0° and 24.0°. The resulting estimates of both rolling and yawing spoiler contributions approximated the wind-tunnel models very well. One possible exception would be their variation with α for large spoiler deflections.

P3F2E77 (30000 ft, Mach 0.9, $\delta_s[0, 36.5]^\circ$, $\alpha[3.9, 7.5]^\circ$)

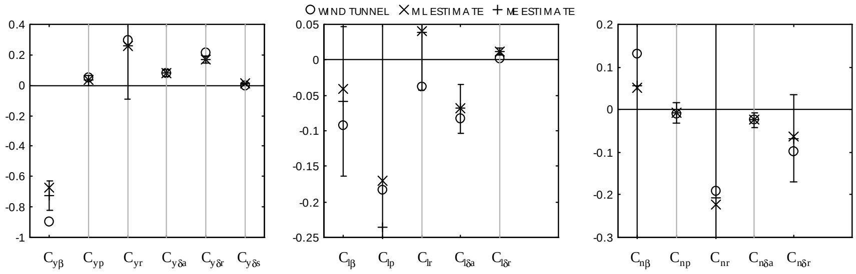

Figure 6-80: P3F2E77 Linear coefficient estimates

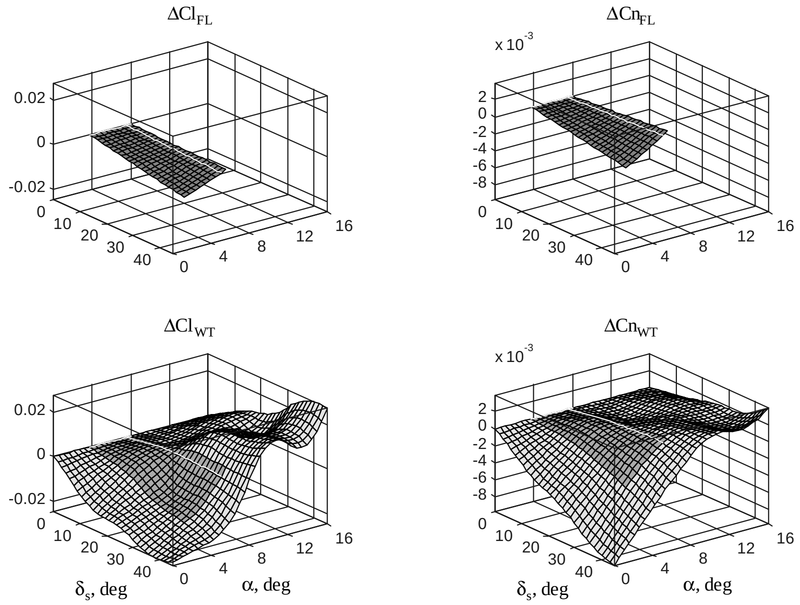

Figure 6-81: P3F2E77 Nonlinear spoiler coefficient estimates

Although the rolling moment coefficients, C_{l_β} and $C_{l_{\delta a}}$ compared reasonably well with their previous estimates, C_{l_p} was notably larger. The estimates of C_{n_r} and $C_{n_{\delta r}}$ also compared well, whereas C_{n_β} was much smaller than its wind-tunnel value. No knots were used for the spoiler contribution models in roll and yaw and thus, only a linear approximation was obtained. The spoilers' rolling contribution estimate followed the wind-tunnel model agreeably, although clearly favouring the low δ_s regime. The yawing contribution also compared well, particularly at low spoiler deflections.

P1F5E13 (40000 ft, Mach 0.9, $\delta_s[0, 44.1]^\circ$, $\alpha[5.7, 10.5]^\circ$)

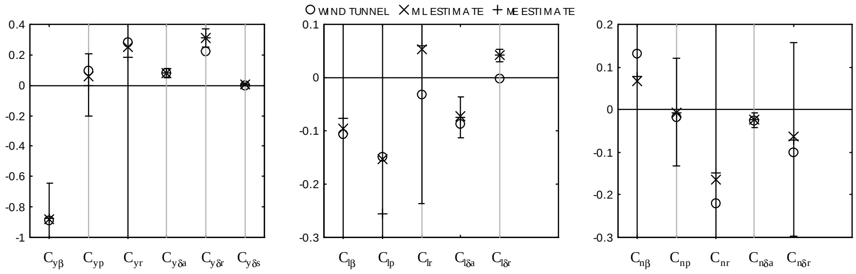

Figure 6-82: P1F5E13 Linear coefficient estimates

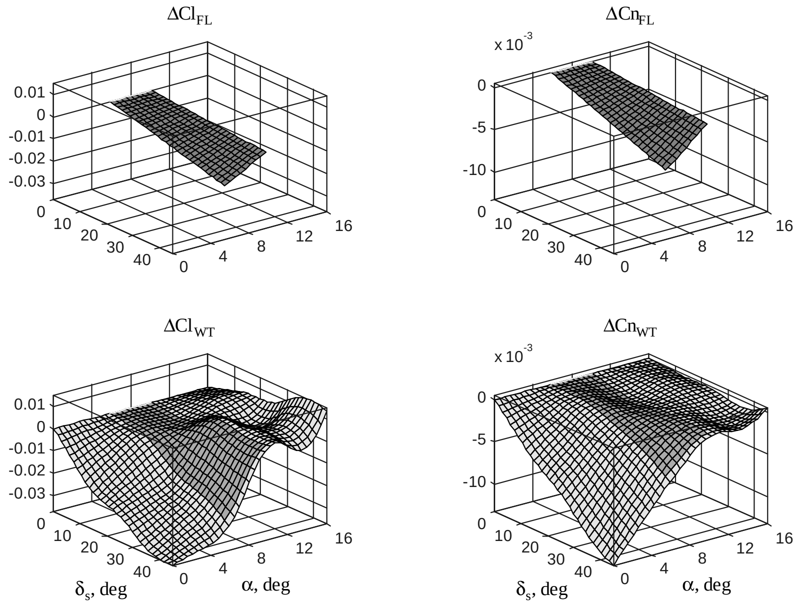

Figure 6-83: P1F5E13 Nonlinear spoiler coefficient estimates

In this case, the estimated C_{y_β} matched both wind-tunnel and ML estimates extremely well. The estimate of C_{l_β} also compared well, however the majority of rolling moment coefficients comprised large standard errors. The yawing moment coefficients were estimated much as before, also with large errors. A predominantly nonlinear variation was anticipated in the spoilers' rolling and yawing contributions, but it was decided to use a linear model for the identification because of data limitations. Nonetheless, the estimated spoiler contributions approximated the wind-tunnel models well.

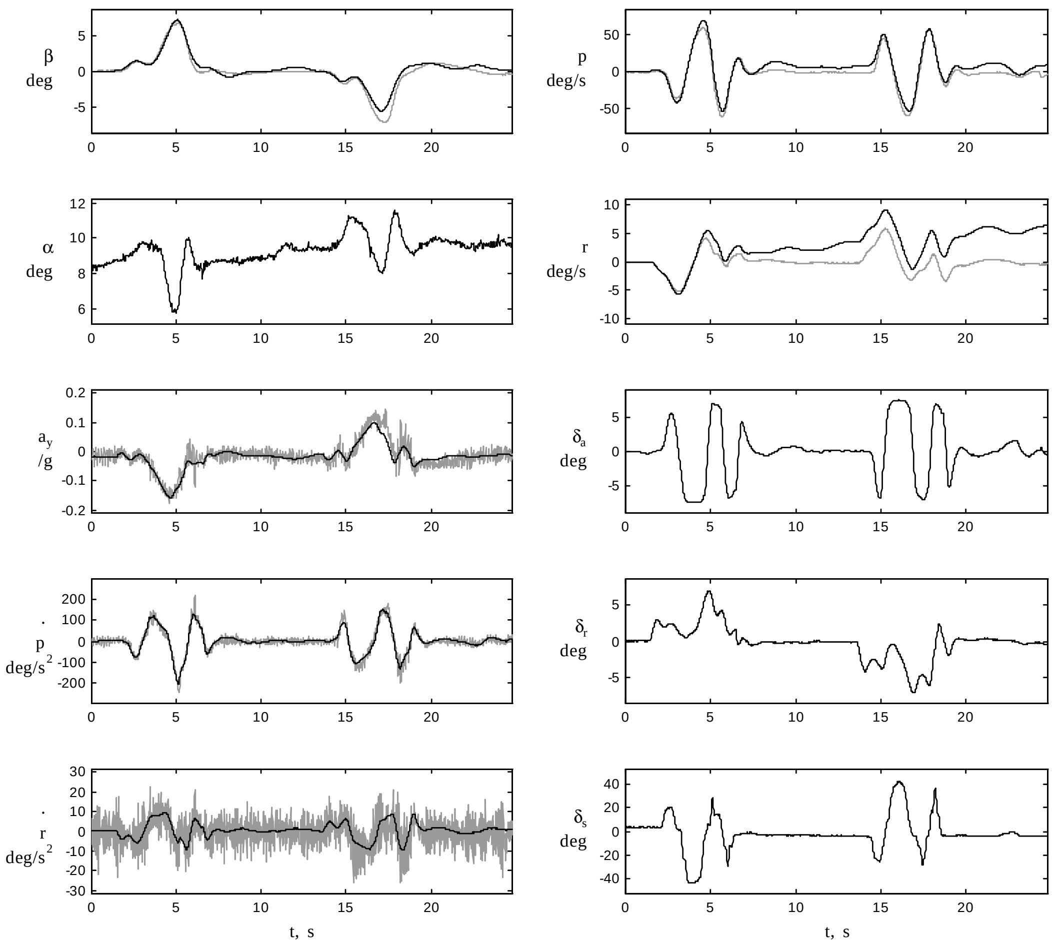

Figure 6-84: P1F5E13 Simulated response comparison

Using the estimated model and the actual control inputs, a response was simulated for verification purposes. In all of the acceleration channels, a considerable amount of measurement noise was present, hence the large confidence bounds produced. This was particularly evident in the roll acceleration and caused differences in the predicted angular response. In contrast, the estimated sideslip followed its measured state very well.

P1F8E26 (30000 ft, Mach 1.0, $\delta_s[0, 36.6]^\circ$, $\alpha[2.4, 5.8]^\circ$)

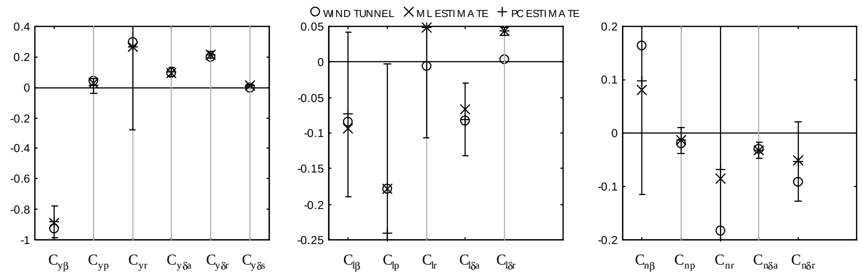

Figure 6-85: P1F8E26 Linear coefficient estimates

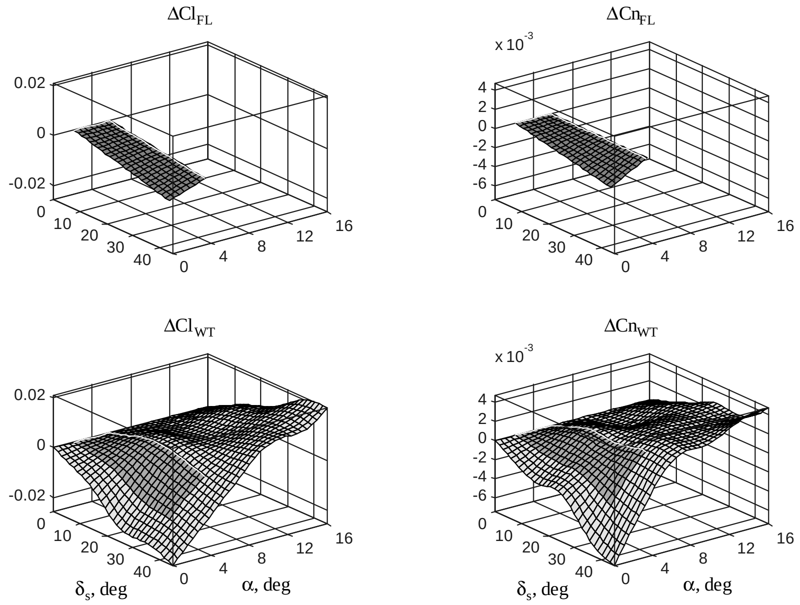

Figure 6-86: P1F8E26 Nonlinear spoiler coefficient estimates

Again, the estimate of C_{y_β} compared very well with both wind-tunnel and ML values. Of note among the rolling moment coefficients is C_{l_p}, which was estimated significantly larger than the previous results. The other terms, C_{l_β} and $C_{l_{\delta a}}$, correlated well, however. The spoiler models were devoid of knots, yielding a linear approximation for both rolling and yawing moment contributions. The estimated $C_{l_{\delta s}}$ and $C_{n_{\delta s}}$ parameters compared well, though the magnitude of the cross-product terms, $C_{l_{\delta s \alpha}}$ and $C_{n_{\delta s \alpha}}$ were much smaller. As a consequence, control reversal was not identified.

P3F6E29 (40000 ft, Mach 1.1, $\delta_s[0, 37.2]^\circ$, $\alpha[4.8, 8.1]^\circ$)

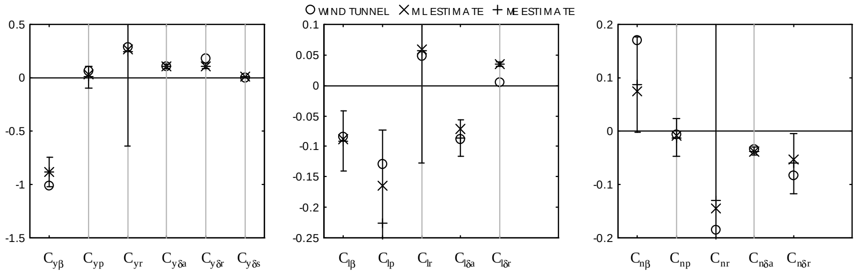

Figure 6-87: P3F6E29 Linear coefficient estimates

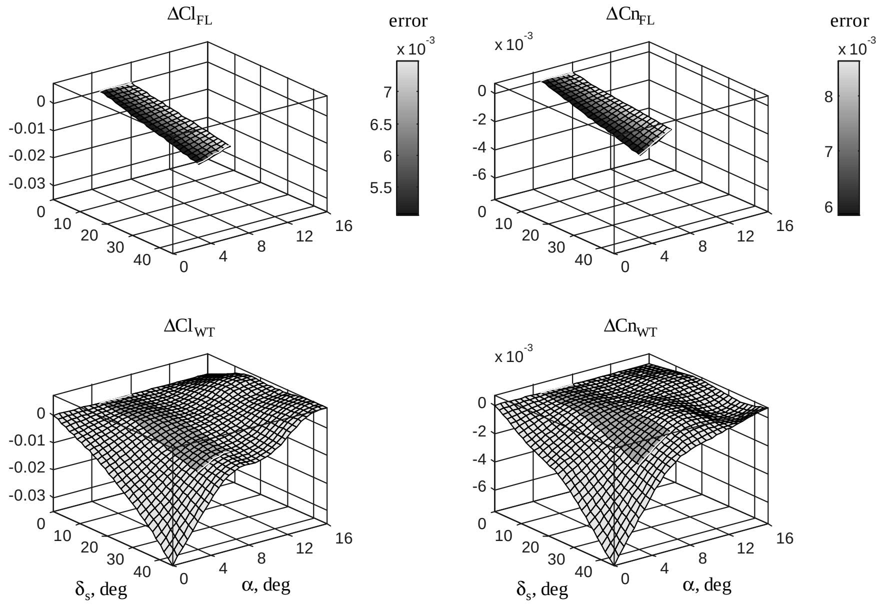

Figure 6-88: P3F6E29 Nonlinear spoiler coefficient estimates

The flight-estimates of C_{y_β} were somewhat smaller than predicted by the wind-tunnel results. Of the rolling moment derivatives, C_{l_β} and $C_{l_{\delta_a}}$ compared well, whereas C_{l_p} was larger than both previous estimates. The estimated yawing moment coefficients generally proved smaller than their wind-tunnel values. A small range in the angle-of-attack prompted a linear identification model, utilising one knot in α at the minimum data point of 4.7°. The model parameters corresponding to the lower region were fixed, due to the absence of data in that region. Both estimated rolling and yawing contribution models compared agreeably with the wind-tunnel models.

6.4 Aerodynamic Behaviour

Having identified a number of salient characteristics in each of the spoiler models from the flight-test data, their aerodynamic significance will now be delineated. In Section 2.5.2, the typical aerodynamic features of spoilers were discussed in relation to those on the F-111C aircraft. Many of these features were identified, as well as some unexpected characteristics.

For all of the cases analysed, the sideforce coefficient, $C_{y_{\delta s}}$, proved extremely small, as indicated by the wind-tunnel results. Since any spoiler contribution to the sideforce (or rolling/yawing moment, for that matter) comes from only one wing, the aerodynamic nature can be equated to that of a single finite spoiler. Clearly, as the wing-sweep angle is increased, a larger component of the spoiler's drag force acts in the y-axis, thus producing a greater sideforce. At the same time, however, the total drag induced by the spoiler will be less, because of the trailing-edge vortices created. Consequently, only a small increase in the sideforce should occur with increasing sweep angle, which corresponded to the behaviour observed in the analysis.

The rolling moment coefficients generally exhibited a decreasing effectiveness as the angle-of-attack was increased. According to the wind-tunnel results, for configurations trimmed at moderate Mach numbers and low angles-of-attack, the control parameter, $C_{l_{\delta s}}$ remained near-constant with α. The rolling contribution then saw a sudden decrease (loss) above a certain angle, eventually resulting in control reversal. In comparison, the estimated rolling effectiveness displayed a similar characteristic in the low-α regime, although it was notably smaller than the wind-tunnel value at low sweep angles. Furthermore, the rapid loss at approximately $8°$ was not detected at low sweep angles ($< 35°$) and low Mach numbers (< 0.5). At moderate Mach numbers, the rapid decrease was identified, but was once again, much smaller than that suggested by the wind-tunnel results. One reasonable explanation for this behaviour would be the difference in Reynold's numbers. Not only was the true spoiler effectiveness overestimated in scaled-model tests, but the change in effectiveness with angle-of-attack was also exaggerated. This difference was most outstanding at low sweep angles and low to moderate Mach numbers. At higher Mach numbers, full control reversal was estimated, occurring at a markedly higher angle-of-attack ($14°$) than the wind-tunnel models.

Even though the flight-identified spoiler contributions were generally lower than their wind-tunnel estimates, they followed basically the same patterns with respect to wing-sweep and Mach number. One of the more obvious trends was the significant degradation of rolling effectiveness for sweep angles above 35°, due to the increased outflow along the wing. Another distinct feature was the rapid loss exhibited above a particular angle-of-attack. As the sweep angle increased, this change occurred at approximately the same value of α. In contrast, as the Mach number increased, the change occurred at an increasingly lower angles-of-attack. This effect can be attributed to the lower-surface shock induced by the deflected spoiler at transonic Mach numbers, as discussed in Section 2.3.4. It was also found that the rolling contribution model became strongly nonlinear with respect to α and δ_s at high Mach numbers as a result of the changing flow field. Moreover, the local effectiveness, $C_{l_{\delta s}}$, generally increased with spoiler deflection, becoming particularly evident at elevated angles-of-attack.

Unfortunately, it was not possible to estimate the spoilers' yawing contribution with as much accuracy as the rolling contribution, because of the excessive measurement noise present. Nonetheless, a significant decrease in $C_{n_{\delta s}}$ with increasing angle-of-attack was identified. This means that the deflected spoilers have a decreasing influence on the wing-drag as the angle-of-attack is increased, which is exactly what would be expected. At very high angles, along with the reversal in rolling contribution, the yawing contribution became adverse. Here, the spoilers were actually reducing the extent of separation over the wing.

An interesting aspect of the yawing contribution is the change in $C_{n_{\delta s}}$ with respect to the angle-of-attack. At low to moderate Mach numbers (< 0.8), this parameter became increasingly positive with α, whereas at higher Mach numbers, it became decreasingly positive. That is, the transonic yawing "effectiveness" tapered off as the angle-of-attack increased. This behaviour corresponds to that observed in the rolling contribution and originates from shock-induced separation on the lower surface.

Generally speaking, the spoilers' estimated yawing contribution was smaller than the wind-tunnel results, for the same reason as proposed above - due to large differences in the Reynold's number.

6.5 Parameter Significance

In the previous two sections, the spoiler coefficient models were identified and assessed with the aim of procuring an accurate representation for each, regardless of the number of parameters included. The significance of individual terms was not considered, since it was assumed that all contributed in some capacity to the aerodynamic model.

In order to obtain a parsimonious model structure that has been resolved using parameter correlation and significance, the Stepwise Regression routine [72, 124, 127, 128, 187] was employed. Figures 6-89 and 6-90 illustrate the iteration sequence and details of the chosen model for one case examined. The left-hand set of axes are relevant to the current (chosen) model only and include the log of F_p along with the critical levels, the Geometric Dilution of Precision, the coefficients themselves, with 95 % confidence bounds and the normal quantile-quantile plot for the residuals. On the right-hand side, the single-value criteria are shown for each step in the iteration sequence, including the initialisation stage.

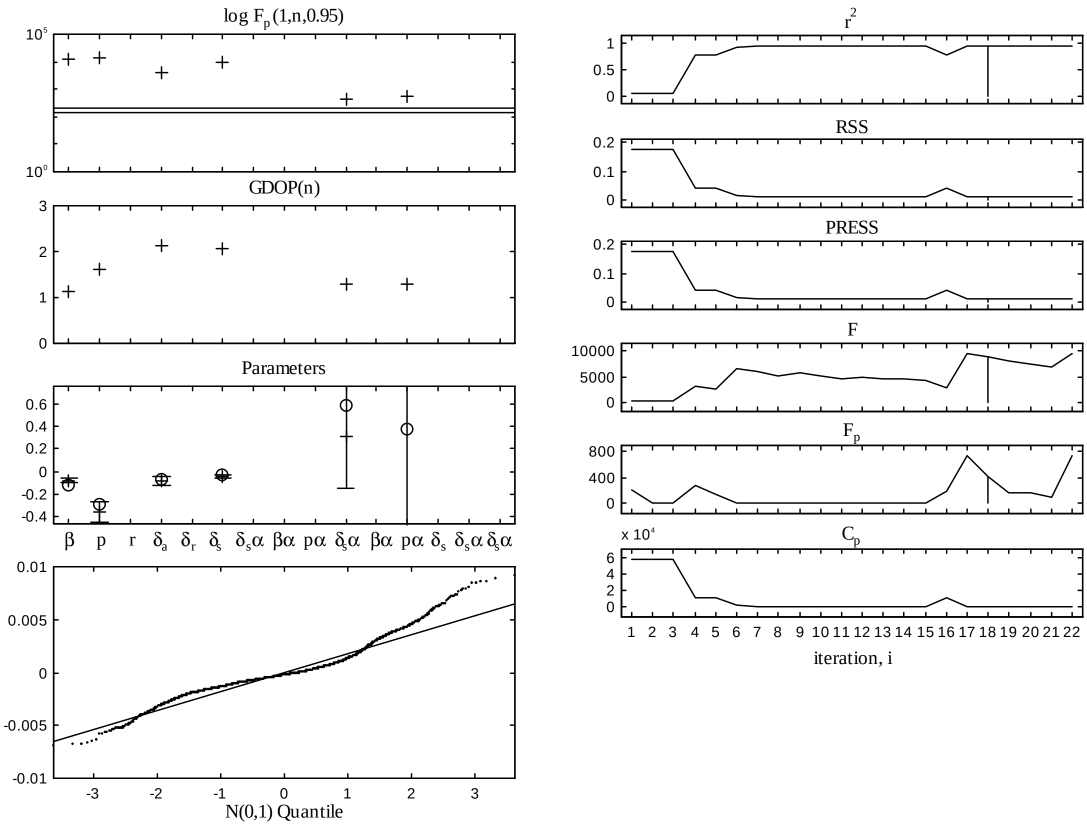

Figure 6-89: Flight P3F1E48 SR iteration details for $\Delta C_l(\delta_s, \alpha)$

The procedure was set up so that, initially, each coefficient was introduced into the regression in sequence, until the full set resided. At this point, the stepwise iteration began and proceeded to eliminate or add variables, depending on their significance. The final model decided upon was, in fact, not the same one arrived at by the algorithm.

Returning to the initial stage, clearly the most important coefficient to the rolling-moment equation was $C_{l_{\delta a}}$, as indicated by many of the single-value criteria at *step (iteration) 4*. After $C_{l_{\delta s}}$ was added to the regression (*step 6*), the criteria changed very little, until *step 15*, whereupon the stepwise iteration began and a number of nonsignificant terms were removed. The model at *step 17*, consisting of C_{l_β}, C_{l_p}, $C_{l_{\delta a}}$, $C_{l_{\delta s}}$ and $C_{l_{p\alpha}}$, was encountered again at *step 22*, which terminated the process. Although this model was favourable in terms of it's small size (and large F statistic), the model chosen was that at *step 18*, because it had a *larger* number of *significant* terms. Hence, the final model was fully significant and gave a better representation of the spoiler aerodynamics, since the cross-product term for the higher (second) region, $C^{(2)}_{l_{\delta s\alpha}}$, was included. The $GDOP$ values were reasonably low, indicating an acceptable level of orthogonality between the variables. Furthermore, apart from the secondary roll-damping term, $C_{l_{p\alpha}}$, the coefficients compared well with their wind-tunnel estimates and led to an effective response model.

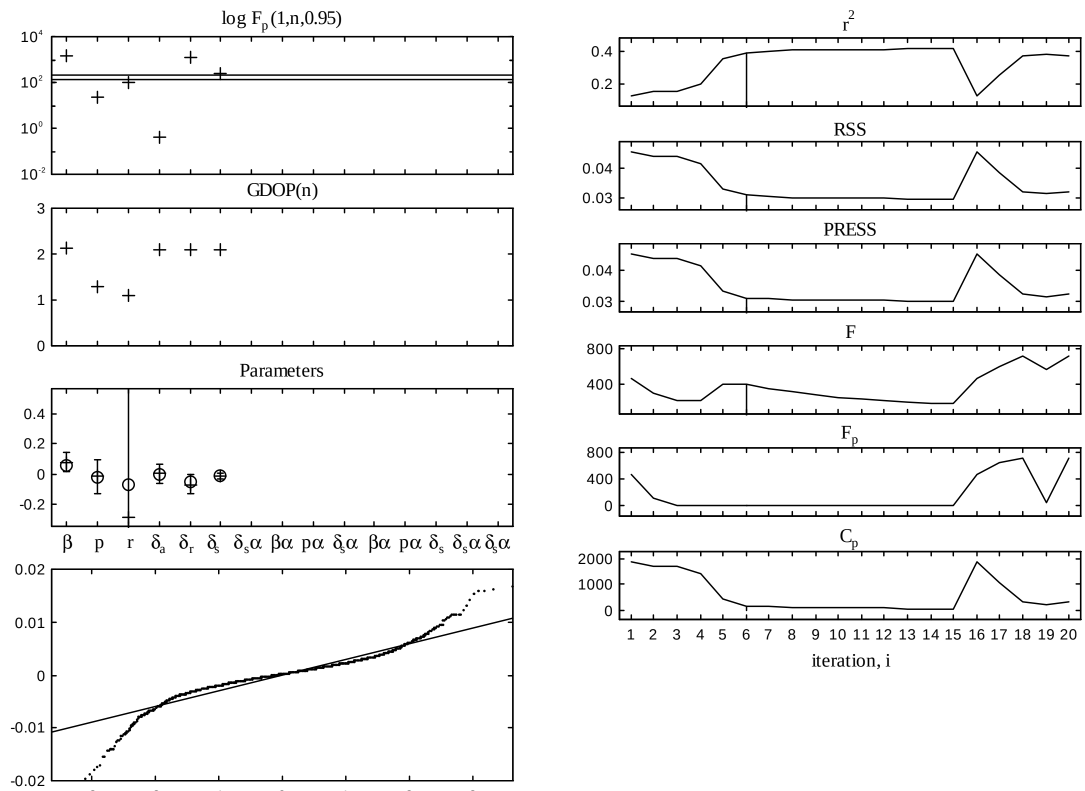

Figure 6-90: Flight P3F1E48 SR iteration details for $\Delta C_n(\delta_s, \alpha)$

Examining the iteration details for the yawing moment equation, it can be seen that most of the improvement in the model came about in the first 6 steps. Thereafter, until the stepwise iteration began at *step 15*, no significant change occurred. The last model (as well as that in *step 18*) consisted of C_{n_β}, $C_{n_{\delta r}}$ and $C^{(2)}_{n_{\delta s}}$ terms. With regard to the spoiler model, this inferred that the yawing contribution at low deflections was nonsignificant. However, the predicted response at *step 6* produced a lower error - seen in r^2, RSS and $PRESS$ - and was therefore chosen as the final model. The difference between this and the other model was simply that $C^{(2)}_{l_{\delta s}}$ was replaced by $C^{(1)}_{l_{\delta s}}$. In order to subsequently reduce this to a fully significant model, one would eliminate the C_{n_r}, $C_{n_{\delta a}}$ and possibly C_{n_r} coefficients. Aside from this latter term, the estimates compared well with the wind-tunnel values and reflected good characteristics.

The resulting spoiler models for roll and yaw are illustrated in Figure 6-91. From this diagram, a number of aspects concerning the flight data analysed become evident.

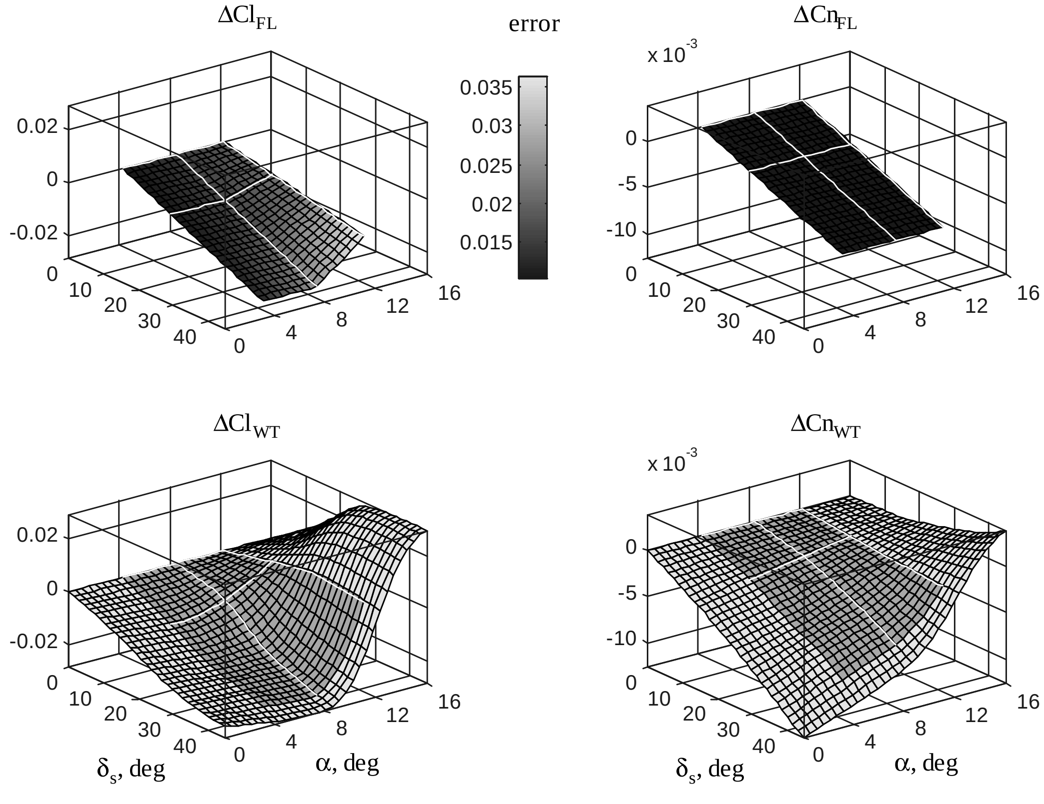

Figure 6-91: Chosen spoiler models for P3F1E48

First, the rapid loss in rolling effectiveness exhibited at high angle-of-attack is significant (at 95% confidence), although of much smaller magnitude than that expected from the wind-tunnel model. In addition, there is no significant change in this contribution with δ_s - indicated by the absence of any lower $C_{l_{\delta s}}$ or $C_{l_{\delta s \alpha}}$ terms. Secondly, the estimated yawing contribution model was constructed with only one $C_{n_{\delta s}}$ parameter, leading to the conclusion that the variation in α is, in fact, nonsignificant. It is important to note, however, that the yawing acceleration signal was heavily corrupted by noise and would undoubtedly affect the significance of all associated model parameters.

6.6 Concluding Remarks

From the identification of the simulated data, a number of relevant aspects emerged. For example, the errors in the estimated sideforce terms were relatively large, whereas the rolling-moment terms were estimated to within 2 % of their actual value. In addition, the standard deviation of the yawing-moment coefficients was quite large, suggesting that the nonlinear model may prove difficult to identify from the real flight-data.

The identification strategy used was essentially the same for each of the flight cases examined, with the exception that the partitioning scheme was tailored to each. In the majority of cases, a Mixed Estimation technique was employed, though in some cases that exhibited a high level of collinearity, a Principal Components Regression was used. Several of the lateral derivatives were represented by splines in α only, whilst the spoiler coefficients were formulated as tensor-product splines in both δ_s and α.

The results obtained from the analysis of the real flight-data were discussed in Section 6.4, with reference to the aerodynamic behaviour associated with each aspect. In summary, the following characteristics were identified:

- the spoilers' sideforce derivative, $C_{y_{\delta_s}}$, was relatively small compared to the other sideforce terms;
- the rolling-moment contribution generally decreased with increasing α ;
- a rapid decrease in the spoilers' effectiveness was identified, although it was much less significant than suggested by the wind-tunnel data and occurred at a higher angle-of-attack;

- continuing from the above, control reversal was also detected, but it was also smaller than expected;
- a gradual decrease in the yawing moment contribution with increasing α was estimated - no rapid change was apparent;
- the yawing-moment contribution also changed sign (becoming adverse) at high angle-of-attack; and
- both rolling- and yawing-moment contributions generally followed the same trends as the wind-tunnel models with sweep angle and Mach number.

Lastly, using a Stepwise Regression procedure, a fully significant model for both rolling and yawing moment coefficients was obtained. This revealed that the sudden rolling moment loss identified at high α was, in fact, significant, although the change with δ_s was not. Likewise, the variation in the yawing moment contribution with α was not deemed significant and therefore omitted from the model.

Chapter 7

Conclusion

Modelling

The mathematical model of an aircraft was detailed in Chapter 3 and comprised parameters that were general functions of the aircraft state. For the F-111C model, these coefficients were dependent on the angle-of-attack, Mach number, altitude and wing-sweep. Since the wing-sweep was constant and the altitude and Mach number changed relatively little during each flight case, however, the coefficients were approximated by functions of the angle-of-attack only. All of the nonlinear coefficients were sufficiently represented by first-order tensor-product splines in α, except for the spoilers' rolling- and yawing-contribution terms, which were expressed as functions of δ_s and α. Spline functions have proven to be ideal for modelling separated-flow characteristics and their effectiveness was further demonstrated by taking advantage of symmetry properties and various simplifications.

Chapter 4 presented a complete description of the identification process, with topics in multiple linear regression, biased estimation and model structure determination. Several new aspects in the application of equation error techniques to flight data were discussed, including a collection of accuracy criteria. The Geometric Dilution of Precision, introduced for assessment of the confidence ellipsoid and the normal quantile-quantile plot, illustrated for examination of the residuals were two such measures. Categorical data was also extensively reviewed and it was suggested that dummy variables could be used, not only in the estimation of partitioned models, but also in the simultaneous analysis of a number of flight cases.

Various model selection procedures were outlined, from which it was determined that the Stepwise Regression algorithm was the most efficient, although the Exhaustive Search was able to cover a greater portion of the model space. In addition, biased estimation techniques were found to affect the model structure determination process. As a consequence of the reduction in their variance, the parameters held higher partial-F values. This meant that the biased terms were *less* likely to be deemed nonsignificant and thus, often kept in the regression during a selection process.

Data Partitioning

There has been very little research on the topic of data partitioning in the identification of nonlinear aircraft models. An attempt was made to fill this gap in Chapter 5. The underlying truth of the matter is that there must always be a compromise between the efficiency of partitioning with respect to the data and with respect to the model. For this reason a manual partitioning scheme, utilising prior information in the form of wind-tunnel models, was employed for the F-111C identification. Unlike the second scheme discussed, which placed an excessive number of knots within the model and then reduced that set, this entailed a more conservative placement of knots. An alternative scheme that added and modified the knots according to their significance was also trialed. However, it employed a crude iteration technique based on several parameters and proved too restrictive for general use.

Two different methods for the identification of partitioned models were investigated. The global regression procedure provided the most accurate results, although it created a large matrix of independent variables, which may not be otherwise possible, depending on the computer's available memory. The sequential regression procedure used smaller matrices, but often encountered problems with divergence - particularly for large models - and was therefore avoided.

In the last section, various partition-optimisation schemes were examined, with particular attention to a continuous approximation which utilised standard unconstrained minimisation techniques. Both nonlinear Least Squares and Simplex algorithms performed well. The former technique implemented a Levenberg-Marquardt method for determination of the search direction and was consistently more efficient. On the other hand, the latter constituted a more robust technique. Furthermore, it was found that the spread of data affected the resulting optimised model, which follows from the first point, above.

F-111C Identification Results

In addition to the research on partitioning, presented in Chapter 5, the results from a spectral analysis of the data were discussed. A second peak in the power spectrum plot at 13 Hz indicated a local pressure fluctuation around the CADS air data system. The high-frequency noise component in the yaw-acceleration channel was also found to be extremely large, yielding a signal-to-noise ratio of approximately 0.57. A correlation analysis of the data revealed a high level of collinearity between the differential-stabilator and spoiler deflections, with a lesser amount between the sideslip and rudder deflection.

The identification results as detailed in Chapter 6 generally agreed with previous estimates. The linear derivatives tended more toward their Maximum Likelihood estimates, while the nonlinear coefficients were smaller than the wind-tunnel results on average. Both rolling- and yawing-contributions were found to decrease with increasing angle-of-attack, although because of the noise in the yaw-acceleration, the latter effect was deemed nonsignificant. A rapid loss in the rolling-contribution was also detected. However, this characteristic was much less marked than exhibited by the wind-tunnel model and control-reversal subsequently occurred at a higher angle-of-attack. The yawing-contribution also changed sign at high angles-of-attack, but did not undergo a sudden change as such. The most reasonable explanation for the disagreement between wind-tunnel and flight-identified results comes from the differences in Reynolds number.

Software

APRE, a program package that performs piecewise regression on aircraft models was developed in the MATLAB interactive environment and was subsequently used and documented. It has the capability to perform unbiased or biased estimation using any of the techniques described herein. The software can also be utilised for model structure determination and subsequent simulation of the dynamic response.

As well as a User's Manual, some of the algorithm details have been included in the appendices.

Conclusion

Piecewise regression can provide a relatively straightforward approach to the determination of nonlinear aircraft models from flight data. However, considerable attention must be paid in formulating the model, as poorly specified parameters can lead to problems with identifiability.

In this thesis, various methods for parameter identification and model structure determination have been examined, including several nonlinear optimisation techniques. Their relative performance has been assessed and problems associated with each were discussed.

The regression procedure was successfully used to identify the nonlinear model of an F-111C aircraft, with particular emphasis placed on evaluating the spoiler characteristics. Among other things, it was found that the Reynold's number can have a significant influence on the effectiveness of these devices.

Bibliography

Parameter Estimation and System Modelling

[1] AGARD : Parameter Identification. *LS 104*. October, 1979.

[2] AGARD : Methods for Aircraft State and Parameter Identification. *CP 172*. November, 1974.

[3] Allen, D.M. : The Prediction Sum of Squares as a Criterion for Selecting Predictor Variables. *University of Kentucky, Department of Statistics*, Technical Report 23. 1971.

[4] Anderson, L.C. : Robust Parameter Identification for Nonlinear Systems Using a Principal Components Regression Algorithm. *AIAA Atmospheric Flight Mechanics Conference Proceedings*, Paper 85-1766. August, 1985. pp. 28-36.

[5] ANSI/AIAA : Recommended Practice for Atmospheric and Space Flight Vehicle Coordinate Systems. *American National Standard Report*, R 004-1992. February, 1992.

[6] Åström, J.J. and Eykhoff, P. : System Identification - a survey. *Automatica*, Vol. 7, No. 2. 1979. pp. 123-162.

[7] Bach, R.E. Jr. : A Variational Technique for Smoothing Flight-Test and Accident Data. *AIAA Atmospheric Flight Mechanics Conference Proceedings*, Paper 80-1601. August, 1980. pp. 383-391.

[8] Bach, R.E. Jr. and Wingrove, R.C. : Applications of State Estimation in Aircraft Flight-Data Analysis. *AIAA Atmospheric Flight Mechanics Conference Proceedings*, Paper 83-2087. August, 1983.

[9] Batterson, J.G. : Estimation of Airplane Stability and Control Derivatives From Large Amplitude Maneuvers. *NASA Technical Memorandum*, TM 83185. 1981.

[10] Batterson, J.G. and Klein, V. : An Application of Parameter Identification to the Oscillatory Motion of an Airplane at High CL. *AIAA Atmospheric Flight Mechanics Conference Proceedings*, Paper 83-2067. August, 1983.

[11] Batterson, J.G. and Klein, V. : Parameter Identification Applied to the Oscillatory Motion of an Airplane Near Stall. *Journal of Aircraft*, Vol. 21, No. 7. July, 1984. pp. 498-504.

[12] Batterson, J.G. and Klein, V. : A Preliminary Analysis of Flight Data from the AFTI/F-16 Airplane. *AIAA Atmospheric Flight Mechanics Conference Proceedings*, Paper 84-2085. August, 1984. pp.140-147.

[13] Batterson, J.G. : STEP and STEPSPL - Computer Programs for Aerodynamic Model Structure Determination and Parameter Estimation. *NASA Technical Memorandum*, TM 86410. January, 1986.

[14] Batterson, J.G. and Klein, V. : Partitioning of Flight Data for Aerodynamic Modeling of Aircraft at High Angles of Attack. *AIAA Atmospheric Flight Mechanics Conference Proceedings*, Paper 87-2621. August, 1987. pp. 444-451 ; *also Journal of Aircraft*, Vol. 26, No. 4. April, 1989. pp. 334-339.

[15] Belsley, D.A., Kuhn, E. and Welsch, R.E. : *Regression Diagnostics: Identifying Influential Data and Sources of Collinearity* © John Wiley & Sons, Inc., 1980.

[16] Bihrle, W. Jr. and Meyer, R.C. : F-14A High-Angle-of-Attack Characteristics. *Journal of Aircraft*, Vol. 13, No. 8. August, 1976. pp. 576-583.

[17] Blackwell, J. : A Maximum Likelihood Parameter Estimation Program for General Non-Linear Systems. *ARL Aerodynamics Technical Memorandum*, ARL-AERO-TM 392. January, 1988.

[18] Blackwell, J. and Feik, R.A. : Identification of Time Delays in Flight Measurements. *Journal of Guidance, Control & Dynamics*, Vol. 14, No. 1. January, 1991. pp. 132-139.

[19] Breeman, J.H., Van Woerkom, K., Jonkers, H.L. and Mulder, J.A. : Aspects of Flight Test Instrumentation. *AGARD : Parameter Identification. LS 104*, Paper 4. October, 1979. pp. 4.1-4.22.

[20] Brown, R.G. and Hwang, P.Y.C. : *Introduction to Random Signals and Applied Kalman Filtering. 2nd Edn.* © John Wiley & Sons, Inc., 1992.

[21] Bryant, W.H. and Hodge, W.F. : A Monte Carlo Analysis of the Effects of Instrumentation Errors on Aircraft Parameter Identification. *AGARD : Methods for Aircraft State and Parameter Identification. CP 172*, Paper 5. November, 1974. pp. 5.1-5.19.

[22] Burton, R.A. : Advancement in Parameter Identification and Aircraft Flight Testing. *AGARD : Methods for Aircraft State and Parameter Identification. CP 172*, Paper 15. November, 1974. pp. 15.1-15.17.

[23] Cannaday, R.L. and Suit, W.T. : Effects of Control Inputs on the Estimation of Stability and Control parameters of a Light Airplane. *NASA Technical Paper*, TP 1043. 1977.

[24] Calico, R.A. Jr. and Fuller, S.G. : Stability of Steady Sideslip Equilibria for High Alpha. *AIAA Journal of Aircraft*, Vol. 20, No. 4. April, 1983. pp. 327-330.

[25] Chen, R.T.N. : Input Design for Aircraft Parameter Identification : Using Time-Optimal Control Formulation. *AGARD : Methods for Aircraft State and Parameter Identification. CP 172*, Paper 13. November, 1974. pp. 13.1-13.15.

[26] Cooper, M.I., Drobik, J.S. and Martin, C.A. : F-111C Flight Data Reduction and Analysis Procedures. *ARL Flight Mechanics Report*, ARL-FM-REP 187. December, 1990.

[27] Curnutt, R.A. : Aerodynamic Data Development for the Turboprop T-44A Operational Flight Trainer. *AIAA Atmospheric Flight Mechanics Conference Proceedings*, Paper 79-1637. August, 1979. pp. 120-128.

[28] Daniel, C. and Mallows, C.L. : *Design, Data and Analysis* © John Wiley & Sons, Inc., 1987.

[29] Donegan, J.J., Robinson, S.W. and Gates, O.B., Jr. : Determination of Lateral-Stability Derivatives and Transfer Function Coefficients from Frequency Response Data for Lateral Motion. *NACA Report*, R 1225. 1955.

[30] Draper, N.R. and Smith, H. : *Applied Regression Analysis* © John Wiley & Sons, Inc., 1981.

[31] Drobik, J.S., Martin, C.A., Cooper, M.I. and Gibbens, P.W. : F-111C Lateral Aerodynamics Flight Data Analysis for Wing Sweeps of 16deg. and 26deg. *ARL Flight Mechanics Report*, ARL-FM-REP 184. December, 1990.

[32] Drobik, J.S., Martin, C.A., Cooper, M.I. and Gibbens, P.W. : F-111C Lateral Aerodynamics Flight Data Analysis for Wing Sweeps of 35deg. and 45deg. *ARL Flight Mechanics Report*, ARL-FM-REP 185. December, 1990.

[33] Ertel, J.E. and Fowlkes, E.B. : Some Algorithms for Linear Spline and Piecewise Multiple Linear Regression. *Journal of the American Statistical Association*, Vol. 71, No. 355. September, 1976.

[34] Etkin, B. : *Dynamics of Atmospheric Flight* © John Wiley & Sons, Inc., 1972.

[35] Eulrich, B.J. and Rynaski, E.G. : Identification of Nonlinear Aerodynamic Stability and Control Parameters at High Angle of Attack. *AGARD : Methods for Aircraft State and Parameter Identification. CP 172*, Paper 2. November, 1974. pp. 2.1-2.15.

[36] Eulrich, B.J. and Harrington, W.W. : Estimation of the Aerodynamic Stability and Control Parameters for the F-106A Aircraft from Flight Data : Maneuver Design and Flight Data Analysis. *AIAA Atmospheric Flight Mechanics Conference Proceedings*, Paper 78-1326. August, 1978. pp. 1-19.

[37] Eustace, R.W., Cooper, M.I. and Martin, C.A. : F-111C Flight Dynamic Model Aerodynamic Data-Base Development and Verification. *ARL Flight Mechanics Technical Memorandum*, ARL-FM-TM 437. December, 1991.

[38] Feik, R.A. : Aircraft Mathematical Model Validation - Comments on the Use of a Systems Identification Procedure. *ARL Aerodynamics Note*, ARL-AERO-NOTE 365. August, 1976.

[39] Feik, R.A. : Longitudinal Aerodynamics Extracted from Flight Tests Using a Parameter Estimation Method. *ARL Aerodynamics Note*, ARL-AERO-NOTE 379. October, 1978.

[40] Feik, R.A. : A Maximum Likelihood Program for Non-Linear System Identification with Application to Aircraft Flight Data Compatibility Checking. *ARL Aerodynamics Note*, ARL-AERO-NOTE 411. July, 1982.

[41] Feik, R.A. : Estimation Programs for Dynamic Flight Test Data Analysis. *ARL Aerodynamics Technical Memorandum*, ARL-AERO-TM 344. January, 1983.

[42] Feik, R.A. : On the Application of Compatibility Checking Techniques to Dynamic Flight Test Data. *ARL Aerodynamics Report*, ARL-AERO-REP 161. June, 1984.

[43] Feik, R.A. : Determination of Instrument Errors by Compatibility Checking - Results from Dynamic Flight Test Data. *ARL Aerodynamics Report*, ARL-AERO-REP 162. September, 1984.

[44] Feik, R.A. : Non-Linear Aerodynamic Characteristics Obtained from the Analysis of Flight Data. *ARL Aerodynamics Technical Memorandum*, ARL-AERO-TM 390. November, 1987.

[45] Fiske, P.H. and Price, C.F. : A New Approach to Model Structure Identification. *AIAA Atmospheric Flight Mechanics Conference Proceedings*, Paper 77-1171. August, 1977. pp. 401-409.

[46] Foch, R.J. and Toot, P.L. : Flight Testing of the Low Altitude/Airspeed Unmanned Research Aircraft (LAURA). *AIAA Atmospheric Flight Mechanics Conference Proceedings*, Paper 90-1262. May, 1990.

[47] Fogarty, L.E. and Howe, R.M. : Computer Mechanization of Six-Degree of Freedom Flight Equations. *NASA Contractor Report*, CR 1344. May, 1969.

[48] Fratter, C. and Stengel, R.F. : Identification of Aerodynamic Coefficients Using Flight Testing Data. *AIAA Atmospheric Flight Mechanics Conference Proceedings*, Paper 83-2099. August, 1983.

[49] Frei, D.R. : Practical Applications of Parameter Identification. *AIAA Atmospheric Flight Mechanics Conference Proceedings*, Paper 77-1136. August, 1977. pp. 134-147.

[50] Gainer, T.G. and Hoffman, S. : Summary of Transformation Equations and Equations of Motion Used in Free-Flight and Wind-Tunnel Data Reduction and Analysis. *NASA Special Publication*, SP 3070. 1972.

[51] Galbraith, T.J. and Keskar, D.A. : Estimation of Nonlinear Aerodynamics From Transport Airplane Certification Maneuvers - A System Identification Approach.

AIAA Atmospheric Flight Mechanics Conference Proceedings, Paper 83-2065. August, 1983.

[52] Gallant, A.R. and Fuller, W.A. : Fitting Segmented Polynomial Regression Models Whose Join Points Have to Be Estimated. *Journal of the American Statistical Association*, Vol. 68, No. 341. March, 1973.

[53] Gates, S.B. and Lyon, H.M. : A Continuation of Longitudinal Stability and Control Analysis. Part I - General Theory. *British Research & Memorandum*, No. 2027, 1944.

[54] Gates, S.B. and Lyon, H.M. : A Continuation of Longitudinal Stability and Control Analysis. Part II - Interpretation of Flight Test. *British Research & Memorandum*, No. 2028, 1944.

[55] Gelb, A. : *Applied Optimal Estimation* © The M.I.T. Press, 1974.

[56] Gerlach, O.H. : The Determination of Stability Derivatives and Performance Characteristics from Dynamic Maneuvers. *SAE Paper*, No. 700236. 1970.

[57] Goman, M. and Khrabrov, A. : State-Space Representation of Aerodynamic Characteristics of an Aircraft at High Angles of Attack. *AIAA Atmospheric Flight Mechanics Conference Proceedings*, Paper 92-4651. August, 1992. pp. 759-766.

[58] Grace, A. : *Optimization Toolbox User's Guide* © The MathWorks, Inc., Natick, 1992.

[59] Greenberg, H. : Determination of Stability Derivatives from Flight Data. *Journal of the Aeronautical Sciences*, Vol. 16, No. 1. 1949. pp. 62.

[60] Greenberg, H. : A Survey of Methods for Determining Stability Derivatives of an Airplane from Dynamic Flight Measurements. *NACA Technical Note*, TN 2340. 1951.

[61] Gunst, R.F. and Mason, R.L. : Biased Estimation Regression; an Evaluation using Mean Squared Error. *Journal of the American Statistical Association*, Vol. 72. 1977. pp. 616-628.

[62] Gupta, N.K. and Hall, W.E. Jr. : Input Design for Identification of Aircraft Stability and Control Derivatives. *NASA Contractor Report*, CR 2493. 1975.

[63] Gupta, N.K. and Hall, W.E. Jr. : Model Structure Determination and Test Input Selection for Identification of Nonlinear Regimes. *U.S. Navy Contractor Report*, ONR-CR 215-213-5. February, 1976.

[64] Gupta, N.K., Hall, W.E. Jr. and Trankle, T.L. : Advanced Methods of Model Structure Determination from Test Data. *AIAA Atmospheric Flight Mechanics Conference Proceedings*, Paper 77-1170. August, 1977. pp. 386-400.

[65] Gupta, N.K. and Iliff, K.W. : Identification of Integro-Differential Systems for Application to Unsteady Aerodynamics and Aeroelasticity. *AIAA Atmospheric Flight Mechanics Conference Proceedings*, Paper 85-1763. August, 1985. pp. 10-21.

[66] Guthery, S.B. : Partition Regression. *Journal of the American Statistical Association*, Vol. 69. December, 1974.

[67] Hall, W.E. Jr., Gupta, N.K. and Tyler, J.S. Jr. : Model Structure Determination and Parameter Identification for Nonlinear Aerodynamic Flight Regimes. *AGARD : Methods for Aircraft State and Parameter Identification. CP 172*, Paper 21. November, 1974. pp. 21.1-21.21.

[68] Hall, W.E. Jr., Gupta, N.K. and Smith, R.G. : Identification of Aircraft Stability and Control Coefficients for the High Angle-of-Attack Regime. *U.S. Navy Contractor Report*, ONR-CR N000014-72-C-0328. March, 1974.

[69] Hamel, P.G. : Aircraft Parameter Identification Methods and Their Applications-Survey and Future Aspects. *AGARD : Parameter Identification. LS 104*, Paper 1. October, 1979. pp. 1.1-1.26.

[70] Hess, R.A. : Effects of Wing Modifications on an Aircraft's Aerodynamic Parameters as Determined from Flight Data. *NASA Technical Memorandum*, TM 87591. 1986.

[71] Hess, R.A. : On the Use of Back Propagation with Feed-Forward Neural Networks for the Aerodynamic Estimation Problem. *AIAA Atmospheric Flight Mechanics Conference Proceedings*, Paper 93-3638. August, 1993. pp. 233-239.

[72] Hinds, H.A. and Cook, M.V. : Preliminary Studies for Aircraft Parameter Estimation Using Modified Stepwise Regression. *Cranfield College of Aeronautics Report*, No. 8911. November, 1989.

[73] Hollkamp, J.J. and Batill, S.M. : Automated Parameter Identification and Order Reduction for Discrete Time Series Models. *AIAA Journal*, Vol. 29, No. 1. January, 1991. pp. 96-103.

[74] Hosman, R.J.A.W. : Advanced Flight Test Instrumentation : Design and Calibration. *AGARD : Methods for Aircraft State and Parameter Identification. CP 172*, Paper 6. November, 1974. pp. 6.1-6.17.

[75] Howard, R.M., Tanner, J.C., Lyons, D.F. and Meeks, D.E. : Flight Test and Numerical Analysis of a Half-Scale Unmanned Air Vehicle. *AIAA Atmospheric Flight Mechanics Conference Proceedings*, Paper 90-1260. May, 1990. pp. 27-33.

[76] Hsia, T.C. : *System Identification* © D.C. Heath & Co., 1977.

[77] Hudson, D.J. : Fitting Segmented Curves Whose Join Points Have to Be Estimated. *American Statistical Association Journal*, Vol. 61. pp. 1097-1129.

[78] Hull, D.G. and Williamson, W.E. : A Nonlinear Method for Parameter Identification Applied to a Trajectory Estimation Problem. *AIAA Atmospheric Flight Mechanics Conference Proceedings*, Paper 77-1137. August, 1977. pp. 148-150.

[79] Idan, M. and Bryson, A.E. : Parameter Identification of Linear Systems Based on Smoothing. *Journal of Guidance, Control & Dynamics*, Vol. 15, No. 4. July, 1992. pp. 901-911.

[80] Idan, M. : Nonlinear Smoothing Identification Algorithm with Application to Data Consistency Checks. *Journal of Guidance, Control & Dynamics*, Vol. 16, No. 2. March, 1993. pp. 337-345.

[81] Iliff, K.W. and Taylor, L.W. Jr. : Determination of Stability Derivatives from Flight Data using a Newton-Raphson Minimization Technique. *NASA Technical Note*, TN D-6579. 1972.

[82] Iliff, K.W. and Maine, R.E. : Practical Aspects of Using a Maximum Likelihood Estimator. *AGARD : Methods for Aircraft State and Parameter Identification. CP 172*, Paper 16. November, 1974. pp. 16.1-16.15.

[83] Iliff, K.W. : Maximum Likelihood Estimates of Lift and Drag Characteristics Obtained from Dynamic Aircraft Maneuvers. *AIAA Atmospheric Flight Mechanics Conference Proceedings*, June, 1976. pp.137-150 ; *also Journal of Aircraft*, Vol. 14, No. 12. December, 1977. pp. 1175-1181.

[84] Iliff, K.W. : Estimation of Characteristics and Stochastic Control of an Aircraft Flying in Atmospheric Turbulence. *AIAA Atmospheric Flight Mechanics Conference Proceedings*, June, 1976. pp. 26-38.

[85] Iliff, K.W. and Maine, R.E. : Further Observations on Maximum Likelihood Estimates of Stability and Control Characteristics Obtained from Flight Data. *AIAA Atmospheric Flight Mechanics Conference Proceedings*, Paper 77-1133. August, 1977. pp. 100-112.

[86] Iliff, K.W., Maine, R.E. and Thornberry Steers, S. : Flight Determined Stability and Control Coefficients of the F-111A Airplane. *NASA Technical Memorandum*, TM 72851. March, 1978.

[87] Iliff, K.W. : Identification and Stochastic Control of an Aircraft Flying in Turbulence. *Journal of Guidance, Control & Dynamics*, Vol. 1, No. 2. 1978. pp. 101-108.

[88] Iliff, K.W. : Aircraft Identification Experience. *AGARD : Parameter Identification. LS 104*, Paper 6. October, 1979. pp. 6.1-6.35.

[89] Iliff, K.W. : Stall/Spin Flight Results for the Remotely Piloted Spin Research Vehicle. *AIAA Atmospheric Flight Mechanics Conference Proceedings*, Paper 80-1563. August, 1980. pp. 62-75.

[90] Iliff, K.W. and Maine, R.E. : More Than You May Want to Know About Maximum Likelihood Estimation. *AIAA Atmospheric Flight Mechanics Conference Proceedings*, Paper 84-2070. August, 1984. pp. 1-24.

[91] Iliff, K.W. and Maine, R.E. : **Bibliography for Aircraft Parameter Estimation**. *NASA Technical Memorandum*, TM 86804. October, 1986.

[92] Iliff, K.W. : Aircraft Parameter Estimation-*AIAA Dryden Lecture in Research for 1987. NASA Technical Memorandum*, TM 88281. January, 1987.

[93] Iliff, K.W. : Parameter Estimation for Flight Vehicles. *AIAA Journal of Guidance, Control & Dynamics*, Vol. 12, No. 5. September, 1989. pp. 609-622.

[94] Jategaonkar, R.V. and Plaetschke, E. : Maximum Likelihood Parameter Estimation from Flight Test Data for General Non-Linear Systems. *DFVLR Forschungsbericht*, FB 83-14. March, 1983.

[95] Jategaonkar, R.V. and Plaetschke, E. : Non-Linear Parameter Estimation from Flight Test Data Using Minimum Search Methods. *DFVLR Forschungsbericht*, FB 83-15. March, 1983.

[96] Jategaonkar, R.V. and Plaetschke, E. : Maximum Likelihood Estimation of Parameters in Linear Systems with Process and Measurement Noise. *DFVLR Forschungsbericht*, FB 87-20. June, 1987.

[97] Jategaonkar, R.V. and Plaetschke, E. : A FORTRAN Program for Maximum Likelihood Estimation of Parameters in Linear Systems with Process and Measurement Noise - User's Manual. *DFVLR Forschungsbericht*, IB 111-87/21. 1987.

[98] Jategaonkar, R.V. and Plaetschke, E. : Estimation of Aircraft Parameters Using Filter Error Methods and Extended Kalman Filter. *DFVLR Forschungsbericht*, FB 88-15. March, 1988.

[99] Jategaonkar, R.V. and Plaetschke, E. : Algorithms for Aircraft Parameter Estimation Accounting for Process and Measurement Noise. *AIAA Journal of Aircraft*, Vol. 26, No. 4. April, 1989. pp. 360-372.

[100] Jategaonkar, R.V. : Identification of the Aerodynamic Model of the DLR Research Aircraft ATTAS from Flight Test Data. *DLR Forschungsbericht*, FB 90-40. July, 1990.

[101] Jobson, J.D. : *Applied Multivariate Data Analysis. VOLUME I. Regression and Experimental Design* © Springer-Verlag New York, 1991.

[102] Jobson, J.D. : *Applied Multivariate Data Analysis. VOLUME II. Categorical and Multivariate Methods* © Springer-Verlag New York, 1992.

[103] Jonkers, H.L. : Application of the Kalman Filter to Flight Path Reconstruction from Flight Data Including Estimation of Instrumental Bias Error Corrections. *Delft University of Technology*, PhD Thesis, 1976.

[104] Kaletka, J. and Fu, K.H. : Frequency-Domain Identification of Unstable Systems Using X-31A Aircraft Flight Test Data. *AIAA Atmospheric Flight Mechanics Conference Proceedings*, Paper 93-3635. August, 1993. pp. 198-222.

[105] Kalviste, J. and Eller, B. : Coupled Static and Dynamic Stability Parameters. *AIAA Atmospheric Flight Mechanics Conference Proceedings*, Paper 89-3362. August, 1989. pp. 129-143.

[106] Kelsey, J.R. and Petersen, D.P. : Aerodynamic Estimation By Means of an Extended Kalman Filter. *AIAA Atmospheric Flight Mechanics Conference Proceedings*, Paper 79-1686. August, 1979. pp. 440-444.

[107] Keskar, D.A. and Klein, V. : Determination of Instrumentation Errors from Measured Data Using Maximum Likelihood Method. *AIAA Atmospheric Flight Mechanics Conference Proceedings*, Paper 80-1602. August, 1980. pp. 392-396.

[108] Kim, W., Lee, J.G. and Lee, D.H. : Application of Recursive Partially Unknown System Identification to Aerodynamic Coefficients Estimation. *AIAA Atmospheric Flight Mechanics Conference Proceedings*, Paper 92-4504. August, 1992. pp. 468-473.

[109] Kirsten, P.W. : A Comparison and Evaluation of Two Methods of Extracting Stability Derivatives from Flight Test Data. *AGARD : Methods for Aircraft State and Parameter Identification. CP 172*, Paper 18. November, 1974. pp. 18.1-18.26.

[110] Kleinbaum, D.G., Kupper, L.L. and Muller, K.E. : *Applied Regression Analysis and Other Multivariable Methods* © PWS-Kent, Inc., 1988.

[111] Klein, R.E. : Identification of Multivalued Parameters in a Class of Noisy Dynamic Processes. *3rd IFAC Identification and System Parameter Estimation Proceedings*, Paper TN-11. June, 1973. pp. 851-856.

[112] Klein, V. and Williams, D.A. : On Some Problems Related to the Identification of Aircraft Parameters. *3rd IFAC Identification and System Parameter Estimation Proceedings*, Paper PT-2. June, 1973. pp.435-444.

[113] Klein, V. : Parameter Identification Applied to Aircraft. *Cranfield Report Aero*, No. 26. December, 1974.

[114] Klein, V. : Longitudinal Aerodynamic Derivatives of a Slender Delta-Wing Research Aircraft Extracted from Flight Data. *Cranfield Report Aero*, No. 27. January, 1975.

[115] Klein, V. : On the Adequate Model for Aircraft Parameter Estimation. *Cranfield Report Aero*, No. 28. March, 1975.

[116] Klein, V. : System Parameter Identification in Aircraft Dynamics. *Cranfield College of Aeronautics Report*. 1975.

[117] Klein, V. : Analysis of Flight Test Data. *Cranfield College of Aeronautics Report*. May, 1975.

[118] Klein, V. and Scheiss, J.R. : Compatibility Check of Measured Aircraft Responses using Kinematic Equations and Extended Kalman Filter. *NASA Technical Note*, TN D-8514. 1977.

[119] Klein, V. : Determination of Longitudinal Aerodynamic Derivatives from Steady-State Measurement of an Aircraft. *AIAA Atmospheric Flight Mechanics Conference Proceedings*, Paper 77-1123. August, 1977. pp. 30-38.

[120] Klein, V. : Aircraft Parameter Estimation in the Frequency Domain. *AIAA Atmospheric Flight Mechanics Conference Proceedings*, Paper 78-1344. August, 1978. pp. 140-147.

[121] Klein, V. : Determination of Stability and Control Parameters of a Light Airplane from Flight Data using Two Estimation Methods. *NASA Technical Paper*, TP 1306. 1979.

[122] Klein, V. : Identification Evaluation Methods. *AGARD : Parameter Identification. LS 104*, Paper 2. October, 1979. pp. 2.1-2.21.

[123] Klein, V. : Maximum Likelihood Method for Estimating Airplane Stability and Control Parameters From Flight Data in Frequency Domain. *NASA Technical Paper*, TP 1637. May, 1980.

[124] Klein, V., Batterson, J.G. and Murphy, P.C. : Determination of Airplane Model Structure From Flight Data by Using Modified Stepwise Regression. *NASA Technical Paper*, TP 1916. 1981.

[125] Klein, V. Batterson, J.G. and Smith, P.L. : On the Determination of Airplane Model Structure from Flight Data. *6th IFAC Identification and System Parameter Estimation Proceedings*, Vol. 2. 1982. pp. 1034-1039.

[126] Klein, V. and Batterson, J.G. : Determination of Airplane Aerodynamic Parameters from Flight Data at High Angles of Attack. *ICAS Proceedings*, Vol. 6.3.3. 1982. pp. 467-474.

[127] Klein, V. and Batterson, J.G. : Determination of Airplane Model Structure From Flight Data Using Splines and Stepwise Regression. *NASA Technical Paper*, TP 2126. March, 1983.

[128] Klein, V., Batterson, J.G. and Murphy, P.C. : Airplane Model Structure Determination from Flight Data. *Journal of Aircraft*, Vol. 20, No. 5. May, 1983. pp. 469-474.

[129] Klein, V., Batterson, J.G. and Abbasy, I. : Determination of Aerodynamic Parameters of a Fighter Airplane from Flight Data at High Angles of Attack. *AIAA Atmospheric Flight Mechanics Conference Proceedings*, Paper 83-2066. August, 1983.

[130] Klein, V. and Batterson, J.G. : Aerodynamic Characteristics of a Fighter Airplane Determined From Flight and Wind Tunnel Data. *NASA Technical Paper*, TP 2483. September, 1985.

[131] Klein, V. and Batterson, J.G. : Aerodynamic Parameters Estimated from Flight and Wind Tunnel Data. *Journal of Aircraft*, Vol. 23, No. 4. 1986. pp. 306-312.

[132] Klein, V. and Mayo, M.H. : Estimation of Aerodynamic Parameters from Flight Data of a High Incidence Research Model. *ICAS Proceedings* Paper No. 86-5.5.2. 1986.

[133] Klein, V. and Morgan, D.R. : Estimation of Bias Errors in Measured Airplane Responses Using Maximum Likelihood Method. *NASA Technical Memorandum*, TM 89059. January, 1987.

[134] Klein, V. : Two Biased Estimation Techniques in Linear Regression-Application to Aircraft. *NASA Technical Memorandum*, TM 100649. July, 1988.

[135] Klein, V. : Estimation of Aircraft Aerodynamic Parameters from Flight Data. *Progress in the Aerospace Sciences*, Vol. 26. 1989. pp. 1-77.

[136] Klein, V., Breneman, K.P. and Ratvasky, T.P. : Aerodynamic Parameters of an Advanced Fighter Aircraft Estimated from Flight Data. Preliminary Results. *NASA Technical Memorandum*, TM 101631. July, 1989.

[137] Klein, V. : On Parameter Estimation of Highly Augmented Aircraft. *AIAA Atmospheric Flight Mechanics Conference Proceedings*, Paper 89-3356. August, 1989. pp. 83-91.

[138] Klein, V., Ratvasky, T.P. and Cobleigh, B.R. : Aerodynamic Parameters of High-Angle-of-Attack Research Vehicle (HARV) Estimated From Flight Data. *NASA Technical Memorandum*, TM 102692. August, 1990.

[139] Klein, V. and Noderer, K.D. : Aerodynamic Parameters of the X-31 Drop Model Estimated from Flight Data at High Angles of Attack. *AIAA Atmospheric Flight Mechanics Conference Proceedings*, Paper 92-4357. August, 1992. pp. 174-181.

[140] Kleingeld, H.W. : Design and Evaluation of a Symmetric Flight-Test Manoeuvre for the Estimation of Longitudinal Performance and Stability and Control Characteristics. *AGARD : Methods for Aircraft State and Parameter Identification. CP 172*, Paper 9. November, 1974. pp. 9.1-9.6.

[141] Koehler, R. and Wilhelm, K. : Closed Loop Aspects of Aircraft Identification. *AGARD : Parameter Identification. LS 104*, Paper 10. October, 1979. pp. 10.1-10.24.

[142] Lee, D.H. and Lee, J.G. : Comparison of Parameter Identification Algorithms for Flight Vehicles. *The Japan Society for Aeronautical and Space Sciences Transactions*, Vol. 36, No. 114. February, 1994. pp. 249-256.

[143] Linse, D.J. and Stengel, R.F. : Identification of Aerodynamic Coefficients Using Computational Neural Networks. *30th Aerospace Sciences Meeting & Exhibit Proceedings*, Paper 92-0172. January, 1993. pp. 1-11.

[144] Little, J.N. and Shure, L. : *Signal Processing Toolbox User's Guide* © The MathWorks, Inc., Natick, 1992.

[145] Ljung, L. : *System Identification : Theory for the User* © Prentace-Hall, New Jersey, 1987.

[146] Long, P.Y., Fratello, D.J., Robelen, D.B. and Makowiec, G.M. : Wind-Tunnel and Flight-Test Investigation of the EXDRONE Remotely Piloted Vehicle Configuration. *AIAA Atmospheric Flight Mechanics Conference Proceedings*, Paper 90-1261. May, 1990. pp. 34-46.

[147] Maine, R.E. : Maximum Likelihood Estimation of Aerodynamic Derivatives for an Oblique Wing Aircraft from Flight Data. *AIAA Atmospheric Flight Mechanics Conference Proceedings*, Paper 77-1135. August, 1977. pp. 124-133.

[148] Maine, R.E. and Iliff, K.W. : Maximum Likelihood Estimation of Translational Acceleration Derivatives from Flight Data. *AIAA Atmospheric Flight Mechanics Conference Proceedings*, Paper 78-1342. August, 1978. pp. 121-131 ; *also Journal of Aircraft*, Vol. 16, No. 10. October, 1979. pp. 674-679.

[149] Maine, R.E. and Iliff, K.W. : Formulation and Implementation of a Practical Algorithm for Parameter Estimation with Process and Measurement Noise. *AIAA Atmospheric Flight Mechanics Conference Proceedings*, Paper 80-1603. August, 1980. pp. 397-411.

[150] Maine, R.E. and Iliff, K.W. : User's Manual for MMLE3, a General FORTRAN Program for Maximum Likelihood Parameter Estimation. *NASA Technical Paper*, TP 1563. November, 1980.

[151] Maine, R.E. and Iliff, K.W. : Programmer's Manual for MMLE3, a General FORTRAN Program for Maximum Likelihood Parameter Estimation. *NASA Technical Paper*, TP 1690. 1980.

[152] Maine, R.E. and Iliff, K.W. : The Theory and Practice of Estimating the Accuracy of Dynamic Flight-Determined Coefficients. *NASA Reference Publication*, RP 1107. 1981.

[153] Maine, R.E. and Iliff, K.W. : Identification of Dynamic Systems - Theory and Formulation. *NASA Reference Publication*, RP 1138. February, 1985.

[154] Maine, R.E. and Murray, J.E. : Application of Parameter Estimation to Highly Unstable Aircraft. *AIAA Atmospheric Flight Mechanics Conference Proceedings*, Paper 86-2020. August, 1986. pp. 25-36.

[155] Maine, R.E. and Iliff, K.W. : Application of Parameter Estimation to Aircraft Stability and Control. The Output-Error Approach. *NASA Reference Publication*, RP 1168. 1986.

[156] Marchand, M. and Koehler, R. : Determination of Aircraft Derivatives by Automatic Parameter Adjustment and Frequency Response Methods. *AGARD : Methods for Aircraft State and Parameter Identification. CP 172*, Paper 17. November, 1974. pp. 17.1-17.18.

[157] Martin, C.A. : Estimation of Aircraft Dynamic States and Instrument Systematic Errors from Flight Test Measurements Using the Carlson Square Root Formulation of the Kalman Filter. *ARL Aerodynamics Note*, ARL-AERO-NOTE 399. September, 1980.

[158] Martin, C.A. and Feik, R.A. : Estimation of Aircraft Dynamic States and Instrument Systematic Errors from Flight Test Measurements. *2nd IEAust Conference on Control Engineering, Newcastle*. August, 1982.

[159] Martin, C.A. : Modelling Aircraft Dynamics. *ARL Aerodynamics Technical Memorandum*, ARL-AERO-TM 400. September, 1988.

[160] Martin, C.A. and Hill, S.D. : Prediction of Aircraft Spin Recovery. *AIAA Atmospheric Flight Mechanics Conference Proceedings*, Paper 89-3363. August, 1989.

[161] Martin, C.A. : Flight Behaviour of Highly Manoeuvrable Aircraft. *3rd Australian Aeronautical Conference Proceedings*. October, 1989. pp. 43-51.

[162] McBrinn, D.E. and Brassell, B.B. : Aerodynamic Parameter Identification for the A-7 Airplane at High Angles of Attack. *AIAA Atmospheric Flight Mechanics Conference Proceedings*. June, 1976. pp. 108-117.

[163] McDowell, J.L., Schutz, B.E., Tapley, B.D. and Williamson, W.E. Jr. : An Analysis of Reentry Vehicle Trajectory Reconstruction and Parameter Identification. *AIAA Atmospheric Flight Mechanics Conference Proceedings*, Paper 79-1685. August, 1979. pp. 474-484.

[164] McGee, V.E. and Willard, T.C. : Piecewise Regression. *Journal of the American Statistical Association*, Vol. 65, No. 331. September, 1970.

[165] Mehra, R.K. : Maximum Likelihood Identification of Aircraft Parameters. *JACC, Atlanta*. 1970.

[166] Mehra, R.K. and Tyler, J.S. : Case Studies in Aircraft Parameter Identification. *3rd IFAC Identification and System Parameter Estimation Proceedings*, Paper C-3. June, 1973. pp. 117-144.

[167] Mehra, R.K., Stepner, D.E. and Tyler, J.S. : Maximum Likelihood Identification of Aircraft Stability and Control Derivatives. *Journal of Aircraft*, Vol. 11, No. 2. February, 1974. pp. 81-89.

[168] Mehra, R.K. and Gupta, N.K. : Status of Input Design for Aircraft Parameter Identification. *AGARD : Methods for Aircraft State and Parameter Identification. CP 172*, Paper 12. November, 1974. pp. 12.1-12.21.

[169] Mehra, R.K. and Carroll, J.V. : Bifurcation Analysis of Aircraft High Angle-of-Attack Flight Dynamics. *AIAA Atmospheric Flight Mechanics Conference Proceedings*, Paper 80-1599. August, 1980. pp. 358-371.

[170] Meyer, T.J. and Mook, D.J. : Robust Identification of Nonlinear Aerodynamic Model Structure. *AIAA Atmospheric Flight Mechanics Conference Proceedings*, Paper 92-4503. August, 1992. pp. 458-467.

[171] Milne, G.W. : Identification of a Dynamic Model of a Helicopter from Flight Tests. *Stanford University, Department of Electrical Engineering*, PhD Thesis, 1986.

[172] Mohler, R.R. : Nonlinear Stability and Control Study of Highly Maneuverable High Performance Aircraft. *Oregon State University ECE Report* NASA 91-01. August, 1991.

[173] Moler, C., Bangert, S., Kleiman, S. and Little, J.N. : *MATLAB User's Guide* © The MathWorks, Inc., Natick, 1990.

[174] Molusis, J.A. : Rotorcraft Derivative Identification from Analytical Models and Flight Test Data. *AGARD : Methods for Aircraft State and Parameter Identification. CP 172*, Paper 24. November, 1974. pp. 24.1-24.31.

[175] Montgomery, D.C. and Peck, E.A. : *Introduction to Linear Regression Analysis* © John Wiley & Sons, Inc., 1982.

[176] MORELLI, E.A. and KLEIN, V. : Optimal Input Design for Aircraft Parameter Estimation Using Dynamic Programming Principles. *AIAA Atmospheric Flight Mechanics Conference Proceedings*, Paper 90-2801. May, 1990. pp. 249-259.

[177] MULDER, J.A. : Estimation of the Aircraft State in Non-Steady Flight. *AGARD : Methods for Aircraft State and Parameter Identification. CP 172*, Paper 19. November, 1974. pp. 19.1-19.21.

[178] MULDER, J.A., JONKERS, H.L., HORSTEN, J.J., BREEMAN, J.H. and SIMONS, J.L. : Analysis of Aircraft Performance, Stability and Control Measurements. *AGARD : Parameter Identification. LS 104*, Paper 5. October, 1979. pp. 5.1-5.87.

[179] MULDER, J.A. : Design and Evaluation of Dynamic Flight Test Maneuvers. *Delft University of Technology*, PhD Thesis, 1986.

[180] MURPHY, P.C. and KLEIN, V. : Maximum Likelihood Algorithm Using an Efficient Scheme for Computing Sensitivities and Parameter Confidence Intervals. *AIAA Atmospheric Flight Mechanics Conference Proceedings*, Paper 84-2084. August, 1984. pp. 131-139.

[181] MURPHY, P.C. : A Methodology for Airplane Parameter Estimation and Confidence Interval Determination in Nonlinear Estimation Problems. *NASA Reference Publication*, RP 1153. 1986.

[182] MURPHY, P.C. : Efficient Computation of Parameter Confidence Intervals. *AIAA Atmospheric Flight Mechanics Conference Proceedings*, Paper 87-2624. August, 1987. pp. 464-473.

[183] PARAMESWARAN, V. and PLAETSCHKE, E. : Flight Path Reconstruction Using Extended Kalman Filtering Techniques. *DLR Forschungsbericht*, FB 90-41. August, 1990.

[184] PARK, G.D. : Determination of Tail-Off Aircraft Parameters Using Systems Identification. *AIAA Atmospheric Flight Mechanics Conference Proceedings*. June, 1976. pp. 128-136.

[185] PEARSON, A.E. : Parameter Identification for Nonlinear Aerodynamic Systems. *Brown University Technical Report*, NAG. 1-1065. November, 1990.

[186] Pearson, A.E. : Discrete Frequency Formats for Linear Differential System Identification. *13th IFAC Congress Proceedings*, Vol. 7. July, 1993. pp. 143-148.

[187] Perkins, A.R. : Use of Stepwise Regression Techniques and Kinematic Compatibility for the Analysis of EAP Flight Data. *AGARD : Manoeuvring Aerodynamics. CP 497*, Paper 14. May, 1991. pp. 14.1-14.12.

[188] Plaetschke, E. and Schulz, G. : Practical Input Signal Design. *AGARD : Parameter Identification. LS 104*, Paper 3. October, 1979. pp. 3.1-3.19.

[189] Press, W.H., Teukolsky, S.A., Vetterling, W.T. and Flannery, B.P. : *Numerical Recipes in C. 2nd Edn.* © Cambridge University Press, 1992.

[190] Proskawetz, K.O. : Identification of the Longitudinal Motion of a Dornier DO 28 Airplane. *10th IFAC Congress Proceedings.* 1987. pp. 133-138.

[191] Quanwei, J. and Qiongkang, C. : Dynamic Model for Real-Time Estimation of Aerodynamic Characteristics. *Journal of Aircraft*, Vol. 26, No. 4. April, 1989. pp. 315-321.

[192] Queijo, M.J., Wells, W.R. and Keskar, D.A. : The Influence of Unsteady Aerodynamics on Extracted Aircraft Parameters. *AIAA Atmospheric Flight Mechanics Conference Proceedings*, Paper 78-1343. August, 1978. pp. 132-139.

[193] Ramachandran, S. and Wells, W.R. : Estimation of Nonlinear Aerodynamic Derivatives of a Variable Geometry Fighter Aircraft from Flight Data. *AIAA Mechanics and Control of Flight Conference Proceedings*, Paper 74-790. August, 1974.

[194] Ramachandran, S., Schneider, H., Mason, J.D. and Stalford, H.L. : Identification of Aircraft Aerodynamic Characteristics at High Angles of Attack and Sideslip Using the Estimation Before Modeling (EBM) Technique. *AIAA Atmospheric Flight Mechanics Conference Proceedings*, Paper 77-1169. August, 1977. pp. 374-385.

[195] Raney, D.L. : Analysis of Lateral Stability of X-29 Drop Model Using System Identification Methodology. *AIAA Atmospheric Flight Mechanics Conference Proceedings*, Paper 87-2625. August, 1987. pp. 474-481.

[196] Rault, A. : Identification Applications to Aeronautics. *3rd IFAC Identification and System Parameter Estimation Proceedings*, Paper S-2. June, 1973. pp. 49-65.

[197] Rohlf, D., Plaetschke, E. and Weiá, S. : X-31A Model Evaluation and Validation via System Identification. *AIAA Atmospheric Flight Mechanics Conference Proceedings*, Paper 91-2875. August, 1991. pp. 1-10.

[198] Rokhsaz, K. and Steck, J.E. : Use of Neural Networks in Control of High-Alpha Maneuvers. *Journal of Guidance, Control & Dynamics*, Vol. 16, No. 5. September, 1993. pp. 934-939.

[199] Ross, A.J. : Determination of Aerodynamic Derivatives from Transient Responses in Manoeuvring Flight. *AGARD : Methods for Aircraft State and Parameter Identification. CP 172*, Paper 14. November, 1974. pp. 14.1-14.10.

[200] Ross, A.J. and Foster, G.W. : FORTRAN Programs for the Determination of Aerodynamic Derivatives from Transient Longitudinal or Lateral Responses of Aircraft. *British Aeronautical Research Council*, ARC Report No. CP1344. 1976.

[201] Ross, A.J. : Identification Experience in Extreme Flight Regimes. *AGARD : Parameter Identification. LS 104*, Paper 8. October, 1979. pp. 8.1-8.15.

[202] Ross, A.J. : Application of Parameter Identification Techniques to Analysis of Flight Data. *Progress in the Aerospace Sciences*, Vol. 18. 1979. pp. 325-350.

[203] Ross, A.J., Edwards, G.F. and Klein, V. : Validation of Aerodynamic Parameters at High Angles of Attack for RAE High-Incidence Research Models. *AIAA Atmospheric Flight Mechanics Conference Proceedings*, Paper 87-2558. August, 1987. pp. 296-304.

[204] Ross, A.J., Edwards, G.F., Klein, V. and Batterson, J.G. : Validation of Aerodynamic Parameters for High-Incidence Research Models. *Journal of Aircraft*, Vol. 26, No. 7. July, 1989. pp. 621-628.

[205] Rynaski, E.G., Andrisani, D. II and Weingarten, N.C. : Identification of the Stability Parameters of an Aeroelastic Airplane. *AIAA Atmospheric Flight Mechanics Conference Proceedings*, Paper 78-1328. August, 1978. pp. 20-27.

[206] Schiff, L.B., Tobak, M. and Malcolm, G.N. : Mathematical Modeling of the Aerodynamics of High-Angle-of-Attack Maneuvers. *AIAA Atmospheric Flight Mechanics Conference Proceedings*, Paper 80-1583. August, 1980. pp. 222-235.

[207] SCHUMAKER, L.L. : *Spline Functions: Basic Theory* © John Wiley & Sons, Inc., 1981.

[208] SCHWANZ, R.C. and WELLS, W.R. : Identification of Aeroelastic Parameters Using a Recursive Sequential Least Squares Method. *AIAA Atmospheric Flight Mechanics Conference Proceedings*, Paper 80-1634. August, 1980. pp. 650-661.

[209] SHAFER, M.F. : Flight Investigation of Various Control Inputs Intended for Parameter Estimation. *AIAA Atmospheric Flight Mechanics Conference Proceedings*, Paper 84-2073. August, 1984. pp. 33-49.

[210] SHILU, C. and XIAOFEI, X. : Parameter Identification of Unsteady Aerodynamic Forces for Elastic Vehicles. *AIAA Atmospheric Flight Mechanics Conference Proceedings*, Paper 92-4505. August, 1992. pp. 474-476.

[211] SHINBROT, M. : A Least Squares Curve Fitting Method with Applications to the Calculation of Stability Coefficients from Transient-Response Data. *NACA Technical Note*, TN 2341. 1951.

[212] SILHOUETTE, X. and STENGEL, R. : Estimation of the Aerodynamic Coefficients of the NAVION Aircraft at High Angles of Attack and Sideslip. *AIAA Atmospheric Flight Mechanics Conference Proceedings*, Paper 87-2622. August, 1987. pp. 452-463.

[213] SIM, A.G. : Flight Characteristics of a Manned, Low-Speed, Controlled Deep Stall Vehicle. *AIAA Atmospheric Flight Mechanics Conference Proceedings*, Paper 84-2074. August, 1984. pp. 50-56.

[214] SPEYER, J.L. and CRUES, E.Z. : On-Line Estimation and Identification of Aircraft Stability Derivatives Using the Modified Gain Extended Kalman Filter. *AIAA Atmospheric Flight Mechanics Conference Proceedings*, Paper 85-1762. August, 1985. pp. 1-9.

[215] SRI-JAYANTHA, M. and STENGEL, R.F. : Determination of Nonlinear Aerodynamic Coefficients Using the Estimation-Before-Modeling Method. *Journal of Aircraft*, Vol. 25, No. 9. September, 1988. pp. 796-804.

[216] Stalford, H.L. : The EBM System Identification Technique and its Application to High α Modeling of Aircraft. *AIAA Atmospheric Flight Mechanics Conference Proceedings*, Paper 80-1631. August, 1980. pp. 619-625.

[217] Stalford, H.L. : High-Alpha Aerodynamic Model Identification of T-2C Aircraft Using the EBM Method. *Journal of Aircraft*, Vol. 18, No. 10. October, 1981. pp. 801-809.

[218] Stengel, R.F. and Linse, D.J. : System Identification for Nonlinear Control Using Neural Networks. *NASA Conference Paper*, CP 3095. December, 1990. pp. 187-192.

[219] Stepner, D.E. and Mehra, R.K. : Maximum Likelihood Identification and Optimal Input Design for Identifying Aircraft Stability and Control Derivatives. *NASA Contractor Report*, CR 2200. 1973.

[220] Stevenson, S.W. : Parameter Identification Modeling for Simulation Aerodynamic Model Updates. *AIAA Atmospheric Flight Mechanics Conference Proceedings*, Paper 91-2878. August, 1991. pp. 298-305.

[221] Stevenson, S.W., Holl, D. and Roman, A. : Parameter Identification of AV-8B Wingborne Aerodynamics for Flight Simulator Model Updates. *AIAA Atmospheric Flight Mechanics Conference Proceedings*, Paper 92-4506. August, 1992. pp. 477-493.

[222] Stuckey, R.A. : Identification of Nonlinear Aircraft Spoiler Parameters. *13th IFAC Congress Proceedings*, Paper 93/0945, Vol. 1. July, 1993. pp. 283-288.

[223] Stuckey, R.A. : Efficient Data Partitioning in the Nonlinear Model Structure Determination of Aircraft. *5th Australian Aeronautical Conference, Proceedings*, Vol. 1. September, 1993. pp. 69-74.

[224] Stuckey, R.A. : Flight-Estimated Spoiler Aerodynamics of the F-111C Aircraft. *AIAA Atmospheric Flight Mechanics Conference Proceedings*, Paper 94-3459. August, 1994. pp. 449-458.

[225] Taylor, L.W. Jr., Iliff, K.W. and Powers, B.G. : A Comparison of Newton-Raphson and Other Methods for Determining Stability Derivatives from Flight Data. *AIAA Conference Proceedings*, Paper 69-315. 1969.

[226] Taylor, L.W. Jr. : Application of a New Criterion for Modeling Systems. *AGARD : Methods for Aircraft State and Parameter Identification. CP 172*, Paper 4. November, 1974. pp. 4.1-4.9.

[227] Toutenburg, H. : *Prior Information in Linear Models* © John Wiley & Sons, Inc., 1982.

[228] Trankle, T.L. and Rabin, U.H. : Filtering Flight Data Prior to Aerodynamic System Identification. *AIAA Atmospheric Flight Mechanics Conference Proceedings*, Paper 83-2098. August, 1983.

[229] Trankle, T.L. and Bachner, S.D. : Identification of a Full Subsonic Envelope Nonlinear Aerodynamic Model of the F-14 Aircraft. *AIAA Atmospheric Flight Mechanics Conference Proceedings*, Paper 93-3634. August, 1993. pp. 187-197.

[230] Travassos, R.H., Gupta, N.K., Iliff, K.W. and Maine, R. : Determination of an Oblique Wing Aircraft's Aerodynamic Characteristics. *AIAA Atmospheric Flight Mechanics Conference Proceedings*, Paper 80-1630. August, 1980. pp.608-618.

[231] Travassos, R. and Kaufman, H. : Parallel Procedures for Aircraft Parameter Identification and State Estimation. *AIAA Atmospheric Flight Mechanics Conference Proceedings*, Paper 79-1636. August, 1979. pp. 111-119.

[232] Verbrugge, R.A., Charon, W. and Marchand, M. : Wind Tunnel and Free-Flight Model Identification Experience. *AGARD : Parameter Identification. LS 104*, Paper 9. October, 1979. pp. 9.1-9.33.

[233] Verhaegen, M.H. : Comparison of Two Numerical Techniques for Aerodynamic Model Identification. *AIAA Atmospheric Flight Mechanics Conference Proceedings*, Paper 87-2620. August, 1987. pp. 436-443.

[234] Vincent, J.H, Gupta, N.K. and Hall, W.E. Jr. : Recent Results in Parameter Identification for High Angle of Attack Stall Regimes. *AIAA Atmospheric Flight Mechanics Conference Proceedings*, Paper 79-1640. August, 1979.

[235] Wells, W.R. : Estimation of Aircraft Parameters in Nonlinear Aerodynamic Models. *3rd IFAC Identification and System Parameter Estimation Proceedings*, Paper PT-4. June, 1973. pp. 445-448.

[236] Wells, W.R. and Ramachandran, S. : Flight Test Design for Efficient Extraction of Aircraft Parameters. *AIAA Atmospheric Flight Mechanics Conference Proceedings*. June, 1976. pp. 101-107.

[237] Wells, W.R. and Queijo, M.J. : Simplified Unsteady Aerodynamic Concepts, with Application to Parameter Estimation. *AIAA Atmospheric Flight Mechanics Conference Proceedings*, Paper 77-1124. August, 1977. pp. 39-45.

[238] Wells, W.R., Banda, S.S. and Quam, D.L. : A Model for Unsteady Effects in Lateral Dynamics for Use in Parameter Estimation. *AIAA Atmospheric Flight Mechanics Conference Proceedings*, Paper 79-1638. August, 1979. pp. 129-134.

[239] Wells, W.R. and Keskar, D.A. : The Relationship of Unsteadiness in Downwash to the Quality of Parameter Estimates. *AIAA Atmospheric Flight Mechanics Conference Proceedings*, Paper 79-1639. August, 1979. pp. 135-142.

[240] Wells, W.R. and Banda, S.S. : Data Analysis for Aircraft Parameter Estimates. *AIAA Atmospheric Flight Mechanics Conference Proceedings*, Paper 81-1864. August, 1981.

[241] Wells, W.R. and Klein, V. : Parameter Estimation Applied to General Aviation Aircraft : A Case Study. *AIAA Atmospheric Flight Mechanics Conference Proceedings*, Paper 82-1313. August, 1982.

[242] Wingrove, R.C. : A Quasi-Linearization Technique for Estimating Aircraft States from Flight Data. *Journal of Aircraft*, Vol. 10, No. 5. 1973. pp. 303-307.

[243] Wingrove, R.C. : Parameter Estimation of Powered-Lift STOL Aircraft Characteristics Including Turbulence and Ground Effects. *AGARD : Methods for Aircraft State and Parameter Identification. CP 172*, Paper 28. November, 1974. pp. 28.1-28.10.

[244] Yazawa, K. : Identification of Aircraft Stability and Control Derivatives in the Presence of Turbulence. *AIAA Atmospheric Flight Mechanics Conference Proceedings*, Paper 77-1134. August, 1977. pp. 113-123.

[245] Young, J.W., Schy, A.A. and Johnson, K.G. : Pseudosteady State Analysis of Nonlinear Aircraft Maneuvers. *AIAA Atmospheric Flight Mechanics Conference Proceedings*, Paper 80-1600. August, 1980. pp. 372-382.

[246] Youssef, H.M. and Juang, J.C. : Estimation of Aerodynamic Coefficients Using Neural Networks. *AIAA Atmospheric Flight Mechanics Conference Proceedings*, Paper 93-3639. August, 1993. pp. 242-245.

[247] Zadeh, L.A. : From Circuit Theory to System Theory. *Proceedings of the IRE*, pp. 856-965. 1962.

Spoiler Aerodynamics

[248] AGARD : Aerodynamic Characteristics of Controls. *CP 262*. May, 1979.

[249] Al-Bahi, A.M. and Ghazi M.A. : An Experimental Investigation on Spoiler Effect. *AIAA Conference Proceedings*, Paper 91-3214. 1991. pp. 109-115.

[250] Ayoub, A., Satynarayana, B. and Karamcheti, K. : Unsteady Flow Patterns Associated with Spoiler Control Devices. *AIAA 20th Aerospace Sciences Meeting Conference Proceedings*, Paper 82-0127. January, 1982.

[251] Barnes, C.S. : A Developed Theory of Spoilers on Airfoils. *British Aeronautical Research Council*, ARC Report No. CP887. July, 1965.

[252] Bodapati, S., Foreman, M.J. and Lee, C.S. : Flow-Field Measurements of an Airfoil with a Deflected Spoiler Using an LDV System. *AIAA 19th Fluid Dynamics, Plasma Dynamics and Lasers Conference Proceedings*, Paper 87-1438. June, 1987. pp. 1-10.

[253] Consigny, H., Gravelle, A. and Molinaro, R. : Aerodynamic Characteristics of a Two-Dimensional Moving Spoiler in Subsonic and Transonic Flow. *AIAA Applied Aerodynamics Conference Proceedings*, Paper 83-1809. July, 1983.

[254] Costes, M. : Comparison Between Experimental and Computational Results for Airfoils Equipped with a Spoiler and a Flap *AIAA 3rd Applied Aerodynamics Conference Proceedings*, Paper 85-5008. October, 1985.

[255] Destuynder, R. and Hönlinger, H. : Multi-Control System in Unsteady Aerodynamics Using Spoilers. *AIAA Conference Proceedings*, Paper 87-0855. 1987. pp. 421-427.

[256] De Young, J : Theoretical Antisymmetric Span Loading for Wings of Arbitrary Planform at Subsonic Speeds. *NACA Technical Report*, TR 1056. 1951.

[257] ESDU : Lift and rolling moment due to spoilers on wings with flaps undeflected at subsonic speeds. *ESDU 90030*. November, 1990.

[258] Francis, M.S., Keesee, J.E., Seiler, F.J., Lang, J.D. and Sparks, G.W. : Aerodynamic Characteristics of an Unsteady Flow. *AIAA Applied Aerodynamics Conference Proceedings*, Paper 79-0283. January, 1979.

[259] Franks, R.W. : Tests in the Ames 40- by 80- Foot Wind Tunnel of the Aerodynamic Characteristics of Airplane Models with Plain Spoiler Ailerons. *NACA Research Memorandum*, RM A54H26. December, 1954.

[260] Franks, R.W. : The Application of a Simplified Lifting-Surface Theory to the Prediction of the Rolling Effectiveness of Plain Spoiler Ailerons at Subsonic Speeds. *NACA Research Memorandum*, RM A54H26a. December, 1954.

[261] Hayes, C. : Roll-Control Effectiveness of Several Spoiler Configurations on an Airplane Model with Wing Sweep of 55° and 75° at Supersonic Mach Numbers. *NASA Technical Memorandum*, TM X-2165. March, 1971.

[262] Henderson, M.L : A Solution to the 2-D Separated Wake Modeling Problem and its use to Predict CLmax of Arbitrary Airfoil Sections. *AIAA Applied Aerodynamics Conference Proceedings*, Paper 78-156, January, 1978.

[263] Hoak, D.E., *et al* : *USAF Stability and Control DatCom*, Vol. 3, Section 6.2 : Asymmetrically Deflected Controls on Wing-Body and Tail-Body Control Combinations. April, 1978.

[264] Jonas, K., Wnnenberg, H. and Horstmann, K.H. : Roll Control by Digitally Controlled Segment Spoilers. *AGARD : Aerodynamic Characteristics of Controls. CP 262*, Paper 7. May, 1979. pp. 7.1-7.8.

[265] Jordan, F. L. Jr, Gato, W., Masiello, M.F., O'Rourke, M.J. and White, E.R. : Experimental Investigation of Unsteady Aerodynamics on a Flap Element Induced by Rapid Spoiler Deflection. *AIAA Conference Proceedings*. 1994.

[266] Kalligas, K.P. : The Dynamic Characteristics of Two-Dimensional Spoilers at Low Speeds. *University of Bristol, Department of Aeronautical Engineering*, PhD Thesis, 1986.

[267] Lê, T.H., Ryan, J. and Morchoisne, Y. : Application of a Fourier Panel Method to 3-D Spoiler Calculations. *AIAA Conference Proceedings*, Paper 87-2417. 1987. pp. 367-370.

[268] Lee, C.S., Bodapati, S. and Karamcheti, K. : Flow Measurements of an Airfoil with Deflected Spoiler. *AIAA 21st Aerospace Sciences Meeting Proceedings*, Paper 83-0365. January, 1983.

[269] Lee, C.S. and Bodapati, S. : A Comparison Between Theoretical and Experimental Flowfields of an Airfoil with Delfected Spoiler. *AIAA 23rd Aerospace Sciences Meeting Proceedings*, Paper 85-0269. January, 1985.

[270] Lee, C.S. and Bodapati, S. : Experimental Investigations of the Flowfield of an Airfoil with Spoiler. *AIAA Journal*, Vol. 25, No. 11. November, 1987. pp. 1411-1416.

[271] Lord, D.R. and Czarnecki, K.R. : Loads Associated with Spoilers at Supersonic Speeds. *NACA Research Memorandum* RML55E12a. June, 1955.

[272] Lowry, J.G. : Data on Spoiler-Type Ailerons. *NACA Research Memorandum*, RM L53124a. October, 1953.

[273] Mack, M.D., Seetharam, H.C., Kuhn, W.G. and Bright, J.T. : Aerodynamics of Spoiler Control Devices. *AIAA Aircraft Systems and Technology Meeting Proceedings*, Paper 79-1873. August, 1979.

[274] McLachlan, B.G. and Karamcheti, K. : Experimental Study of the Flowfield of an Airfoil with Deflected Spoiler. *AIAA 20th Aerospace Sciences Meeting Proceedings*, Paper 82-0126. January, 1982.

[275] McLachlan, B.G., Karamcheti, K., Ayoub, A. and Hadjidakis, G. : A Study of the Unsteady Flow Field of an Airfoil with Deflected Spoiler. *AIAA Atmospheric Flight Mechanics Conference Proceedings*, Paper 83-2131. August, 1983.

[276] McLachlan, B.G. and Karamcheti, K. : An Experimental Study of Airfoil-Spoiler Aerodynamics. *NASA Contractor Report*, CR 177328. February, 1985.

[277] Myers, P.G. : A Two-Dimensional Spoiler of Arbitrary Chordwise Position in a Low Speed Flow. *University of Bristol, Department of Aeronautical Engineering*, PhD Thesis, 1990.

[278] Seetharam, H.C. and Wentz, W.H. Jr : Experimental Studies of Flow Separation and Stalling on a Two-Dimensional Airfoil at Low Speeds. *NASA Contractor Report*, CR 2560. 1975.

[279] Siddalingappa, S.R. and Hancock, G.J. : Unsteady Aerodynamics of Two Dimensional Spoilers at Low Speeds. *AGARD : Aerodynamic Characteristics of Controls. CP 262*, Paper 21. May, 1979. pp. 21.1-21.13.

[280] Siddalingappa, S.R. and Hancock, G.J. : An Introduction to the Aerodynamics of Spoilers. *Queen Mary College, London*, QMC/EP 1034. August, 1980.

[281] Vogler, R.D. : Wind-Tunnel Investigation at High Subsonic Speeds of Spoilers of Large Projection on an NACA 65A006 Wing with Quarter-Chord Line Swept Back 32.6°. *NACA Research Memorandum*, RM L51L10. January, 1952.

[282] Weick, F.E. and Shortal, J.A. : Wind-Tunnel Research Comparing Lateral Control Devices, Particularly at High Angles of Attack : V. Spoilers and Ailerons on Rectangular Wings. *NACA Report*, R 439. 1932.

[283] Weick, F.E. and Jones, R.T. : Resumé of N.A.C.A. Lateral Control Research. *NACA Report*, R 605. 1937.

[284] Woods, L.C. : Theory of Airfoil Spoilers *British Research & Memorandum*, No. 2969, 1956.

Appendix A

Aircraft Equations of Motion

A.1 Frames of reference

In order to describe the motion of an aircraft in flight, it is first neccessary to define a set of appropriate coordinate systems. The systems proposed in references [50] and more recently, [5] are commonly employed as standards for flight dynamics and shall be summarised here. Essentially, there are three reference frames of importance, illustrated in Figure A-1. Each is Cartesian in nature and can be related to the others through a linear transformation of coordinates.

Earth/Inertial Axes

The first set of axes, required in most dynamic systems, is for all intensive purposes assumed 'fixed'. The Earth Axes provide a frame to which all motions can be referred. Its origin is set at some point on the Earth's surface with the x, y and z axes aligned North, East and downward, respectively, forming an orthogonal *right-handed* system. One can define the location of a free-flying aircraft using this reference system and along with the Body Axes, the aircraft's orientation.

Body Axes

These orthogonal axes, denoted x_b, y_b and z_b, are located at the aircraft's centre of gravity and aligned towards the fuselage nose, the starboard wing and the fuselage belly, respectively. Orientation of the aircraft, with respect to the Earth Axes can be described by the Euler angles, (ϕ, θ, ψ), given in Section A.3. Additionally, the angular rates about each body axis are given by the roll, pitch and yaw: p, q and r.

Wind Axes

This last set of axes also has its origin fixed at the aircraft's centre of gravity, however, it is orientated such that the x_w axis is aligned with the relative-wind vector (i.e. the incident airstream). The Wind Axes are related to the Earth Axes via the Bank, Climb and Heading angles, (ϕ_w, θ_w, ψ_w) and they are related to the Body Axes through the Angle-of-Attack, α and Sideslip angle, β. The principal function of the Wind Axes is to define the orientation of the vehicle resultant velocity vector with respect to the Earth Axes.

A detailed development of the reference system, with associated coordinate transformations may be sought from Etkin [34]. Only the basic equations of relevance to the current work have been presented here.

A.2 The dynamic system

The rigid-body equations of motion for an aircraft in flight are obtained from application of Newton's 2^{nd} law. This states:

> *"The rate of change in linear momentum of a body is equal to the sum of all external forces acting on that body and the rate of change in angular momentum is equal to the sum of all external moments"*

Both (time) rates of change in linear and angular momentum are referred to the fixed inertial frame. This law can be expressed in terms of the force and moment vector quantities, $\vec{\mathbf{F}}$ and $\vec{\mathbf{M}}$ and subsequently applied to an aircraft in its body axes:

$$\vec{\mathbf{F}} = m\frac{\mathrm{d}\vec{\mathbf{v}}}{\mathrm{d}t} + m(\vec{\omega} \times \vec{\mathbf{v}}) \tag{A.1}$$

$$\vec{\mathbf{M}} = \frac{\mathrm{d}\vec{\mathbf{H}}}{\mathrm{d}t} + \vec{\omega} \times \vec{\mathbf{H}} \tag{A.2}$$

where m is the mass of the aircraft and the vectors, $\vec{\mathbf{F}} = F_x\,\vec{i} + F_y\,\vec{j} + F_z\,\vec{k}$ represents the total force, $\vec{\mathbf{M}} = L\,\vec{i} + M\,\vec{j} + N\,\vec{k}$ the total moment, $\vec{\mathbf{v}} = u\,\vec{i} + v\,\vec{j} + w\,\vec{k}$ the velocity, $\vec{\omega} = p\,\vec{i} + q\,\vec{j} + r\,\vec{k}$ the angular velocity and

$$\vec{\mathbf{H}} = \int_{\mathcal{V}} \vec{\mathbf{r}} \times [\vec{\omega} \times \vec{\mathbf{r}}]\ \mathrm{d}m \tag{A.3}$$

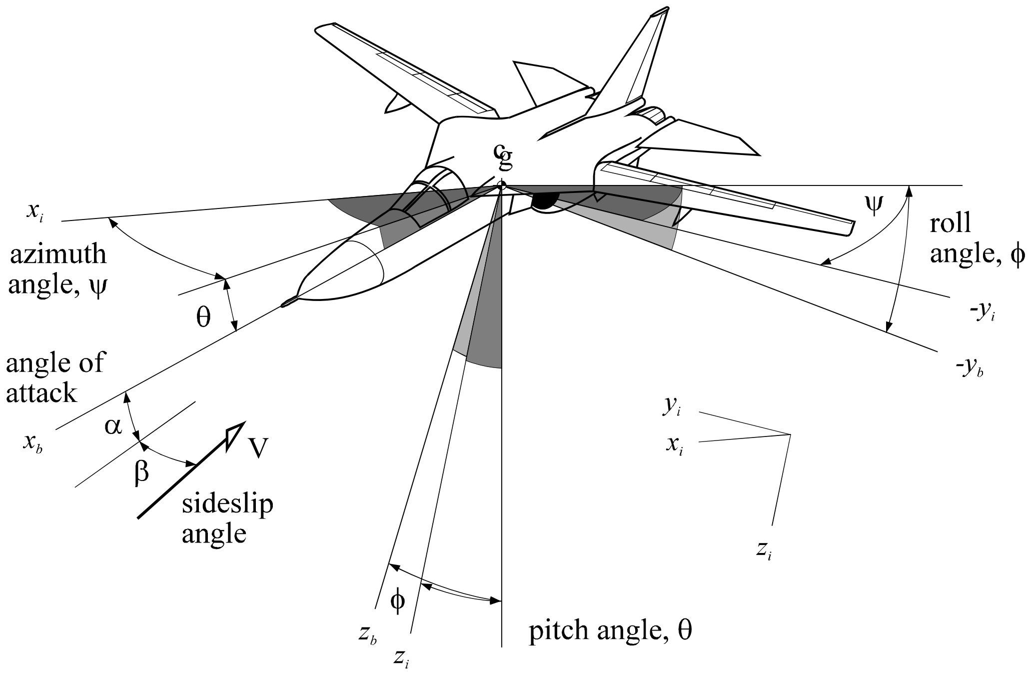

Figure A-1: Fixed inertial and body reference frames represents the total angular momentum. The inner term containing $\vec{\mathbf{r}} = x\,\vec{\imath} + y\,\vec{\jmath} + z\,\vec{k}$ must be integrated over the aircraft's volume to obtain $\vec{\mathbf{H}}$. Defining the mass moments and products of inertia, respectively:

$$I_{xx} = \textstyle\int_{\mathcal{V}} (\,y^2 + z^2)\ \mathrm{d}m \qquad I_{yy} = \int_{\mathcal{V}} (\,x^2 + z^2)\ \mathrm{d}m \qquad I_{zz} = \int_{\mathcal{V}} (\,x^2 + y^2)\ \mathrm{d}m$$
$$I_{xy} = \textstyle\int_{\mathcal{V}} xy\ \mathrm{d}m \qquad I_{xz} = \int_{\mathcal{V}} xz\ \mathrm{d}m \qquad I_{yz} = \int_{\mathcal{V}} yz\ \mathrm{d}m$$

The equations, (A.1), (A.2) and (A.3) completely describe the motion of a rigid aircraft in free-flight. If each body axis component is now considered separately, the following scalar equations can be obtained:

$$\begin{aligned} \dot{u} - vr + wq &= \frac{1}{m} F_x \\ \dot{v} + ur - wp &= \frac{1}{m} F_y \\ \dot{w} - uq + vp &= \frac{1}{m} F_z \end{aligned} \tag{A.4}$$

which describes the linear motion and, assuming symmetry about the xz plane ($I_{xy} = I_{yz} = 0$), the equations:

$$\begin{aligned} \dot{p} - \frac{I_{xz}}{I_x}(\,\dot{r} + pq) + \frac{I_z - I_y}{I_x} qr &= \frac{1}{I_x} L \\ \dot{q} + \frac{I_x - I_z}{I_y} pr + \frac{I_{xz}}{I_y}(\,p^2 - r^2) &= \frac{1}{I_y} M \\ \dot{r} - \frac{I_{xz}}{I_z}(\,\dot{p} - qr) + \frac{I_y - I_x}{I_z} pq &= \frac{1}{I_z} N \end{aligned} \tag{A.5}$$

describe the angular motion.

A.3 Orientation of the Aircraft

In order to calculate the position and orientation of the aircraft at any point in time, the relationship between earth and body axes must be formulated. There exist several ways in which the body axes orientation can be described, relative to an inertial frame. The first to be presented is the widely used Euler angle system.

Refer to Figure A-1. This system utilises three *consecutive* rotations, whose order is crucial. The sequence is:

1. rotation about body axis, z, through yaw angle, ψ ;
2. rotation about displaced y axis through pitch angle, θ ; and
3. rotation about displaced x axis through roll angle, ϕ.

Having defined the Euler angles, it is now possible to determine the Euler rates in terms of the body angular rates:

$$\begin{aligned} \dot{\phi} &= p + (q \sin\phi + r\cos\phi)\tan\theta \\ \dot{\theta} &= q\cos\phi - r\sin\phi \\ \dot{\psi} &= (q\sin\phi + r\cos\phi)\sec\theta \end{aligned} \tag{A.6}$$

forming a set of nonlinear differential equations. There is, however, a singularity at $\theta = \pm 90°$ and thus, the second angular representation to be presented is often a more favourable choice. The set of *quaternions* are derived from an instantaneous axis of rotation plus a single rotation about that axis. They are related to the body rates through:

$$\begin{aligned} \dot{e}_0 &= \frac{1}{2}(-p\,e_1 - q\,e_2 - r\,e_3) \\ \dot{e}_1 &= \frac{1}{2}(p\,e_0 + r\,e_2 - q\,e_3) \\ \dot{e}_2 &= \frac{1}{2}(q\,e_0 - r\,e_1 + p\,e_3) \\ \dot{e}_3 &= \frac{1}{2}(r\,e_0 + q\,e_1 - p\,e_2) \end{aligned} \tag{A.7}$$

where e_0, e_1, e_2 and e_3 denote the quaternion values, which range from -1 to 1. The above time-varying differential equations, like the Euler equations (A.6), can be solved to yield the instantaneous attitude.

The 'absolute' velocity, angle-of-attack and sideslip angle provide alternative states by which the orientation of the body axes, with reference to the wind axes, can be measured. They may be calculated using the following relationships:

$$\begin{aligned} V &= \sqrt{u^2 + v^2 + w^2} \\ \beta &= \sin^{-1}\frac{v}{V} \\ \alpha &= \tan^{-1}\frac{w}{u} \end{aligned} \tag{A.8}$$

A.4 Forces and Moments

The forces and moments in each body axis, given by Equations (A.4) and (A.5), can be divided into their aerodynamic, thrust and gravitational components via:

$$\begin{aligned} F_x &= X_A + X_T - mg\sin\theta & L &= L_A + L_T \\ F_y &= Y_A + Y_T + mg\sin\phi\cos\theta & M &= M_A + M_T \\ F_z &= Z_A + Z_T + mg\cos\phi\cos\theta & N &= N_A + N_T \end{aligned} \tag{A.9}$$

Euler angles have been utilised here to express the gravitational components, though an equivalent representation can be formulated using quaternions, if required.

A.5 Perturbation Theory

By assuming that the motion of the aircraft consists of small deviations about some 'trim' flight condition, the rigid-body equations of motion are able to be linearised. Considering each state variable as a Taylor series expansion about its trim state, the equations of motion can be rewritten and divided into a set of trim equations and a set of corresponding perturbation equations. The formulation can be further simplified by neglecting all second- and higher-order terms. Hence, each state variable is written in the form:

$$x = x_1 + \Delta x \tag{A.10}$$

where the subscript 1 denotes trim and Δx is the perturbed state. The trim equations take on the same form as the general equations, (A.4) and (A.5) above. Consequently, the perturbation equations are, for the linear velocities:

$$\begin{aligned} \Delta\dot{u} - v_1\Delta r - r_1\Delta v + w_1\Delta q + q_1\Delta w &= \frac{1}{m}\Delta X - g\Delta\theta\cos\theta_1 \\ \Delta\dot{v} + u_1\Delta r + r_1\Delta u - w_1\Delta p - p_1\Delta w &= \frac{1}{m}\Delta Y - g\Delta\theta\sin\phi_1\sin\theta_1 + g\Delta\phi\cos\phi_1\cos\theta_1 \\ \Delta\dot{w} - u_1\Delta q - q_1\Delta u + v_1\Delta p + p_1\Delta v &= \frac{1}{m}\Delta Z - g\Delta\theta\cos\phi_1\sin\theta_1 - g\Delta\phi\sin\phi_1\cos\theta_1 \end{aligned} \tag{A.11}$$

and for the angular velocities:

$$
\begin{aligned}
\Delta\dot{p} - \frac{I_{xz}}{I_x}\Delta\dot{r} - \frac{I_{xz}}{I_x}(p_1\Delta q + q_1\Delta p) + \frac{I_z - I_y}{I_x}(q_1\Delta r + r_1\Delta q) &= \frac{1}{I_x}\Delta L \\
\Delta\dot{q} + \frac{I_x - I_z}{I_y}(p_1\Delta r + r_1\Delta p) + 2\frac{I_{xz}}{I_y}p_1\Delta p - 2\frac{I_{xz}}{I_y}r_1\Delta r &= \frac{1}{I_y}\Delta M \\
\Delta\dot{r} - \frac{I_{xz}}{I_z}\Delta\dot{p} + \frac{I_y - I_x}{I_z}(p_1\Delta q + q_1\Delta p) + \frac{I_{xz}}{I_z}(q_1\Delta r + r_1\Delta q) &= \frac{1}{I_z}\Delta N
\end{aligned}
\tag{A.12}
$$

In addition, the perturbed Euler angles are written

$$
\begin{aligned}
\Delta\dot{\phi} &= \Delta p + \Delta q \sin\phi_1 \tan\theta_1 + \Delta r \cos\phi_1 \tan\theta_1 + \ldots \\
&\quad + \Delta\phi(q_1 \cos\phi_1 - r_1 \sin\phi_1)\tan\theta_1 + \Delta\theta(q_1 \sin\phi_1 + r_1 \cos\phi_1)\sec^2\theta_1 \\
\Delta\dot{\theta} &= \Delta q \cos\phi_1 - \Delta r \sin\phi_1 - \Delta\phi(q_1 \sin\phi_1 + r_1 \cos\phi_1) \\
\Delta\dot{\psi} &= \Delta q \sin\phi_1 \sec\theta_1 + \Delta r \cos\phi_1 \sec\theta_1 + \ldots \\
&\quad + \Delta\phi(q_1 \cos\phi_1 - r_1 \sin\phi_1)\sec\theta_1 + \Delta\theta(q_1 \sin\phi_1 + r_1 \cos\phi_1)\tan\theta_1 \sec\theta_1
\end{aligned}
\tag{A.13}
$$

assuming $\sin\Delta\phi \approx \Delta\phi$, $\sin\Delta\theta \approx \Delta\theta$ and $\cos\Delta\theta \approx \cos\Delta\phi \approx 1$, since $\Delta\phi$ and $\Delta\theta$ are considered small.

It is also possible to substitute the wind axes states, V, β and α into Equations (A.11) using the linearised approximation:

$$
\Delta V \approx \Delta u \qquad \Delta\beta \approx \frac{\Delta v}{V_1} \qquad \Delta\alpha \approx \frac{\Delta w}{V_1} \tag{A.14}
$$

from the Equations (A.8). The above sets of equations are first-order linear differential equations in the perturbation quantities, with constant coefficients at each trim condition. Their numerical solution is therefore reasonably straightforward.

Before proceeding though, expressions for the aerodynamic and propulsive forcing functions are required. For conventional aircraft and flight conditions, these functions are likely to be dependent on the aircraft's states and control deflections as well as a number of external random inputs, such as turbulence. An approximation to the perturbation forcing functions is obtained through series expansion about a trim condition, in the same way the equations of motion were linearised to form a perturbation model. Neglecting any external disturbances, the first-order expansions for force and moment perturbations have the form:

$$\Delta X = \sum_j \frac{\partial X}{\partial x_j} \Delta x_j \tag{A.15}$$

where $\partial X/\partial x_j$ are the dimensional stability derivatives in each state and control variable, and Δx_j represent the corresponding perturbation variables. These partial derivative terms are dimensional and are normally substituted into the equations of motion as:

$$\begin{array}{lll} X_\alpha = \frac{1}{m}\frac{\partial F_x}{\partial \alpha} & Z_\alpha = \frac{1}{m}\frac{\partial F_z}{\partial \alpha} & Y_\beta = \frac{1}{m}\frac{\partial F_y}{\partial \beta} \\ L_\beta = \frac{1}{I_{xx}}\frac{\partial L}{\partial \beta} & M_\alpha = \frac{1}{I_{yy}}\frac{\partial M}{\partial \alpha} & N_\beta = \frac{1}{I_{zz}}\frac{\partial N}{\partial \beta} \end{array}$$

and so on, for each state/control variable. The dimensional derivatives can also be expressed in terms of their non-dimensional counterparts - the usual format for presentation of the aircraft's aerodynamic characteristics - outlined in the following Section.

A.6 State-space Representation

Since the perturbation equations of motion are all linear with respect to the state variables, they can be expressed in matrix differential form via:

$$\begin{aligned} \dot{\mathbf{x}} &= \mathbf{A}\mathbf{x} + \mathbf{B}\mathbf{u} \\ \mathbf{y} &= \mathbf{C}\mathbf{x} + \mathbf{D}\mathbf{u} \end{aligned} \tag{A.16}$$

in which the state, (partial) output and control vectors are:

$$\begin{aligned} \mathbf{x} &= \begin{bmatrix} \Delta V & \Delta\beta & \Delta\alpha & \Delta p & \Delta q & \Delta r & \Delta\phi & \Delta\theta & \Delta\psi \end{bmatrix}^T \\ \mathbf{y} &= \begin{bmatrix} \Delta a_x & \Delta a_y & \Delta a_z & \Delta\dot{p} & \Delta\dot{q} & \Delta\dot{r} \end{bmatrix}^T \qquad \mathbf{u} = \begin{bmatrix} \Delta\delta_j & \cdots \end{bmatrix}^T \end{aligned} \tag{A.17}$$

based on the wind axes and Euler states. The state and control transition matrices can be constructed using sub-matrices:

$$\begin{aligned} \mathbf{A} &= \begin{bmatrix} \mathbf{A}_{11} - \mathbf{A}_{12} & \mathbf{0} \\ \mathbf{0} & \mathbf{I} \end{bmatrix}^{-1} \begin{bmatrix} \begin{bmatrix} \mathbf{A}_{21} & \mathbf{0} \end{bmatrix} + \mathbf{A}_{22} \\ \mathbf{A}_{23} \end{bmatrix} \\ \mathbf{B} &= \begin{bmatrix} \mathbf{A}_{11} - \mathbf{A}_{12} & \mathbf{0} \\ \mathbf{0} & \mathbf{I} \end{bmatrix}^{-1} \begin{bmatrix} \mathbf{B}_{11} \\ \mathbf{0} \end{bmatrix} \end{aligned} \tag{A.18}$$

as can the corresponding output matrices:

$$\begin{aligned}
\mathbf{C} &= \mathbf{A}_{11}\left[\begin{array}{c}\mathbf{A}_{11}-\mathbf{A}_{12}\end{array}\right]^{-1}\left[\left[\begin{array}{cc}\mathbf{A}_{21} & \mathbf{0}\end{array}\right]+\mathbf{A}_{22}\right]-\left[\begin{array}{c}\mathbf{C}_{11}\\ \mathbf{0}\end{array}\right] \\
\mathbf{D} &= \mathbf{A}_{11}\left[\begin{array}{c}\mathbf{A}_{11}-\mathbf{A}_{12}\end{array}\right]^{-1}\mathbf{B}_{11}
\end{aligned} \tag{A.19}$$

For simplification, define the following moment of inertia ratios:

$$\begin{array}{lll}
I_1^* = \frac{I_{xz}}{I_x} & I_2^* = \frac{I_y-I_z}{I_x} & I_3^* = \frac{I_z-I_x}{I_y} \\
I_4^* = \frac{I_{xz}}{I_y} & I_5^* = \frac{I_x-I_y}{I_z} & I_6^* = \frac{I_{xz}}{I_z}
\end{array}$$

as well as several diagonal matrices to be used in coefficient dimensionalising:

$$\mathbf{d}_1 = diag\begin{Bmatrix}\frac{QS}{m}\\ \frac{QS}{m}\\ \frac{QS}{m}\\ \frac{QSb}{I_x}\\ \frac{QS\bar{c}}{I_y}\\ \frac{QSb}{I_x}\end{Bmatrix} \qquad \mathbf{d}_2 = diag\begin{Bmatrix}\frac{1}{V_1}\\ 1\\ 1\\ \frac{b}{2V_1}\\ \frac{\bar{c}}{2V_1}\\ \frac{b}{2V_1}\end{Bmatrix} \qquad \mathbf{d}_3 = diag\begin{Bmatrix}\frac{\bar{c}}{2V_1}\\ \frac{b}{2V_1}\\ \frac{\bar{c}}{2V_1}\\ \frac{b}{2V_1}\\ \frac{\bar{c}}{2V_1}\\ \frac{b}{2V_1}\end{Bmatrix}$$

The general form of each sub-matrix is presented below. Only those coefficients of relative importance have been included in each forcing function.

$$\mathbf{A}_{11} = diag\begin{Bmatrix}1\\ V_1\\ V_1\\ 1\\ 1\\ 1\end{Bmatrix} \qquad \mathbf{A}_{12} = \mathbf{d}_1\begin{bmatrix}\circ & \circ & C_{x_{\dot{\alpha}}} & \circ & \circ & \circ\\ \circ & C_{y_{\dot{\beta}}} & \circ & \circ & \circ & \circ\\ \circ & \circ & C_{z_{\dot{\alpha}}} & \circ & \circ & \circ\\ \circ & C_{l_{\dot{\beta}}} & \circ & \circ & \circ & \circ\\ \circ & \circ & C_{m_{\dot{\alpha}}} & \circ & \circ & \circ\\ \circ & C_{n_{\dot{\beta}}} & \circ & \circ & \circ & \circ\end{bmatrix}\mathbf{d}_2\mathbf{d}_3 + \begin{bmatrix}\circ & \circ & \circ & \circ & \circ & \circ\\ \circ & \circ & \circ & \circ & \circ & \circ\\ \circ & \circ & \circ & \circ & \circ & \circ\\ \circ & \circ & \circ & \circ & \circ & I_1\\ \circ & \circ & \circ & \circ & \circ & \circ\\ \circ & \circ & \circ & I_6 & \circ & \circ\end{bmatrix}$$

$$\mathbf{A}_{21} = \mathbf{d}_1\begin{bmatrix}C_{x_V} & \circ & C_{x_\alpha} & \circ & C_{x_q} & \circ\\ \circ & C_{y_\beta} & \circ & C_{y_p} & \circ & C_{y_r}\\ C_{z_V} & \circ & C_{z_\alpha} & \circ & C_{z_q} & \circ\\ \circ & C_{l_\beta} & \circ & C_{l_p} & \circ & C_{l_r}\\ C_{m_V} & \circ & C_{m_\alpha} & \circ & C_{m_q} & \circ\\ \circ & C_{n_\beta} & \circ & C_{n_p} & \circ & C_{n_r}\end{bmatrix}\mathbf{d}_2 \qquad \mathbf{B}_{11} = \mathbf{d}_1\begin{bmatrix}C_{x_\delta} & \cdots\\ C_{y_\delta} & \cdots\\ C_{z_\delta} & \cdots\\ C_{l_\delta} & \cdots\\ C_{m_\delta} & \cdots\\ C_{n_\delta} & \cdots\end{bmatrix}$$

$$
\mathbf{A}_{22} = \begin{bmatrix}
\circ & r_1 V_1 & -q_1 V_1 & \circ & -\alpha_1 V_1 & \beta_1 V_1 & \circ & -gC_{\theta_1} & \circ \\
-r_1 & \circ & p_1 V_1 & \alpha_1 V_1 & \circ & -V_1 & gC_{\phi_1} C_{\theta_1} & -gS_{\phi_1} S_{\theta_1} & \circ \\
q_1 & -p_1 V_1 & \circ & -\beta_1 V_1 & V_1 & \circ & -gS_{\phi_1} C_{\theta_1} & -gC_{\phi_1} S_{\theta_1} & \circ \\
\circ & \circ & \circ & I_1^* q_1 & I_1^* p_1 + I_2^* r_1 & I_2^* q_1 & \circ & \circ & \circ \\
\circ & \circ & \circ & I_3^* r_1 - 2I_4^* p_1 & \circ & I_3^* p_1 + 2I_4^* r_1 & \circ & \circ & \circ \\
\circ & \circ & \circ & I_5^* q_1 & I_5^* p_1 - I_6^* r_1 & -I_6^* q_1 & \circ & \circ & \circ
\end{bmatrix}
$$

$$
\mathbf{A}_{23} = \begin{bmatrix}
\circ & \circ & \circ & 1 & S_{\phi_1} T_{\theta_1} & C_{\phi_1} T_{\theta_1} & (q_1 C_{\phi_1} - r_1 S_{\phi_1}) T_{\theta_1} & (q_1 S_{\phi_1} + r_1 C_{\phi_1}) \frac{1}{C_{\theta_1}^2} & \circ \\
\circ & \circ & \circ & \circ & C_{\phi_1} & -S_{\phi_1} & -(q_1 S_{\phi_1} + r_{1C_{\phi_1})} & \circ & \circ \\
\circ & \circ & \circ & \circ & \frac{S_{\phi_1}}{C_{\theta_1}} & \frac{C_{\phi_1}}{C_{\theta_1}} & (q_1 C_{\phi_1} - r_1 S_{\phi_1}) \frac{1}{C_{\theta_1}} & (q_1 S_{\phi_1} + r_1 C_{\phi_1}) \frac{T_{\theta_1}}{C_{\theta_1}} & \circ
\end{bmatrix}
$$

$$
\mathbf{C}_{11} = \begin{bmatrix}
\circ & r_1 V_1 & -q_1 V_1 & \circ & -\alpha_1 V_1 & \beta_1 V_1 & \circ & \circ & \circ \\
-r_1 & \circ & p_1 V_1 & \alpha_1 V_1 & \circ & -V_1 & \circ & \circ & \circ \\
q_1 & -p_1 V_1 & \circ & -\beta_1 V_1 & V_1 & \circ & \circ & \circ & \circ
\end{bmatrix}
$$

where $S_{\phi_1} \equiv \sin\phi_1$, $T_{\theta_1} \equiv \tan\theta_1$, $C_{\phi_1} \equiv \cos\phi_1$, *etc.*

Appendix B

F-111C Flight Testing

B.1 Instrumentation Data

Table B.1 details the instrumentation used in flight testing, including the range and accuracy for each unit. The signals were measured at a rate of 60 Hz using an Airborne Flight-Test Recording and Analysis System (AFTRAS).

Time shifts were applied to the flight data, in order to compensate for instrument signal conditioning and recording lags, summarised in Table B.2. In this table, a positive integer lag corresponds to a lag of n time-samples with respect to the control deflection signals.

B.2 Flight Test Program

The matrix of flight test cases examined is outlined in Table B.3 for both phases of the program. Each case is denoted by a marker, where $\circ \sim$ *phase1* and $\bullet \sim$ *phase 2*. At each test point, the following manoeuvres were performed:

1. accurate trim, pitch input;
2. trim, reversed pitch input;
3. accurate trim, rudder step input followed by aileron doublet. Rudder and aileron released;
4. trim, reversed rudder and aileron input; trim.

These manoeuvres were designed to produce an aircraft response that was optimum for the determination of stability and control derivatives. Large, rapid control inputs were

QUANTITY	INSTRUMENTATION	RANGE	ACCURACY
a_x	linear accelerometer	$\pm 5\,g$	± 0.05
a_y	"	$\pm 5\,g$	± 0.05
a_z	"	$\pm 10\,g$	± 0.05
p	rate gyro	$\pm 300\,\deg/s$	± 3
q	"	$\pm 100\,\deg/s$	± 1
r	"	$\pm 50\,\deg/s$	± 0.5
$\dot{p}$	angular accelerometer	$\pm 10\,\mathrm{rad}/s^2$	± 0.05
$\dot{q}$	"	$\pm 5\,\mathrm{rad}/s^2$	± 0.05
$\dot{r}$	"	$\pm 5\,\mathrm{rad}/s^2$	± 0.05
ϕ	attitude gyro	$\pm 180\,\deg$	± 0.5
θ	"	$\pm 180\,\deg$	± 0.5
α	NBTU wind vanes	$-3 \rightarrow 25\,\deg$	± 0.5
β	"	$\pm 24\,\deg$	± 0.5
V	NBTU pitot probe	$0 \rightarrow 900\,kt$	± 10
M	"	$0.3 \rightarrow 1.8$	± 0.001
h	"	$-500 \rightarrow 55000\,ft$	± 1.5
Λ	transducing unit	$16 \rightarrow 72.5\,\deg$	± 0.05
δ_{e_R}	"	$-30 \rightarrow 15\,\deg$	± 0.1
δ_{e_R}	"	$-30 \rightarrow 15\,\deg$	± 0.1
δ_r	"	$\pm 30\,\deg$	± 0.1
δ_{s_R}	"	$0 \rightarrow 45\,\deg$	± 0.1
δ_{s_R}	"	$0 \rightarrow 45\,\deg$	± 0.1

Table B.1: Range and accuracy of acquisition units

Channel	*phase 1*	*phase 2*
δ_j	0	0
α	2	-2
β	0	0
θ	0	2
ϕ	0	0
p	2	2
q	3	3
r	2	2
$\dot{q}$	–	3
a_n	4	4

Table B.2: Instrumentation time lags

necessary to provide sufficient excitation of the aircraft's natural modes, with the automatic flight control system engaged.

Supplementary manoeuvres were also conducted to enhance the prediction capability of the validated ARL flight dynamic model. These included lateral oscillatory manoeuvres, dutch rolls and steady-heading sideslips.

For a more complete description of each flight case, the spoiler deflection and angle-of-attack ranges have been illustrated in Figure B-1. The spoilers' nonlinear behaviour was expected to be most pronounced at high angles-of-attack, so manoeuvres in this regime were favoured for analysis. Referring to the figure, several flights did reach angles of 14° or more, however the α-range was consistently modest, thus restricting the size of the identification models.

Alt., ft	Λ, deg	Mach number							
		0.4	0.5	0.6	0.7	0.8	0.9	1.0	1.1
5000	16								
	26	●●		○					
	35	○		○					
	45		●	○					
10000	16	○		○					
	26	○							
	35	○	●						
	45		●	●		●			
20000	16	○	●	○●					
	26	○	●	○					
	35		●	○					
	45			○	●		○●		
30000	16			○●	●	○			
	26			○●	●	○			
	35			○	●	○			
	45				●	○	●	○	
40000	16								
	26								
	35					○	●	●	
	45						○		●

Table B.3: Matrix of flight test points

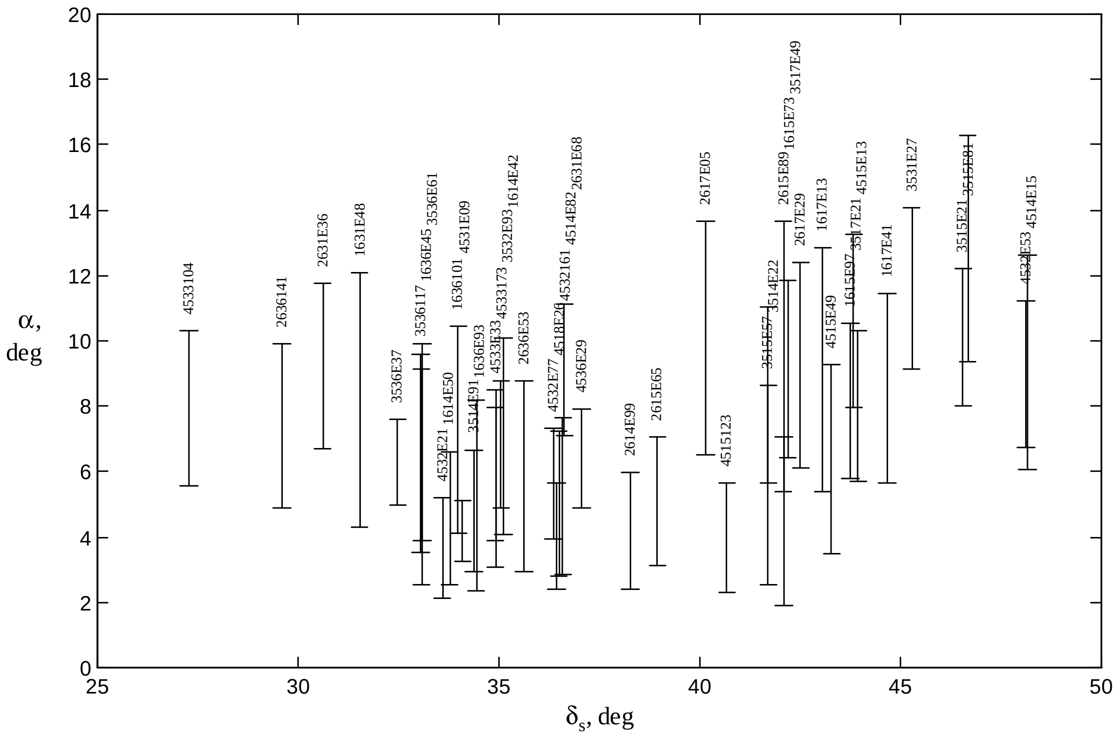

Figure B-1: Flight test manoeuvre range in δ_s and α

Appendix C

Algorithm Details

C.1 Distribution Functions

Algorithms designed for the determination of special distribution functions will often involve some fairly convoluted operations. This section was included to detail the formulation of those distributions used in the identification procedure. Some of the following routines have been taken from Press, *et al* [189] and appropriately modified for use in MATLAB.

C.1.1 F-distribution

For two random samples, the F statistic gives the ratio of one variance to the other. If the first sample's underlying distribution actually has a smaller variance than the second's, the *probability* that F would be as large as it is, can be written $Q(F\,|\nu_1, \nu_2)$. Here, ν_1 and ν_2 represent the number of degrees of freedom in the first and second samples, respectively. The function `FDIST.M`, used to compute the probability distribution of F, is evaluated via the Incomplete Beta function where

$$Q(F\,|\nu_1, \nu_2) = I_x(a, b) \tag{C.1}$$

The variable, $x = \frac{\nu_2}{\nu_2 + \nu_1 F}$, denotes the upper limit on the integral in β, with degrees of freedom, $a = \frac{1}{2}\nu_2$ and $b = \frac{1}{2}\nu_1$. The Incomplete Beta function is defined by:

$$I_x(a, b) = \frac{\beta_x(a, b)}{\beta(a, b)} \tag{C.2}$$

where the Beta function,

$$\begin{aligned}\beta_x(a,b) &= \int_0^x t^{a-1}(1-t)^{b-1}\,dt \quad ; \quad a,b>0 \\ \beta(a,b) &\equiv \beta_1(a,b)\end{aligned}$$

$I_x(a,b)$ is computed in `BETAI.M`. A series expansion exists for $\beta_x(a,b)$, however for numerical evaluation, the continued fraction representation has proven to be a more useful form. This is exploited in the C routine, `BETACF.C` and is given by:

$$\beta_x(a,b) = \frac{x^a(1-x)^b}{a}\left[\frac{1}{1+}\frac{d_1}{1+}\frac{d_2}{1+}\cdots\right] \tag{C.3}$$

for the constants,

$$\begin{aligned}d_{2m+1} &= -\frac{(a+m)(a+b+m)x}{(a+2m)(a+2m+1)} \\ d_{2m} &= \frac{m(b-m)x}{(a+2m)(a+2m-1)}\end{aligned}$$

The continued fraction converges rapidly for $x < (a+1)/(a+b+2)$, taking in the worst case, of order $\mathrm{O}(\sqrt{\max(a,b)})$ iterations. A MEX function was created to interface the C code with MATLAB, since the formulation is necessarily recursive and thus inefficient as an M function. In order to obtain the Incomplete Beta function, the (complete) beta function, $\beta(a,b)$, must also be evaluated. To accomplish this, the relationship between Beta and Gamma functions is employed:

$$\beta(a,b) = \frac{\Gamma(a)\Gamma(b)}{\Gamma(a+b)} \tag{C.4}$$

where the Gamma function is defined by the integral:

$$\Gamma(a) = \int_0^\infty t^{a-1}e^{-t}\,dt \tag{C.5}$$

There are a variety of methods for use in calculating the function, $\Gamma(a)$ numerically. The scheme chosen was based on the following expression, valid for certain integer choices of γ and N, and coefficients, $c_0, c_1, c_2, \ldots, c_N$.

$$\Gamma(a+1) = (a+\gamma+\frac{1}{2})^{a+\frac{1}{2}}e^{-(z+\gamma+\frac{1}{2})}\sqrt{2\pi}\left[c_0+\frac{c_1}{a+1}+\frac{c_2}{a+2}+\ldots+\frac{c_N}{a+N}+\epsilon\right] \tag{C.6}$$

In GAMMLN.M, the natural log of the Gamma function is evaluated instead, to avoid numerical overflow, which can occur for even modest values of x.

C.1.2 Cumulative Normal Distribution

The *cumulative normal* distribution is a useful comparative tool for the examination of noisy data. One can ascertain the normality of a random sequence, for example, by looking at a quantile-quantile plot which utilises the distribution function.

Rewriting Equation (4.73), the cumulative standard normal distribution is given by:

$$\Phi(x) = \frac{1}{\sqrt{2\pi}} \int_{-\infty}^{x} e^{-t^2/2}\, dt \tag{C.7}$$

which has the same form as the *error function*:

$$\mathrm{erf}\,(x) = \frac{2}{\sqrt{\pi}} \int_{0}^{x} e^{-t^2}\, dt \tag{C.8}$$

Fortunately, an inbuilt function for fast calculation of the error function is provided in MATLAB through ERF.M. Therefore, $\Phi(x)$ can be computed efficiently using the relationship:

$$\Phi(x) = \frac{1}{2}[1 + \mathrm{erf}\,(\frac{1}{\sqrt{2}}x)] \tag{C.9}$$

Conversely, the variable, x can be found using the inverse operator (through ERFINV.M):

$$x = \sqrt{2}\,\mathrm{erf}^{-1}(2\Phi - 1) \equiv \Phi^{-1} \tag{C.10}$$

The M files, NORMF.M and NORMFINV.M were written to perform these functions in MATLAB.

C.2 Partition Optimisation

A wide range of methods exist for unconstrained optimisation, which can be categorised according to the level of derivative information that is used. Search methods that use only function evaluations are most suitable for problems which are very nonlinear or have a number of discontinuities. Gradient methods are generally more efficient when the function to be minimised is continuous in its first derivative. Higher-order methods, such as

Newton's method, are really only suitable when the second-order information is readily and easily calculated since calculation of such information, using numerical differentiation, is computationally expensive.

The MATLAB *Optimisation Toolbox* provides a collection of functions that perform minimisation on general nonlinear functions. The principal algorithms for unconstrained minimisation are the Nelder-Mead simplex search and the BFGS (Broyden, Fletcher, Goldfarb and Shanno) quasi-Newton methods. For constrained minimisation, a variation of Sequential Quadratic Programming is used. Nonlinear Least Squares problems use the Gauss-Newton and Levenberg-Marquardt methods. This section will briefly examine various schemes trialed for the optimisation of data-partitions (*see* Section 5.4.3). A more complete coverage of the algorithms is given in the User's Guide [58].

C.2.1 Unconstrained Optimisation

Both functions, `FMINS.M` and `FMINU.M` find the minimum of a scalar function of several variables, starting from an initial estimate. This can be mathematically stated as

$$\underset{\mathbf{x}\in\Re^n}{\text{minimise}}\ f(\mathbf{x}) \tag{C.11}$$

where f is a scalar function of the vector, $\mathbf{x}$. `FMINS` uses the simplex search method of Nelder and Mead. The default algorithm for `FMINU` is a quasi-Newton method, which implements the BFGS formula for updating the Hessian approximation. Quasi-Newton methods compile curvature information at each iteration to formulate a quadratic model of the form:

$$f(\mathbf{x}) = \tfrac{1}{2}\mathbf{x}^T\mathbf{H}\mathbf{x} + \mathbf{b}^T\mathbf{x} + c \tag{C.12}$$

In this expression, $\mathbf{H}$ represents the Hessian, which is a positive-definite symmetric matrix, $\mathbf{b}$ and c denote constants. These methods avoid the expensive numerical calculation of $\mathbf{H}$, instead making an approximation by using the observed behaviour of $f(\mathbf{x})$ and $\nabla\mathbf{f}(\mathbf{x})$ to build up curvature information. The formulation of Broyden, Fletcher, Goldfarb and Shanno is commonly thought to be the most effective for use in a general purpose. It is given by:

$$\mathbf{H}_{k+1} = \mathbf{H}_k + \frac{\mathbf{q}_k\mathbf{q}_k^T}{\mathbf{q}_k^T\mathbf{s}_k} - \frac{\mathbf{H}_k^T\mathbf{H}_k}{\mathbf{s}_k^T\mathbf{H}_k\mathbf{s}_k} \tag{C.13}$$

where the coefficients:

$$\begin{aligned}\mathbf{s}_k &= \mathbf{x}_{k+1} - \mathbf{x}_k \\ \mathbf{q}_k &= \nabla\mathbf{f}(\mathbf{x}_{k+1}) - \nabla\mathbf{f}(\mathbf{x}_k)\end{aligned}$$

An efficient line-search algorithm, such as the safeguarded mixed quadratic and cubic polynomial interpolation/extrapolation method avoids computation of the gradients every iteration.

C.2.2 Nonlinear Least Squares

The same line search procedure as that above is used in conjunction with the nonlinear Least Squares optimisation routine, `LEASTSQ.M`. In the Least Squares problem, a function, $\mathbf{F}(\mathbf{x})$ is minimised with respect to the elements in $\mathbf{x}$.

$$\underset{\mathbf{x}\in\Re^n}{\text{minimise}}\ \mathbf{F}(\mathbf{x}) \tag{C.14}$$

where the function,

$$\mathbf{F}(\mathbf{x}) = \sum_{i=1}^{n} f_i^{\,2}(\mathbf{x}) = \mathbf{f}(\mathbf{x})^T\mathbf{f}(\mathbf{x}) \tag{C.15}$$

Although the function can be minimised using a general unconstrained minimisation technique, certain characteristics of the problem can be exploited to improve the iterative efficiency of the solution procedure. The Levenberg-Marquardt method provides a robust means for determining the search direction during the optimisation. The search direction, $\mathbf{d}_k$, is obtained at each major iteration, k, which is a solution of the linear set of equations:

$$(\mathbf{J}(\mathbf{x}_k)^T\mathbf{J}(\mathbf{x}_k) + \lambda_k\mathbf{I})\mathbf{d}_k = -\mathbf{J}(\mathbf{x}_k)\,\mathbf{f}(\mathbf{x}_k) \tag{C.16}$$

Here the scalar, λ_k, controls both the magnitude and direction of $\mathbf{d}_k$. It can be shown that the method uses a search direction which is a cross between the Gauss-Newton direction and the steepest descent. The term, λ_k, is effectively controlled to ensure descent even when second-order terms, which restrict the efficiency of the Gauss-Newton method, are encountered.

C.2.3 Constrained Optimisation

In constrained optimisation, the general aim is to transform the problem into an easier sub-problem which can then be solved and used as the basis of an iterative process. `CONSTR.M` finds the constrained minimum of a scalar function of several variables, starting at an initial estimate. This can be mathematically stated as:

$$\underset{\mathbf{x}\in\Re^n}{\text{minimise}}\ f(\mathbf{x}) \quad \text{subject to:} \quad \mathbf{G}(\mathbf{x}) \leq \mathbf{0} \tag{C.17}$$

Earlier methods, now considered relatively inefficient, have been replaced by methods which focus on the solution of the Kuhn-Tucker (KT) equations. The KT equations are necessary conditions for optimality of a constrained optimisation problem. At the optimal solution point, $\mathbf{x}^*$, they can be written:

$$\nabla\mathbf{f}(\mathbf{x}^*) + \sum_{i=1}^{n} \lambda_i^* \nabla\mathbf{g}_i(\mathbf{x}^*) = 0 \tag{C.18}$$

where

$$\begin{aligned} \lambda_i^* \nabla\mathbf{g}_i(\mathbf{x}^*) &= \mathbf{0} \quad ; \quad i = 1, \ldots, m_e \\ \lambda_i^* &\geq \mathbf{0} \quad ; \quad i = m_e + 1, \ldots, m \end{aligned}$$

The Lagrangian multipliers, λ_i, are necessary to balance the deviations in magnitude of the objective function and constraint gradients. Since only active constraints are included in this cancelling operation, constraints which are not active are given Lagrangian multipliers equal to zero. The solution of the KT equations can be achieved via direct computation of the Lagrangian multipliers using constrained quasi-Newton methods. These methods are often referred to as Sequential Quadratic Programming (SQP) methods, since a QP sub-problem is solved at each major iteration. Based on the work of Biggs, Han and Powell, the method used closely mimics Newton's method for unconstrained optimisation. At each major iteration, an approximation is made of the Hessian of the Lagrangian function using a quasi-Newton updating method, such as the BFGS updating scheme. This is then used to generate a QP sub-problem, whose solution is used to form a search direction for a line search procedure.

The QP sub-problem is obtained by linearising the nonlinear constraints.

$$\underset{\mathbf{x}\in\Re^n}{\text{minimise}}\ \frac{1}{2}\mathbf{d}^T\mathbf{H}_k\mathbf{d} + \nabla\mathbf{f}(\mathbf{x}_k)^T\mathbf{d} \tag{C.19}$$

where

$$\begin{aligned}
\nabla\mathbf{g}_i(\mathbf{x})^T\mathbf{d} + \mathbf{g}_i(\mathbf{x}) &= 0 \quad ; \quad i = 1, \ldots, m_e \\
\nabla\mathbf{g}_i(\mathbf{x})^T\mathbf{d} + \mathbf{g}_i(\mathbf{x}) &\leq 0 \quad ; \quad i = m_e + 1, \ldots, m
\end{aligned}$$

An active set strategy, or projection method was implemented to solve the QP problem, because of its fast convergence.

A nonlinearly constrained problem can often be solved in fewer iterations using SQP than an unconstrained problem, since the limits on the feasible area are used informatively in the search procedure.

Appendix D

PRE User's Manual

D.1 Introduction

The *PRE* software package provides tools for the estimation of partitioned models from measured data, within the MATLAB interactive environment. A piecewise regression technique is used, as well as various procedures such as Stepwise Regression for determination of the model structure.

The primary script file, `APRE.M`, was written specifically for the identification of aircraft models from flight-data. By utilising the mathematical description for atmospheric flight dynamics, the initialisation procedure has been greatly simplified. All that is required by the program are a number of pre-defined options and the flight-data itself. Upon execution, the procedure attempts to identify the nominated model parameters and associated accuracies, along with various statistical information. The user is also given an opportunity to interactively modify the model structure and is supplied with several selection criteria to base their decision on. This step takes place in the function, `REG.M`, which conducts the model structure determination process and is independent of the system dynamics.

For graphical output of the (estimated) aircraft coefficients and subsequent simulation of the nonlinear dynamic reponse, a secondary script, `FLYT.M`, has also been included. This program was designed so that it could be initialised either by a separate set of input options, or by the identification routine, `APRE.M`.

In addition to the operating code, several demonstration problems have been compiled for verification of the algorithms and illustration of their use. The demonstrations outlined here are:

- F_DEMO1 - Flight dynamic response simulation of the F-111C aircraft.
- A_DEMO1 - Aircraft piecewise regressive estimation of the model simulated above.
- R_DEMO1 - Model structure determination using Stepwise Regression.

D.2 Piecewise Regression

The piecewise regression procedure operates on data subsets, partitioned according to the location of 'knots' in the model. These knots define regions of unique variation, that are parametrized by polynomial splines. The spline coefficients, along with other linear derivatives are compiled into a set of equations representing the aircraft dynamics and then estimated.

At the heart of the routine, a multiple linear regression is formulated and the mean square error of the predicted response minimised, using a Least Squares solution. Assuming the model is correct, this will provide an unbiased solution if the equation error is stationary and uncorrelated, and there is no noise in the independent variables. It has been shown, however, that even in the presence of measurement noise, the LS solution can yield accurate estimates. Furthermore, if each error observation is identically distributed and independent with zero mean, the estimates will also be consistent and efficient. This means that for long data sequences, the error in the estimates will have zero mean and minimum variance among all other unbiased estimators.

Several approaches exist for the determination of an adequate model structure incorporating both linear and nonlinear coefficients. These can be divided into two groups:

Parameter selection methods available include Stepwise Regression and Exhaustive Selection. The former is utilises each parameter's correlation with the response and their individual significance for sequential addition to and elimination from the model.

Partition optimisation methods include Significant-region Expansion and various nonlinear optimisation algorithms to position the knots in the model. Two optimisation schemes that have been used successfully are the Simplex Search and nonlinear Least Squares.

D.3 Model Accuracy

D.3.1 Collinearity

Data collinearity may be assessed for each regression in the model structure determination procedure, using several measures. These include the correlation coefficient, R, the variance inflation factor, VIF, eigen-condition index, η_j, and variance-decomposition proportion, π_{kj}. The correlation coefficient measures the correlation between pairs of variables in the regression, whereas the variance inflation factor reflects the correlation between each variable and a linear combination of the others. Single elements in R will approach unity when two regressors are highly correlated and VIF will increase toward infinity. An eigensystem analysis of the regression is possible using both η_j and π_{kj}. The condition index measures the degree of ill-conditioning that can be attributed to each eigenvector. Furthermore, the make-up of each eigenvector in terms of the regression variables can be examined, using the variance-decomposition proportion. For any small eigenvalue, or large η_j, two or more variables with large values of π_{kj} will indicate a possible collinearity problem.

D.3.2 Confidence Bounds

Assuming that the measurement error is normally distributed, confidence intervals may be evaluated for the estimates and predicted response. The confidence is based on a pre-selected significance level of α_p. In addition to constructing confidence bounds, the assumption of normality allows hypothesis tests to be conducted, which form the crux of parameter selection methods.

It is important to note that if the prediction error is not white, possibly due to modelling errors, the bounds can be quite optimistic. Furthermore, any measurement noise in the independent variables will affect the confidence intervals, so it is best kept to a minimum.

As well as the individual confidence bounds, the eccentricity of the joint confidence ellipsoid can be assessed using the geometric dilution of precision, or $GDOP$. The elements of this are equal to the ratio of the the furthest projection of the uncertainty ellipsoid onto each parameter axis, divided by the parameter value where the ellipsoid intersects that axis. Clearly, if two or more parameters have large $GDOP$'s, their correlation will be high and thus, their joint confidence poor.

D.3.3 Accuracy Criteria

A number of criteria are also provided in the regression algorithm for diagnosis of model accuracy and significance. These criteria are particularly useful in model structure determination, as they present single measures for each model trialed. They consist of the following:

- R^2 - the squared multiple squared correlation coefficient, which is simply the ratio of the predicted response variance divided by the actual (sample) variance;
- RSS - the residual sum of squares, which should approach a minimum;
- $PRESS$ - the prediction sum of squares, although similar to RSS, provides additional information concerning the predictive capabilities of the regression model;
- The F statistic - which gives a good indication of the significance of the overall regression. It will yield a maximum value for an *efficient* model;
- $F_{p_{\min}}$ - the minimum partial-F statistic, among the set corresponding to each variable, will highlight the least significant variable in the regression; and
- The C_p statistic - which provides a similar measure to F, in that both the model accuracy and size are taken into account.

In addition to these parameters, the residuals themselves can be examined via a time-history plot, and a normal quantile-quantile plot. An autocorrelation plot of the predicted and actual responses provides further comparison, based on their spectral content.

D.4 Algorithm Formulation

The Least Squares solution to the normal equations is achieved in MATLAB using orthogonal-triangular decomposition. If a biased solution is required, either Mixed Estimation (ME) or Principal Components Regression (PCR) techniques can be employed. The weighting matrix utilised in the ME routine is based on the expected variance of the estimates, which can be set by the user. In the PCR routine, the 'small' eigenvectors with two or more high variance-decomposition proportions are removed, thus reducing the rank by an integer amount.

Model structure determination is possible through a number of different methods implemented in the identification code. Stepwise Regression is one of the more efficient methods by which a parsimonious model can be resolved. In this approach, the parameters are sequentially added to the regression according to their partial correlations, or removed if their contribution is judged nonsignificant. An option has also been provided, to prevent the algorithm from terminating with an empty model, if a significant set of parameters exists. Following completion of the iteration sequence, the user may select any of the intermediate models as the final solution. The second parameter-selection approach of Exhaustive Selection is obviously far more time-consuming and quite possibly unjustified for substantial models. However, a greater range of combinations may be covered, allowing the "best" model to be chosen. As a default, the model with the largest F statistic is selected.

Of the partition-optimisation techniques available, the most efficient is the nonlinear Least Squares. This algorithm utilises a Levenberg-Marquardt method to determine the search direction during optimisation, which has proven to be a robust approach for this type of application. The Nelder-Mead Simplex Search technique is more cumbersome, though it will often provide more consistent results since gradient information is not used. Lastly, the Significant-region Expansion technique can be used to place the knots in one-dimensional splines effectively, producing a fully significant model.

D.5 Speed and Efficiency

Depending on whether any model structure determination is undertaken, the majority of execution time will be spent in either the construction stage, or the identification stage. For example, the demonstration routine, A_DEMO1, took around 6 mins to run on a 486/33 PC with 16M Ram. Since this involved a simple linear regression on an aircraft model incorporating several spline coefficients, most of the time was spent in building the model. If, however, a Stepwise Regression procedure was chosen, the routine might take much longer, depending on the options selected.

Naturally, the CPU time expended in an optimisation of the partitons can be an order of magnitude greater, since an entirely new model must be generated for each iteration. The Nonlinear Least Squares algorithm also makes finite-difference gradient calculations, which adds to the number of model evaluations. This gradient information is utilised most effectively however, and the algorithm can consistently outperform the Simplex Search optimisation.

The key to creating efficient code in MATLAB is *vectorisation.* Whenever possible, vectorised algorithms were implemented in place of loops, such as in the functions RCSOLVN.M, RSSOLV1.M and within REG.M. In some cases though, the code could not be vectorised, yet speed was still crucial. It was in these situations that MEX files were neccessary - a good example is the bottleneck computation done in BETACF.C.

In MATLAB, the allowable matrix size is limited only by the computer's memory. It therefore provides an ideal environment in which this type of analysis can be performed. The largest matrix generated in the main routine, APRE, is the global regressor matrix. It has N rows of observations and ($n_L + n_c(n_{kx} * n_{kz} - 1) + n_s(n_{kz} - 1)$) columns of independent variables, where n_L is the number of linear terms, n_c is the number of carpet coefficients, n_s is the number of spline coefficients and n_{kx} and n_{kz} represent the number of knots in x and z, respectively. In A_DEMO1, which operates on just one flight case, this matrix reaches a size of approximately $[2400 \times 44]$.

D.6 Important Functions

Over 200 files constitute the *PRE Toolbox* - many of them standalone functions - a list of which has been compiled in CONTENTS.M (*see* Appendix E). Although there are some very useful routines for general purposes, not all are crucial to the identification or simulation procedures. The primary functions tied in with the identification procedure are:

- APRE.M, APRE_*.M

  The main script is run as a 'procedure', making many internal parameters available to the user. Most of the accompanying routines are also scripts, invoked from APRE. These include APRE_XZ.M, which creates the regressor sub-matrices and APRE_PAR.M, which cycles through the partitioned data regions, either compiling a global regressor matrix, or performing successive identifications. The functions, APRE_TRN.M and APRE_OPT.M are used in the partition optimisation procedure - they essentially transform the (unbounded) optimisation variables to knots and output an error measure.

- REG.M, ME.M, PCR.M

  All of the estimation and if required, model structure determination, is done inside REG. This function resides at the centre of the identification procedure and returns the parameter estimates, along with their standard errors. Within REG.M, the Mixed Estimation and Principal Components Regression functions, ME.M and PCR.M, are called.

The 'second-half' of the entire process comprises display and simulation of the aircraft model, generated either by APRE, or by the user. This includes such functions as:

- `FLYT.M, FLYT_*.M, ODE.M, RSPLOT.M, RCMESH.M`

  As with `APRE.M`, the main script, `FLYT.M`, is run as a procedure, which in turn invokes the associated routines as required. Some of these functions are used to construct the state, control and observation matrices including `FLYT_TRM.M` and `FLYT_STM.M`. They are passed through to `ODE.M`, which performs the actual integration. `RSPLOT.M` and `RCMESH.M` display the nonlinear coefficients in one and two dimensions, respectively.

Other useful routines that can be executed from the workspace are:

- `POINTS.M, SIGNAL.M, COLLCHK.M, UIKNOTS.M, EXTRAP2.M, RSPLYN.M, RCARPT.M, INNOVATE.M, INTERPN.M, MATLOADR.MEX, SAVERMF.M`

  The help facility can be utilised to outline these functions adequately, including inputs and outputs, and will therefore not be covered here. To obtain a description of any of these files, or any other file in the Toolbox, simply type:

  >> **`help <mfile.m>`**

  at the command-line, where **`<mfile.m>`** is the name of the file.

- `F_DEMO.M, A_DEMO.M, R_DEMO.M`

The demonstration files are discussed in Section D.10. They can be run from `ACDEMS.M` and include some helpful comments for initialisation.

D.7 Operation

D.7.1 Construction of the Model

If the postulated model structure incorporates spline coefficients, then the variables in the regression will be collected from partitioned data subsets. It is then possible to estimate those coefficients in one of two ways:

1. Solve the local regression for each region; or

2. Compile the variables from each region into one regression and then solve.

The first option involves stepping through each region and performing a regression on the data *in that region only.* The contribution of the parameters estimated at each step is then subtracted from the response and the next region analysed. This procedure is less efficient than the next and can lead to a diverging solution. It should only be used if the maximum allowable matrix size is small, or if a Significant-region Expansion is being conducted.

The second option will produce a more accurate solution, without any problem of divergence. It entails stepping through each region, as before, although this time the variables are appended to a global regressor matrix. Once complete, a single regression is performed to obtain a solution for the entire parameter set. The Partiton-Optimisation procedure uses this approach to estimate each model in the iteration.

D.7.2 Performing the Identification

For a model that produces a prediction of the response $\hat{\mathbf{y}}$, the Least-Squares (LS) estimate minimises the cost function:

$$J = (\mathbf{y} - \hat{\mathbf{y}})^T (\mathbf{y} - \hat{\mathbf{y}})$$

The two biased estimation techniques use essentially the same approach, except that the regression matrices are augmented or transformed in some way as to favour certain parameters. Prior to identification, the data is centered to remove the bias term - this reduces the size of the matrices and improves the efficiency of the procedure. Two methods for parameter selection are available in REG and include:

1. Stepwise Regression; and

2. Exhaustive Search.

Stepwise Regression constitutes the most efficient algorithm, as it employs an iterative process in which the parameters' significance and correlation are examined at each step. First, a pre-defined initial variable set is introduced into the regression in an order set by the user. Once complete, the iteration begins on the model - either removing variables deemed nonsignificant from a partial-F test, or adding variables not yet in the regression, according to their partial-correlation. The algorithm is terminated when no further variables can be eliminated and no new variables added. At this point, the user may revisit any of the intermediate models along with several selection criteria, in order to find a suitable representation.

The Exhaustive Search simply steps through every combination of model parameters, regardless of their significance. Upon completion, the model having the largest F statistic is chosen, unless the option allowing external selection has been set. As mentioned previously, this algorithm is far more time-consuming, however a greater range of models is formulated as a result.

D.8 Installation

STEP 1.

Copy all of the files from the disk into a new sub-directory: `\matlab\toolbox\pre`. Append the MATLABPATH variable in the `matlab.rc` file with this new diectory. Alternatively, within MATLAB, the command:

>> `path=(path,'\matlab\toolbox\pre');`

will temporarily augment the MATLABPATH.

STEP 2.

Start MATLAB and at the command-line, type:

>> `acdems`

This will begin the demonstration shell. To try a different problem, continue as below.

STEP 3.

Create an initialisation script as described in the next section, to create the inputs neccessary for APRE. Direct keyboard input is possible, but it is not recommended since a number of parameters are required. Use the demonstration file, A_DEMO1 as a rough guide. Execute this script and then run APRE. The estimates can be displayed and an equivalent response simulated by running FLYT immediately after.

D.9 Inputs and Outputs

D.9.1 The Data Matrix

The format of the flight-data matrix is defined such that each column represents a unique observation variable and each row a set of single measurements in time. In APRE and

FLYT, the columns are ordered as follows:

$$\mathbf{M} = \left[\begin{array}{cccccccccccccccccccc} V & \beta & \alpha & p & q & r & \phi & \theta & \psi & a_x & a_y & a_z & \dot{p} & \dot{q} & \dot{r} & h & M & \delta_1 & \cdots & \delta_{nu} \end{array}\right]$$

where the number of control inputs, nu, is optional. The first six state variables plus the control variables, δ_j, constitute the minimum size data matrix required by the routines.

D.9.2 Inputs

The input parameters required by APRE are detailed below. Those variables which are *optional* are shown in parentheses `[ ]`.

- `fm1` - A matrix of strings containing the file name(s) of `.MAT` file(s) that are to be loaded. These files **must** each contain either a single flight-data matrix `F`, or both the simulated data-matrix, `M`, and coefficient matrices output from FLYT. The data matrices are joined so that multiple flight cases can be analysed collectively.

- `fm1n` - An index vector that describes the columns in `F` (or `M`) in which each variable is found. Zeros may be used to indicate nonexistant variables. Hence, if all variables are present, the matrix, `F( : ,fm1n)`, should be ordered as above.

- `[fm2]` - A string matrix similar to `fm1`, however the flight-data matrices and coefficient matrices contained therein are used for *comparison* purposes only.

- `[fm2n]` - The corresponding index vector for `fm2`.

- `[fm3]` - A string vector containing the file name to be used for initialisation and output files. The initialisation files, saved upon entry into APRE and FLYT, are given the extensions `.MET` and `.MYT` respectively. The output `.MAT` file is saved at the end of FLYT and holds a simulated data matrix and several coefficient matrices.

- `[fl1]` - A string vector with the file name to be used for a diary record of the regression procedure. The extension of this text file is `.LOG`. Inclusion of this parameter will flag REG to output the solution details to both screen and file.

- `[fl2]` - The file name to be used for a diary record of the identification procedure. Inclusion of this string vector will flag APRE to output the general identification details - along with the estimates - to screen and file.

- `ws` - The sample-frequency of the flight-data in Hz.

- `[trm]` - An optional integer vector, giving the data indices over which the data is to be averaged, for definition of the aircraft's trim state.

- `I` - The initialisation matrix. Each column corresponds to a particular constant of the aircraft in flight. These are, in order:

$$\begin{bmatrix} S & \bar{c} & b & m & I_x & I_y & I_z & I_{xz} & \rho_0 & g \end{bmatrix}$$

  Each row in the matrix corresponds to a particular flight case, or row, in `fm1`.

- `[k]` - An index vector with the *coefficient matrix* (*see* `La`*, below*) column numbers of variables which are to be utilised as axes in the spline functions. Both $[x, z]$ axes can be defined for two-dimensional splines (carpets), or just the z axis, for one-dimensional splines. For example, `k = [10,3]` implies δ_s as the x-axis and α as the z-axis.

- `[kx]` - The knot vector associated with the x-axis of all carpet functions. Note, both `kx(1)` and `kz(1)` must be equal to zero.

- `[kz]` - The knot vector associated with the z-axis of all carpet functions and all (1-D) spline functions.

- `[Ra]` - The carpet coefficient initialisation matrix. Each column of `Ra` corresponds to a unique nonlinear coefficient in the model. The rows of `Ra` consist of the following:

  `Ra(1:2,i)` - coefficient matrix row and column numbers, respectively.

  = `1,2,...,6` and `1,2,...,nu+7`

  Note that `Ra(2,i) = nu+7` corresponds to an incremental coefficient, rather than a derivative, since there are actually only `nu+6` coefficient matrix columns.

  `Ra(3:4,i)` - the carpet (integer) order in x and z axes, respectively.

  = `0,1,2,...`

  `Ra(5:6,i)` - the carpet symmetry flags for x and z axes.

  = `-1` (anti-symmetric),`0` (non-symmetric),`1` (symmetric)

`Ra(7:?,i)` - the *a-priori* coefficient sub-matrix, resized as a vector. That is, if

$$r = \begin{bmatrix} D_{x_0,z_0} & D_{x_1,z_0} & \cdots \\ D_{x_0,z_1} & D_{x_1,z_1} & \cdots \\ \vdots & \vdots & \end{bmatrix} \quad \text{then} \quad \texttt{Ra(7:?,i)} \equiv r^T(:) = \begin{bmatrix} D_{x_0,z_0} \\ D_{x_1,z_0} \\ \vdots \end{bmatrix}$$

- `[rU],[rB],[rF]` - Carpet *a-priori* coefficient sub-matrix index vectors for unbiased, biased and fixed parameters.

- `[Pa]` - The spline coefficient initialisation matrix. Each column of `Pa` corresponds to a unique nonlinear coefficient in the model. The rows of `Pa` consist of the following:

`Pa(1:2,i)` - coefficient matrix row and column numbers, respectively.

= `1,2,...,6` and `1,2,...,nu+7`

`Pa(3,i)` - the spline (integer) order in the z axis.

= `0,1,2,...`

`Pa(4,i)` - the spline symmetry flag for the z axis.

= `-1` (anti-symmetric),`0` (non-symmetric),`1` (symmetric)

`Pa(5:?,i)` - the *a-priori* coefficient sub-vector. That is,

$$\texttt{Pa(5:?,i)} \equiv p = \begin{bmatrix} D_{z_0} \\ D_{z_1} \\ \vdots \end{bmatrix}$$

- `[pU],[pB],[pF]` - Spline *a-priori* coefficient sub-vector indices for unbiased, biased and fixed parameters.

- `[Lda]` - The linear 'dynamic' *a-priori* coefficient matrix.

$$\texttt{Lda} \equiv \begin{bmatrix} C_{x_{\dot V}} & C_{x_{\dot\beta}} & C_{x_{\dot\alpha}} & C_{x_{\dot p}} & C_{x_{\dot q}} & C_{x_{\dot r}} \\ C_{y_{\dot V}} & C_{y_{\dot\beta}} & C_{y_{\dot\alpha}} & C_{y_{\dot p}} & C_{y_{\dot q}} & C_{y_{\dot r}} \\ C_{z_{\dot V}} & C_{z_{\dot\beta}} & C_{z_{\dot\alpha}} & C_{z_{\dot p}} & C_{z_{\dot q}} & C_{z_{\dot r}} \\ C_{l_{\dot V}} & C_{l_{\dot\beta}} & C_{l_{\dot\alpha}} & C_{l_{\dot p}} & C_{l_{\dot q}} & C_{l_{\dot r}} \\ C_{m_{\dot V}} & C_{m_{\dot\beta}} & C_{m_{\dot\alpha}} & C_{m_{\dot p}} & C_{m_{\dot q}} & C_{m_{\dot r}} \\ C_{n_{\dot V}} & C_{n_{\dot\beta}} & C_{n_{\dot\alpha}} & C_{n_{\dot p}} & C_{n_{\dot q}} & C_{n_{\dot r}} \end{bmatrix}$$

- [ldU],[ldB],[ldF] - Linear dynamic *a-priori* coefficient matrix indices for unbiased, biased and fixed parameters.

- [La] - The linear 'static' *a-priori* coefficient matrix.

$$\texttt{La} \equiv \begin{bmatrix} C_{x_V} & C_{x_\beta} & C_{x_\alpha} & C_{x_p} & C_{x_q} & C_{x_r} & C_{x_{\delta j}} & \cdots \\ C_{y_V} & C_{y_\beta} & C_{y_\alpha} & C_{y_p} & C_{y_q} & C_{y_r} & C_{y_{\delta j}} & \cdots \\ C_{z_V} & C_{z_\beta} & C_{z_\alpha} & C_{z_p} & C_{z_q} & C_{z_r} & C_{z_{\delta j}} & \cdots \\ C_{l_V} & C_{l_\beta} & C_{l_\alpha} & C_{l_p} & C_{l_q} & C_{l_r} & C_{l_{\delta j}} & \cdots \\ C_{m_V} & C_{m_\beta} & C_{m_\alpha} & C_{m_p} & C_{m_q} & C_{m_r} & C_{m_{\delta j}} & \cdots \\ C_{n_V} & C_{n_\beta} & C_{n_\alpha} & C_{n_p} & C_{n_q} & C_{n_r} & C_{n_{\delta j}} & \cdots \end{bmatrix}$$

  All coefficient matrices use the row and column numbers of this matrix, for reference to particular derivatives in the model.

- [lU],[lB],[lF],[lC] - Linear static *a-priori* coefficient matrix indices for unbiased, biased, fixed and constrained parameters. `lC` is actually a matrix of 3 rows, where the corresponding estimated coefficient elements, `Lh(lC(1,:))./Lh(lC(2,:))` = `lC(3,:)`. Hence, the ratio between those estimates is retained.

- [alf] - The significance level required to construct confidence bounds and perform hypothesis tests.

- [Ji] - A $[1 \times 3]$ vector of flags, indicating which terms are to be postulated in the initial regression model. The three elements indicate the linear 'dynamic' terms, the linear 'static' terms and the nonlinear terms, repectively.

  `Ji(i) = 0,1`

- [Nr] - The nonlinear solution recalculation (integer) frequency. This sets the frequency at which the aircraft state matrix is 're-trimmed' in the dynamic simulation routine, ODE. For a full nonlinear response, use `Nr = 1`.

- `[opt]` - FLYT and APRE routine solution options. The elements are, in order:

  `ode` - solution technique

  = `-1` (no solution),
  `0` (linear time-invariant time response - requires *Control System Toolbox*),
  `1` (nonlinear 1^{st}-order Runge-Kutta),
  `2` (n/l $2, 3^{rd}$-order R-K),
  `3` (n/l $4, 5^{th}$-order R-K)

  `axis` - axes format for state matrix = `0` (wind),`1` (body)

  `angle` - angular displacement format for state matrix = `0` (Euler),`1` (quaternion)

  `pause` - pause flag = `0,1`

  `disp` - display option = `0` (no output),`1` (write to ascii data file),`2` (print)

  `id` - piecewise identification procedure

  = `0` (accumulation),
  `1` (sequential),
  `2` (significant region expansion),
  `3` (Simplex partition optimisation - requires *Optimisation Toolbox*),
  `4` (nonlinear LS partition optimisation - requires *Optimisation Toolbox*)

  `reg` - regression scheme = `0` (Linear),`1` (Stepwise),`2` (exhaustive)

  `init` - initial variable entry to regression = `0` (direct),`1` (ordered),`2` (correlated)

  `biastype` - biased estimation technique

  = `0` (none),`1` (Mixed Estimation),`2` (Principal Components)

  `user` - user-input flag = `0,1`

- `[adsp]` - APRE display option flags. The elements are, in order:

  `path` - plot coefficient paths = `0,1`

  `model` - plot intermediate model response = `0,1`

  `region` - plot current regression data-region = `0,1`

- `[fdsp]` - FLYT display options. The elements are, in order:

`fdsp(1:2)` - nonlinear coefficient plot size in $[x, z]$ = `0` (none),`1` (half),`2` (full)

`fdsp(3:?)` - ODE routine disply options

= `'c'` (% completion),`'m'` (state/control matrices),`dA` (plot observations)

Note that the indices in vector, `dA`, will vary according to `angle` (= `opt(3)`).

- `[Nyc]` - Number of interpolants for carpet/spline plots in x and z, respectively.
- `[mxe]` - The maximum number of elements allowed in the regression matrices.
- `[opt_]` - General GLOBAL options. In order, the elements are:

`acc` - accurate anglular accelerations flag. If `acc` = `0`, the angular rates are differentiated.

`rates` - accurate anglular rates flag. If `rates` = `0`, the angular accelerations are integrated.

`couple` - include cross-coupling flag.

`frac` - knot fraction for coefficient gradient calculation. This is used if one of the nonlinear coefficients has been formulated as a contribution and a linear reponse chosen (`opt(2)` = `0`), in which case a derivative is needed.

`Ir` - update initialisation vector at recalculation flag. That is, update the *dimensional* derivatives at each recalculation step.

`grav` - include gravity contribution in linear accelerations flag.

`randseed` - random (time-based) initial seed for noise flag. Do not choose this option unless a unique noise sequence is required each simulation.

`rlim` - correlation coefficient limit. Values under this limit will not be displayed.

`viflim` - variance inflation factor limit, for display.

`klim` - eigen condition number limit. In Principal Components Regression, eigenvectors with condition numbers above `klim` and two or more high variance decomposition proportions (greater than `pkjlim`) are removed.

`pkjlim` - variance decomposition proportion limit.

`bias` - fraction of unbiased coefficient variance desired for biased coefficient variance. This sets the 'weighting' factor toward the bias terms. For example, the default of `0.01` corresponds to a standard deviation which is 10 % of the unbiased result.

`freq` - approximate measurement noise frequency (Hz). Not currently used.

`condtol` - matrix condition tolerance. If either of these tolerances (`condtol`, `rsstol`) are triggered, the procedure can be terminated.

`rsstol` - residual sum of squares tolerance.

`step` - robust stepwise selection flag. The algorithm avoids selecting empty model.

`color` - display color flag.

The default `opt_` vector is:

```
[ 1 1 1 0.1 1 1 0 0.8 0 1e3 0.5 0.01 30 1e-12 1e-6 1 1 ]
```

D.9.3 Outputs

As well as the input parameters, `fm1`, `fm1n`, `fm2`, `fm2n`, `fm3`, `ws`, `trm`, `Nr`, `I`, `k`, `kx`, `kz`, `opt`, `fdsp`, `Nyc`, `mxe` and `opt_`, a number of outputs are returned by APRE. These consist of:

- `H` - A matrix comprising the number of data points enclosed by each partition, for use in the coefficient plots.
- `Rh` - The estimated carpet coefficient matrix. `Rh` essentially corresponds to the initialisation matrix, `Ra`, however the first few rows are augmented as detailed:

  `Rh(1:2,i)` - coefficient matrix row and column numbers, respectively.

  = `1,2,...,6` and `1,2,...,nu+7`

  `Ra(3:6,i)` - the carpet order for the first and upper regions in x and z, respectively.

  `Ra(3:4,i)` = `(Ra(5:6,i)~=0)`

  `Ra(5:6,i)` = `0,1,2,...`

  `Ra(7:10,i)` - the carpet symmetry flags for the first and upper regions in x and z.

  `Ra(7:8,i)` = `Ra(9:10,i)-(~Ra(9:10,i))`

  `Ra(9:10,i)` = `-1,0,1`

  `Ra(11:?,i)` - the estimated coefficient sub-matrix, resized as a vector.

- `Rhe` - The standard error of the estimated coefficient sub-matrix, `Ra(11:?,:)`.
- `Ph` - The estimated spline coefficient matrix. `Ph` corresponds to the initialisation matrix `Pa` with the first few rows augmented as detailed:

`Ph(1:2,i)` - coefficient matrix row and column numbers, respectively.

= `1,2,...,6` and `1,2,...,nu+7`

`Pa(3:4,i)` - the spline order for the first and upper regions in z.

`Pa(3,i)` = `(Pa(4,i)~=0)`

`Pa(4,i)` = `0,1,2,...`

`Pa(5:6,i)` - the spline symmetry flags for the first and upper regions in the z axis.

`Pa(5,i)` = `Pa(6,i)-(~Pa(6,i))`

`Pa(6,i)` = `-1,0,1`

`Pa(7:?,i)` - the estimated coefficient vector.

- `Phe` - The standard error of the estimated coefficient vector, `Pa(7:?,:)`.
- `Ldh` - The estimated linear 'dynamic' coefficient matrix.
- `Ldhe` - The standard error of `Ldh`.
- `Lh` - The estimated linear 'static' coefficient matrix.
- `Lhe` - The standard error of `Lh`.
- `cput` - APRE's base CPU execution time.
- `units_` - `'imperial'` or `'metric'`.

Following subsequent execution of FLYT, the variables that are written to `fm3` and left in the workspace include:

- `DATE` - A record of the time & date.
- `R1,R1e` - The final (estimated) carpet coefficient matrix and its standard error.
- `P1,P1e` - The final spline coefficient matrix and its standard error.
- `Ld1,Ld1e` - The final linear dynamic coefficient matrix and its standard error.
- `L1,L1e` - The final linear static coefficient matrix and its standard error.

- `Yc` - A matrix built from sub-matrices of interpolated carpet ordinates. It is constructed as follows:

$$\texttt{Yc} \equiv \left[\begin{bmatrix} 0 & \mathbf{x} \\ \mathbf{z} & \mathbf{Y}_1 \end{bmatrix} \begin{bmatrix} 0 & \mathbf{x} \\ \mathbf{z} & \mathbf{Y}_2 \end{bmatrix} \cdots \right]$$

- `Yp` - A matrix built from vectors of interpolated spline ordinates.

$$\texttt{Yp} \equiv \begin{bmatrix} \mathbf{z} & \mathbf{y}_1 & \mathbf{y}_2 & \cdots \end{bmatrix}$$

- `M` - The simulated flight-data matrix (outlined previously).

D.10 Demonstration Routines

To run any of the demonstrations, simply install the files as explained in Section D.8 and at the command line, type either **`acdems`** or the name of the demo itself. Several have been created and three of these are presented here. The script files have also been included in Appendix E.

D.10.1 F_DEMO1

This demonstration simulates the flight response of an F-111C aircraft undergoing a combined lateral manoeuvre. The aircraft's geometric and inertial constants are used, as well as the control inputs recorded on the corresponding flight. The aerodynamic model is constructed from wind-tunnel results and previous flight estimates. In this model, the spoilers' rolling and yawing moment contributions have been represented by splines in δ_s and α, whereas the derivatives, C_{l_β}, C_{l_p}, C_{n_β} and C_{n_r} are all expressed as splines in α only. Measurement noise, of similar magnitude to that present in the actual flight data, is added in order to make the resulting signals more realistic.

D.10.2 A_DEMO1

In the next demonstration, the response data simulated above is analysed to examine the effects of measurement noise on the solution. The structure of the postulated model can be given exactly the same form as in the simulation, so that each parameter can be compared directly. Alternatively, the user may determine a suitable partitioning scheme, based on the spread of data and resulting variance of each region. A biased mixed estimation technique is utilised and no attempt made to select a significant parameter set. If this is desired, change `opt(7)` and `opt(10)` to `1`.

D.10.3 R_DEMO1

This last demonstration is taken from an example in reference [30] and is used to verify the Stepwise Regression algorithm, REG. It is based on the problem of finding an adequate model for the process of cement hardening. Figure D-1 illustrates the REG 'Control Panel' for selection of the final model.

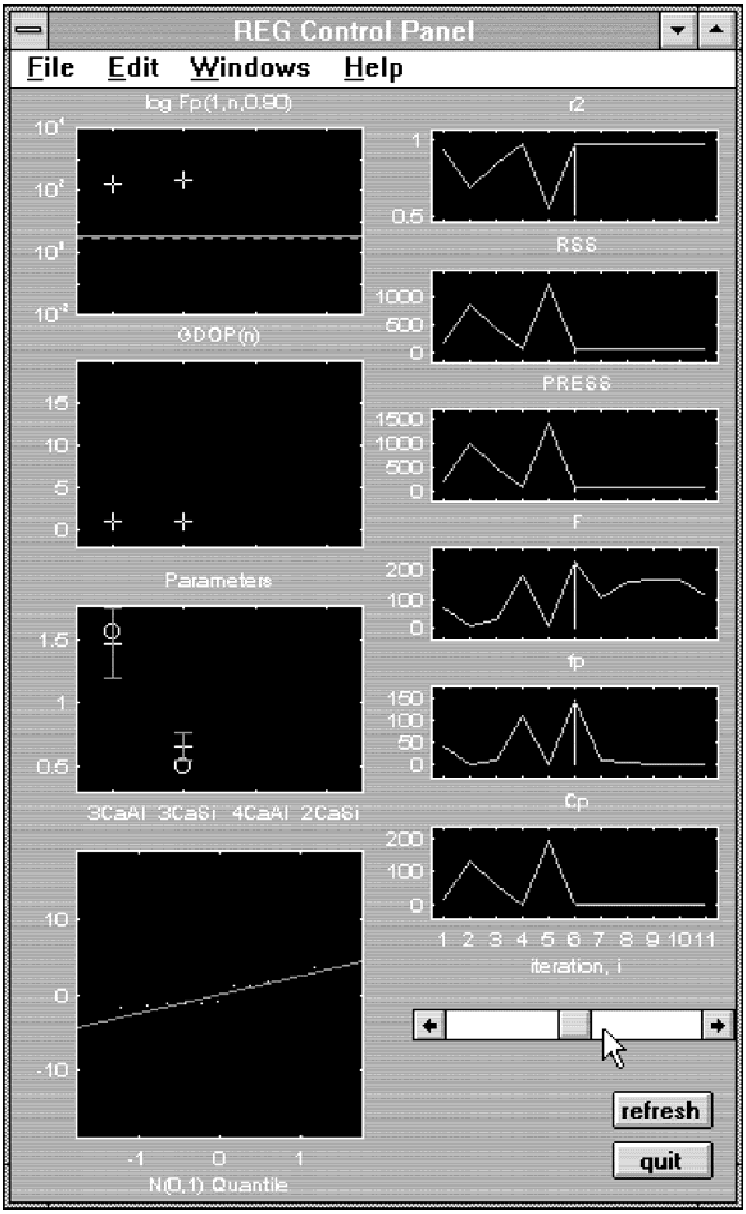

Figure D-1: REG Control Panel for model selection

Appendix E

MATLAB Files

Listings for three of the demonstration files have been included here, as well as the contents file for the *PRE Toolbox*. This last file gives a one-line description of most of the M files in the Toolbox.

E.1 F_DEMO1: F-111C aircraft response simulation

```
% F_DEMO1 : Demonstration 1 - Flight dynamic response simulation
%
%           Simulates the nonlinear dynamic response of an F-111C aircraft to
%           lateral control input. The high angle-of-attack aerodynamic
%           characteristics are modelled using tensor splines.
%
%           See A_DEMO1, ACDEMS

% The response of a General Dynamics F-111C aircraft to a combined control
% input is demonstrated in this example. The spoilers on the F-111C, used for
% lateral (roll) control, have inherently nonlinear characteristics. As the
% angle-of-attack is increased, this contribution changes, particularly for
% large deflections. The control inputs used in the simulation those of the
% actual flight data.
%
% Intialising :

% Flight response initialisation file names
%
fm1=['F1E48A';'F1E48B'];

% fm1 observation vector column no's = order of Z in F, where
%
%          1  2  3  4  5  6  7  8  9  10 11 12 13 14 15 16 17 18 19 20 21
% fm1:  F[ ax ay az p  q  r  h  M  V  a  b  pd qd rd th ph dh da dr ds ]
% FLYT: Z[ V  b  a  p  q  r  ph th .  ax ay az pd qd rd h  M  dh da dr ds ]
%
fm1n =   [ 9  11 10 4  5  6  16 15 0  1  2  3  12 13 14 7  8  17 18 19 20 ];

% Initialisation and output flight response file name
%
fm3=['F_DEMO1'];

% Sample frequency
%
ws=60;

% Set trim indices (2)
%
F=matloadr([fm1(1,:),'.MAT'],'F'); F=scale(centre(F)); n=[1:size(F,1)]';

plot(n,F(:,9:11)+2,'y',n,F(:,4:6)+1,'m',n,F(:,17:20),'c')
xlabel('n'), title('( V,b,a ) ; ( p,q,r ) ; ( dh,da,dr,ds )')

trm=uiknots'; close(gcf), size(trm);
if ~all(ans), trm=[1,1]; elseif ans(2)<2, trm=[1,trm]; end
trm=round(trm([1,2]));

% Write knot vectors to file
%
fid=fopen('TRIM.M','at'); fprintf(fid,'trm=[ %g:%g ];\n',trm); fclose(fid);

trm=[trm(1):trm(2)];

% Include geometric, mass and inertial characteristics, atmospheric constants
% and trim states.

% Initialisation vector
%
I=[    550        ... % wing area (ft^2)
         8.8      ... % MAC (ft)
        70        ... % wing span (ft)
      2247.63     ... % aircraft mass (slug)
     73602.1      ... % x-inertia (slugft^2)
    359989        ... % y-inertia (slugft^2)
    426433        ... % z-inertia (slugft^2)
      4020.85     ... % xz-inertia (slugft^2)
         0.002378 ... % s/l density (slug/ft^3)
        32.174    ] ; % gravity const. (ft/s^2)
                      % trim states/outputs obtained from flight data
I=[1,1]'*I;
```

```
% The spoilers' lateral contribution may be expressed as functions of both
% spoiler deflection and angle-of-attack. We will use a carpet (2-d spline)
% representation for these. Furthermore, the Clb, Clp, Cnb and Cnr derivatives
% all exhibit a significant nonlinearity in angle-of-attack, so a spline
% representation will be used. The data was obtained from scaled model
% wind-tunnel tests. Of interest is the control reversal (change of sign in
% dCl) at higher angles of attack.

% Coefficient matrix column no's (spoiler deflection,alpha)
%
k=[ 10 3 ];

% x-axis carpet knots (ds)
%
kx=[ 0 10 20 30 45 ]'; % deg

% z-axis carpet knots (a)
%
kz=[ 0 4 8 12 16 ]'; % deg

% Carpet ordinate matrix
%
R=[  4  6    % coeff' matrix row # : l,n
    11 11    % coeff' matrix col # : const.
     1  1    % x (ds) carpet order
     1  1    % z (a)  carpet order
    -1 -1    % x (ds) symmetry format : anti-symmetric
     0  0 ]; % z (a)  symmetry format : non-symmetric
%
%  +--ds
%  |
%  a
%     [ dCl ]
[  0 -0.0089 -0.0191 -0.0293 -0.0397
   0 -0.0101 -0.0210 -0.0305 -0.0429
   0 -0.0077 -0.0192 -0.0311 -0.0437
   0 -0.0008 -0.0024 -0.0062 -0.0148
   0  0.0061  0.0145  0.0188  0.0141 ]'; R(7:31,1)=ans(:);
%     [ dCn ]
[  0 -0.0019 -0.0039 -0.0064 -0.0105
   0 -0.0011 -0.0028 -0.0046 -0.0084
   0 -0.0005 -0.0015 -0.0029 -0.0059
   0  0.0001  0.0001  0.0001  0.0001
   0  0.0006  0.0016  0.0030  0.0061 ]'; R(7:31,2)=ans(:);

% Spline ordinate matrix
%
P=[  4  4  6  6    % coeff' matrix row # : l,n
     2  4  2  6    % coeff' matrix col # : const.
     1  1  1  1    % z (a)  carpet order
     0  0  0  0 ]; % z (a)  symmetry format : non-symmetric
%
% [ Clb       Clp       Cnb       Cnr ]
%
[ -0.0669 -0.4613  0.1343 -0.2654
  -0.0841 -0.4728  0.1358 -0.2697
  -0.1127 -0.3121  0.1437 -0.2988
  -0.1329 -0.1696  0.1278 -0.2826
  -0.1408 -0.1808  0.0827 -0.2533 ]; P(5:9,:)=ans;

% Dynamic coefficients include Cyb and Cza. For this flight case, all stability
% and control derivatives apart from the spoiler terms can be linearly
% approximated for all angles of attack (and spoiler deflections). These values
% were estimated from the flight-data using a Maximum Likelihood technique
% and are somewhat more accurate than the wind-tunnel results.

% Linear dynamic coefficient matrix
%
Ld=[  0       0       0       0       0       0
      0 -0.1401       0       0       0       0
      0       0 -2.9901       0       0       0
      0 -0.0198       0       0       0       0
      0       0 -5.7862       0       0       0
      0  0.0319       0       0       0       0 ];
```

```
% Linear static coefficient matrix
%
L=[  0       0       0       0        0       0       0       0       0       0
     0 -0.7219       0  0.0691        0  0.3105       0  0.0195  0.2097  0.0011
     0       0 -5.3572       0  -5.3377       0 -0.9683       0       0       0
     0       0       0       0        0  0.1243       0 -0.0739  0.0069       0
     0       0 -0.9225       0 -25.5955       0 -1.9022       0       0       0
     0       0       0 -0.0254        0       0       0 -0.0040 -0.0647       0 ];

% In order to make the simulated data more realistic, we will add Gaussian
% noise to the measurements (observations), excluding the controls. If the
% SIGNAL PROCESSING Toolbox is available, use the following commands to
% obtain a variance estimate of the flight data :
%
% >> matloadr([fm1(1,:),'.MAT'],'F'); f2zu(ans,fm1n);
% >> innovate(ans,4,3/(ws/2)); % 4th order, 3Hz lowpass freq.
% >> GG=[diag(ans)',zeros(1,4)];

% Discrete measurement noise covariance :
%                                                                .    .    .
%  [  V    b    a    p    q    r    ph   th   ps   ax   ay   az   p    q    r   ...
%     h    M    dh   da   dr   ds  ]

GG=[ 9e-2 4e-4 1e-3 2e-2 1e-3 5e-4 4e-3 4e-3 0e+0 2e-5 3e-5 1e-4 3e+1 3e+0 9e+0 ...
     1e+0 1e-7 0    0    0    0    ];

% To subsequently remove measurement noise from M (only if opt_(7)=0) use :
%
% >> randn('seed',0)
% >> M=M-randn(size(M))*sqrt(diag(GG));

% Setup ode solution parameters and display preferences.

% Re-calculation frequency (nonlinear)
%
Nr=1;

% Routine solution options
%
opt=[  2 ... % sol'n algorithm  : Runge-Kutta 2/3rd order
       0 ... % axes format      : Wind
       0 ... % angular rotation : Euler
       1 ... % pause flag
       0 ];  % display output   : none

% FLYT display/plot options ; number intermediate x,z points
%
fdsp=[ 1 1 ...                      % x,z plot size : half
       2 3 4 6 7 11 13 15 19:21 ]; % ode display   : [ b a p r ph da dr ds ]
Nyc=[ 61 61 ];

% Global options
%
global opt_

opt_=[ 1   ... % accurate angular accelerations flag
       1   ... % accurate angular rates flag
       1   ... % inherent inertial cross-coupling flag
       0.1 ... % knot fraction for coeff' differentiation     > not used here
       0   ... % update initialisation (trim) vector flag
       0   ... % implicit gravity acceleration component flag
       0   ];  % random noise time-based initial seed flag

% This takes around 41 mins on a 486/33 PC with 16M.

clear F n fid ans

% . . . . . . . . . . . . . . . . . . . . . . . . . . . . . . . . . . . . . . .
flyt
% . . . . . . . . . . . . . . . . . . . . . . . . . . . . . . . . . . . . . . .
```

E.2 A_DEMO1: Identification of simulated F-111C model

```
% A_DEMO1 : Demonstration 1 - Aircraft piecewise regressive estimation
%
%           Identifies the F-111C aircraft model simulated in F_DEMO1. The data
%           must be partitoned according to knots set by the user, in order to
%           estimate the nonlinear aerodynamic coefficients.
%
%           See A_DEMO2, ACDEMS

% We will use the response data simulated with the model of the F-111C aircraft
% from F_DEMO1 in this demostration. The spoilers on the F-111C, used for
% lateral (roll) control, have inherently nonlinear characteristics. As the
% angle-of-attack is increased, this contribution changes, particularly for
% large deflections. The control inputs used in the simulation those of the
% actual flight data.
%
% Intialising :

% Flight response initialisation file names
%
fm1=['F_DEMO1'];

% fm1 observation vector column no's = order of Z in F, where
%
%          1  2  3  4  5  6  7  8  9  10 11 12 13 14 15 16 17 18 19 20 21
%
% fm1:  F[ V  b  a  p  q  r  ph th ps ax ay az pd qd rd h  M  dh da dr ds ]
% FLYT: Z[ V  b  a  p  q  r  ph th ps ax ay az pd qd rd h  M  dh da dr ds ]
%
fm1n =   [ 1  2  3  4  5  6  7  8  9  10 11 12 13 14 15 16 17 18 19 20 21 ];

% Flight response comparison file names (data will be concatenated)
%
fm2=['F1E48A';'F1E48B'];

% fm2 observation vector column no's
%
% fm2:  F[ ax ay az p  q  r  h  M  V  a  b  pd qd rd th ph dh da dr ds ]
%
fm2n =   [ 9  11 10 4  5  6  16 15 0  1  2  3  12 13 14 7  8  17 18 19 20 ];

% Initialisation and output flight response file name
%
fm3=['A_DEMO1'];

% Output log file name
%
fl2=['A_DEMO1'];

% Sample frequency ; trim indices ; re-calculation frequency (linear approx'n)
%
ws=60; trm=[ 1:10 ];

% Include geometric, mass and inertial characteristics, atmospheric constants
% and trim states. These should all be identical to those in F_DEMO1.

% Initialisation vector
%
I=[    550        ... % wing area (ft^2)
         8.8      ... % MAC (ft)
        70        ... % wing span (ft)
      2247.63     ... % aircraft mass (slug)
     73602.1      ... % x-inertia (slugft^2)
    359989        ... % y-inertia (slugft^2)
    426433        ... % z-inertia (slugft^2)
      4020.85     ... % xz-inertia (slugft^2)
         0.002378 ... % s/l density (slug/ft^3)
        32.174    ]'; % gravity const. (ft/s^2)
```

```
% As we saw in F_DEMO1, the spoilers' lateral contribution may be expressed as
% functions of both spoiler deflection and angle-of-attack. This (2-D) spline
% function is defined on two sets of knots, or values of spoiler deflection and
% angle-of-attack. One method used in placing these knots is to examine the
% spread of data and place each knot, such that the enclosed region contains
% both a sufficient number of data points and has significant variation. The
% function UIKNOTS can be used for manual positioning ...
%
% The same knots as those in the original model have been postulated intially,
% for direct comparison of the coefficients. If these are chosen, however, we
% are disregarding the spread of data and as a result, may get some bad
% estimates.

% Coefficient matrix column no's (spoiler deflection,alpha)
%
k=[ 10 3 ];

% First load flight data from F_DEMO1.MAT. Load carpet and spline ordinate
% matrices and knot vectors from F_DEMO1.MYT setup file (saved at FLYT startup).
%
M=matloadr([fm1,'.MAT'],'M'); x=abs(M(:,21)); z=M(:,3);

R=matloadr([fm1,'.MYT'],'R'); P=matloadr([fm1,'.MYT'],'P');
kx0=matloadr([fm1,'.MYT'],'kx'); kz0=matloadr([fm1,'.MYT'],'kz');

% Plot abs(ds) v. alpha for UIKNOTS. (abs(ds) from symmetry)
%
plot(x,z,'.r'), set(gca,'YDir','reverse')
xlabels(['|ds|, deg'],0.4), ylabels(['a, ';'deg'])

% Start with the original knots, with x_max and z_max to indicate the data
% limits, prior to manual input. Remember to avoid creating regions enclosing
% small quantities of data. (Regions with NO data will be skipped)
%
kx=kx0; max(x)+1e-4; kx(kx>ans)=[]; kx=[kx;ans];
kz=kz0; max(z)+1e-4; kz(kz>ans)=[]; kz=[kz;ans];

[kx,kz]=uiknots(kx,kz); close(gcf)

% Check zero knots and prepend if neccessary.
%
if kx(1), kx=[0;kx]; end
if kz(1), kz=[0;kz]; end
nkx=size(kx,1); nkz=size(kz,1); nk=nkx*nkz;

% Write knot vectors to file.
%
fid=fopen('KXKZ.M','at');
fprintf(fid,['kx = [',mtx2str(kx'),' ]'';\nkz = [',mtx2str(kz'),' ]'';\n']);
fclose(fid);

% Check partition sizes.
%
disp(mtx2str(hol(kx,kz,x,z),' %4.0f'))

% Check variance proportions for each region. These must be evaluated manually.
% Either a small number of data points, or a low variance-proportion may lead
% to inaccurate estimates.

C1=zeros(nkz-1,nkx-1); C2=C1; C3=C1; V=[x'*x,z'*z,x'*z];

for i=1:nkz-1
   for j=1:nkx-1
      K=findk([mapx(kx(j:j+1),x),mapx(kz(i:i+1),z)],[-1,-1,-1,0]',[j,i]');
      if isempty(K), NaN*[1,1,1]; else, [x(K)'*x(K),z(K)'*z(K),x(K)'*z(K)]./V; end
      C1(i,j)=ans(1); C2(i,j)=ans(2); C3(i,j)=ans(3);
   end
end

blanks(1,ceil((5*(nkx-1)+2-13)/2));
[ans,'  % var(|ds|)',ans,ans,'   % var(a)  ',ans,ans,'% var(|ds|*a)'];
disp(ans), disp(' ')

ones(nkz-1,1)*[' |'];
[ans,mtx2str(C1,' %4.2f'),ans,mtx2str(C2,' %4.2f'),ans,mtx2str(C3,' %4.2f')];
disp(ans)
```

```
% Interpolate on carpet ordinates, R using new knot vectors to generate a
% compatible carpet ordinate matrix. Do the same for the splines, P.

for i=1:size(R,2)
   zeros(5,5); ans(:)=R(7:size(R,1),i); ans=ans'; clf

   surface(kx0',kz0,ans,'EdgeColor',0.5*[ 1 1 1 ],'FaceColor','none')
   set(gca,'View',[ 52.5 30 ]), hold on
   xlabel('ds, deg'), ylabel('a, deg')

   extrap2(kx0',kz0,ans,kx',kz);
   surface(kx',kz,ans,'EdgeColor',[ 0 1 0 ],'FaceColor','none'), hold off

   ans=ans'; R(7:nk+6,i)=ans(:); pause
end
R=R(1:nk+6,:); close(gcf)

P(5:nkz+4,:)=extrap1(kz0,P(5:size(P,1),:),kz); P=P(1:nkz+4,:);

% Solve for the carpet and spline coefficients and insert them into their
% initialisation matrices. Now all biased & fixed terms will be correctly
% matched.
%
rcarpt(R(7:nk+6,:),kx,kz,R(3:4,:)); Ra=[R(1:6,:);ans];
rsplyn(P(5:nkz+4,:),kz,P(3,:)); Pa=[P(1:4,:);ans];

% Since (dC{y,l,n}@ds=0) = 0 for all alpha, we can fix those to their a-priori
% (zero) values. We will leave all terms unbiased for now. They may in fact,
% need to be biased, depending on the patrtitioning, though.

% Carpet index vectors
%
[ [[ 0 ; 3*ones(nkz-1,1) ] ones(nkz,nkx-1) ]' , ...
  [[ 0 ; 3*ones(nkz-1,1) ] ones(nkz,nkx-1) ]' ]; resize(ans,nk);
%
rU=find(ans==1); % unbiased estimation terms
rB=find(ans==2); % biased estimation terms
rF=find(ans==3); % fixed terms

% Spline index vectors
%
[ ones(nkz,1) ones(nkz,1) ones(nkz,1) ones(nkz,1) ];
%
pU=find(ans==1); % unbiased estimation terms
pB=find(ans==2); % biased estimation terms
pF=find(ans==3); % fixed terms
%                                .       .
% Dynamic coefficients include Cyb and Cza. For this flight case, all stability
% and control derivatives apart from the spoiler terms can be linearly
% approximated for all angles of attack (and spoiler deflections). These values
% were estimated from the flight-data using a Maximum Likelihood technique
% and are somewhat more accurate than the wind-tunnel results.

% A-priori linear dynamic coefficient matrix
%
Lda=matloadr([fm1,'.MAT'],'Ld1');

% Linear dynamic coefficient index vectors
% .  .  .  .  .  .
% V  b  a  p  q  r
%
[ 0  0  0  0  0  0    % x
  0  2  0  0  0  0    % y
  0  0  0  0  0  0    % z
  0  2  0  0  0  0    % l
  0  0  0  0  0  0    % m
  0  2  0  0  0  0 ]; % n
%
ldU=find(ans==1); % unbiased estimation terms
ldB=find(ans==2); % biased estimation terms
ldF=find(ans==3); % fixed terms

% All of the 'weaker' terms in the model will be biased. That is, those terms
% that have a small effect on the aircraft's response and hence, are difficult
% to estimate accurately. The dynamic coefficients will also be biased, since
% collinearity with the other variables can cause gross errors.
```

```
% A-priori linear static coefficient matrix
%
La=matloadr([fm1,'.MAT'],'L1');

% Linear static coefficient index vectors
%
% V  b  a  p  q  r  dh da dr ds
%
[ 0  0  0  0  0  0  0  0  0  0    % x
  0  1  0  1  0  1  0  1  1  1    % y
  0  0  0  0  0  0  0  0  0  0    % z
  0  0  0  0  0  1  0  1  1  0    % l
  0  0  0  0  0  0  0  0  0  0    % m
  0  0  0  1  0  0  0  1  1  0 ]; % n
%
lU=find(ans==1); % unbiased estimation terms
lB=find(ans==2); % biased estimation terms
lF=find(ans==3); % fixed terms

% Significance level ; initial postulated coeff's
%
alf=0.05; Ji=[ 1 1 1 ];

% Re-calculation frequency (linear approx')
%
Nr=0;

% Routine solution options
%
opt=[  0 ... % sol'n algorithm          : LTITR kernel
       0 ... % axes format              : Wind
       0 ... % angular rotation         : Euler
       0 ... % pause flag
       0 ... % display output           : none
       0 ... % identification procedure : accumulation
       0 ... % regression scheme        : linear
       0 ... % variable entry           : direct
       1 ... % biased estimation        : mixed estimation
       0 ];  % user input flag          : no

% APRE & FLYT display/plot options ; number intermediate x,z points
%
adsp=[ 0 0 0 ]; % plot coeff' paths ; model responses ; regression region
fdsp=[ 1 1 ...             % x,z plot size : half
       2 3 4 6 7 17:19 ]; % ode display   : [ á à p r í ëa ër ës ] plot
Nyc=[ 61 61 ];

% Global options
%
global opt_

opt_=[ 1      ... % accurate angular accelerations flag
       1      ... % accurate angular rates flag
       1      ... % inherent inertial cross-coupling flag
       0.1    ... % knot fraction for coeff' differentiation
       0      ... % update initialisation (trim) vector flag
       0      ... % implicit gravity acceleration component flag
       0      ... % random noise time-based initial seed flag
       0.8    ... % correlation coefficient limit
       0      ... % variance inflation factor limit
       1e3    ... % eigen condition number limit
       0.5    ... % variance-decomposition proportion limit
       0.01   ... % biased fraction of estimated unbiased variance
      30      ... % approx. measurement noise frequency
       1e-12  ... % matrix condition tolerance
       1e-6   ... % residual sum-of-squares tolerance
       1      ];  % robust stepwise selection flag

% This takes around 6 mins on a 486/33 PC with 16M

clear M x z ans

% . . . . . . . . . . . . . . . . . . . . . . . . . . . . . . . . . . . . . . .
apre
% . . . . . . . . . . . . . . . . . . . . . . . . . . . . . . . . . . . . . . .
```

E.3 R_DEMO1: Hald data model structure determination

```
% R_DEMO1 : Demonstration of REG Data Regression Routine
%
%           Estimates a parsimonious model structure for the relationship
%           between the constituents of Portland cement and the heat evolved
%           during hardening.
%
%           See ACDEMS
%
% For more information, see
%
% [1] Hald, A. :
%     "Statistical Theory with Engineering Applications" John Wiley & Sons Inc.
% [2] Draper, N.R. & Smith, H. :
%     "Applied Regression Analysis" John Wiley & Sons Inc. (c) 1966

% The data used in this example is from a 4-variable problem on the effect of
% composition of Portland cement on heat evolved during hardening, given by
% [1], pp.647. This particular problem was chosen because it illustrates some
% typical difficulties which occur in regression analysis.
%
% Results may be directly compared with those published in [2], pp.397-492.
%
% Some additional variables, required by REG, have been added to the script
% and the initial data matrix has been augmented.
%
% Initialising :

% Extra rows will be added to X - these will not be used in regression and are
% simply to indicate possible discontinuities.

% Matrix of regressors and response
%
% [ 3CaO.Al O  3CaO.SiO  4CaO.Al O .Fe O  2CaO.SiO  Heat evolved (cal/g) ]
%          2 3         2        2 3   2 3        2
X=[     7         26              6          60          78.5
        1         29             15          52          74.3
       11         56              8          20         104.3
       11         31              8          47          87.6
        7         52              6          33          95.9
       11         55              9          22         109.2
        3         71             17           6         102.7
        1         31             22          44          72.5
        2         54             18          22          93.1
       21         47              4          26         115.9
        1         40             23          34          83.8
       11         66              9          12         113.3
       10         68              8          12         109.4 ];

X=X([1:4,4,4,5:7,7,7,8:10,10,11:13],:);

% Index vector (unique rows in X only)
%
k=find([1;diff(X(:,5))])';

% Vector of discontinuities
%
NN=[];

% Use least-squares estimates for a-priori values. For this example, we will
% not bias any parameters in the model.

% a-priori matrix
%      ^
%      c     bias flag
ci=[  1.5511    0      % 3CaO.Al..
      0.5102    0      % 3CaO.Si..
      0.1019    0      % 4CaO.Al..
     -0.1441    0 ];   % 2CaO.Si..
```

```
% Significance level, 10% for hypothesis tests and confidence intervals
%
alf=0.1;

% Initial columns for regression
%
ji=[1:3];

% Title & regressor text matrix for plots
%
fx4=['Heat ';'3CaAl';'3CaSi';'4CaAl';'2CaSi'];

% Output log (diary) file
%
fl1=[];%'R_DEMO1.LOG';

% Routine solution options
%
opt=[ 1 ... % regression procedure : stepwise
      2 ... % regression entry     : correlated
      0 ... % biased estimation    : none
      1 ... % user input flag
      1 ... % intermediate model response plot flag
      0 ];  % pause flag

% Global options
%
global opt_

opt_=[ 1     ... % )
       1     ... % |
       1     ... % (
       0.1   ... % > not used (reserved for FLYT & APRE)
       0     ... % (
       0     ... % |
       0     ... % )
       0.8   ... % correlation coefficient limit
      20     ... % variance inflation factor limit
       1e3   ... % eigen condition number limit
       0.5   ... % variance-decomposition proportion limit
       0.01  ... % biased fraction of estimated unbiased variance
      30     ... % approx. measurement noise frequency
       1e-12 ... % matrix condition tolerance
       1e-6  ... % residual sum-of-squares tolerance
       1     ];  % robust stepwise selection flag

% . . . . . . . . . . . . . . . . . . . . . . . . . . . . . . . . . . . . . . . .

[c0,c,sec]=reg(X(:,[1:4]),X(:,5),alf,k,NN,ci,ji,fx4,fl1,opt);

% . . . . . . . . . . . . . . . . . . . . . . . . . . . . . . . . . . . . . . . .

fprintf('%% Compare estimates against a-priori coefficients\n\n')
fprintf(['                ^          ^   \n', ...
        '       c       c       se(c)\n\n'])

disp([fx4(2:5,:),mtx2str([ci(:,1),c,sec],' %7.4f')]), fprintf('\n')
```

E.4 CONTENTS: *PRE Toolbox* M files

```
% PRE Piecewise Regressive Estimation Toolbox
%
% Version 1.0, 11/04/95
% R.A. Stuckey
% Copyright (c) 1995, University of Sydney
%
%
% Aircraft simulation.
%   alt2sig     - Altitude -> density ratio conversion.
%   alt2temp    - Altitude -> temperature conversion.
%   aplot       - State response output plot.
%   b2i         - Convert direction matrix ; Body -> Inertial axes.
%   b2w         - Convert air vectors ; Body -> Wind axes.
%   b2w1        - Convert single-point air vectors ; Body -> Wind axes.
%   cw2cb1      - Convert single-point aerodynamic derivatives ; Wind -> Body axes.
%   e2q         - Convert angular positions ; Euler -> Quaternion representation.
%   e2q1        - Convert single point angular positions. Requires CONTROL Tool.
%   flyt        - Aircraft Dynamic Response Simulation.
%   flyt_app    - Append flight data matrix.
%   flyt_chk    - Check FLYT input parameters.
%   flyt_com    - Create state companion matrix.
%   flyt_dim    - Create coefficient dimensioning matrices.
%   flyt_lod    - Load flight data.
%   flyt_pre    - Augment state pre-multiplier matrix.
%   flyt_rc     - Create carpet coefficient matrix.
%   flyt_rs     - Create spline coefficient matrix.
%   flyt_stm    - Create global state matrix.
%   flyt_trm    - Augment trim state coefficient matrix.
%   glops       - Augment global options vector.
%   i2b         - Convert direction matrix ; Inertial -> Body axes.
%   i2i1        - Augments initialisation vector.
%   ode         - ODE solution for nonlinear systems. Can use CONTROL Tool.
%   points      - Input signal generation with explicit points.
%   q2e         - Convert angular positions ; Quaternion -> Euler representation.
%   sig2alt     - Density ratio -> altitude conversion.
%   signal      - Input signal generation with input parameters.
%   temp2a      - Temperature -> speed of sound conversion.
%   temp2nu     - Temperature -> viscosity coefficient conversion.
%   w2b         - Convert air vectors ; Wind -> Body axes.
%   w2b1        - Convert single-point air vectors ; Wind -> Body axes.
%
% Identification.
%   amle        - Aircraft Maximum Likelihood Estimation. Requires SSSID Tool.
%   amle_chk    - Check APME input parameters.
%   amle_p2s    - Parameter to state-space conversion function.
%   apre        - Aircraft Piecewise Regressive Estimation.
%   apre_chk    - Check APRE input variables.
%   apre_dkz    - Iterative placement of knots based on significance.
%   apre_dsp    - Display active regression region.
%   apre_ini    - Initialise identification matrices.
%   apre_knt    - Modify/append knot vectors.
%   apre_opt    - Optimise knot positioning.
%   apre_out    - Display a-priori coefficients and estimates.
%   apre_par    - Evaluate partitioned regions.
%   apre_reg    - Perform regression.
%   apre_trn    - Transform knot vectors for optimisation.
%   apre_xz     - Construct regression matrix.
%   centre      - Centre matrix columns.
%   collchk     - Check for collinearity between matrix columns.
%   confr2      - Create 2-D confidence ellipse in cartesian coordinates.
%   decupl      - Decouple angular accelerations.
%   degrav      - Gravitational contribution to linear accelerations.
%   knots       - Manually allocate knots in data.
%   me          - Mixed Estimation.
%   pcr         - Principal Components Regression.
%   reg         - Data Regression Routine. Uses SYSID Tool if present.
%   reg_uiit    - UIControl macro for slider in REG.
%   scale       - Normalise (scale) columns in X.
%   uiknots     - Manually allocate knots in data using UIControls.
```

```
% Splines.
%   extrap1    - 1-D data inter-/extrapolation (table lookup).
%   extrap2    - 2-D data inter-/extrapolation (table lookup).
%   findk      - Find data in axis quadrants.
%   findx      - Find kk-matrix elements in axis quadrants.
%   mapx       - Map matrix elements in axis regions.
%   rcarpt     - Multiple carpet function.
%   rcfind     - Multiple carpet finder.
%   rcmesh     - Evaluate, display and compare single carpet function.
%   rcsolv     - Multiple carpet solution.
%   rcsolvn    - Carpet array solution.
%   rcsolv1    - Single-point multiple carpet solution.
%   rsfind     - Multiple spline finder.
%   rsplot     - Evaluate, display and compare multiple spline functions.
%   rsplyn     - Multiple spline function.
%   rssolv     - Multiple spline solution.
%   rssolvn    - Multiple spline array solution.
%   rssolv1    - Single-point multiple spline solution.
%
% Distribution functions.
%   betai      - Incomplete beta function.
%   fdist      - F-distribution probability.
%   fdisti     - Compute F statistic. Requires OPTIM Tool.
%   fdisti_a   - Auxiliary function for FDISTI.
%   ftable     - Table-lookup of F statistic.
%   gammln     - Natural log of the complete gamma function.
%   normf      - The Standard Normal distribution function N(0,1).
%   normfinv   - Inverse of the Standard Normal distribution function.
%   qq_norm    - Create indices for normal quantile-quantile plot.
%
% Signal Processing.
%   dff        - Numerical differential.
%   dfffix     - Differential error correction.
%   dfffix_e   - Integral error calculation.
%   innovate   - Innovation covariance estimate. Requires SYSID Tool.
%   int        - Numerical integral.
%   outliers   - Find outliers in columns of data matrix.
%   seed       - Random time-based initial seed.
%
% Miscellaneous.
%   combine    - Calculate binary combination matrix.
%   comply     - Arrange two matrices so that their row dimensions are equal.
%   contents   - This file.
%   ffind      - Find text string in file.
%   groups     - Size of groups in vectors.
%   gsum       - Sum groups appearing in a vector.
%   index      - Create index matrix.
%   interpn    - Nth degree linear data interpolation.
%   interset   - Intersecting set.
%   interval   - Divide integer vector into intervals.
%   list       - Output variable list to text matrix.
%   listmat    - Output .MAT file variable list to text matrix.
%   m2m        - Concatenate/divide User Data Matrices.
%   matloadr   - Load full, real matrix from .MAT file.
%   meq        - Matrix inequality.
%   mget       - Get property values from a vector of handles.
%   mset       - Set property values to a vector of handles.
%   mtx2str    - Convert numeric matrix to equivalent string matrix.
%   mtxcmp     - Matrix comparison.
%   ncr        - Total number of r-combinations in n.
%   polyfitx   - Tensor-polynomial curve fitting.
%   polyvalx   - Tensor-polynomial evaluation.
%   resize     - Resize matrix.
%   savermf    - Save REAL variables in .M file format.
%   setf       - Sort and remove multiple occurences in a vector.
%   shift      - Shift matrix columns.
%   union      - Union set.
%   width      - Returns the width of matrix X.
```

```
% General graphics.
%   clip       - Manual clipping for plots.
%   clrbar     - Create colour-bar for colour plots.
%   count      - Window counter & expected time until completion.
%   gryd       - Creates user-defined grid.
%   gtex       - Place text on 2-D graph using mouse.
%   intplots   - Plot intermediate regions.
%   ishandle   - Determine handle existance and type.
%   tex        - A function to allow the use of special characters in plots.
%   texts      - Place text with respect to axis.
%   titles     - Place titles above plot.
%   xlabels    - Place labels on x axis.
%   ylabels    - Place labels on y axis.
%
% .MEX functions.
%   betacf     - Continued fraction for incomplete beta function.
%   matlist    - List variables in .MAT file.
%   matloadr   - Load full, real matrix from .MAT file.
%
% Data file interface.
%   f111_ini   - Create F-111C initialisation and flight data files.
%   f111l_sp   - Create .MAT format wind-tunnel spoiler derivative database.
%   f111l_wt   - Create .MAT format wind-tunnel lateral derivative database.
%   f2zu       - Conversion from flight data matrix to observation/control matrices.
%   latdb_cg   - Convert wind-tunnel coefficient and derivative values.
%   latdb_sp   - Convert wind-tunnel spoiler coefficients.
%   p2pa       - Set up knot vector and convert spline matrix.
%   r2ra       - Set up knot vectors and convert carpet matrix.
%
% Demos.
%   a_demo1    - Demonstration 1 - Aircraft piecewise regressive estimation.
%   acdems     - Set up Aircraft Parameter Identification demos for the MATLAB Expo.
%   f_demo1    - Demonstration 1 - Flight dynamic response simulation.
%   f_demo2    - Demonstration 2 - Flight dynamic response simulation.
%   f_demo3    - Demonstration 3 - Flight dynamic response simulation.
%   r_demo1    - Demonstration of REG Data Regression Routine.
%   s_demo1    - Demonstration of 1-D spline functions.
%   s_demo2    - Demonstration of 2-D spline functions.
```